



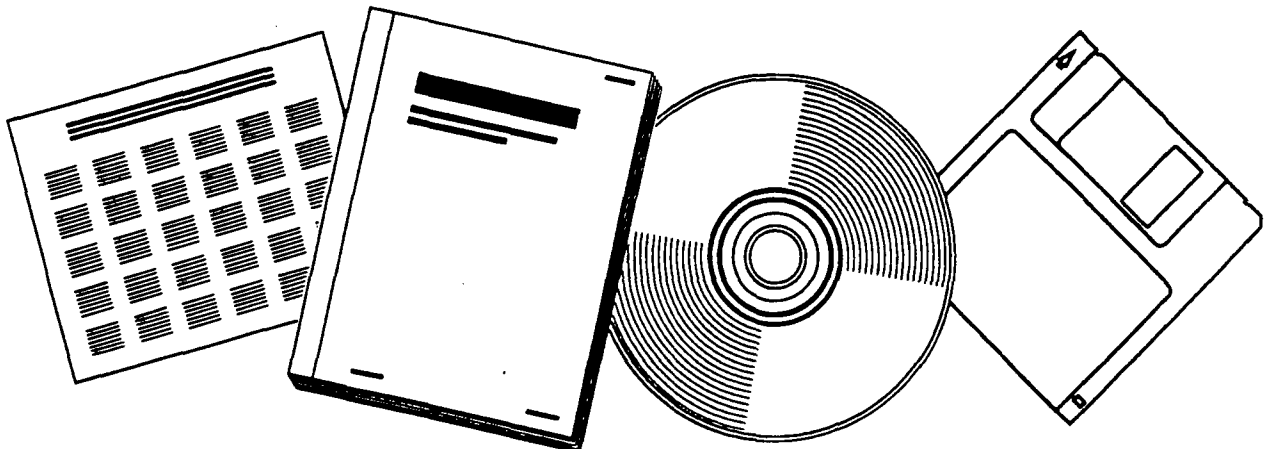
PB97-163935

NTIS[®]
Information is our business.

DETERMINATION OF PILE DRIVEABILITY AND CAPACITY FROM PENETRATION TESTS. VOLUME 1 FINAL REPORT

GOBLE, RAUSCHE, LIKINS AND ASSOCIATES, INC., CLEVELAND, OH

MAY 97



U.S. DEPARTMENT OF COMMERCE
National Technical Information Service





PB97-163935

Determination of Pile Driveability and Capacity From Penetration Tests

Volume I: Final Report

PUBLICATION NO. FHWA-RD-96-179

MAY 1997



U.S. Department of Transportation
Federal Highway Administration

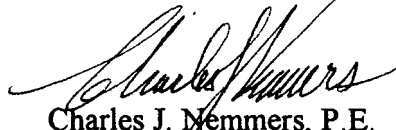
Research and Development
Turner-Fairbank Highway Research Center
6300 Georgetown Pike
McLean, VA 22101-2296



REPRODUCED BY: **NTIS**
U.S. Department of Commerce
National Technical Information Service
Springfield, Virginia 22161

FOREWORD

This report, *Determination of Pile Driveability and Capacity from Penetration Tests*, is comprised of three volumes. Volume I (FHWA-RD-96-179), contained here, summarizes the design and experimental use of a method that extracts dynamic soil resistance parameters as the Standard Penetration Test is being performed. Extensive correlations with full scale load tests were made based on these results. Volume II (FHWA-RD-96-180) of the series describes the data bank that has been assembled as part of the study and contains dynamic and static load test data. Volume III (FHWA-RD-96-181) documents the results of a literature study and summarizes available information on dynamic soil models and their parameters.




Charles J. Memmers, P.E.
Office of Engineering
Research and Development

NOTICE

This document is disseminated under the sponsorship of the Department of Transportation in the interest of information exchange. The United States Government assumes no liability for its contents or use thereof. This report does not constitute a standard, specification, or regulation.

The United States Government does not endorse products or manufacturers. Trade and manufacturers' names appear in this report only because they are considered essential to the object of the document.

Technical Report Documentation Page

1. Report No. FHWA-RD-96-179		2.  PB97-163935		3. Recipient's Catalog No.	
4. Title and Subtitle DETERMINATION OF PILE DRIVEABILITY AND CAPACITY FROM PENETRATION TESTS Volume I: Final Report				5. Report Date May 1997	
				6. Performing Organization Code	
7. Author(s) Rausche, F., Thendean, G., Abou-matar, H., Likins, G.E., Goble, G.G.				8. Performing Organization Report No.	
9. Performing Organization Name and Address Goble Rausche Likins and Associates, Inc. 4535 Renaissance Parkway Cleveland, Ohio 44128				10. Work Unit No. (TRAIS) 3E3A-0193	
				11. Contract or Grant No. DTFH61-93-C-00047	
12. Sponsoring Agency Name and Address Office of Engineering R&D Federal Highway Administration 6300 Georgetown Pike McLean, Virginia 22101-2296				13. Type of Report and Period Covered Final Report October 1991 - September 1994	
				14. Sponsoring Agency Code	
15. Supplementary Notes FHWA Contracting Officer's Technical Representative: Carl Ealy, HNR-30 FHWA Technical Consultant: Jerry DiMaggio, HNG-31					
16. Abstract <p>Research has been conducted on the potential improvement of dynamic wave equation analysis methodology using in-situ soil testing techniques. As a basis for this investigation, the literature was reviewed and a summary was compiled of efforts made to date on the development of models and associated parameters for pile driving analysis. Furthermore a data base was developed containing more than 150 cases of test piles with static load tests, dynamic restrrike tests, soil information, driving system data and installation records. One hundred data base cases were subjected to correlation studies using both wave equation and CAPWAP. This work yielded dynamic soil model parameters which did not indicate a specific relationship with soil grain size.</p> <p>The in-situ soil testing device utilized was a Modified SPT which yielded data from both static and dynamic measurements. Either static uplift or torque tests yielded static ultimate shaft resistance, and uplift tests also indicated a shaft resistance quake. Static compressive tests on a special tip indicated ultimate end bearing and associated toe quake. Indirectly, by signal matching, soil damping parameters were calculated. These quantities were then used for the prediction of full-scale pile behavior. Data from the Modified SPT were gathered and analyzed on six sites with previous full-scale static pile tests and on three sites where static load tests were to be performed at a later date.</p> <p>Recommendations derived from these tests pertain to the current soil model and to proposals for future changes. In general, the current approach was found to yield, on the average, very reasonable results for end of installation situations. For restrrike tests, standard parameters may be misleading. Any necessary modifications to the current approach, for example, the use of particularly large toe quakes or low toe damping factors should be based on Modified SPT measurements. Differences between prediction and full-scale pile field behavior were attributed to soil strength changes over relatively small distances which cannot be detected with standard SPT spacings of 5 ft (1.5 m).</p> <p>This volume is the first in a series. Other volumes in the series are: FHWA-RD-96-180 Volume II: Appendixes FHWA-RD-96-181 Volume III: Literature Review, Data Base and Appendixes</p>					
17. Key Words Pile driving, foundation, pile foundation, wave equation, CAPWAP, standard penetration test, in-situ test, pile capacity, pile driveability, pile data base, energy, static load test, dynamic load test, soil damping.			18. Distribution Statement No restrictions. This document is available to the public through the National Technical Information Service, Springfield, Virginia 22161.		
19. Security Classif. (of this report) Unclassified		20. Security Classif. (of this page) Unclassified		21. No. of Pages 242	22. Price

SI* (MODERN METRIC) CONVERSION FACTORS

APPROXIMATE CONVERSIONS TO SI UNITS

APPROXIMATE CONVERSIONS FROM SI UNITS

Symbol	When You Know	Multiply By	To Find	Symbol	Symbol	When You Know	Multiply By	To Find	Symbol
LENGTH					LENGTH				
in	inches	25.4	millimeters	mm	mm	millimeters	0.039	inches	in
ft	feet	0.305	meters	m	m	meters	3.28	feet	ft
yd	yards	0.914	meters	m	m	meters	1.09	yards	yd
mi	miles	1.61	kilometers	km	km	kilometers	0.621	miles	mi
AREA					AREA				
in ²	square inches	645.2	square millimeters	mm ²	mm ²	square millimeters	0.0016	square inches	in ²
ft ²	square feet	0.093	square meters	m ²	m ²	square meters	10.764	square feet	ft ²
yd ²	square yards	0.836	square meters	m ²	m ²	square meters	1.195	square yards	yd ²
ac	acres	0.405	hectares	ha	ha	hectares	2.47	acres	ac
mi ²	square miles	2.59	square kilometers	km ²	km ²	square kilometers	0.386	square miles	mi ²
VOLUME					VOLUME				
fl oz	fluid ounces	29.57	milliliters	mL	mL	milliliters	0.034	fluid ounces	fl oz
gal	gallons	3.785	liters	L	L	liters	0.264	gallons	gal
ft ³	cubic feet	0.028	cubic meters	m ³	m ³	cubic meters	35.71	cubic feet	ft ³
yd ³	cubic yards	0.765	cubic meters	m ³	m ³	cubic meters	1.307	cubic yards	yd ³
NOTE: Volumes greater than 1000 l shall be shown in m ³ .									
MASS					MASS				
oz	ounces	28.35	grams	g	g	grams	0.035	ounces	oz
lb	pounds	0.454	kilograms	kg	kg	kilograms	2.202	pounds	lb
T	short tons (2000 lb)	0.907	megagrams (or "metric ton")	Mg (or "t")	Mg (or "t")	megagrams (or "metric ton")	1.103	short tons (2000 lb)	T
TEMPERATURE (exact)					TEMPERATURE (exact)				
°F	Fahrenheit temperature	5(F-32)/9 or (F-32)/1.8	Celcius temperature	°C	°C	Celcius temperature	1.8C + 32	Fahrenheit temperature	°F
ILLUMINATION					ILLUMINATION				
fc	foot-candles	10.76	lux	lx	lx	lux	0.0929	foot-candles	fc
fl	foot-Lamberts	3.426	candela/m ²	cd/m ²	cd/m ²	candela/m ²	0.2919	foot-Lamberts	fl
FORCE and PRESSURE or STRESS					FORCE and PRESSURE or STRESS				
lbf	poundforce	4.45	newtons	N	N	newtons	0.225	poundforce	lbf
lbf/in ²	poundforce per square inch	6.89	kilopascals	kPa	kPa	kilopascals	0.145	poundforce per square inch	lbf/in ²

* SI is the symbol for the International System of Units. Appropriate rounding should be made to comply with Section 4 of ASTM E380.

TABLE OF CONTENTS

<u>Volume I Final Report</u>	<u>Page</u>
1. INTRODUCTION	1
2. WAVE EQUATION CORRELATIONS AND SOIL PARAMETER CALCULATIONS ...	5
2.1 OBJECTIVES	5
2.2 DESCRIPTION OF THE DATA BASE	5
2.3 VALUE OF THE DATA BASE	6
2.4 WAVE EQUATION SOIL MODELS INVESTIGATED	7
2.5 CORRELATION EFFORTS AND PARAMETER CALCULATIONS	9
2.6 RESULTS ..	12
2.6.1 Capacity Predictions	12
2.6.2 Dynamic Soil Model Properties	20
2.6.3 Apparent Setup Factors	25
3. CAPWAP CORRELATION AND SOIL PARAMETER CALCULATIONS	31
3.1 INTRODUCTION	31
3.2 TIME RATIO	36
3.3 PILE TYPE	37
3.4 COMPARISON BETWEEN AUTOMATIC, BEST MATCH, RADIATION DAMPING RESULTS	37
3.5 DYNAMIC SOIL PARAMETERS	43
3.6 GUIDELINES FOR USING RADIATION DAMPING	43
4. THE MODIFIED SPT PROCEDURE	49
4.1 INTRODUCTION	49
4.2 THE MODIFIED SPT PROCEDURE CONCEPT	49
4.3 SPT EQUIPMENT MODIFICATIONS	50
4.3.1 Dynamic Force and Velocity Measurements	50
4.3.2 Oversized Tips	52
4.3.3 Hammer Performance Analyzer™	52
4.4 ADDITIONAL VERIFICATION TESTS	52
4.4.1 General Remarks	52
4.4.2 Axial Static Load Test	54
4.4.2.1 Reaction Frame	54
4.4.2.2 Load Transducers	54
4.4.2.3 Displacement Transducers	57
4.4.2.4 Spacers	57
4.4.2.5 Data Acquisition and Software	58
4.4.3 Torque Static Test	58
4.4.4 Instrumented Sampler	60
4.4.5 Cone Penetration Test	60
4.5 THE MODIFIED SPT TEST PROCEDURE	61
4.6 LOCATION OF TEST SITES	63
4.6.1 Correlation Study Sites	63
4.6.2 Verification Sites	66

TABLE OF CONTENTS (Continued)

<u>Volume I Final Report</u>	<u>Page</u>
5. DATA REDUCTION, ANALYSES, AND RESULTS	67
5.1 STATIC RESULTS	67
5.1.1 Background	67
5.1.2 Uplift and Compression	68
5.1.3 Comparison of Flat and Cone Tip	69
5.1.4 Scale Factor for Unit End Bearing Prediction	70
5.1.5 Rate Effect of Soil	73
5.1.6 Soil Setup	78
5.1.7 Torque Test	81
5.1.8 Pile Capacity Determination Using CPT Results	85
5.2 DYNAMIC RESULTS	89
5.2.1 Analytical Background	89
5.2.2 Verification of the Method	92
5.2.3 Determination of Wave Equation Soil Constants	95
5.2.4 GRLWEAP Analysis	96
5.2.5 SPT Result Summary	96
5.2.6 Dynamic Data Collection	99
5.2.7 Dynamic Data Analysis and Results of SPT	100
5.2.8 Discussion of Shaft Results	109
5.2.9 Discussion of Toe Results	110
5.2.10 Shaft Soil Model Studies	115
5.2.11 Toe Soil Model Studies	116
6. WAVE EQUATION ANALYSIS OF FULL-SCALE PILES	119
6.1 INTRODUCTION	119
6.2 DIRECT PILE CAPACITY CALCULATION FROM MODIFIED SPT	120
6.2.1 St. Mary, Cleveland, Ohio	130
6.2.2 Fore River Bridge, Portland, Maine	130
6.2.3 C&D Canal, Pier 17, Delaware	131
6.2.4 C&D Canal, Pier 21, Delaware	132
6.2.5 White City Bridge, TP3, Florida	133
6.2.6 Apalachicola River Bridge, Florida	133
6.2.7 Correlation of Directly Calculated Capacity Values	134
6.3 DYNAMIC SOIL PARAMETER CALCULATION	135
6.4 DRIVEABILITY ANALYSES	136
6.4.1 St. Mary, Cleveland, Ohio	136
6.4.2 Fore River Bridge, Portland, Maine	145
6.4.3 C&D Canal, Pier 17, Delaware	145
6.4.4 C&D Canal, Pier 21, Delaware	146
6.4.5 White City Bridge, TP3, Florida	148
6.4.6 Apalachicola River Bridge, Florida	148
6.5 BEARING GRAPH CALCULATIONS	150
6.6 TOE PARAMETER STUDY	159
6.7 DISCUSSION OF RESULTS	168

TABLE OF CONTENTS (Continued)

<u>Volume I Final Report</u>	<u>Page</u>
6.7.1 Blow Count Predictions	168
6.7.2 Capacity Predictions	168
6.7.3 Toe Parameter Study	170
7. PILE CAPACITY AND BLOW COUNT PREDICTION	173
7.1 INTRODUCTION	173
7.2 MODIFIED SPT DATA ANALYSIS	173
7.3 PILE CAPACITY PREDICTION	174
7.3.1 Aucilla River Bridge Florida	180
7.3.2 Vilano Bridge - East Embankment, Florida	181
7.3.3 Vilano Bridge - West Embankment, Florida	181
7.3.4 Discussion of Pile Capacity Prediction	182
7.4 DRIVEABILITY ANALYSIS AND BEARING GRAPHS	182
8. CONCLUSIONS	199
8.1 THE WAVE EQUATION MODEL	199
8.2 THE DATA BASE	200
8.3 DYNAMIC SOIL PARAMETERS	200
8.4 THE MODIFIED SPT	201
9. RECOMMENDATIONS	203
 <u>Volume II Appendixes</u>	
APPENDIX A - WAVE EQUATION ANALYSIS RESULTS	1
APPENDIX B - SPT STATIC LOAD TEST RESULTS	111
APPENDIX C - TORQUE TEST RESULTS	131
APPENDIX D - DYNAMIC TEST RESULTS	137
APPENDIX E - SUMMARY OF SPT ROD TOP MEASUREMENTS	243
APPENDIX F - TEST SITES INFORMATION	251
APPENDIX G - TRANSDUCER CALIBRATION RESULTS	301
APPENDIX H - LABORATORY TESTING RESULTS	311
REFERENCES	393

TABLE OF CONTENTS (Continued)

<u>Volume III Literature Review, Data Base and Appendixes</u>	<u>Page</u>
1. INTRODUCTION	1
2. LITERATURE REVIEW ON DYNAMIC PILE ANALYSIS MODELS	3
2.1 INTRODUCTION	3
2.2 REVIEW OF LITERATURE ON DYNAMIC SOIL MODELS	3
2.3 REVIEW OF LITERATURE ON EXPERIMENTAL STUDIES	12
2.4 PARAMETERS FOR SMITH'S SOIL MODELS	13
2.5 SOIL CONSTANTS FROM CAPWAP	18
2.6 SOIL CONSTANTS FROM IN-SITU TESTS	19
2.7 SOIL SETUP AND RELAXATION BEHAVIOR	24
3. DESCRIPTION OF DATA BASE	27
3.1 DATA BASE REQUIREMENTS	27
3.2 DATA BASE STATISTICS (January 1996)	28
APPENDIX A - INTRODUCTION INTO THE MECHANICS OF TRAVELING WAVES IN A SLENDER, ELASTIC ROD	43
APPENDIX B - INVESTIGATION OF DYNAMIC SOIL RESISTANCE ON PILES USING GRLWEAP	51
APPENDIX C - WAVE EQUATION ANALYSIS	57
APPENDIX D - DYNAMIC PILE TESTING AND ANALYSIS: CASE METHOD AND CAPWAP	71
APPENDIX E - GROUND SURFACE MEASUREMENTS DURING SPT AND PILE DRIVING	97
APPENDIX F - RESULTS FROM SENSITIVITY STUDY	103
APPENDIX G - DOCUMENTED LARGE QUAKE CASES	105
APPENDIX H - DOCUMENTED HIGH SOIL DAMPING CASES	113
REFERENCES	123

LIST OF FIGURES

Volume I: Final Report

<u>Figure</u>	<u>Page</u>
2.1	GRLWEAP EOD Capacity Correlations Using Standard Smith Soil Model . . . 14
2.2	GRLWEAP BOR Capacity Correlations Using Standard Smith Soil Model . . . 14
2.3	GRLWEAP EOD Capacity Correlations Using Smith Soil Model and Adjusted Hammer/Driving System Parameters 15
2.4	GRLWEAP BOR Capacity Correlations Using Smith Soil Model and Adjusted Hammer/Driving System Parameters 15
2.5	Capacity Correlation for Static Formula Prediction 16
2.6(a)	Frequency Distribution and Probability Density Function of Adjusted WEAP (EOD) 17
2.6(b)	Frequency Distribution and Probability Density Function of Adjusted WEAP (BOR) 17
2.7	Log-Normal Probability Density for EOD and BOR Predictions with Standard Smith Model, and With and Without Adjusted Hammer/Driving System Parameters 18
2.8	Log-Normal Probability Density for EOD and BOR Predictions (as in figure 2.7 but With Results Averaged for Same Site) 18
2.9	Log-Normal Probability Density for BOR Predictions with Several Methods 19
2.10	Log-Normal Probability Density for BOR Predictions (as in figure 2.8 but With Results Averaged for Same Site) 19
2.11	Adjusted GRLWEAP BOR Capacity Correlation for Different Time Ratio 21
2.12	Log Normal Probability Density For Adjusted GRLWEAP BOR Capacity with Three Different Time Ratios 22
2.13	Log Normal Probability Density for Adjusted GRLWEAP BOR Capacity with Two Different Time Ratios 22
2.14	Smith Shaft Damping Factors Back-Calculated for Piles with More Than 30 Percent Shaft Resistance 24
2.15	Smith Toe Damping Factor Back-calculated For Piles with Less Than 70 Percent Shaft Resistance 24
2.16	Increasing Tendency of Shaft Damping with Time (Svinkin and Teferra, 1994) 25
2.17	Correlated Setup Factors for Piles with More Than 50 Percent Friction 26
2.18	Standard Setup Factors from Unadjusted Wave Equation EOD Analysis 27
2.19	Setup Factors Based on Standard Smith EOD Analyses with Adjusted Hammer/Driving System Parameters 28
2.20	Average Standard Setup Factors and Recommended Setup Factors 28
2.21	Log-Normal Probability Density for Standard EOD and CAPWAP EOD Factored with Conservative Setup Factors (Apply Only to Non End Bearing Pile) 29
2.22	Apparent Setup Factors for Various States (Load Test / Adjusted WEAP-EOD) 29
2.23	Apparent Setup Factors for Various States (Load Test / CAPWAP-EOD) 30

LIST OF FIGURES (continued)

Volume I: Final Report

<u>Figure</u>	<u>Page</u>
3.1(a) CAPWAP (Automatic) Capacity versus Static Load Test Capacity Showing Different Time Ratios	33
3.1(b) Log-Normal Probability Density Function for CAPWAP (Automatic) Capacity Prediction at Different Time Ratios	33
3.2(a) CAPWAP (Best Match) Capacity versus Static Load Test Capacity Showing Different Time Ratios	34
3.2(b) Log-Normal Probability Density Function for CAPWAP (Best Match) Capacity Prediction at Different Time Ratios	34
3.3(a) CAPWAP (Radiation Damping) Capacity versus Static Load Test Capacity Showing Different Time Ratios	35
3.3(b) Log-Normal Probability Density Function for CAPWAP (Radiation Damping) Capacity Prediction at Different Time Ratios	35
3.4(a) CAPWAP (Automatic) Capacity versus Static Load Test Capacity Showing Different Pile Types	38
3.4(b) CAPWAP (Automatic) Capacity versus Static Load Test Capacity Showing Displacement and Nondisplacement Piles	38
3.5(a) CAPWAP (Best Match) Capacity versus Static Load Test Capacity Showing Different Pile Types	39
3.5(b) CAPWAP (Best Match) Capacity versus Static Load Test Capacity Showing Displacement and Nondisplacement Piles	39
3.6(a) CAPWAP (Radiation Damping) Capacity versus Static Load Test Capacity Showing Different Pile Types	40
3.6(b) CAPWAP (Radiation Damping) Capacity versus Static Load Test Capacity Showing Displacement and Nondisplacement Piles	40
3.7 Log-Normal Probability Density Function for Automatic, Best Match, and Radiation Damping CAPWAP Capacity Prediction	42
3.8 Log-Normal Probability Density Function for Original and Version 1.993-1 + Radiation Damping CAPWAP Capacity Prediction	42
3.9(a) Smith Shaft Damping versus Soil Types from Best Match CAPWAP	45
3.9(b) Smith Shaft Damping versus Soil Types from Radiation Damping CAPWAP	45
3.10(a) Smith Toe Damping versus Soil Types from Best Match CAPWAP	46
3.10(b) Smith Toe Damping versus Soil Types from Radiation Damping CAPWAP	46
3.11(a) Shaft Quake versus Soil Types from Best Match CAPWAP	47
3.11(b) Shaft Quake versus Soil Types from Radiation Damping CAPWAP	47
3.12(a) Toe Quake versus Soil Types from Best Match CAPWAP	48
3.12(b) Toe Quake versus Soil Types from Radiation Damping CAPWAP	48
4.1 Instrumented SPT Rod	51
4.2 Oversized Tips - Flat End and Cone	53
4.3 The Modified SPT Procedure with HPA Measurement	53
4.4 Schematic Static Uplift and Compression Test Setup	55
4.5(a) Static Uplift Test Setup at White City, TP3, FL Site	56
4.5(b) Static Compression Test Setup at White City, TP6, FL Site	56
4.6 Instrumented Torque Rod	59

LIST OF FIGURES (continued)

Volume I: Final Report

<u>Figure</u>	<u>Page</u>
4.7 Torque Test Being Performed	60
5.1 Typical Load <i>versus</i> Displacement for Clay and Sand	68
5.2 Load <i>versus</i> Displacement for Flat End and Cone Tip at Portland Site	71
5.3 Load <i>versus</i> Displacement for Flat End and Cone Tip at CD21 Site	71
5.4 Load <i>versus</i> Displacement for Flat End Tip and Full-Scale Pile, Portland Site	74
5.5 Load <i>versus</i> Displacement for Flat End Tip and Full-Scale Pile, AP Site	74
5.6 Bottom Force from Various Hammer Drop Heights	76
5.7 Bottom Velocity from Various Hammer Drop Heights	76
5.8 Rate Effect Study for CH Type Soil	78
5.9 Setup Evaluation for Three Sites	81
5.10 Summary of Torque Test Results from 20 Sites	84
5.11 Torque Resistance <i>versus</i> Uplift Resistance	86
5.12 Torque Test Results from Vilano Bridge - West, FL	86
5.13(a) Comparison of CPT and Modified SPT Data for AP Site	87
5.13(b) Comparison of CPT and Modified SPT Data for Aucilla Site	87
5.13(c) Comparison of CPT and Modified SPT Data for VE Site	88
5.13(d) Comparison of CPT and Modified SPT Data for VW Site	88
5.14 Procedure for Estimating Pile Tip Bearing Capacity from the Measured Cone Resistance (After Vanikar, FHWA-DP-66-1, 1986)	90
5.15(a) Force and Velocity Measured at the Top	94
5.15(b) Comparison Between Measured and Calculated Bottom Force	94
5.15(c) Comparison Between Measured and Calculated Bottom Velocity	94
5.16(a) Comparison Between GRLWEAP and Measured Top Force and Velocity from St. Mary Site	97
5.16(b) Comparison Between GRLWEAP and Measured Bottom Force and Velocity from St. Mary Site	97
5.17(a) Comparison Between GRLWEAP and Measured Top Force and Velocity from Apalachicola Site	98
5.17(b) Comparison Between GRLWEAP and Measured Bottom Force and Velocity from Apalachicola Site	98
5.18 Comparison Between GRLWEAP and Measured Blow Count from SPT Driving System	107
5.19(a) Comparison Between Ultimate Toe Resistance from Static Compression Tests and Dynamic Analyses	113
5.19(b) Comparison of Toe Damping Factors from "Static" and "Dynamic" Analyses for Static $R_u >$ Dynamic R_u	113
5.20 Measured and GRLWEAP Computed Dynamic Force vs Dynamic Displacement, and Static Force vs Displacement (For SPT Sampler at St. Mary 65 ft or 19.8 m)	115
5.21 Measured and GRLWEAP Computed Dynamic Force vs Dynamic Displacement, and Static Force vs Displacement for Flat End Tip at St. Mary 105 ft or 32 m	117

LIST OF FIGURES (continued)

Volume I: Final Report

Figure

Page

5.22	Measured and GRLWEAP Computed Dynamic Force vs Dynamic Displacement, and Static Force vs Displacement for Flat End Tip at White City 35 ft or 10.7 m	118
6.1	Driveability Graphs for St. Mary, Cleveland, OH	144
6.2	Driveability Graphs for Fore River Bridge, Portland, ME	144
6.3	Driveability Graphs for C&D Canal, Pier 17, DE	144
6.4	Driveability Graphs for C&D Canal, Pier 21, DE	144
6.5	Driveability Graphs for White City Bridge, TP3, FL	150
6.6	Driveability Graphs for Apalachicola Bridge, FL	150
6.7	Bearing Graphs for St. Mary, Cleveland, OH	158
6.8	Bearing Graphs for Fore River Bridge, Portland, ME	158
6.9	Bearing Graphs for C&D Canal, Pier 17, DE	158
6.10	Bearing Graphs for C&D Canal, Pier 21, DE	158
6.11	Bearing Graphs for White City Bridge, TP3, FL	159
6.12	Bearing Graphs for Apalachicola Bridge, FL	159
6.13	Effects of Toe Quake Variations on GRLWEAP Calculated Top Quantities	163
6.14	Effects of Toe Quake on GRLWEAP Calculated Bottom Quantities	163
6.15	Effects of Hyperbolic Factor F1 on GRLWEAP Calculated Top Quantities	164
6.16	Effects of Hyperbolic Factor F1 on GRLWEAP Calculated Bottom Quantities	164
6.17	Effects of Toe Damping on GRLWEAP Calculated Top Quantities	165
6.18	Effects of Toe Damping on GRLWEAP Calculated Bottom Quantities	165
6.19	Effects of Toe Gap on GRLWEAP Calculated Top Quantities	166
6.20	Effects of Toe Gap on GRLWEAP Calculated Bottom Quantities	166
6.21	Effects of Toe Unloading Quake on GRLWEAP Calculated Top Quantities	167
6.22	Effects of Toe Unloading Quake on GRLWEAP Calculated Bottom Quantities	167
7.1	Bearing Graph for Aucilla River Bridge, FL from Various Analysis Methods	192
7.2	Bearing Graph for Vilano Bridge - East, FL from Various Analysis Methods	193
7.3	Bearing Graph for Vilano Bridge - West, FL from Various Analysis Methods	194
7.4	Driveability Graph for Aucilla River Bridge, FL from Various Analysis Methods	195
7.5	Driveability Graph for Vilano Bridge - East, FL from Various Analysis Methods	196
7.6	Driveability Graph for Vilano Bridge - West, FL from Various Analysis Methods	197

LIST OF FIGURES (continued)

Volume II: Appendixes

<u>Figure</u>	<u>Page</u>
A.1	Bearing Graph STD-ST Analysis for St. Mary, OH 6
A.2	Bearing Graph SPT-ST Analysis for St. Mary, OH 7
A.3	Bearing Graph SPT-DYN Analysis for St. Mary, OH 8
A.4	Bearing Graph MDF-ST Analysis for St. Mary, OH 9
A.5	Bearing Graph STD-ST Analysis for Portland, ME 10
A.6	Bearing Graph SPT-ST Analysis for Portland, ME 11
A.7	Bearing Graph SPT-DYN Analysis for Portland, ME 12
A.8	Bearing Graph MDF-ST Analysis for Portland, ME 13
A.9	Bearing Graph MDF-Cap-STD Analysis for Portland, ME 14
A.10	Bearing Graph MDF-Cap-SPT Analysis for Portland, ME 15
A.11	Bearing Graph STD-ST C&D Canal, Pier 17, DE 16
A.12	Bearing Graph SPT-ST C&D Canal, Pier 17, DE 17
A.13	Bearing Graph SPT-DYN C&D Canal, Pier 17, DE 18
A.14	Bearing Graph MDF-ST C&D Canal, Pier 17, DE 19
A.15	Bearing Graph MDF-Cap-STD C&D Canal, Pier 17, DE 20
A.16	Bearing Graph MDF-Cap-SPT C&D Canal, Pier 17, DE 21
A.17	Bearing Graph STD-ST, C&D Canal, Pier 21, DE 22
A.18	Bearing Graph SPT-ST, C&D Canal, Pier 21, DE 23
A.19	Bearing Graph SPT-DYN, C&D Canal, Pier 21, DE 24
A.20	Bearing Graph MDF-ST, C&D Canal, Pier 21, DE 25
A.21	Bearing Graph MDF-Cap-STD, C&D Canal, Pier 21, DE 26
A.22	Bearing Graph MDF-Cap-SPT, C&D Canal, Pier 21, DE 27
A.23	Bearing Graph STD-ST, White City Bridge, FL 28
A.24	Bearing Graph SPT-ST, White City Bridge, FL 29
A.25	Bearing Graph SPT-DYN, White City Bridge, FL 30
A.26	Bearing Graph STD-ST, Apalachicola, FL 31
A.27	Bearing Graph SPT-ST, Apalachicola, FL 32
A.28	Bearing Graph SPT-DYN, Apalachicola, FL 33
A.29	Bearing Graph MDF-ST, Apalachicola, FL 34
A.30	Bearing Graph MDF-Cap-STD, Apalachicola, FL 35
A.31	Bearing Graph MDF-Cap-SPT, Apalachicola, FL 36
A.32	Bearing Graph STD-ST Analysis for Aucilla, FL 37
A.33	Bearing Graph STD-DYN Analysis for Aucilla, FL 38
A.34	Bearing Graph SPT-ST Analysis for Aucilla, FL 39
A.35	Bearing Graph SPT-DYN Analysis for Aucilla, FL 40
A.36	Bearing Graph MDF-ST Analysis for Aucilla, FL 41
A.37	Bearing Graph MDF-DYN Analysis for Aucilla, FL 42
A.38	Bearing Graph STD (FHWA) Analysis for Aucilla, FL 43
A.39	Bearing Graph STD-ST Analysis for Vilano - East, FL 44
A.40	Bearing Graph STD-DYN Analysis for Vilano - East, FL 45
A.41	Bearing Graph SPT-ST Analysis for Vilano - East, FL 46
A.42	Bearing Graph SPT-DYN Analysis for Vilano - East, FL 47
A.43	Bearing Graph MDF-ST Analysis for Vilano - East, FL 48

LIST OF FIGURES (continued)

Volume II: Appendixes

<u>Figure</u>	<u>Page</u>
A.44	Bearing Graph MDF-DYN Analysis for Vilano - East, FL 49
A.45	Bearing Graph STD (FHWA) Analysis for Vilano - East, FL 50
A.46	Bearing Graph STD-ST Analysis for Vilano - West, FL 51
A.47	Bearing Graph STD-DYN Analysis for Vilano - West, FL 52
A.48	Bearing Graph SPT-ST Analysis for Vilano - West, FL 53
A.49	Bearing Graph SPT-DYN Analysis for Vilano - West, FL 54
A.50	Bearing Graph MDF-ST Analysis for Vilano - West, FL 55
A.51	Bearing Graph MDF-DYN Analysis for Vilano - West, FL 56
A.52	Bearing Graph STD (FHWA) Analysis for Vilano - West, FL 57
A.53	Driveability Graph STD-ST Analysis for St. Mary, OH 58
A.54	Driveability Graph SPT-ST Analysis for St. Mary, OH 59
A.55	Driveability Graph SPT-DYN Analysis for St. Mary, OH 60
A.56	Driveability Graph MDF-ST Analysis for St. Mary, OH 61
A.57	Driveability Graph STD-ST Analysis for Portland, ME 62
A.58	Driveability Graph SPT-ST Analysis for Portland, ME 63
A.59	Driveability Graph SPT-DYN Analysis for Portland, ME 64
A.60	Driveability Graph STD-ST Analysis for Portland, ME 65
A.61	Driveability Graph MDF-Cap-STD Analysis for Portland, ME 66
A.62	Driveability Graph MDF-Cap-SPT Analysis for Portland, ME 67
A.63	Driveability Graph STD-ST Analysis for C&D Canal, Pier 17, DE 68
A.64	Driveability Graph SPT-ST Analysis for C&D Canal, Pier 17, DE 69
A.65	Driveability Graph SPT-DYN Analysis for C&D Canal, Pier 17, DE 70
A.66	Driveability Graph MDF-ST Analysis for C&D Canal, Pier 17, DE 71
A.67	Driveability Graph MDF-Cap-STD Analysis for C&D Canal, Pier 17, DE 72
A.68	Driveability Graph MDF-Cap-SPT Analysis for C&D Canal, Pier 17, DE 73
A.69	Driveability Graph STD-ST Analysis for C&D Canal, Pier 21, DE 74
A.70	Driveability Graph SPT-ST Analysis for C&D Canal, Pier 21, DE 75
A.71	Driveability Graph SPT-DYN Analysis for C&D Canal, Pier 21, DE 76
A.72	Driveability Graph MDF-ST Analysis for C&D Canal, Pier 21, DE 77
A.73	Driveability Graph MDF-Cap-STD Analysis for C&D Canal, Pier 21, DE 78
A.74	Driveability Graph MDF-Cap-SPT Analysis for C&D Canal, Pier 21, DE 79
A.75	Driveability Graph STD-ST Analysis for White City Bridge, FL 80
A.76	Driveability Graph SPT-ST Analysis for White City Bridge, FL 81
A.77	Driveability Graph SPT-DYN Analysis for White City Bridge, FL 82
A.78	Driveability Graph STD-ST Analysis for Apalachicola, FL 83
A.79	Driveability Graph SPT-ST Analysis for Apalachicola, FL 84
A.80	Driveability Graph SPT-DYN Analysis for Apalachicola, FL 85
A.81	Driveability Graph MDF-ST Analysis for Apalachicola, FL 86
A.82	Driveability Graph MDF-Cap-STD Analysis for Apalachicola, FL 87
A.83	Driveability Graph MDF-Cap-SPT Analysis for Apalachicola, FL 88
A.84	Driveability Graph STD-ST Analysis for Aucilla, FL 89
A.85	Driveability Graph STD-DYN Analysis for Aucilla, FL 90
A.86	Driveability Graph SPT-ST Analysis for Aucilla, FL 91

LIST OF FIGURES (continued)

Volume II: Appendixes

<u>Figure</u>	<u>Page</u>
A.87	Driveability Graph STD-DYN Analysis for Aucilla, FL 92
A.88	Driveability Graph MDF-ST Analysis for Aucilla, FL 93
A.89	Driveability Graph MDF-DYN Analysis for Aucilla, FL 94
A.90	Driveability Graph STD (FHWA) Analysis for Aucilla, FL 95
A.91	Driveability Graph STD-ST Analysis for Vilano - East, FL 96
A.92	Driveability Graph STD-DYN Analysis for Vilano - East, FL 97
A.93	Driveability Graph SPT-ST Analysis for Vilano - East, FL 98
A.94	Driveability Graph SPT-DYN Analysis for Vilano - East, FL 99
A.95	Driveability Graph MDF-ST Analysis for Vilano - East, FL 100
A.96	Driveability Graph MDF-DYN Analysis for Vilano - East, FL 101
A.97	Driveability Graph STD (FHWA) Analysis for Vilano - East, FL 102
A.98	Driveability Graph STD-ST Analysis for Vilano - West, FL 103
A.99	Driveability Graph STD-DYN Analysis for Vilano - West, FL 104
A.100	Driveability Graph SPT-ST Analysis for Vilano - West, FL 105
A.101	Driveability Graph SPT-DYN Analysis for Vilano - West, FL 106
A.102	Driveability Graph MDF-ST Analysis for Vilano - West, FL 107
A.103	Driveability Graph MDF-DYN Analysis for Vilano - West, FL 108
A.104	Driveability Graph STD (FHWA) Analysis for Vilano - West, FL 109
B.1	Load versus Displacement for St. Mary, Cleveland, OH at depth of 40 ft . . . 116
B.2	Load versus Displacement for St. Mary, Cleveland, OH at depth of 65 ft . . . 116
B.3	Load versus Displacement for St. Mary, Cleveland, OH at depth of 100 ft . . . 116
B.4	Load versus Displacement for St. Mary, Cleveland, OH at depth of 100 ft (15 h) 116
B.5	Load versus Displacement for St. Mary, Cleveland, OH at depth of 103.5 ft . . 117
B.6	Load versus Displacement for St. Mary, Cleveland, OH at depth of 105 ft . . . 117
B.7	Load versus Displacement for Fore River Bridge, Portland, ME at depth of 42 ft 117
B.8	Load versus Displacement for Fore River Bridge, Portland, ME at depth of 54 ft 117
B.9	Load versus Displacement for Fore River Bridge, Portland, ME at depth of 56 ft 118
B.10	Load versus Displacement for C&D Canal, Pier 17, DE at depth of 14 ft 118
B.11	Load versus Displacement for C&D Canal, Pier 17, DE at depth of 50 ft 118
B.12	Load versus Displacement for C&D Canal, Pier 17, DE at depth of 55 ft 118
B.13	Load versus Displacement for C&D Canal, Pier 17, DE at depth of 55 ft (1 h) 119
B.14	Load versus Displacement for C&D Canal, Pier 17, DE at depth of 55 ft (14 h) 119
B.15	Load versus Displacement for C&D Canal, Pier 17, DE at depth of 60 ft 119
B.16	Load versus Displacement for C&D Canal, Pier 17, DE at depth of 60 ft (1 h) 119
B.17	Load versus Displacement for C&D Canal, Pier 17, DE at depth of 65 ft 120

LIST OF FIGURES (continued)

Volume II: Appendixes

<u>Figure</u>	<u>Page</u>	
B.18	Load versus Displacement for C&D Canal, Pier 17, DE at depth of 65 ft (2 h)	120
B.19	Load versus Displacement for C&D Canal, Pier 17, DE at depth of 70 ft	120
B.20	Load versus Displacement for C&D Canal, Pier 21, DE at depth of 40 ft	120
B.21	Load versus Displacement for C&D Canal, Pier 21, DE at depth of 40 ft (1 h)	121
B.22	Load versus Displacement for C&D Canal, Pier 21, DE at depth of 55 ft	121
B.23	Load versus Displacement for C&D Canal, Pier 21, DE at depth of 55 ft (1 h)	121
B.24	Load versus Displacement for C&D Canal, Pier 21, DE at depth of 65 ft	121
B.25	Load versus Displacement for C&D Canal, Pier 21, DE at depth of 70 ft	122
B.26	Load versus Displacement for C&D Canal, Pier 21, DE at depth of 71 ft	122
B.27	Load versus Displacement for White City Bridge, TP3, FL at depth of 32 ft . .	122
B.28	Load versus Displacement for White City Bridge, TP3, FL at depth of 35 ft . .	122
B.29	Load versus Displacement for Apalachicola River Bridge, FL at depth of 55 ft	123
B.30	Load versus Displacement for Apalachicola, FL at depth of 55 ft (15 min & 1 h)	123
B.31	Load versus Displacement for Apalachicola River Bridge, FL at depth of 75 ft	123
B.32	Load versus Displacement for Apalachicola, FL at depth of 75 ft (15 min & 1 h)	123
B.33	Load versus Displacement for Apalachicola River Bridge, FL at depth of 89 ft	124
B.34	Load versus Displacement for Sunshine Skyway Bridge, FL at depth of 45 ft	124
B.35	Load versus Displacement for Sunshine Skyway Bridge, FL at depth of 45.5 ft	124
B.36	Load versus Displacement for Sunshine Skyway Bridge, FL at depth of 50 ft	124
B.37	Load versus Displacement for Sunshine Skyway Bridge, FL at depth of 53 ft	125
B.38	Load versus Displacement for Aucilla River Bridge, FL at depth of 10 ft	125
B.39	Load versus Displacement for Aucilla River Bridge, FL at depth of 20 ft	125
B.40	Load versus Displacement for Aucilla River Bridge, FL at depth of 30 ft	125
B.41	Load versus Displacement for Aucilla River Bridge, FL at depth of 42 ft	126
B.42	Load versus Displacement for Aucilla River Bridge, FL at depth of 45 ft	126
B.43	Load versus Displacement for Aucilla River Bridge, FL at depth of 63 ft	126
B.44	Load versus Displacement for Aucilla River Bridge, FL at depth of 67.5 ft . . .	126
B.45	Load versus Displacement for Vilano Bridge - East, FL at depth of 15 ft	127
B.46	Load versus Displacement for Vilano Bridge - East, FL at depth of 20 ft	127
B.47	Load versus Displacement for Vilano Bridge - East, FL at depth of 25 ft	127

LIST OF FIGURES (continued)

Volume II: Appendixes

<u>Figure</u>	<u>Page</u>	
B.48	Load versus Displacement for Vilano Bridge - East, FL at depth of 30 ft (Compression)	127
B.49	Load versus Displacement for Vilano Bridge - East, FL at depth of 30 ft (Uplift)	128
B.50	Load versus Displacement for Vilano Bridge - East, FL at depth of 35 ft	128
B.51	Load versus Displacement for Vilano Bridge - East, FL at depth of 40 ft	128
B.52	Load versus Displacement for Vilano Bridge - West, FL at depth of 30 ft	128
B.53	Load versus Displacement for Vilano Bridge - West, FL at depth of 35 ft	129
B.54	Load versus Displacement for Vilano Bridge - West, FL at depth of 45 ft	129
B.55	Load versus Displacement for Vilano Bridge - West, FL at depth of 50 ft	129
B.56	Load versus Displacement for Vilano Bridge - West, FL at depth of 52 ft	129
B.57	Load versus Displacement for Vilano Bridge - West, FL at depth of 55 ft	130
B.58	Load versus Displacement for Vilano Bridge - West, FL at depth of 59 ft	130
B.59	Load versus Displacement for Vilano Bridge - West, FL at depth of 62 ft	130
B.60	Load versus Displacement for Vilano Bridge - West, FL at depth of 67 ft	130
C.1	Torque versus Rotation for Apalachicola River Bridge, FL at depth of 55 ft	133
C.2	Torque versus Rotation for Apalachicola River Bridge, FL at depth of 75 ft	133
C.3	Torque versus Rotation for Sunshine Skyway Bridge, FL at depth of 45.5 ft	133
C.4	Torque versus Rotation for Sunshine Skyway Bridge, FL at depth of 50 ft	133
C.5	Torque versus Rotation for Aucilla River Bridge, FL at depth of 10 ft	134
C.6	Torque versus Rotation for Aucilla River Bridge, FL at depth of 20 ft	134
C.7	Torque versus Rotation for Aucilla River Bridge, FL at depth of 30 ft	134
C.8	Torque versus Rotation for Aucilla River Bridge, FL at depth of 45 ft	134
C.9	Torque versus Rotation for Vilano Bridge - East, FL at depth of 30 ft	135
C.10	Torque versus Rotation for Vilano Bridge - West, FL at depth of 30 ft	135
C.11	Torque versus Rotation for Vilano Bridge - West, FL at depth of 35 ft	135
C.12	Torque versus Rotation for Vilano Bridge - West, FL at depth of 45 ft	135
C.13	Torque versus Rotation for Vilano Bridge - West, FL at depth of 50 ft	136
C.14	Torque versus Rotation for Vilano Bridge - West, FL at depth of 55 ft	136
C.15	Torque versus Rotation for Vilano Bridge - West, FL at depth of 59 ft	136
D.1a	Top F-V Time History for St. Mary, Cleveland, OH at depth of 40 ft	142
D.1b	Bottom F-V Time History for St. Mary, Cleveland, OH at depth of 40 ft	142
D.1c	Bottom Force Time History (Static) for St. Mary, Cleveland, OH at depth of 40 ft	142
D.1d	Bottom Force Time History (Dynamic) for St. Mary, Cleveland, OH at depth of 40 ft	142
D.2a	Top F-V Time History for St. Mary, Cleveland, OH at depth of 65 ft	143
D.2b	Bottom F-V Time History for St. Mary, Cleveland, OH at depth of 65 ft	143
D.2c	Bottom Force Time History (Static) for St. Mary, Cleveland, OH at depth of 65 ft	143
D.2d	Bottom Force Time (Dynamic) History for St. Mary, Cleveland at depth of 65 ft	143
D.3a	Top F-V Time History for St. Mary, Cleveland, OH at depth of 65 ft (25 min)	144

LIST OF FIGURES (continued)

Volume II: Appendixes

<u>Figure</u>	<u>Page</u>	
D.3b	Bottom F-V Time History for St. Mary, Cleveland, OH at depth of 65 ft (25 min)	144
D.4a	Top F-V Time History for St. Mary, Cleveland, OH at depth of 65 ft (2 h)	145
D.4b	Bottom F-V Time History for St. Mary, Cleveland, OH at depth of 65 ft (2 h) . .	145
D.4c	Bottom Force Time History (Static) for St. Mary, OH at depth of 65 ft (2 h) . .	145
D.4d	Bottom Force Time History (Dynamic) for St. Mary, at depth of 65 ft (2 h) . . .	145
D.5a	Top F-V Time History for St. Mary, Cleveland, OH at depth of 100 ft	146
D.5b	Bottom F-V Time History for St. Mary, Cleveland, OH at depth of 100 ft	146
D.5c	Bottom Force Time History (Static) for St. Mary, Cleveland at depth of 100 ft	146
D.5d	Bottom Force Time History (Dynamic) for St. Mary, Cleveland at depth of 100 ft	146
D.6a	Top F-V Time History for St. Mary, Cleveland, OH at depth of 100 ft (15 h) . .	147
D.6b	Bottom F-V Time History for St. Mary, Cleveland, OH at depth of 100 ft (15 h)	147
D.6c	Bottom Force Time History (Static) for St. Mary, OH at depth of 100 ft (15 h)	147
D.6d	Bottom Force Time History (Dynamic) for St. Mary, OH at depth of 100 ft (15 h)	147
D.7a	Top F-V Time History for St. Mary, Cleveland, OH at depth of 103.5 ft	148
D.7b	Bottom F-V Time History for St. Mary, Cleveland, OH at depth of 103.5 ft . . .	148
D.7c	Bottom Force Time History (Static) for St. Mary, OH at depth of 103.5 ft	148
D.7d	Bottom Force Time History (Dynamic) for St. Mary, OH at depth of 103.5 ft . .	148
D.8a	Top F-V Time History for St. Mary, Cleveland, OH at depth of 105 ft	149
D.8b	Bottom F-V Time History for St. Mary, Cleveland, OH at depth of 105 ft	149
D.8c	Bottom Force Time History (Static) for St. Mary, Cleveland at depth of 105 ft	149
D.8d	Bottom Force Time History (Dynamic) for St. Mary, Cleveland at depth of 105 ft	149
D.9a	Top F-V Time History for Fore River Bridge, Portland, ME at depth of 20 ft . .	150
D.9b	Bottom F-V Time History for Fore River Bridge, Portland, ME at depth of 20 ft	150
D.9c	Bottom Force Time History (Dynamic) for Fore River Bridge at depth of 20 ft	150
D.10a	Top F-V Time History for Fore River Bridge, Portland, ME at depth of 30 ft . .	151
D.10b	Bottom F-V Time History for Fore River Bridge, Portland, ME at depth of 30 ft	151
D.10c	Bottom Force Time History (Dynamic) for Fore River Bridge at depth of 30 ft	151
D.11a	Top F-V Time History for Fore River Bridge, Portland, ME at depth of 40 ft . .	152
D.11b	Bottom F-V Time History for Fore River Bridge, Portland, ME at depth of 40 ft	152

LIST OF FIGURES (continued)

Volume II: Appendixes

<u>Figure</u>	<u>Page</u>
D.11c	152
D.12a	153
D.12b	153
D.12c	153
D.12d	153
D.13a	154
D.13b	154
D.13c	154
D.13d	154
D.14a	155
D.14b	155
D.14c	155
D.14d	155
D.15a	156
D.15b	156
D.15c	156
D.15d	156
D.16a	157
D.16b	157
D.17a	158
D.17b	158
D.18a	159
D.18b	159
D.18c	159
D.18d	159
D.19a	160
D.19b	160
D.20a	161
D.20b	161
D.20c	161

LIST OF FIGURES (continued)

Volume II: Appendixes

<u>Figure</u>	<u>Page</u>
D.20d	161
Bottom Force Time History (Dynamic) for C&D Pier 17 at depth of 55 ft (14 h)	
D.21a	162
Top F-V Time History for C&D Canal, Pier 17, DE at depth of 60 ft	
D.21b	162
Bottom F-V Time History for C&D Canal, Pier 17, DE at depth of 60 ft	
D.21c	162
Bottom Force Time History (Static) for C&D Canal, Pier 17 at depth of 60 ft	
D.21d	162
Bottom Force Time History (Dynamic) for C&D Canal, Pier 17 at depth of 60 ft	
D.22a	163
Top F-V Time History for C&D Canal, Pier 17, DE at depth of 60 ft (1 h)	
D.22b	163
Bottom F-V Time History for C&D Canal, Pier 17, DE at depth of 60 ft (1 h)	
D.22c	163
Bottom Force Time History (Static) for C&D Canal, Pier 17 at depth of 60 ft (1 h)	
D.22d	163
Bottom Force Time History (Dynamic) for C&D Canal, Pier 17 at depth of 60 ft (1 h)	
D.23a	164
Top F-V Time History for C&D Canal, Pier 17, DE at depth of 65 ft	
D.23b	164
Bottom F-V Time History for C&D Canal, Pier 17, DE at depth of 65 ft	
D.23c	164
Bottom Force Time History (Static) for C&D Canal, Pier 17 at depth of 65 ft	
D.23d	164
Bottom Force Time History (Dynamic) for C&D Canal, Pier 17 at depth of 65 ft	
D.24a	165
Top F-V Time History for C&D Canal, Pier 17, DE at depth of 65 ft (2 h)	
D.24b	165
Bottom F-V Time History for C&D Canal, Pier 17, DE at depth of 65 ft (2 h)	
D.24c	165
Bottom Force Time History (Static) for C&D Canal, Pier 17 at depth of 65 ft (2 h)	
D.24d	165
Bottom Force Time History (Dynamic) for C&D Canal, Pier 17 at depth of 65 ft (2 h)	
D.25a	166
Top F-V Time History for C&D Canal, Pier 17, DE at depth of 70 ft	
D.25b	166
Bottom F-V Time History for C&D Canal, Pier 17, DE at depth of 70 ft	
D.25c	166
Bottom Force Time History (Static) for C&D Canal, Pier 17 at depth of 70 ft	
D.25d	166
Bottom Force Time History (Dynamic) for C&D Canal, Pier 17 at depth of 70 ft	
D.26a	167
Top F-V Time History for C&D Canal, Pier 21, DE at depth of 40 ft	
D.26b	167
Bottom F-V Time History for C&D Canal, Pier 21, DE at depth of 40 ft	
D.26c	167
Bottom Force Time History (Static) for C&D Canal, Pier 21 at depth of 40 ft	
D.27a	168
Top F-V Time History for C&D Canal, Pier 21, DE at depth of 40 ft (1 h)	
D.27b	168
Bottom F-V Time History for C&D Canal, Pier 21, DE at depth of 40 ft (1 h)	
D.28a	169
Top F-V Time History for C&D Canal, Pier 21, DE at depth of 55 ft	
D.28b	169
Bottom F-V Time History for C&D Canal, Pier 21, DE at depth of 55 ft	
D.28c	169
Bottom Force Time History (Static) for C&D Canal, Pier 21 at depth of 55 ft	
D.28d	169
Bottom Force Time History (Dynamic) for C&D Canal, Pier 21 at depth of 55 ft	
D.29a	170
Top F-V Time History for C&D Canal, Pier 21, DE at depth of 55 ft (1 h)	
D.29b	170
Bottom F-V Time History for C&D Canal, Pier 21, DE at depth of 55 ft (1 h)	
D.29c	170
Bottom Force Time History (Static) for C&D Canal, Pier 21 at depth of 55 ft (1 h)	

LIST OF FIGURES (continued)

Volume II: Appendixes

<u>Figure</u>	<u>Page</u>
D.29d	Bottom Force Time History (Dynamic) for C&D Canal, Pier 21 at depth of 55 ft (1 h) 170
D.30a	Top F-V Time History for C&D Canal, Pier 21, DE at depth of 65 ft 171
D.30b	Bottom F-V Time History for C&D Canal, Pier 21, DE at depth of 65 ft 171
D.30c	Bottom Force Time History (Static) for C&D Canal, Pier 21 at depth of 65 ft 171
D.30d	Bottom Force Time History (Dynamic) for C&D Canal, Pier 21 depth of 65 ft 171
D.31a	Top F-V Time History for C&D Canal, Pier 21, DE at depth of 70 ft 172
D.31b	Bottom F-V Time History for C&D Canal, Pier 21, DE at depth of 70 ft 172
D.32a	Top F-V Time History for C&D Canal, Pier 21, DE at depth of 71 ft 173
D.32b	Bottom F-V Time History for C&D Canal, Pier 21, DE at depth of 71 ft 173
D.32c	Bottom Force Time History (Static) for C&D Canal, Pier 21 at depth of 71 ft 173
D.32d	Bottom Force Time History (Dynamic) for C&D Canal, Pier 21 at depth of 71 ft 173
D.33a	Top F-V Time History for White City Bridge, TP3, FL at depth of 20 ft 174
D.33b	Bottom F-V Time History for White City Bridge, TP3, FL at depth of 20 ft 174
D.34a	Top F-V Time History for White City Bridge, TP3, FL at depth of 29 ft 175
D.34b	Bottom F-V Time History for White City Bridge, TP3, FL at depth of 29 ft 175
D.34c	Bottom Force Time History (Dynamic) for White City Bridge, TP3, FL at depth of 29 ft 175
D.35a	Top F-V Time History for White City Bridge, TP3, FL at depth of 31 ft 176
D.35b	Bottom F-V Time History for White City Bridge, TP3, FL at depth of 31 ft 176
D.36a	Top F-V Time History for White City Bridge, TP3, FL at depth of 32 ft 177
D.36b	Bottom F-V Time History for White City Bridge, TP3, FL at depth of 32 ft 177
D.36c	Bottom Force Time History (Static) for White City Bridge at depth of 32 ft 177
D.36d	Bottom Force Time History (Dynamic) for White City Bridge at depth of 32 ft 177
D.37a	Top F-V Time History for White City Bridge, TP3, FL at depth of 35 ft 178
D.37b	Bottom F-V Time History for White City Bridge, TP3, FL at depth of 35 ft 178
D.37c	Bottom Force Time History (Static) for White City Bridge at depth of 35 ft 178
D.37d	Bottom Force Time History (Dynamic) for White City Bridge at depth of 35 ft 178
D.38a	Top F-V Time History for White City Bridge, TP6, FL at depth of 16 ft 179
D.38b	Bottom F-V Time History for White City Bridge, TP6, FL at depth of 16 ft 179
D.39a	Top F-V Time History for White City Bridge, TP6, FL at depth of 32 ft 180
D.39b	Bottom F-V Time History for White City Bridge, TP6, FL at depth of 32 ft 180
D.39c	Bottom Force Time History (Dynamic) for White City Bridge, TP6, FL at depth of 32 ft 180
D.40a	Top F-V Time History for White City Bridge, TP6, FL at depth of 33 ft 181
D.40b	Bottom F-V Time History for White City Bridge, TP6, FL at depth of 33 ft 181
D.41a	Top F-V Time History for Apalachicola River Bridge, FL at depth of 20 ft 182
D.41b	Bottom F-V Time History for Apalachicola River Bridge, FL at depth of 20 ft 182
D.42a	Top F-V Time History for Apalachicola River Bridge, FL at depth of 25 ft 183
D.42b	Bottom F-V Time History for Apalachicola River Bridge, FL at depth of 25 ft 183

LIST OF FIGURES (continued)

Volume II: Appendixes

<u>Figure</u>	<u>Page</u>
D.42c Bottom Force Time History (Dynamic) for Apalachicola River Bridge, FL at depth of 25 ft	183
D.43a Top F-V Time History for Apalachicola River Bridge, FL at depth of 25 ft (14 h)	184
D.43b Bottom F-V Time History for Apalachicola River Bridge, FL at depth of 25 ft (14 h)	184
D.43c Bottom Force Time History (Static) for Apalachicola, FL at depth of 25 ft (14 h)	184
D.44a Top F-V Time History for Apalachicola River Bridge at depth of 55 ft	185
D.44b Bottom F-V Time History for Apalachicola River Bridge, FL at depth of 55 ft .	185
D.44c Bottom Force Time History (Static) for Apalachicola, FL at depth of 55 ft . . .	185
D.44d Bottom Force Time History (Dynamic) for Apalachicola, FL at depth of 55 ft	185
D.45a Top F-V Time History for Apalachicola River Bridge, FL at depth of 55 ft (1 h)	186
D.45b Bottom F-V Time History for Apalachicola, FL at depth of 55 ft (1 h)	186
D.45c Bottom Force Time History (Static) for Apalachicola, FL at depth of 55 ft (1 h)	186
D.45d Bottom Force Time History (Dynamic) for Apalachicola at depth of 55 ft (1 h)	186
D.46a Top F-V Time History for Apalachicola River Bridge, FL at depth of 75 ft	187
D.46b Bottom F-V Time History for Apalachicola River Bridge, FL at depth of 75 ft .	187
D.46c Bottom Force Time History (Static) for Apalachicola River at depth of 75 ft . .	187
D.46d Bottom Force Time History (Dynamic) for Apalachicola River at depth of 75 ft	187
D.47a Top F-V Time History for Apalachicola River Bridge, FL at depth of 75 ft (1 h)	188
D.47b Bottom F-V Time History for Apalachicola, FL at depth of 75 ft (1 h)	188
D.47c Bottom Force Time History (Static) for Apalachicola, FL at depth of 75 ft (1 h)	188
D.47d Bottom Force Time History (Dynamic) for Apalachicola, FL at depth of 75 ft (1 h)	188
D.48a Top F-V Time History for Apalachicola River Bridge, FL at depth of 89 ft	189
D.48b Bottom F-V Time History for Apalachicola River Bridge, FL at depth of 89 ft .	189
D.48c Bottom Force Time History (Static) for Apalachicola River at depth of 89 ft . .	189
D.48d Bottom Force Time History (Dynamic) for Apalachicola River at depth of 89 ft	189
D.49a Top F-V Time History for Aucilla River Bridge, FL at depth of 5 ft	190
D.49b Bottom F-V Time History for Aucilla River Bridge, FL at depth of 5 ft	190
D.49c Bottom Force Time History (Dynamic) for Aucilla River, FL at depth of 5 ft . .	190
D.50a Top F-V Time History for Aucilla River Bridge, FL at depth of 10 ft	191
D.50b Bottom F-V Time History for Aucilla River Bridge, FL at depth of 10 ft	191
D.50c Bottom Force Time History (Static) for Aucilla River, FL at depth of 10 ft	191

LIST OF FIGURES (continued)

Volume II: Appendixes

<u>Figure</u>	<u>Page</u>
D.50d	Bottom Force Time History (Dynamic) for Aucilla River, FL at depth of 10 ft 191
D.51a	Top F-V Time History for Aucilla River Bridge, FL at depth of 15 ft 192
D.51b	Bottom F-V Time History for Aucilla River Bridge, FL at depth of 15 ft 192
D.51c	Bottom Force Time History (Dynamic) for Aucilla River, FL at depth of 15 ft 192
D.52a	Top F-V Time History for Aucilla River Bridge, FL at depth of 20 ft 193
D.52b	Bottom F-V Time History for Aucilla River Bridge, FL at depth of 20 ft 193
D.52c	Bottom Force Time History (Static) for Aucilla River, FL at depth of 20 ft 193
D.52d	Bottom Force Time History (Dynamic) for Aucilla River, FL at depth of 20 ft 193
D.53a	Top F-V Time History for Aucilla River Bridge, FL at depth of 20 ft (1 h) 194
D.53b	Bottom F-V Time History for Aucilla River Bridge, FL at depth of 20 ft (1 h) 194
D.53c	Bottom Force Time History (Static) for Aucilla River, FL at depth of 20 ft (1 h) 194
D.53d	Bottom Force Time History (Dynamic) for Aucilla River at depth of 20 ft (1 h) 194
D.54a	Top F-V Time History for Aucilla River Bridge, FL at depth of 25 ft 195
D.54b	Bottom F-V Time History for Aucilla River Bridge, FL at depth of 25 ft 195
D.54c	Bottom Force Time History (Dynamic) for Aucilla River, FL at depth of 25 ft 195
D.55a	Top F-V Time History for Aucilla River Bridge, FL at depth of 30 ft 196
D.55b	Bottom F-V Time History for Aucilla River Bridge, FL at depth of 30 ft 196
D.55c	Bottom Force Time History (Static) for Aucilla River, FL at depth of 30 ft 196
D.55d	Bottom Force Time History (Dynamic) for Aucilla River, FL at depth of 30 ft 196
D.56a	Top F-V Time History for Aucilla River Bridge, FL at depth of 30 ft (11 h) 197
D.56b	Bottom F-V Time History for Aucilla River Bridge, FL at depth of 30 ft (11 h) 197
D.56c	Bottom Force Time History (Static) for Aucilla River, FL at depth of 30 ft (11 h) 197
D.56d	Bottom Force Time History (Dynamic) for Aucilla, FL at depth of 30 ft (11 h) 197
D.57a	Top F-V Time History for Aucilla River Bridge, FL at depth of 35 ft 198
D.57b	Bottom F-V Time History for Aucilla River Bridge, FL at depth of 35 ft 198
D.57c	Bottom Force Time History (Dynamic) for Aucilla River, FL at depth of 35 ft 198
D.58a	Top F-V Time History for Aucilla River Bridge, FL at depth of 40 ft 199
D.58b	Bottom F-V Time History for Aucilla River Bridge, FL at depth of 40 ft 199
D.58c	Bottom Force Time History (Dynamic) for Aucilla River, FL at depth of 40 ft 199
D.59a	Top F-V Time History for Aucilla River Bridge, FL at depth of 42 ft 200
D.59b	Bottom F-V Time History for Aucilla River Bridge, FL at depth of 42 ft 200
D.59c	Bottom Force Time History (Static) for Aucilla River, FL at depth of 42 ft 200
D.59d	Bottom Force Time History (Dynamic) for Aucilla River, FL at depth of 42 ft 200
D.60a	Top F-V Time History for Aucilla River Bridge, FL at depth of 45 ft 201
D.60b	Bottom F-V Time History for Aucilla River Bridge, FL at depth of 45 ft 201
D.60c	Bottom Force Time History (Static) for Aucilla River, FL at depth of 45 ft 201
D.60d	Bottom Force Time History (Dynamic) for Aucilla River, FL at depth of 45 ft 201
D.61a	Top F-V Time History for Aucilla River Bridge, FL at depth of 50 ft 202
D.61b	Bottom F-V Time History for Aucilla River Bridge, FL at depth of 50 ft 202
D.61c	Bottom Force Time History (Dynamic) for Aucilla River, FL at depth of 50 ft 202

LIST OF FIGURES (continued)

Volume II: Appendixes

<u>Figure</u>	<u>Page</u>
D.62a	Top F-V Time History for Aucilla River Bridge, FL at depth of 55 ft 203
D.62b	Bottom F-V Time History for Aucilla River Bridge, FL at depth of 55 ft 203
D.62c	Bottom Force Time History (Dynamic) for Aucilla River, FL at depth of 55 ft 203
D.63a	Top F-V Time History for Aucilla River Bridge, FL at depth of 60 ft 204
D.63b	Bottom F-V Time History for Aucilla River Bridge, FL at depth of 60 ft 204
D.63c	Bottom Force Time History (Dynamic) for Aucilla River, FL at depth of 60 ft 204
D.64a	Top F-V Time History for Aucilla River Bridge, FL at depth of 63 ft 205
D.64b	Bottom F-V Time History for Aucilla River Bridge, FL at depth of 63 ft 205
D.64c	Bottom Force Time History (Static) for Aucilla River, FL at depth of 63 ft 205
D.64d	Bottom Force Time History (Dynamic) for Aucilla River, FL at depth of 63 ft 205
D.65a	Top F-V Time History for Aucilla River Bridge, FL at depth of 65 ft 206
D.65b	Bottom F-V Time History for Aucilla River Bridge, FL at depth of 65 ft 206
D.65c	Bottom Force Time History (Dynamic) for Aucilla River, FL at depth of 65 ft 206
D.66a	Top F-V Time History for Aucilla River Bridge, FL at depth of 67.5 ft 207
D.66b	Bottom F-V Time History for Aucilla River Bridge, FL at depth of 67.5 ft 207
D.66c	Bottom Force Time History (Static) for Aucilla River, FL at depth of 67.5 ft 207
D.66d	Bottom Force Time History (Dynamic) for Aucilla River, FL at depth of 67.5 ft 207
D.67a	Top F-V Time History for Vilano Bridge - East, FL at depth of 10 ft 208
D.67b	Bottom F-V Time History for Vilano Bridge - East, FL at depth of 10 ft 208
D.68a	Top F-V Time History for Vilano Bridge - East, FL at depth of 15 ft (Tip) 209
D.68b	Bottom F-V Time History for Vilano Bridge - East, FL at depth of 15 ft (Tip) 209
D.68c	Bottom Force Time History (Static) for Vilano - East, FL at depth of 15 ft (Tip) 209
D.68d	Bottom Force Time History (Dynamic) for Vilano - East at depth of 15 ft (Tip) 209
D.69a	Top F-V Time History for Vilano Bridge - East, FL at depth of 15 ft 210
D.69b	Bottom F-V Time History for Vilano Bridge - East, FL at depth of 15 ft 210
D.69c	Bottom Force Time History (Dynamic) for Vilano - East, FL at depth of 15 ft 210
D.70a	Top F-V Time History for Vilano Bridge - East, FL at depth of 20 ft 211
D.70b	Bottom F-V Time History for Vilano Bridge - East, FL at depth of 20 ft 211
D.70c	Bottom Force Time History (Static) for Vilano - East, FL at depth of 20 ft 211
D.70d	Bottom Force Time History (Dynamic) for Vilano - East, FL at depth of 20 ft 211
D.71a	Top F-V Time History for Vilano Bridge - East, FL at depth of 25 ft (Tip) 212
D.71b	Bottom F-V Time History for Vilano Bridge - East, FL at depth of 25 ft (Tip) 212
D.71c	Bottom Force Time History (Static) for Vilano - East, FL at depth of 25 ft (Tip) 212
D.71d	Bottom Force Time History (Dynamic) for Vilano - East at depth of 25 ft (Tip) 212
D.72a	Top F-V Time History for Vilano Bridge - East, FL at depth of 25 ft 213
D.72b	Bottom F-V Time History for Vilano Bridge - East, FL at depth of 25 ft 213
D.72c	Bottom Force Time History (Dynamic) for Vilano - East, FL at depth of 25 ft 213
D.73a	Top F-V Time History for Vilano Bridge - East, FL at depth of 30 ft (Tip) 214

LIST OF FIGURES (continued)

Volume II: Appendixes

<u>Figure</u>	<u>Page</u>
D.73b	Bottom F-V Time History for Vilano Bridge - East, FL at depth of 30 ft (Tip) . . . 214
D.73c	Bottom Force Time History (Static) for Vilano Bridge - East, FL at depth of 30 ft (Tip) 214
D.73d	Bottom Force Time History (Dynamic) for Vilano Bridge - East, FL at depth of 30 ft (Tip) 214
D.74a	Top F-V Time History for Vilano Bridge - East, FL at depth of 30 ft 215
D.74b	Bottom F-V Time History for Vilano Bridge - East, FL at depth of 30 ft 215
D.74c	Bottom Force Time History (Static) for Vilano - East, FL at depth of 30 ft . . . 215
D.74d	Bottom Force Time History (Dynamic) for Vilano - East, FL at depth of 30 ft . 215
D.75a	Top F-V Time History for Vilano Bridge - East, FL at depth of 35 ft (Tip) 216
D.75b	Bottom F-V Time History for Vilano Bridge - East, FL at depth of 35 ft (Tip) . . 216
D.75c	Bottom Force Time History (Static) for Vilano - East, FL at depth of 35 ft (Tip) 216
D.75d	Bottom Force Time History (Dynamic) for Vilano - East at depth of 35 ft (Tip) 216
D.76a	Top F-V Time History for Vilano Bridge - East, FL at depth of 35 ft 217
D.76b	Bottom F-V Time History for Vilano Bridge - East, FL at depth of 35 ft 217
D.76c	Bottom Force Time History (Dynamic) for Vilano - East, FL at depth of 35 ft . 217
D.77a	Top F-V Time History for Vilano Bridge - East, FL at depth of 40 ft 218
D.77b	Bottom F-V Time History for Vilano Bridge - East, FL at depth of 40 ft 218
D.77c	Bottom Force Time History (Static) for Vilano - East, FL at depth of 40 ft . . . 218
D.77d	Bottom Force Time History (Dynamic) for Vilano - East, FL at depth of 40 ft . 218
D.78a	Top F-V Time History for Vilano Bridge - West, FL at depth of 30 ft 219
D.78b	Bottom F-V Time History for Vilano Bridge - West, FL at depth of 30 ft 219
D.78c	Bottom Force Time History (Static) for Vilano - West, FL at depth of 30 ft . . . 219
D.78d	Bottom Force Time History (Dynamic) for Vilano - West, FL at depth of 30 ft . 219
D.79a	Top F-V Time History for Vilano Bridge - West, FL at depth of 35 ft 220
D.79b	Bottom F-V Time History for Vilano Bridge - West, FL at depth of 35 ft 220
D.79c	Bottom Force Time History (Static) for Vilano - West, FL at depth of 35 ft . . . 220
D.79d	Bottom Force Time History (Dynamic) for Vilano - West, FL at depth of 35 ft . 220
D.80a	Top F-V Time History for Vilano Bridge - West, FL at depth of 35 ft (1 h) . . . 221
D.80b	Bottom F-V Time History for Vilano Bridge - West, FL at depth of 35 ft (1 h) . 221
D.80c	Bottom Force Time History (Static) for Vilano - West, FL at depth of 35 ft (1 h) 221
D.80d	Bottom Force Time History (Dynamic) for Vilano - West, FL at depth of 35 ft (1 h) 221
D.81a	Top F-V Time History for Vilano Bridge - West, FL at depth of 40 ft 222
D.81b	Bottom F-V Time History for Vilano Bridge - West, FL at depth of 40 ft 222
D.81c	Bottom Force Time History (Static) for Vilano - West, FL at depth of 40 ft . . . 222
D.81d	Bottom Force Time History (Dynamic) for Vilano - West, FL at depth of 40 ft . 222
D.82a	Top F-V Time History for Vilano Bridge - West, FL at depth of 42 ft 223
D.82b	Bottom F-V Time History for Vilano Bridge - West, FL at depth of 42 ft 223
D.82c	Bottom Force Time History (Dynamic) for Vilano - West, FL at depth of 42 ft . 223

LIST OF FIGURES (continued)

Volume II: Appendixes

<u>Figure</u>	<u>Page</u>
D.83a	Top F-V Time History for Vilano Bridge - West, FL at depth of 45 ft 224
D.83b	Bottom F-V Time History for Vilano Bridge - West, FL at depth of 45 ft 224
D.83c	Bottom Force Time History (Static) for Vilano - West, FL at depth of 45 ft . . . 224
D.83d	Bottom Force Time History (Dynamic) for Vilano - West, FL at depth of 45 ft . 224
D.84a	Top F-V Time History for Vilano Bridge - West, FL at depth of 45 ft (1 h) . . . 225
D.84b	Bottom F-V Time History for Vilano Bridge - West, FL at depth of 45 ft (1 h) . 225
D.84c	Bottom Force Time History (Static) for Vilano - West, FL at depth of 45 ft (1 h) 225
D.84d	Bottom Force Time History (Dynamic) for Vilano - West, FL at depth of 45 ft (1 h) 225
D.85a	Top F-V Time History for Vilano Bridge - West, FL at depth of 50 ft 226
D.85b	Bottom F-V Time History for Vilano Bridge - West, FL at depth of 50 ft 226
D.86a	Top F-V Time History for Vilano Bridge - West, FL at depth of 50 ft (1 h) . . . 227
D.86b	Bottom F-V Time History for Vilano Bridge - West, FL at depth of 50 ft (1 h) . 227
D.86c	Bottom Force Time History (Dynamic) for Vilano - West, FL at depth of 50 ft (1 h) 227
D.87a	Top F-V Time History for Vilano Bridge - West, FL at depth of 50 ft (14 h) . . . 228
D.87b	Bottom F-V Time History for Vilano Bridge - West, FL at depth of 50 ft (14 h) 228
D.88a	Top F-V Time History for Vilano Bridge - West, FL at depth of 52 ft 229
D.88b	Bottom F-V Time History for Vilano Bridge - West, FL at depth of 52 ft 229
D.88c	Bottom Force Time History (Static) for Vilano - West, FL at depth of 52 ft . . . 229
D.88d	Bottom Force Time History (Dynamic) for Vilano - West, FL at depth of 52 ft . 229
D.89a	Top F-V Time History for Vilano Bridge - West, FL at depth of 55 ft 230
D.89b	Bottom F-V Time History for Vilano Bridge - West, FL at depth of 55 ft 230
D.89c	Bottom Force Time History (Static) for Vilano - West, FL at depth of 55 ft . . . 230
D.89d	Bottom Force Time History (Dynamic) for Vilano - West, FL at depth of 55 ft . 230
D.90a	Top F-V Time History for Vilano Bridge - West, FL at depth of 55 ft (1 h) . . . 231
D.90b	Bottom F-V Time History for Vilano Bridge - West, FL at depth of 55 ft (1 h) . 231
D.90c	Bottom Force Time History (Static) for Vilano - West, FL at depth of 55 ft (1 h) 231
D.90d	Bottom Force Time History (Dynamic) for Vilano - West at depth of 55 ft (1 h) 231
D.91a	Top F-V Time History for Vilano Bridge - West, FL at depth of 55 ft (1 h and 20 in Drop) 232
D.91b	Bottom F-V Time History for Vilano Bridge - West, FL at depth of 55 ft (1 h and 20 in Drop) 232
D.92a	Top F-V Time History for Vilano Bridge - West, FL at depth of 59 ft 233
D.92b	Bottom F-V Time History for Vilano Bridge - West, FL at depth of 59 ft 233
D.92c	Bottom Force Time History (Static) for Vilano - West, FL at depth of 59 ft . . . 233
D.92d	Bottom Force Time History (Dynamic) for Vilano - West, FL at depth of 59 ft . 233
D.93a	Top F-V Time History for Vilano Bridge - West, FL at depth of 59 ft (1 h and 5 in) 234

LIST OF FIGURES (continued)

Volume II: Appendixes

<u>Figure</u>	<u>Page</u>	
D.93b	Bottom F-V Time History for Vilano - West, FL at depth of 59 ft (1 h and 5 in)	234
D.93c	Bottom Force Time History (Static) for Vilano - West, FL at depth of 59 ft (5 in)	234
D.93d	Bottom Force Time History (Dynamic) for Vilano - West at depth of 59 ft (5 in)	234
D.94a	Top F-V Time History for Vilano - West, FL at depth of 59 ft (1 h and 30 in)	235
D.94b	Bottom F-V Time History for Vilano - West, FL at depth of 59 ft (1 h and 30 in)	235
D.94c	Bottom Force Time History (Static) for Vilano - West, FL at depth of 59 ft (30 in)	235
D.94d	Bottom Force Time History (Dynamic) for Vilano - West, FL at depth of 59 ft (30 in)	235
D.95a	Top F-V Time History for Vilano Bridge - West, FL at depth of 62 ft	236
D.95b	Bottom F-V Time History for Vilano Bridge - West, FL at depth of 62 ft	236
D.96a	Top F-V Time History for Vilano Bridge - West, FL at depth of 62 ft (ASLT) . .	237
D.96b	Bottom F-V Time History for Vilano Bridge - West, FL at depth of 62 ft (ASLT)	237
D.96c	Bottom Force Time History (Static) for Vilano - West at depth of 62 ft (ASLT)	237
D.96d	Bottom Force Time History (Dynamic) for Vilano-West at depth of 62 ft (ASLT)	237
D.97a	Top F-V Time History for Vilano Bridge - West, FL at depth of 64 ft	238
D.97b	Bottom F-V Time History for Vilano Bridge - West, FL at depth of 64 ft	238
D.97c	Bottom Force Time History (Dynamic) for Vilano - West, FL at depth of 64 ft .	238
D.98a	Top F-V Time History for Vilano Bridge - West, FL at depth of 67 ft	239
D.98b	Bottom F-V Time History for Vilano Bridge - West, FL at depth of 67 ft	239
D.99a	Top F-V Time History for Vilano Bridge - West, FL at depth of 67 ft (ASLT) . .	240
D.99b	Bottom F-V Time History for Vilano Bridge - West, FL at depth of 67 ft (ASLT)	240
D.99c	Bottom Force Time History (Static) for Vilano - West at depth of 67 ft (ASLT)	240
D.99d	Bottom Force Time History (Dynamic) for Vilano-West at depth of 67 ft (ASLT)	240
D.100a	Top F-V Time History for Vilano Bridge - West, FL at depth of 68 ft	241
D.100b	Bottom F-V Time History for Vilano Bridge - West, FL at depth of 68 ft	241
E.1	Transfer Efficiencies of Various SPT Safety Hammer Systems	249
E.2	Hammer Kinetic Energies of Various SPT Safety Hammer Systems	250
F.1a	Site Plan - St. Mary	252
F.1b	Soil Boring Log - St. Mary	253
F.1c	Pile Driving Record - St. Mary	255
F.1d	Static Load Test Results - St. Mary	256

LIST OF FIGURES (continued)

Volume II: Appendixes

<u>Figure</u>		<u>Page</u>
F.2a	Site Plan - Portland	257
F.2b	Soil Boring Log - Portland	258
F.2c	Pile Driving Record	259
F.2d	Static Load Test Result - Portland	260
F.3a	Site Plan - CD17	261
F.3b	Soil Boring Log - CD17	262
F.3c	Pile Driving Log - CD17	267
F.3d	Static Load Test Result - CD17	268
F.4a	Site Plan - CD21	269
F.4b	Soil Boring Log - CD21	270
F.4c	Pile Driving Log - CD21	275
F.4d	Static Load Test Result - CD21	276
F.5a	Site Plan - White City	277
F.5b	Soil Boring Log - White City	278
F.5c	Pile Driving Log - White City, TP3	279
F.5d	Pile Driving Log - White City, TP6	280
F.5e	Static Load Test Result - White City, TP3	281
F.5f	Static Load Test Result - White City, TP6	281
F.6a	Site Plan - Apalachicola	283
F.6b	Soil Boring Log - Apalachicola	284
F.6c	CPT Results - Apalachicola	285
F.6d	Pile Driving Log - Apalachicola	286
F.6e	Static Load Test Result - Apalachicola	287
F.7a	Site Plan - Aucilla	288
F.7b	Soil Boring Log - Aucilla	289
F.7c	CPT Results - Aucilla	290
F.8a	Site Plan - Vilano - West	292
F.8b	Site Plan - Vilano - Center	293
F.8c	Site Plan - Vilano - East	294
F.8d	Soil Boring Log - Vilano - West	295
F.8e	Soil Boring Log - Vilano - Center	296
F.8f	Soil Boring Log - Vilano - East	297
F.8g	CPT Results - Vilano - East	298
F.8h	CPT Results - Vilano - West	299
G.1	Piezoresistive Accelerometer (SN# P035) Calibration Results	302
G.2	Piezoresistive Accelerometer (SN# P036) Calibration Results	302
G.3	Piezoelectric Accelerometer (SN# 10469) Calibration Results	303
G.4	Piezoelectric Accelerometer (SN# 10470) Calibration Results	303
G.5a	Load Transducer (SPT Rod #22) Calibration Results	304
G.5b	Load Transducer (SPT Rod #22) Calibration Plot	305
G.6a	Load Transducer (SPT Rod #23) Calibration Results	306
G.6b	Load Transducer (SPT Rod #23) Calibration Plot	307
G.7	Displacement Transducer (PSITRONIX, No. 93-310) Calibration Results	308

LIST OF FIGURES (continued)

Volume II: Appendixes

<u>Figure</u>	<u>Page</u>
G.8	Displacement Transducer (PSITRONIX No. 93-311) Calibration Results 308
G.9	Torque Transducer (SPT Rod 7A) Calibration Results 309
G.10	Torque Transducer (SPT Rod 7B) Calibration Results 309
H.1	Soil Classification for St. Mary, Cleveland, OH at depth of 40 ft 314
H.2	Soil Classification for St. Mary, Cleveland, OH at depth of 65 ft 316
H.3	Soil Classification for St. Mary, Cleveland, OH at depth of 100 ft 319
H.4	Soil Classification for St. Mary, Cleveland, OH at depth of 103.5 ft 322
H.5	Soil Classification for Fore River Bridge, Portland, ME at depth of 30 ft 325
H.6	Soil Classification for Fore River Bridge, Portland, ME at depth of 40 ft 327
H.7	Soil Classification for Fore River Bridge, Portland, ME at depth of 50 ft 329
H.8	Soil Classification for C&D Canal, Pier 17, DE at depth of 14 ft 331
H.9	Soil Classification for C&D Canal, Pier 17, DE at depth of 30 ft 334
H.10	Soil Classification for C&D Canal, Pier 17, DE at depth of 40 ft 336
H.11	Soil Classification for C&D Canal, Pier 17, DE at depth of 50 ft 339
H.12	Soil Classification for C&D Canal, Pier 17, DE at depth of 55 ft 341
H.13	Soil Classification for C&D Canal, Pier 17, DE at depth of 60 ft 344
H.14	Soil Classification for C&D Canal, Pier 17, DE at depth of 65 ft 346
H.15	Soil Classification for C&D Canal, Pier 21, DE at depth of 41 ft 348
H.16	Soil Classification for C&D Canal, Pier 21, DE at depth of 55 ft 351
H.17	Soil Classification for C&D Canal, Pier 21, DE at depth of 65 ft 353
H.18	Soil Classification for White City Bridge, TP3, FL at depth of 30.5 ft 355
H.19	Soil Classification for White City Bridge, TP6, FL at depth of 15.5 ft 357
H.20	Soil Classification for Apalachicola River Bridge, FL at depth of 20 ft 359
H.21	Soil Classification for Apalachicola River Bridge, FL at depth of 25 ft 361
H.22	Soil Classification for Apalachicola River Bridge, FL at depth of 55 ft 363
H.23	Soil Classification for Apalachicola River Bridge, FL at depth of 75 ft 366
H.24	Soil Classification for Sunshine Skyway Bridge, FL at depth of 15 ft 368
H.25	Soil Classification for Sunshine Skyway Bridge, FL at depth of 25 ft 370
H.26	Soil Classification for Sunshine Skyway Bridge, FL at depth of 27.5 ft 372
H.27	Soil Classification for Sunshine Skyway Bridge, FL at depth of 30 ft 374
H.28	Soil Classification for Sunshine Skyway Bridge, FL at depth of 35 ft 376
H.29	Soil Classification for Sunshine Skyway Bridge, FL at depth of 40 ft 378
H.30	Soil Classification for Sunshine Skyway Bridge, FL at depth of 45.5 ft 380
H.31	Soil Classification for Sunshine Skyway Bridge, FL at depth of 50 ft 382
H.32	Soil Classification for Aucilla River Bridge, FL at depth of 5 ft 384
H.33	Soil Classification for Aucilla River Bridge, FL at depth of 10 ft 385
H.34	Soil Classification for Vilano Bridge - East, FL at depth of 5 ft 386
H.35	Soil Classification for Vilano Bridge - East, FL at depth of 25 ft 387
H.36	Soil Classification for Vilano Bridge - East, FL at depth of 35 ft 388
H.37	Soil Classification for Vilano Bridge - East, FL at depth of 45 ft 389
H.38	Soil Classification for Vilano Bridge - West, FL at depth of 64 ft 390
H.39	Unconfined Compression Test Results for Apalachicola River Bridge, FL 391

LIST OF FIGURES (continued)

Volume III: Literature Review, Data Base and Appendixes

<u>Figure</u>	<u>Page</u>
2.1 Smith Soil Resistance Model	4
2.2 Smith Resistance Components Plotted versus Displacement (Top), Time (Middle), and Velocity (Bottom)	5
2.3 The Coyle-Gibson Resistance versus Velocity Plot	6
2.4 The Randolph Simon Shaft Soil Model	9
A.1 Wave Travel in a Rod	44
A.2 Example of a Downward Traveling Wave	44
A.3 Wave Balance at Pile With Bottom Resistance	46
A.4 Reflection At a Free Pile Bottom	46
A.5 Generation of Resistance Waves	48
A.6 Resistance Wave Reflections	49
B.1 Smith's soil model	52
B.2 Velocity force and damping forces over time for Smith-1 (top) and Smith-2 damping approach	53
B.3 Multipliers for conversion of Gibson to Smith-1 damping factors	54
B.4 Velocities, forces at pile top and damping forces as a function of time for Gibson and Gibson-GRL damping approaches	55
B.5 Conversion of Smith to GRL damping factors	55
C.1 Segmentation of a Non-Uniform Pile	58
C.2 Diesel Hammer Thermodynamics	61
C.3 Force Deformation of Non-linear Springs	62
C.4 Static Soil Resistance versus Pile Displacement	64
C.5 Dynamic Soil Resistance versus Pile Velocity	65
C.6 Forces Acting on Segment i	66
D.1 Waves Caused by a Resistance R_x , at Location x Below the Pile Top Generated by an Impact Wave Which Started to Move Down the Pile at Time t_1	72
D.2 Typical Resistance vs. Time Plot For a Pile Showing the Total Resistance $R(t)$, the Static Resistance $R_s(t)$, and Other Selected Resistance Values	75
D.3 Typical Plots of Pile Top Force and Velocity of a Damaged Pile	77
D.4 The Smith Soil Resistance Model (Viscous Damping Model Instead of a Strict Smith Damping is Shown)	80
D.5 Static Shaft Resistance	84
D.6 Static Toe Resistance	84
D.7 The Extended CAPWAP Soil Resistance Model (a) Shaft (b) Toe	87
D.8 Slack Model	91
D.9 Error Evaluation - CAPWAP	95
E.1 H-Pile at 78 ft (23.8 m) Depth; $V_s = 35.5/(1328 - 1235)$ $= 382$ ft/s (116 m/s)	98
E.2 H-Pile at 106 ft (32.3 m) Depth; $V_s = 35.5/(615.8 - 532.2)$ $= 42.5$ ft/s (130 m/s)	98
E.3 SPT Results	100
E.4 SPT Results, 25 ft	101

LIST OF FIGURES (continued)

Volume III: Literature Review, Data Base and Appendixes

<u>Figure</u>		<u>Page</u>
E.5	SPT Results, 50 ft, 6 s	101
E.6	SPT Results, 50 ft, 2 s	102
E.7	SPT Results, 50 ft, 250 ms	102
G.1	Load-set Curves from Static and Dynamic Test, ID# 24	107
G.2	Load-set Curves for Static and Dynamic Test, ID# 63	108
G.3	Load-set Curves from Static and Dynamic Test, ID# 75	109
G.4	Load-set Curves for Static and Dynamic Test, ID# 27	111

LIST OF TABLES

Volume I: Final Report

<u>Table</u>	<u>Page</u>	
2.1	Outline of Correlation Procedure	10
2.2	Statistical Summary of Capacity Ratios (Predicted/Static Load Test)	13
2.3	Statistical Summary of Capacity Ratios at Different Time Ratios	21
3.1	Summary CAPWAP Capacity Prediction at Different Time Ratio	32
3.2	Statistical Summary of CAPWAP Capacity Prediction	37
4.1	The Modified SPT Procedure	62
4.2	Summary of Test Sites	64
5.1	Comparison between Flat End and Cone Tip	72
5.2	Study of Scale Factor for Unit End Bearing	73
5.3	Summary of Rate Effect from Static Tests	75
5.4	Summary Uplift Capacity versus Time from Three Sites	80
5.5	Comparison of Initial Shear Strength and N_{60}	80
5.6	Summary of Torque Resistance and Uplift Resistance	83
5.7	Summary of the Smith Soil Constants for the St. Mary Site, Cleveland, Ohio .	101
5.8	Summary of the Smith Soil Constants for the Fore River Bridge, Portland, Maine	102
5.9	Summary of the Smith Soil Constants for the C&D Canal Site, Pier 17, Delaware	103
5.10	Summary of the Smith Soil Constants for the C&D Canal Site, Pier 21, Delaware	104
5.11	Summary of the Smith Soil Constants for the White City Bridge, Florida	105
5.12	Summary of the Smith Soil Constants for the Apalachicola River Bridge Site, Florida	106
5.13	Comparison Between Measured and GRLWEAP Blow Count for SPT Driving System (EOD Condition)	108
5.14	Ultimate Resistance and Toe Damping Factor Calculated by "Static" and "Dynamic" Analyses for Static $R_u >$ Dynamic R_u	111
5.15	Comparison of Toe Quakes from Modified SPT Compression Tests (Flat End Tip)	114
5.16	Comparison of Full Scale Pile Toe Quakes from CAPWAP Results	114
5.17	GRLWEAP Study of New Toe Soil Models on SPT Flat End Tip	117
6.1	Pile Capacity Prediction for St. Mary Site, Cleveland, Ohio	122
6.2	Pile Capacity Prediction for Fore River Bridge, Portland, Maine	123
6.3	Pile Capacity Prediction for C&D Canal, Pier 17, Delaware	124
6.4	Pile Capacity Prediction for C&D Canal, Pier 21, Delaware	125
6.5	Pile Capacity Prediction for White City Bridge, TP3, Florida	126
6.6	Pile Capacity Prediction for Apalachicola River Bridge, Florida	127
6.7	Comparison of Capacity Values from Different Methods	128
6.8	Soil Resistance Distribution and Smith Soil Constants for St. Mary, OH	137
6.9	Soil Resistance Distribution and Smith Soil Constants for Portland, ME	138
6.10	Soil Resistance Distribution and Smith Soil Constants for C&D Pier 17, DE . .	139

LIST OF TABLES (continued)

Volume I: Final Report

<u>Table</u>	<u>Page</u>
6.11	Soil Resistance Distribution and Smith Soil Constants for C&D Pier 21, DE . . . 140
6.12	Soil Resistance Distribution and Smith Soil Constants for White City, TP3, FL 141
6.13	Soil Resistance Distribution and Smith Soil Constants for Apalachicola, FL . . . 142
6.14	Blow Count Comparison for St. Mary, Cleveland, Ohio 143
6.15	Blow Count Comparison for Fore River Bridge, Portland, Maine 143
6.16	Blow Count Comparison for C&D Canal, Pier 17, Delaware 147
6.17	Blow Count Comparison for C&D Canal, Pier 21, Delaware 147
6.18	Blow Count Comparison for White City Bridge, TP3, Florida 149
6.19	Blow Count Comparison for Apalachicola River Bridge, Florida 149
6.20	Bearing Graph Comparison for St. Mary, Cleveland, Ohio 151
6.21	Bearing Graph Comparison for Fore River Bridge, Portland, Maine 152
6.22	Bearing Graph Comparison for C&D Canal, Pier 17, Delaware 153
6.23	Bearing Graph Comparison for C&D Canal, Pier 21, Delaware 154
6.24	Bearing Graph Comparison for White City Bridge, TP3, Florida 155
6.25	Bearing Graph Comparison for Apalachicola River Bridge, Florida 156
6.26a	Comparison of Capacity Predictions from Dynamic SPT, GRLWEAP, and Static Load Test 157
6.26b	Method Description 157
6.27	Summary of Toe Parameter Study 161
6.28	Final Blow Count Comparison Driveability Studies 169
7.1	Summary of the Smith Soil Constants for Aucilla River Bridge, Florida 175
7.2	Summary of the Smith Soil Constants for Vilano Bridge-East, Florida 176
7.3	Summary of the Smith Soil Constants for Vilano Bridge-West, Florida 177
7.4	Aucilla River Bridge, Florida (PSC Pile 18 in Square) 178
7.5	Vilano Bridge - East Embankment, Florida (PSC Pile 18 in Square) 179
7.6	Vilano Bridge - West Embankment, Florida (PSC Pile 18 in Square) 179
7.7	Summary of the Capacity Calculation 183
7.8	Resistance Distribution and Dynamic Parameters for Driveability Analyses of Aucilla River Bridge, Florida 184
7.9	Resistance Distribution and Dynamic Parameters for Driveability Analyses of Vilano Bridge - East Embankment, Florida 185
7.10	Resistance Distribution and Dynamic Parameters for Driveability Analyses of Vilano Bridge - West Embankment, Florida 186
7.11	Blow Count Prediction for Aucilla River Bridge, Florida 188
7.12	Blow Count Prediction for Vilano Bridge - East Embankment, Florida 188
7.13	Blow Count Prediction for Vilano Bridge - West Embankment, Florida 189
7.14	Bearing Graph Prediction for Aucilla River Bridge, Florida 189
7.15	Bearing Graph Prediction for Vilano Bridge - East Embankment, Florida 190
7.16	Bearing Graph Prediction for Vilano Bridge - West Embankment, Florida 191

LIST OF TABLES (continued)

Volume II: Appendixes

<u>Table</u>		<u>Page</u>
A.1	Summary of Bearing Graph Analysis Results	2
A.2	Summary of Driveability Analysis Results	4
B.1	Summary of SPT Static Load Test Results	112
C.1	Summary of Torque Test Results	132
D.1	Summary of Dynamic Test Results	138
E.1	SPT Rod Top Measurements	244
H.1	Summary of Soil Classifications	312

LIST OF TABLES (continued)

Volume III: Literature Review, Data Base and Appendixes

<u>Table</u>	<u>Page</u>
2.1a	Damping Values from Literature with $n = 1$ 14
2.1b	Damping Values from Literature with $n \neq 1$ 15
2.2	Quake Values from Literature 16
2.3	Comparison of GRLWEAP with CAPWAP Soil Models 20
3.1	General and Pile Data Information 29
3.2	Driving Data 30
3.3	Hammer and Driving System Information 31
3.4	Dynamic Analysis Summary Information 32
3.5	CAPWAP Results (one spreadsheet each for EOD and all restrikes) 33
3.6	Subsurface and Static Load Information 34
3.7	Correlation Analysis Summary 35
3.8	Additional Spreadsheets 37
3.9	General Description of Data Base Entries 38
B.1	Input details of Case study 53
B.2	Comparison of GRLWEAP damping approaches with standard Smith damping results 54
D.1	CAPWAP Unknowns 94
F.1	Summary of Sensitivity Study from Three Hammer-Pile Combinations 104
G.1	Summary of Large Toe Quake Case 112
H.1	Summary of High Toe Damping Cases Based On Restrike Tests 116
H.2	Summary of High Shaft Damping Cases 119

LIST OF SYMBOLS

Volume I: Final Report

A	-	cross section area or setup parameter
A ₃	-	average of the three highest shaft resistance per unit length
A _s	-	pile soil contact area
A _{toe}	-	toe area
B	-	pile width
Cl	-	circumference of the pile
c	-	velocity of wave propagation
E	-	modulus of elasticity
F ₁	-	loading toe quake multiplier (hyperbolic model)
F ₂	-	unloading toe quake multiplier (hyperbolic model)
F _m (t)	-	force measured near the top of drill string
F [↓] (t)	-	downward traveling force wave
F [↑] (t)	-	upward traveling force wave
f _s	-	average unit sleeve friction
J or J _c	-	Smith damping constant
J _s	-	shaft damping
J _t	-	Toe damping
L	-	pile length below gauges
MS	-	shaft support soil mass
NFac	-	ratio of number of pile segments to soil segments
K	-	ratio of unit pile friction to unit sleeve friction
k	-	cushion stiffness
m	-	mass constant
N	-	SPT N-value
N ₆₀	-	SPT N-value corrected to 60 percent transfer efficiency
n	-	damping exponent
q	-	quake
Q _p	-	pile toe resistance
Q _s	-	pile shaft resistance or shaft quake
Q _t	-	toe quake
q _{c1} , q _{c2} , q _{c3}	-	average cone tip resistance
R	-	total measured toe resistance
R(t)	-	toe resistance force
R _a	-	inertia or acceleration dependent resistance
R _{cT}	-	total calculated toe resistance
R _d	-	dynamic or velocity dependent resistance

LIST OF SYMBOLS (continued)

Volume I: Final Report

R_s	-	static or displacement dependent resistance
R_u	-	ultimate static capacity
SK	-	shaft radiation damping parameter
$u(t)$	-	displacement at the toe
$\dot{u}(t)$	-	velocity of soil
$\ddot{u}(t)$	-	acceleration
\dot{u}_m	-	measured velocity
V_{impact}	-	SPT hammer impact velocity
Z1	-	impedance of the very top pile segment
ϕ_a	-	toe radiation damping constant
τ_o	-	soil shear strength at time t_0
$\tau(t)$	-	soil shear strength at time t
Δ_i	-	final displacement

Volume III: Literature Review, Data Base and Appendixes

A	-	setup factor
C_1	-	frequency dependent parameter for toe soil stiffness (Mitwally and Novak, 1988)
C_2	-	frequency dependence parameter for toe soil damping (Mitwally and Novak, 1988)
c_H	-	damping factor at toe (Holeyman, 1988)
c_s	-	frequency dependent shaft damping (Mitwally and Novak, 1988)
c_t	-	frequency dependent toe damping (Mitwally and Novak, 1988)
c_u	-	undrained shear strength
E	-	elastic modulus
E'	-	modulus of viscosity (Holeyman, 1988)
E_i	-	initial tangent modulus (Holeyman, 1988)
f_s	-	cone shaft friction or unit shaft resistance
G	-	soil's shear modulus
G_b	-	toe soil shear modulus (Mitwally and Novak, 1988)
I_p	-	influence coefficient (Hussein, 1992)
J	-	Smith damping factor
J_c	-	Coyle-Gibson exponent damping factor
J_G	-	toe damping prior to failure (Lee et al., 1988)
J_G'	-	toe damping during failure (Lee et al., 1988)

LIST OF SYMBOLS (continued)

Volume III: Literature Review, Data Base and Appendixes

J_L'	-	shaft damping prior to failure (Lee et al., 1988)
J_M	-	purely viscous damping factor (Middendorp and Brederode, 1984)
$J_{R,toe}$	-	toe damping value (Randolph and Simons, 1986)
J_s	-	shaft damping
J_t	-	toe damping
k	-	soil stiffness
k_H	-	soil stiffness at toe (Holeyman, 1988)
k_s	-	shaft soil stiffness
k_t	-	soil stiffness (Randolph and Simons, 1986)
m_s	-	soil mass
n	-	Coyle-Gibson damping exponent
p_c	-	cone tip pressure
p_y	-	yield pressure (Liang and Sheng, 1992)
q	-	quake
q_r	-	ultimate strength at the base (Holeyman, 1988)
q_s	-	shaft quake
q_t	-	toe quake
q_{ut}	-	unit toe resistance
r_o	-	pile radius
r_H	-	cone bottom radius (Holeyman, 1988)
r_m	-	radius of zone of soil deformation (Nguyen et al., 1988)
R_d	-	total dynamic soil resistance
R_f	-	failure load (Lee et al., 1988)
R_t	-	total shaft resistance (Middendorp and Brederode, 1984)
R_s	-	total static soil resistance
R_u	-	ultimate resistance
R_{t1}	-	failure load at time t_1
R_{t2}	-	failure load at time t_2
S_1	-	frequency dependent parameter for shaft soil stiffness (Mitwally and Novak, 1988)
S_2	-	frequency dependent parameter for shaft soil damping (Mitwally and Novak, 1988)
t_f	-	time to failure
u	-	displacement of pile segment
\dot{u}	-	velocity of pile segment
\ddot{u}	-	acceleration of pile segment

LIST OF SYMBOLS (continued)

Volume III: Literature Review, Data Base and Appendixes

u_p	-	pore water pressure
v_1	-	pile velocity (Briaud and Garland, 1984)
v_2	-	pile static reference velocity (Briaud and Garland, 1984)
v_s	-	shear wave velocity
σ	-	stress
ϵ	-	strain
ϵ_l	-	average volumetric locking strain (Liang and Hussein, 1992)
ρ	-	soil mass density
τ_{max}	-	maximum shear strain (Nguyen et al., 1988)
τ_o	-	soil shear strength (Liang and Hussein, 1992)
τ_u	-	ultimate shear stress
ν	-	Poisson's ratio
ϕ	-	friction angle of soil
ω	-	frequency

CHAPTER 1

INTRODUCTION

When a new technology is introduced into practice, three things will invariably happen. First, the promotor will fuel enthusiasm of the profession; then, when left alone, the new user will become disappointed or bewildered, and finally, practitioners force the developers to make the new procedure work under a variety of conditions in practice.

The wave equation technology is now probably in the third stage of development. The enthusiasm of the first phase occurred in the seventies when the obvious advantages of this analysis type over simple formulas were realized. In the second phase, the profession recognized the difficulty of finding proper hammer and soil models. For example, in 1986, a thorough study of the Wave Equation Analysis of Pile Driving (WEAP) diesel hammer model was conducted and improvements were achieved through changes of the mathematical models, particularly for atomized fuel injection. Stress and transferred energy predictions today agree favorably with field measurements and the emphasis for improvements of the wave equation approach has shifted to the more complex question of soil model performance.

There are two basic criticisms of the Smith (1960) soil representation that is the basis for current wave equation analyses. First, the approach is sometimes called "crude" since it only involves an elasto-plastic spring and a viscous dashpot, the latter being of the rather unique "Smith-type" (i.e., the damping constant is the product of static resistance and damping factor). Second, the model does not allow for a calculation of soil constants from standard geotechnical soil properties or otherwise measurable soil responses to laboratory or in-situ testing. Of course, if the Smith approach would always accurately predict blow counts or pile bearing capacity, then nobody would worry about its lack of elegance. However, the method does not always produce sufficiently accurate results. The research presented in this report attempted to improve the current State-of-the-Art of wave equation analyses.

The following report was written after 3 years of intensive research on the mechanics of pile soil interaction during a hammer blow. The primary objective of this effort was a better wave equation prediction of (a) pile driveability based on in-situ soil tests and (b) an improved prediction of pile bearing capacity based on end of driving or restrrike pile penetration observations.

Several distinctly different methods were employed to meet the objectives of the study. In summary,

a literature study was performed for an assessment of soil models and parameters for the dynamic analysis of impact driven piles;

a data base was generated and correlation studies were conducted for an assessment of the accuracy or potential improvement of the current methodology;

a new wave equation model was proposed, built into the GRLWEAP¹ program, based on the results of the literature study, and, to a limited degree, tested against measurements taken during the study;

a Modified Standard Penetration Test (SPT) procedure and equipment were designed and employed;

using the Modified SPT, dynamic and static tests were performed at six sites with existing full-scale load test results and at 3 sites with future static tests;

static and dynamic analysis results of the Modified SPT data taken near existing or future static load test piles were evaluated, yielding predictions of bearing capacities and blow counts which were compared with actual full-scale results.

In 1992, during the course of this investigation, the contractor issued an Interim Report (GRL and Associates, Inc., 1992) which summarized (a) literature search, (b) correlation study using the then created data base and (c) a proposal for both dynamic and static in-situ tests. Since that time additional work was performed including a thorough review of the data contained in the data base and the addition of a considerable number of new cases since not all of the earlier submitted cases met stringent requirements. Therefore, the correlation work was repeated and several additional correlation studies were conducted. These new correlation results contained in chapters 2 and 3 of the present final report, therefore, replace equivalent conclusions of the Interim Report (GRL, 1992).

¹GRLWEAP is a proprietary version of the WEAP program; it is the most widely used wave equation analysis program for piles, has been accepted for use on public projects by American Association of State Highway and Transportation Officials (AASHTO), U.S. Army Corps of Engineers and other U.S. government agencies. This program was used for the analyses presented in this report. In fact several figures and tables were generated by this program and therefore bear the GRLWEAP name as an identifier. However, the publication of this name should not be construed as a promotion or endorsement of this software.

The present Final Report describes the Modified SPT system (chapter 4) which was built, tested and then employed on nine different sites. Descriptions of the analyses performed and results obtained based on data collected by the Modified SPT are presented in chapter 5. Chapters 6 and 7 present predictions of full-scale pile performance using Modified SPT results for existing and future load test sites, respectively. Conclusions derived from this study are included in chapter 8. Chapter 9 summarizes recommendations for future work.

Several appendixes in this report present detailed results and analyses of the data collected using the new in-situ test system (Modified SPT). Appendix A contains GRLWEAP analysis results of full-scale correlation test piles described in chapters 6 and 7. Appendixes B and C include the Modified SPT static load and torque test results, respectively. Modified SPT dynamic test results are included in appendix D. Summaries of SPT blow counts and dynamic SPT measurements are presented in appendix E. Transducer calibrations and soil laboratory testing results are included in appendixes G and H, respectively.

The literature study of the Interim Report (GRL, 1992) along with the background appendixes of the Interim Report is considered an important part of the total research effort. For this reason, a second volume of this Final Report is issued containing those parts of the Interim Report that are not repeated in one form or another in this first volume. The second volume also contains a description of the data base and background information for dynamic testing and analysis methods of impact driven piles.

CHAPTER 2

WAVE EQUATION CORRELATIONS AND SOIL PARAMETER CALCULATIONS

2.1 OBJECTIVES

Several objectives were considered when work on the data base was commenced. First, a means would be available to back-calculate dynamic soil model parameters such as damping and quake. Secondly, new wave equation dynamic soil models and their parameters could be tested. Furthermore, a variety of methods for bearing capacity and driveability could be compared. Finally, with sufficiently many data base cases available, a statistical evaluation of the reliability of a prediction would be possible. The following sections describe the efforts taken to meet these objectives, in particular, the value and quality of the data base will be evaluated and the wave equation models will be reviewed. It should be mentioned that the data base since the writing of the Interim Report (GRL, 1992) has been reviewed, expanded and, where necessary, corrected. A description of the data base is included in chapter 3 of volume II.

2.2 DESCRIPTION OF THE DATA BASE

Approximately 100 complete cases were available for analysis meeting the critical review by several of the contractor's engineers who had different research objectives. For example, in one study (not part of the work presented here) the soil data was subjected to a various static analyses; in another study (reported in chapter 3) Case Pile Wave Analysis Program (CAPWAP) analyses were critically reevaluated. As a consequence of these reviews, several cases, originally considered acceptable were now rejected for a variety of reasons (excessively high blow counts; borings not deep enough; static load test not run to failure, etc.) To make up for the resulting deficit, additional cases were selected and included in the data base. In this way, a total of 100 cases meeting very stringent requirements were now available. In addition, more than 50 cases meeting less demanding criteria were also included in the data base.

In order to salvage valuable data, the criteria for case acceptance in the data base were slightly relaxed compared to criteria originally contemplated. The requirements for an acceptable data set may be summarized as follows:

- A static load test carried to failure according to Davisson's failure criterion. If the load-set curve does not reach the Davisson criterion then an extrapolation would be allowed to at most 110 percent of the maximum applied static test load.

- An instrumented restrrike with (a) a waiting time between pile installation and restrrike that is comparable to the time between driving and static load test (obviously, this rule leaves room for interpretation) and (b) meeting any one of the following three blow count requirements (the original requirement of 240 blows/ft (800 blows/m) for the beginning of restrrike (BOR) was relaxed to allow more cases into the data base, particularly if those cases did not indicate a resistance activation problem during the restrrike):

the BOR blow count shall be less than the equivalent of 360 blows/ft (1200 blows/m)

or

the BOR blow count shall be less than 480 blows/ft (1600 blows/m) if the standard GRLWEAP analysis overpredicts the load test capacity or is within 5 percent of it

or

the BOR may be at absolute refusal if both standard GRLWEAP and CAPWAP overpredict or predict the load test within 5 percent

- A soil boring performed within the vicinity of the load test pile extending below the bottom of the pile. This rule was actually violated in one case (Data base ID# 92). At that site many tests had been performed and the geology was therefore relatively well known.
- A driving record indicating as a minimum the end of driving (EOD) and BOR blow counts, the date of installation and restrrike, the hammer and hammer setting used for driving or restriking.

2.3 VALUE OF THE DATA BASE

Obviously, the data base thus established cannot be used for all types of investigation. A purely statistical use of the data base may be hampered by the fact that it has the following shortcomings:

- Only well engineered cases are included, *i.e.*, those with instrumented restrrike tests.
- Instrumented restrrike tests are normally performed on sites where also the initial installation was instrumented; if poor hammer performance was present during the installation, it was likely to be corrected before the restrrike.

- Sites with high soil setup, compared to the end of driving resistance, probably would be excluded from the data base, either because of the static load test restriction or the maximum BOR blow count criterion.
- On a significant number of sites, several piles were tested and their data were included in the data base. Unless these test sites were for important or large projects, the large number of test piles may indicate that the soil behavior at these sites was considered unusual or difficult.
- One acceptable data set (Data base ID# 122) was submitted by a Chinese user. This data set indicated an extremely high increase in blow count between EOD and BOR thereby strongly affecting the wave equation analysis capacity prediction. To reduce the likelihood of this one data point affecting statistical conclusions, it was removed from the correlation summaries.

For the current study, these data base shortcomings are not a major problem since the primary objective is the calculation of dynamic soil parameters and not a blind statistical investigation. However, caution should be exercised when attempting to draw general conclusions from the results presented here.

For the purpose of these correlation studies, the static load test was assumed to be correctly performed according to American Society of Testing and Materials (ASTM) D1143, although in reality it is recognized that the test may contain errors in either the force or displacement measurements, or in both. The "*static load test capacity*" was determined based on Davisson's failure criterion (Vanikar, 1986). Of course, other failure definitions would result in a range of failure loads for the same test. In many soils, the pile capacity changes with time due to soil setup or relaxation. For this reason many specifications require a wait period after installation before the static load test can be applied. Since in the usual case, the static and dynamic tests were not performed the same day, further differences in capacity should be expected. Potential measurement errors, alternative failure definitions, differences in time of testing after installation and other reasons make perfect correlations of static with dynamic test results impossible.

2.4 WAVE EQUATION SOIL MODELS INVESTIGATED

During the course of the project, several new model features were introduced in the wave equation program GRLWEAP. These model components included:

- Toe plug.
- Toe gap.
- Hyperbolic static toe resistance vs toe displacement.
- Reduced unloading quake for shaft resistance.
- Exponential damping.
- Radiation damping for both shaft and toe.

A test of these model components was made by comparing calculated with measured dynamic resistance histories at the SPT sampler. The toe plug, toe gap, and hyperbolic toe resistance proved to be useful for the matching procedures described in chapter 5.

The unloading quake modification caused a lot of complexity in the code, plus an uncertain blow count calculation. It became apparent that energy losses in the static resistance vs penetration cycle during unloading would be negligible compared to the losses due to soil damping. For this reason, no additional efforts were made to find a better algorithm for the unloading behavior.

The radiation damping approach was incorporated in the GRLWEAP program (GRL and Associates, Inc., 1995). This model also made the blow count calculation rather erratic and an improvement of the prediction of the test pile capacities was not realized. Thus, a routine method for the implementation of this model has not yet been found.

Attempts aimed at finding exponential rate effects with the Modified SPT are described in chapter 5. Although conducted successfully, these tests did not indicate that the exponent should be chosen different from unity. In other words, the current linear model was not proven inadequate, at least for the soil types tested and for maximum pile velocities above 3.3 ft/s (1 m/s).

Toe plug and the hyperbolic toe resistance law were essential for matching the SPT data. So far, however, for full-scale piles no clear improvement of correlations could be established.

The expanded wave equation soil model has not been tested enough to yield improved results for standard predictions of bearing capacity or driveability. Further correlation work is necessary to advance the state of the art.

Other GRLWEAP program changes, probably more important for future driveability studies, included the addition of the pile circumference and the effective toe diameter. This latter change allows for an automated calculation of quake values based on pile size. More importantly, for driveability calculations the unit soil strength can now be converted by the program to segment resistance forces. The most important consequence of this change is the possibility to analyze non-uniform piles for driveability in a more realistic manner. For the correlation studies, this change in the program was without consequence.

2.5 CORRELATION EFFORTS AND PARAMETER CALCULATIONS

Using almost 100 data sets from the data base, several studies were performed. Their objectives and certain problems encountered are listed in the following:

- (a) The first correlation effort was a rather obvious one: comparing bearing capacities from wave equation predictions based on (a) the end of driving (EOD) blow count and (b) the beginning of restrrike (BOR) blow count observed in the field, and using the standard wave equation model. This effort includes steps 1, 2 and 3 of table 2.1.

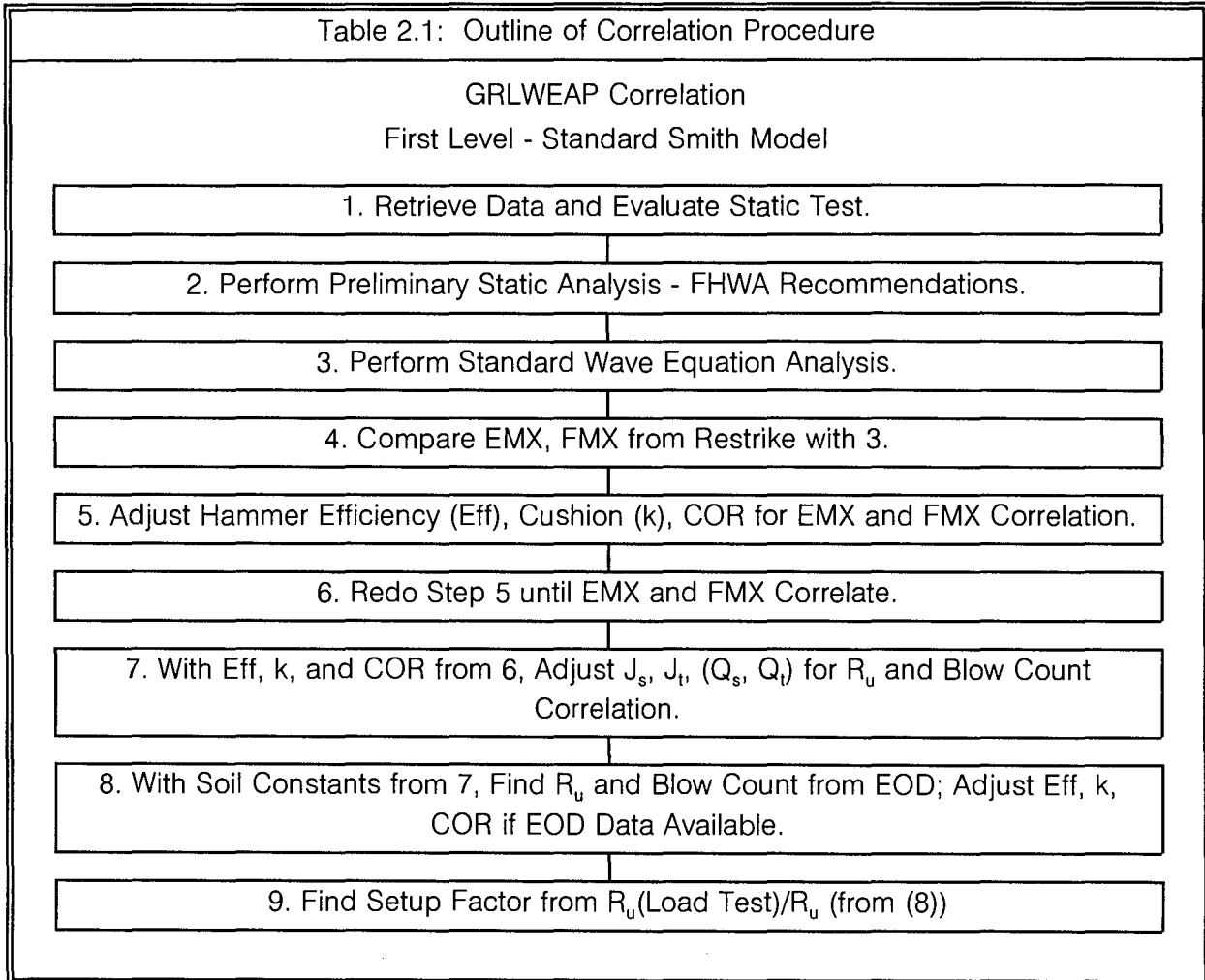
Comment (a1): The so-called EOD standard Smith capacity utilized the recommendations of the GRLWEAP manual for hammer, driving system, pile, and soil modeling. Thus, no effort was made to use information from measurements taken during installation.

(a2): The process of determining BOR capacities, based on the beginning of restrrike blow count, was particularly difficult (actually a guessing game) when both hammer energy and the set (inverse of the equivalent blow count) under the first few hammer blows were highly variable. The restrrike equivalent blow count is difficult to measure and its reliability is often suspect.

- (b) The second correlation effort used the dynamic monitoring restrrike results: maximum force and maximum transferred energy with wave equation analyses adjusted to match these measurements. The results equivalent to those obtained under (a) were calculated. Table 2.1, steps 4, 5 and 6 were involved in this procedure.

Comment (b1): The energy and force adjustment process turned out to be rather time consuming. Sometimes very low hammer efficiency inputs were required to match the measurement results. It is not clear whether the hammer

Table 2.1: Outline of Correlation Procedure



Notes:

1. Requirements for Minimum Data Set: Static Load Test with clear indication of failure. Note that if Davisson's failure load is not reached, it should be possible to extrapolate it to within 10 percent of the maximum load applied.
Generally, blow count of BOR must be less than 240 blows/ft (790 blows/m) unless dynamic results (CAPWAP, Standard GRLWEAP, Case Method) predict high (equal to or greater than static load test).
2. Use Beta Method, Alpha Method, and Norlund Method.
3. Standard Wave Equation uses GRLWEAP Manual and Hammer File Recommendations.
4. For concrete pile, adjust pile cushion, not hammer cushion properties. Agreement within 10 percent is sufficient for EMX, FMX correlation.
5. Agreement within 5 percent is sufficient for R_u and Blow count.
Use J_s only for piles with more than 70 percent shaft resistance.
Use J_t only for piles with more than 70 percent toe resistance.
For intermediate values of shaft and toe resistance, increase/decrease J_s and J_t by the same percentage. Use Q_t only for "bouncy" soils, *i.e.* where CAPWAP Q_t + Toe Gap > 2 times GRLWEAP recommendation.

and driving system parameters chosen for matching of measurement results produced a realistic model. For example, in some instances, adjustments of coefficients of restitution could have been more realistic than changes of hammer efficiency.

- (c) With EOD capacities from the adjusted (b) wave equation and the static load test results known, setup factors were calculated and averaged for similar soil types. These averaged setup factors for shaft soil types were then reused to predict the piles' static load test capacity based on EOD blow counts. (table 2.1, Steps 7, 8 and 9.)

Comment (c1): The term "setup" factor may be criticized since the bearing capacity at EOD is only an estimate. However, this estimated setup factor would be the one that would allow for a prediction of bearing capacity based on a simple, uninstrumented EOD observation.

(c2): The process of setup factor calculation and then reuse for capacity predictions is incestuous. Setup factor reuse was based on "similar" soil types. Of course, only if statistically meaningful results for each soil type were available would this process be truly satisfactory.

- (d) The results of (a) and (b) were also calculated with capacity predictions of several static load test piles on the same site averaged. In this way, the overweighting of certain sites with several load test piles was avoided.

Comment (d1): For several sites, data was available from more than one statically and dynamically tested pile. Only average results for the test piles at a particular site were included in the correlations. This was made possible by expressing correlation results in the form of a ratio: predicted divided by static load test capacity. Averaging reduced the number of observations in the correlations from 99 to 45. The reduced number of 45 sites included 20 sites with only one test pile and 25 sites with two or more test piles.

- (e) The main correlation effort with the wave equation analysis was directed at a back-calculation of wave equation soil damping parameters by matching restrrike based capacity results with the static load test. The rules adhered to in this study are summarized in table 2.1.

Comment (e1): The parameter back-calculation used a fixed shaft quake of 0.1 in (2.5 mm), and either the toe quake as per GRLWEAP manual or that from

CAPWAP if the latter exceeded the former by a factor greater than 2. Therefore, no quake values were calculated in this study. For predominantly shaft resistance piles with more than 70 percent shaft resistance according to static capacity calculations, only the shaft damping factor was calculated. For piles with more than 70 percent end bearing, only toe damping factors were calculated. For all other piles, shaft and toe damping factors were proportionately adjusted starting with the standard GRLWEAP recommendation..

- (f) Calculated damping factors from (e) were compiled for a limited number of cases for which several restrrike test results (with several waiting times) were available for the same site.

Comment (f1): Damping values back-calculated from restrrike observations were not identical as commonly expected for the same pile, under the same hammer and driven in the same soil. Apparently, the setup behavior of the soil not only affected the static strength but also the dynamic soil resistance parameters. Another reason for these varying damping factors might be the reduction of pile velocities as the static soil strength increased. Reduced pile velocities sometimes do require higher damping factors (an effect closely linked to the exponential damping behavior which could not be confirmed in our SPT study). It is recommended that the cases included in the restrrike damping factor study be subjected to an exponential damping correlation.

- (g) Results from static capacity calculations were correlated with static load tests.

Comment (g1): Static capacity calculations (static formula) followed the recommendations of Vanikar, 1986. These calculations were not performed where refusal SPT N-values made the static analysis difficult and therefore could only be performed for 89 cases.

2.6 RESULTS

2.6.1 Capacity Predictions

Figures 2.1 through 2.4 present the EOD and BOR correlations obtained with and without correction for hammer performance. Table 2.2 (lines 1, 3, 5, 7) summarizes these graphs statistically as described below. Each point in the figures represents a pile for which the

capacity was calculated based on bearing graph and observed blow count. The general tendency of the EOD results to underpredict is obvious. On the other hand, restrrike based results tend to overpredict, even after adjustment for hammer-driving system performance. The static formula predictions, based on SPT and Vanikar (1986) are shown in figure 2.5 and in line 11 of table 2.2.

A better means of comparing prediction methods than by scattergrams is desirable. Thus, following the statistical evaluation method, presented by Briaud et al. (1988) for pile capacities calculated by various methods, the predictions were divided by the static load test capacities.

The resulting ratio was statistically investigated by computation of mean and coefficient of variation (C.O.V) in table 2.2. If a normal distribution of these capacity ratios were assumed, there would be some probability of a negative ratio which is, of course, meaningless. Briaud's approach avoids this problem by plotting log normal distributions. Figures 2.6(a) and 2.6(b) show histograms of the capacity ratio for both EOD and BOR. Briaud's log normal probability density function is plotted on the same graph for comparison. The figures show that the BOR log-normal curve follows the frequency distribution quite well. Therefore, for the purpose of

Table 2.2: Statistical Summary of Capacity Ratios (Predicted/Static Load Test)

Line	Prediction Method	Status	Number of Piles/Sites	Mean	Standard Deviation	Coefficient of Variation (C.O.V)
1	Standard GRLWEAP	EOD	99	0.82	0.36	0.44
2		EOD-Avg	45	0.89	0.34	0.38
3		BOR	99	1.22	0.43	0.35
4		BOR-Avg	45	1.23	0.39	0.32
5	(EMX,FMX) Adjusted GRLWEAP	EOD	99	0.74	0.32	0.43
6		EOD-Avg	45	0.79	0.29	0.37
7		BOR	99	1.16	0.41	0.35
8		BOR-Avg	45	1.13	0.35	0.31
9	CAPWAP	BOR	99	0.92	0.20	0.22
10		BOR-Avg	45	0.94	0.15	0.16
11	Static Formula	All	89	1.30	0.88	0.68
12		Avg	43	1.34	0.97	0.72

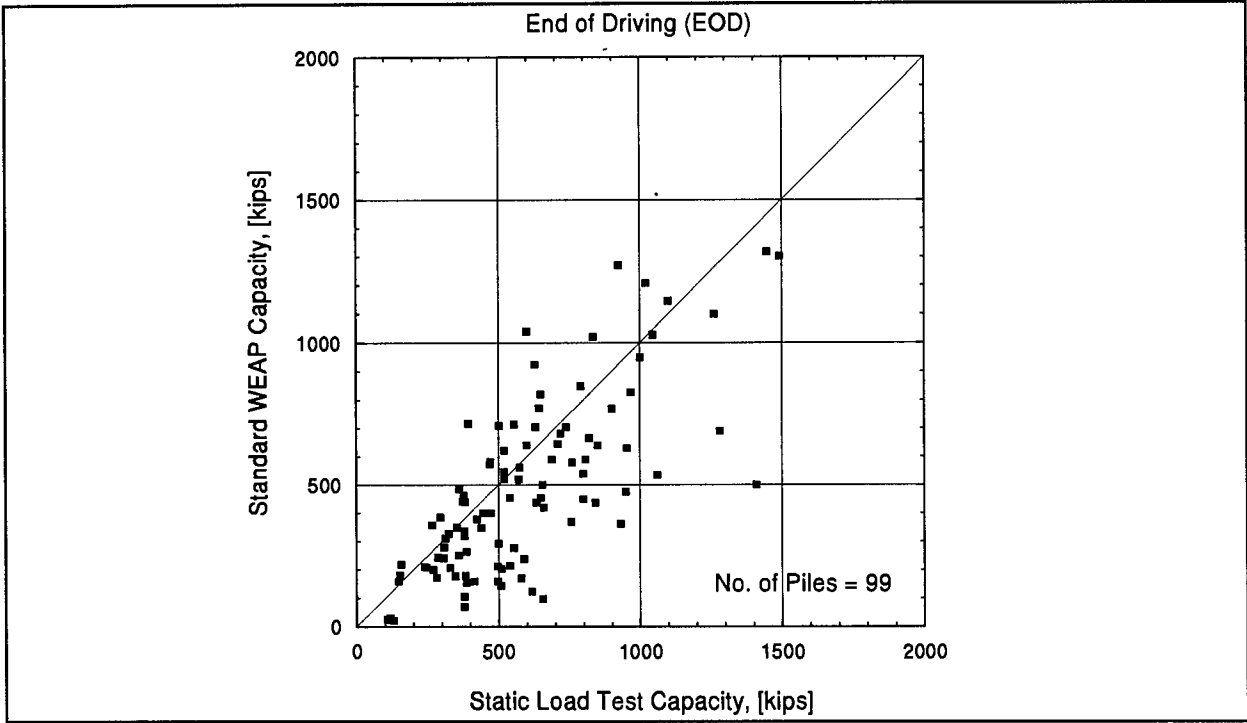


Figure 2.1: GRLWEAP EOD Capacity Correlations Using Standard Smith Soil Model

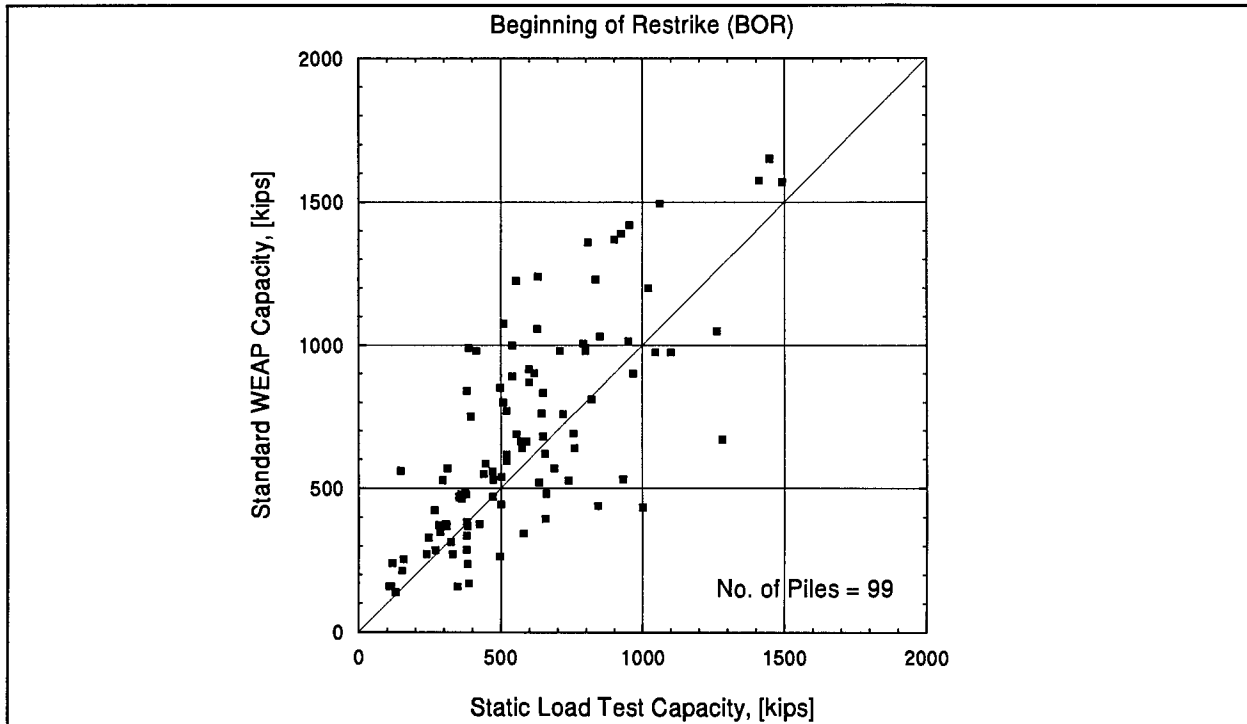


Figure 2.2: GRLWEAP BOR Capacity Correlations Using Standard Smith Soil Model

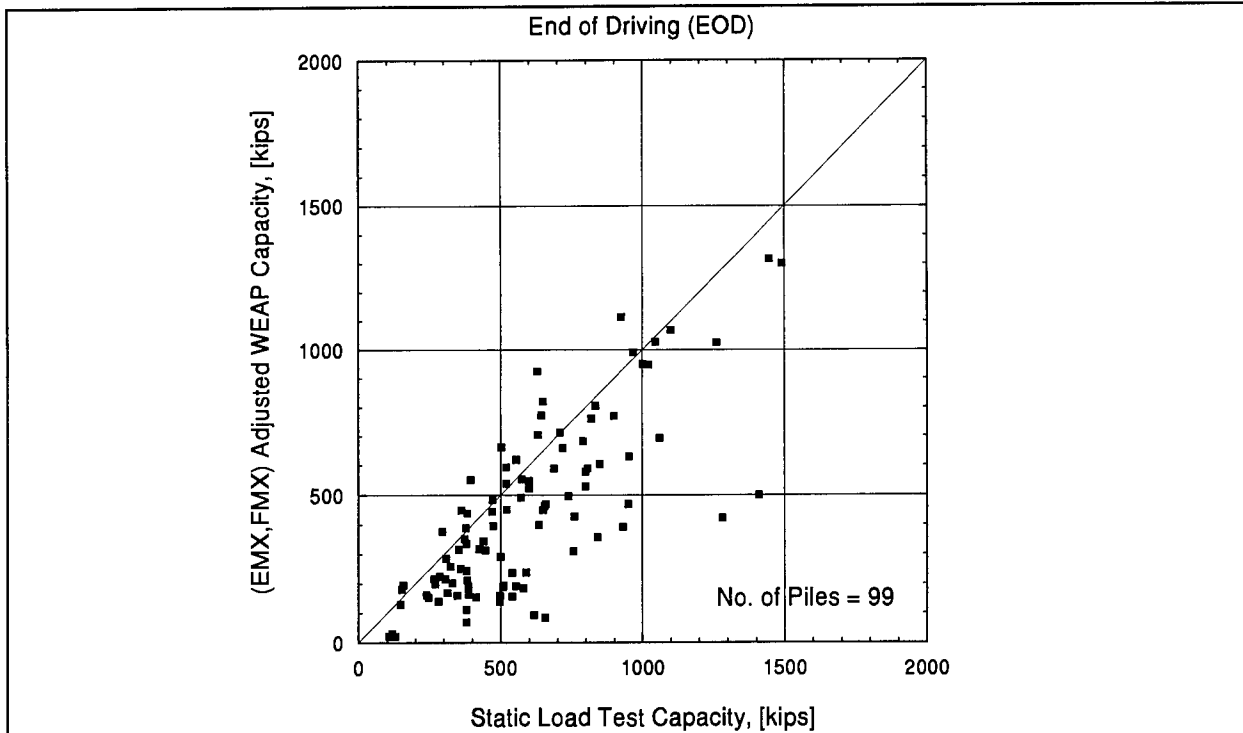


Figure 2.3: GRLWEAP EOD Capacity Correlations Using Smith Soil Model and Adjusted Hammer/Driving System Parameters

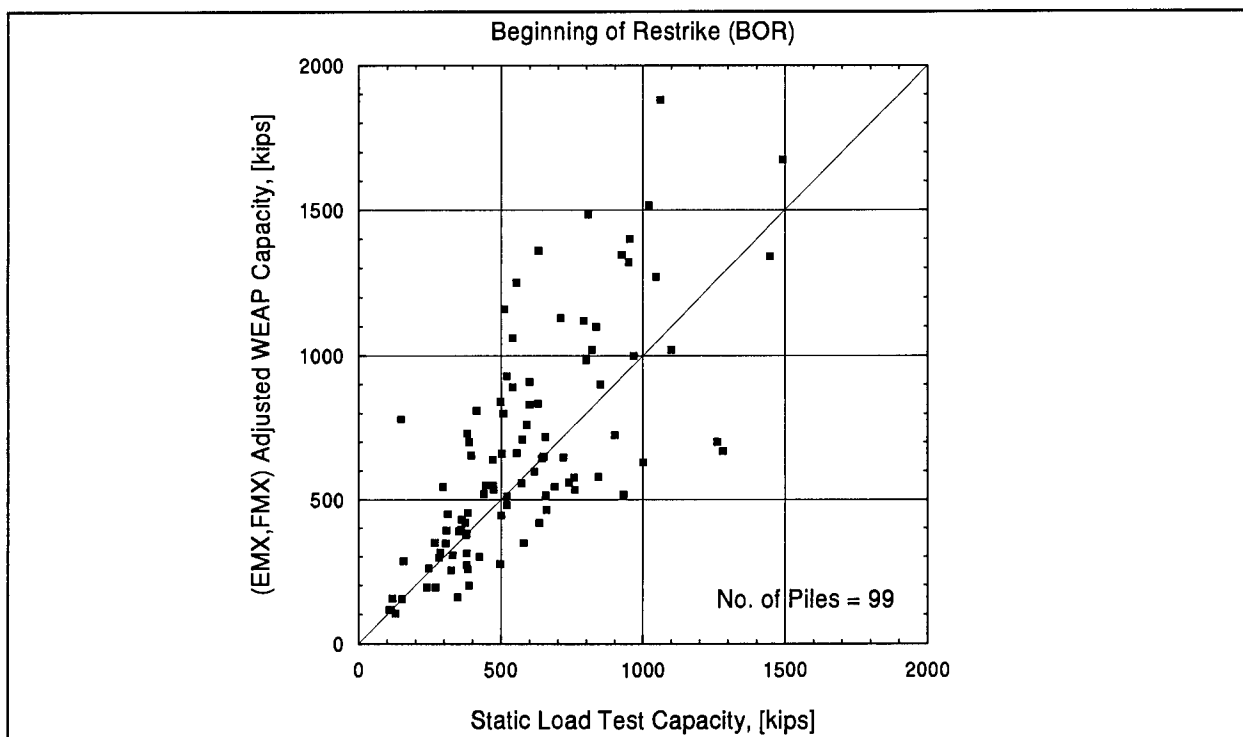


Figure 2.4: GRLWEAP BOR Capacity Correlations Using Smith Soil Model and Adjusted Hammer/Driving System Parameters

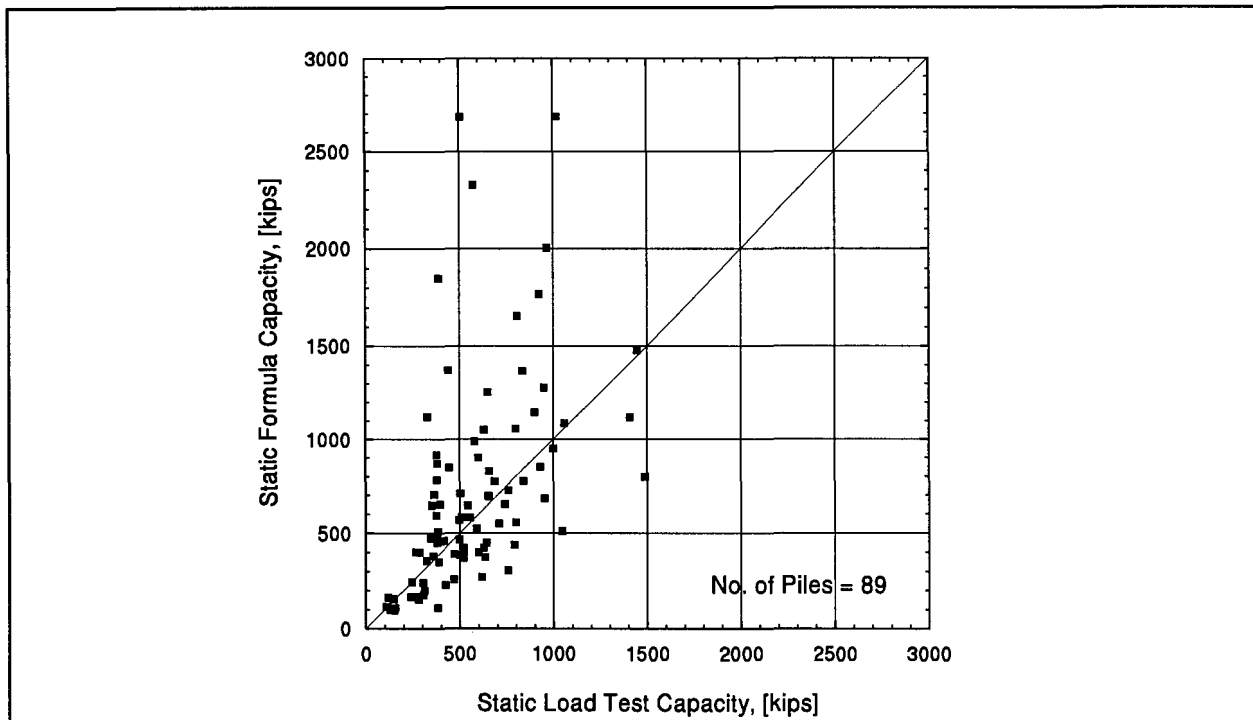


Figure 2.5: Capacity Correlation for Static Formula Prediction

discussion in chapters 2 and 3, histograms are replaced by the log-normal distributions. Of course, erratic histograms like EOD, will always be difficult to cast into a meaningful analytic form.

A log-normal curve was calculated for each capacity ratio and presented in figure 2.7. These curves aid in the relative evaluation of capacity predictions. The higher and narrower the curve of a particular method the better the precision of its prediction. The areas under the curve to the left or right of the perfect ratio 1.0 indicate whether the method would tend to underpredict or overpredict. Overpredictions appear with much greater prominence to the right of capacity ratio 1; underpredictions are squeezed between capacity ratios of 0 and 1. While it is reasonable to treat overpredictions with a greater emphasis than underpredictions, this feature might explain why underpredicting methods appear to have a somewhat greater precision than overpredicting ones.

Because of the potential for overemphasizing the peculiarities of a particular site (Correlation effort (d) in the previous section) for which more than one load test pile was included, figure 2.8 was constructed; it summarizes the prediction results for sites rather than piles (see also lines 2, 4, 6, and 8 of table 2.2). The somewhat narrower and higher curves, compared to those of figure 2.7) suggest that sites with several load tests had unusually complex properties.

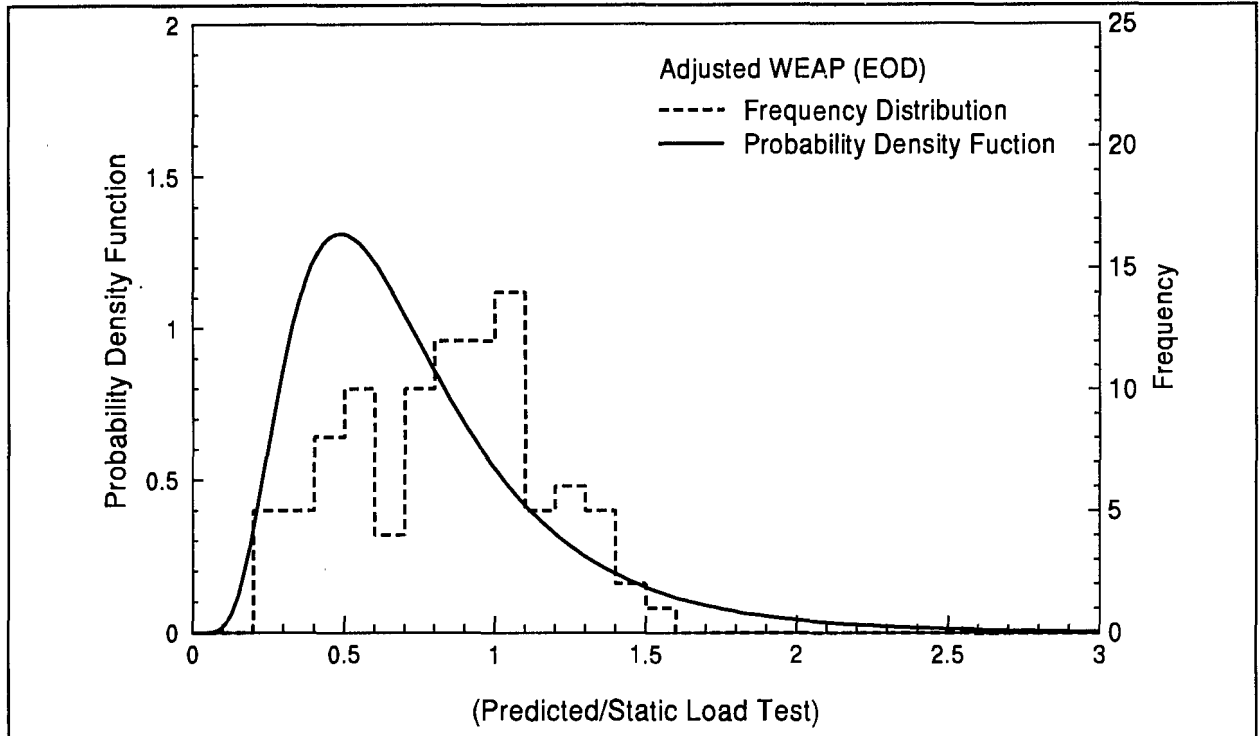


Figure 2.6(a): Frequency Distribution and Probability Density Function of Adjusted WEAP (EOD)

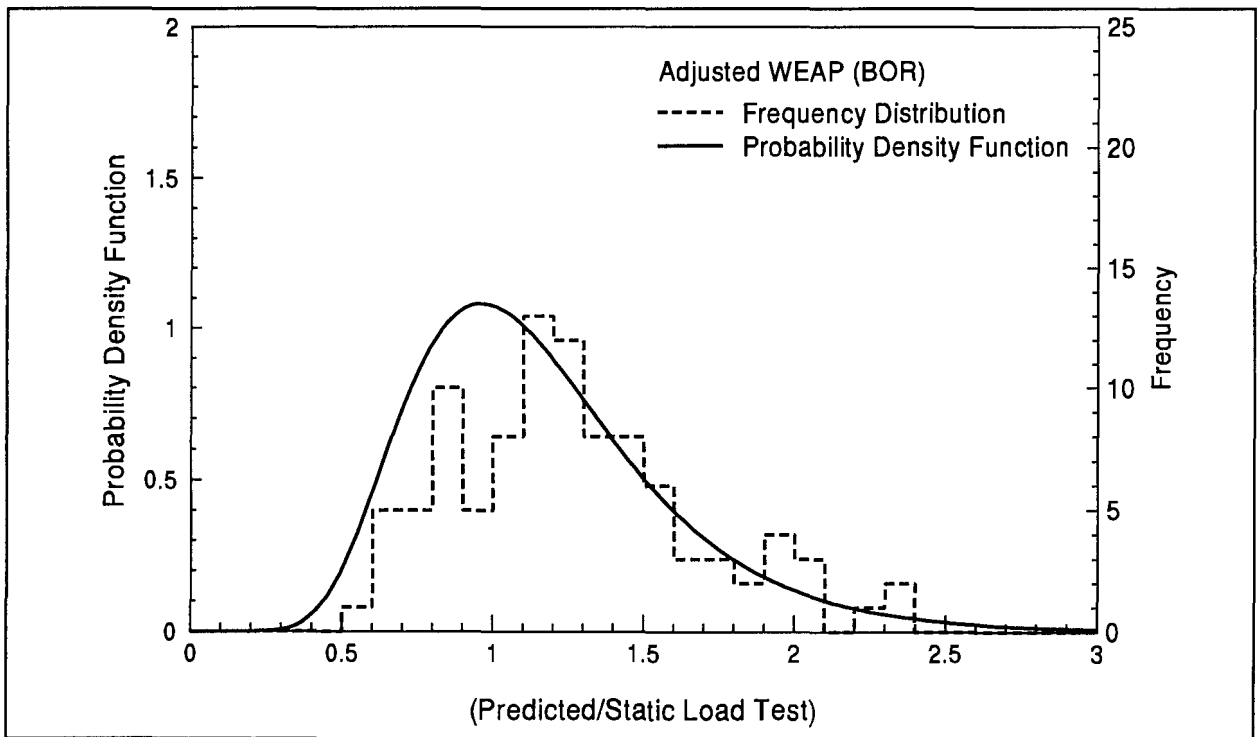


Figure 2.6(b): Frequency Distribution and Probability Density Function of Adjusted WEAP (BOR)

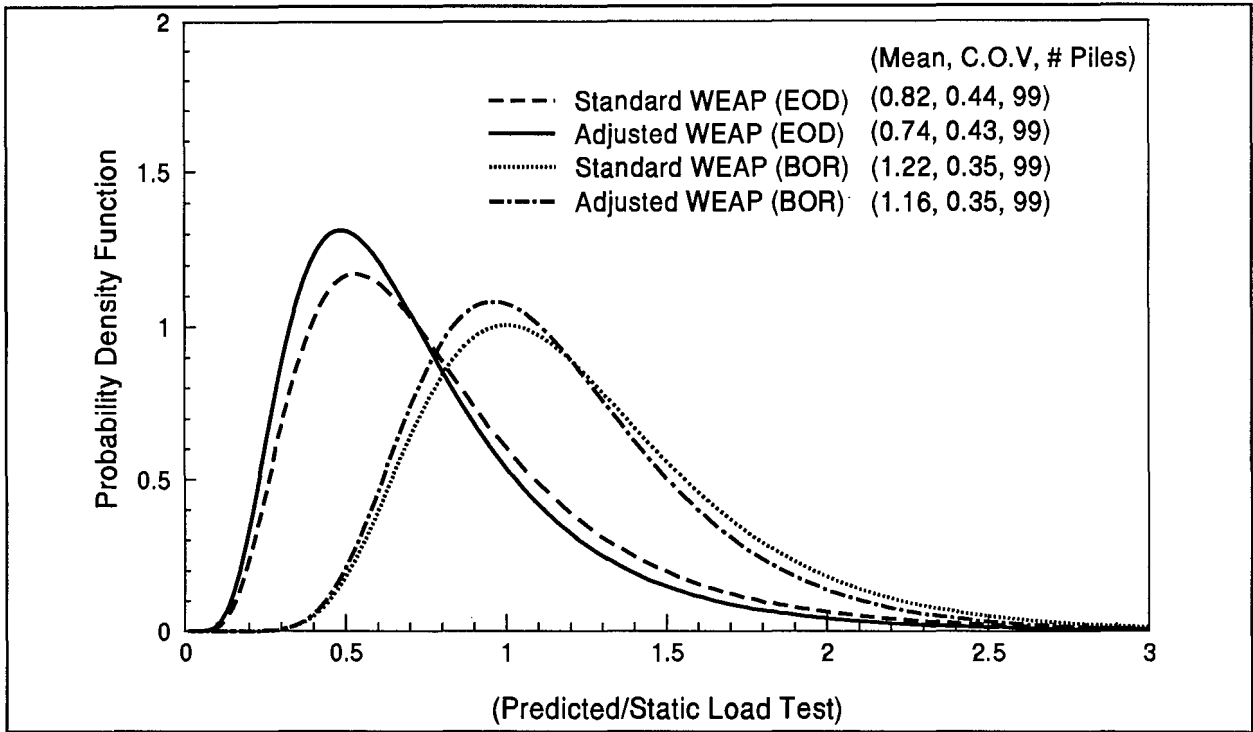


Figure 2.7: Log-Normal Probability Density for EOD and BOR Predictions with Standard Smith Model, and With and Without Adjusted Hammer/Driving System Parameters

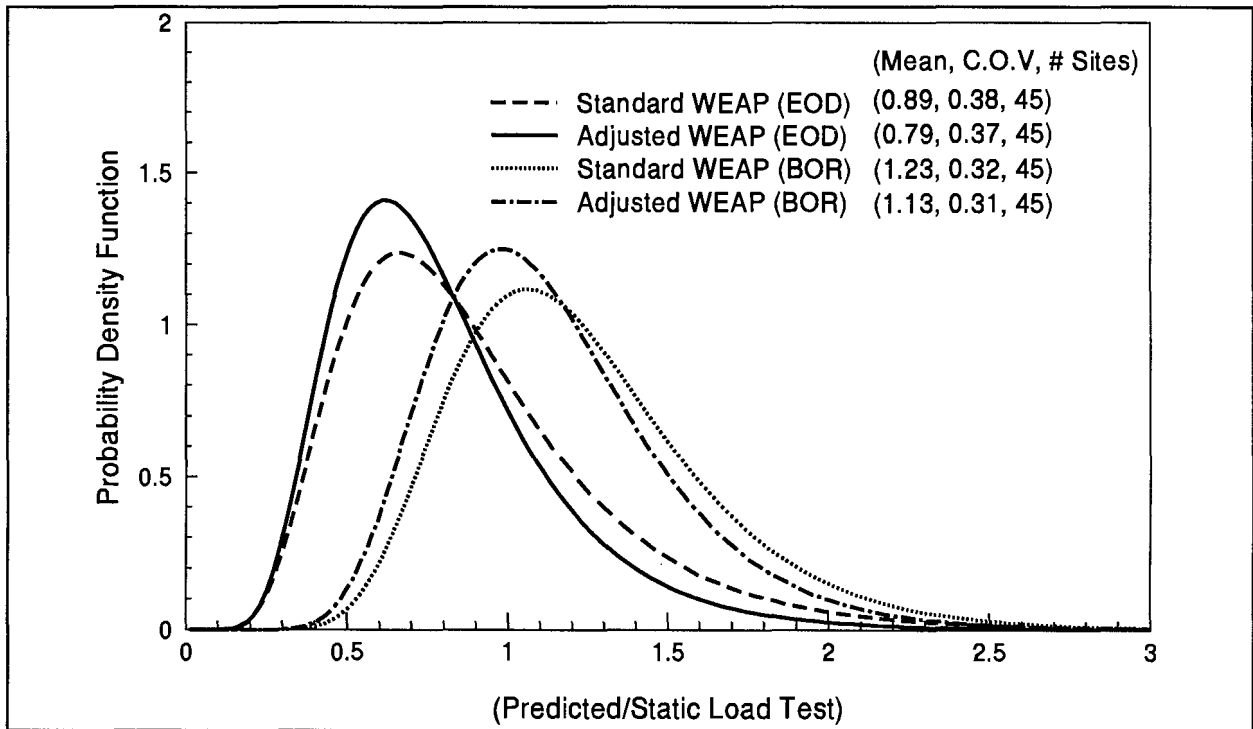


Figure 2.8: Log-Normal Probability Density for EOD and BOR Predictions (as in figure 2.7 but With Results Averaged for Same Site)

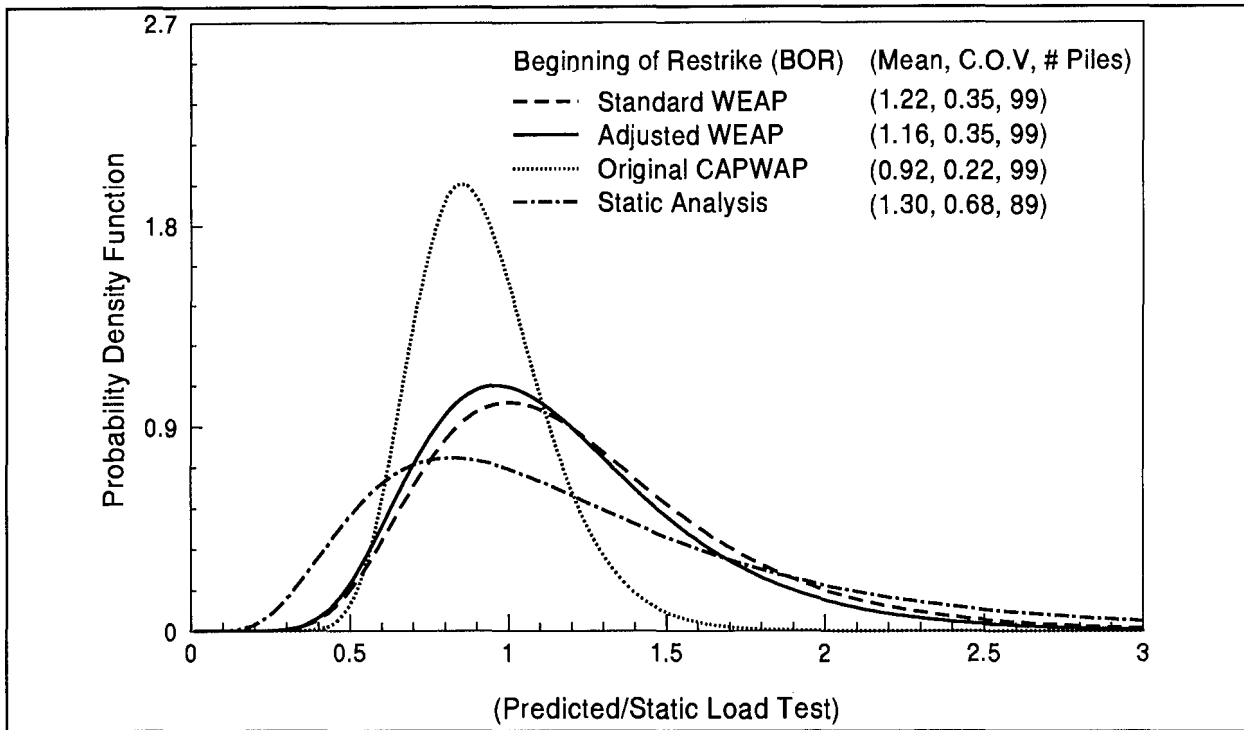


Figure 2.9: Log-Normal Probability Density for BOR Predictions with Several Methods

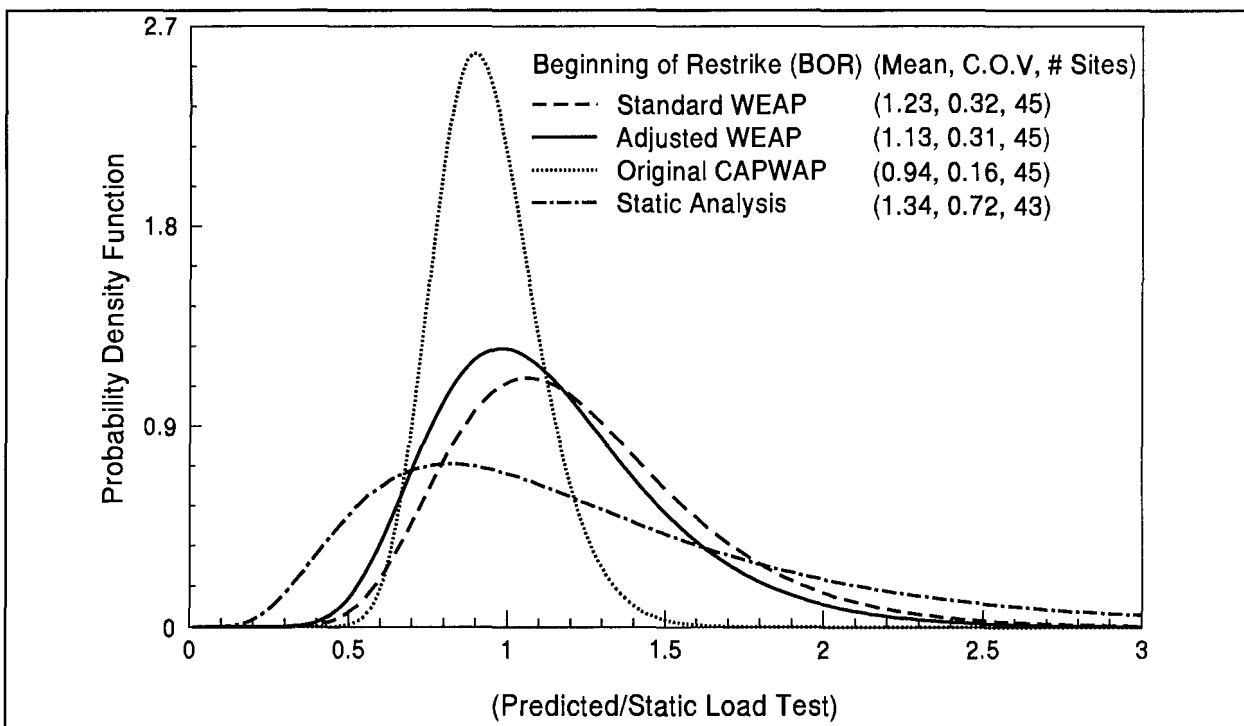


Figure 2.10: Log-Normal Probability Density for BOR Predictions (as in figure 2.8 but With Results Averaged for Same Site)

As a further comparison, the original CAPWAP restrrike predictions (line 9, table 2.2) to be discussed in chapter 3 were also plotted in figure 2.9, together with wave equation restrrike predictions (equivalent to figures 2.2 and 2.4) and the static formula approach (equivalent to figure 2.5). Figure 2.10 shows the same results averaged for sites.

It is well known that pile capacity changes with time after installation. Therefore, it is important to take into account the time difference when comparing the static load test capacity with the GRLWEAP prediction. To study these effects, the time difference between the static load test and the restrrike test is expressed as a ratio $T1/T2$, which is the number of days between the end of driving and static load test ($T1$), divided by the number of days between the end of driving and the restrrike test ($T2$). Thus, a time ratio ($T1/T2$) less than one means that the static load test was performed before the restrrike test. A ratio of 3.0 would mean that the static load test was performed three times later than the restrrike test.

Both the standard and (EMX,FMX) adjusted GRLWEAP capacity predictions were investigated for time effect. The static load test capacity vs the adjusted GRLWEAP (BOR) capacity (similar to figure 2.4) is presented in figure 2.11 distinguishing three different time ratios: less than 0.8, 0.8 to 3.0, and greater than 3.0. For a more quantitative assessment of figure 2.11, the log normal probability density for each time ratio group is presented in figure 2.12. The time ratio less than 0.8 has the highest and narrowest curve indicating best prediction. However, due to its relatively small sample ($N = 10$) compared to the other two time ratios, and since the means of the time ratio less than 0.8 and the time ratio of 0.8 to 3.0 were the same, the data set from these two time ratios were combined in figure 2.13. Table 2.3 summarizes the GRLWEAP capacity correlation for the two time ratios. Obviously, the time of restriking, relative to the time of static testing plays a major role in achieving a quality prediction. Early restriking appears to be one of the reasons why wave equation BOR predictions are sometimes disappointing.

2.6.2 Dynamic Soil Model Properties

The procedure for back-calculating damping parameters is described in table 2.1. This procedure attempted to overcome the problem of non-uniqueness: a higher shaft damping factor could be compensated for by a lower toe damping factor or increases in quakes could be compensated for by decreases in damping. Therefore, quakes were fixed and damping factors proportionately adjusted or fixed when the associated static resistance was low. Results are presented in figures 2.14 and 2.15 for shaft and toe damping, respectively. The soil classifications represent the average properties indicated in the borings (obviously this is an unprecise classification). For the toe damping factors, the associated SPT N-values are also shown in the figure. Back-calculated results vary strongly within the same soil types and, surprisingly, even the averages show very little correlation with soil type. In fact, the omitted case, Data base ID# 122 (see section 2.3) indicated a shaft damping factor of 3.5 s/ft (greater

Table 2.3: Statistical Summary of Capacity Ratios at Different Time Ratios					
Prediction Method	Time Ratio ¹	Number of Piles	Mean	Standard Deviation	Coefficient of Variation (C.O.V)
Standard GRLWEAP	less than 3	59	1.25	0.38	0.30
	greater than 3	40	1.19	0.50	0.42
(EMX,FMX) Adjusted GRLWEAP	less than 3	59	1.18	0.35	0.30
	greater than 3	40	1.14	0.49	0.43

Note: 1 - Time Ratio = (Time of Static Load Test / Time of Restrike Test)
 < 1 when Static Load Test is performed before Restrike Test
 > 1 when Static Load Test is performed after Restrike Test.

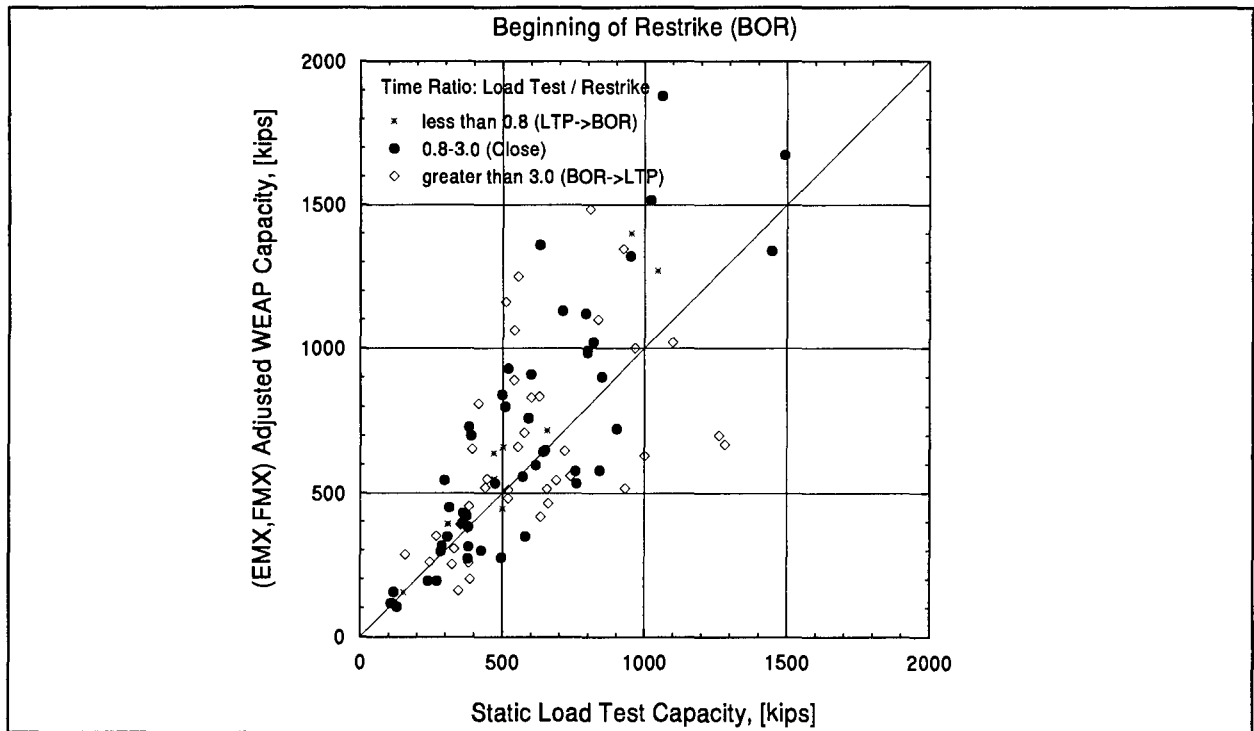


Figure 2.11: Adjusted GRLWEAP BOR Capacity Correlation for Different Time Ratio

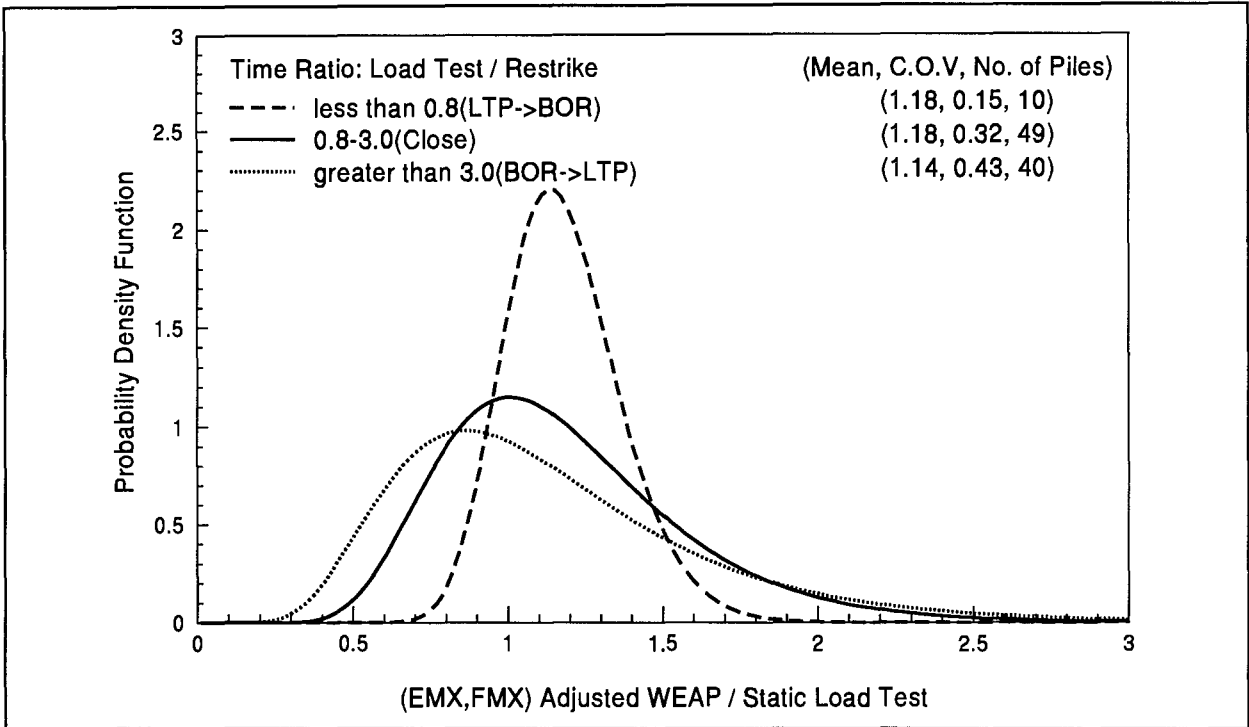


Figure 2.12: Log Normal Probability Density for Adjusted GRLWEAP BOR Capacity with Three Different Time Ratios

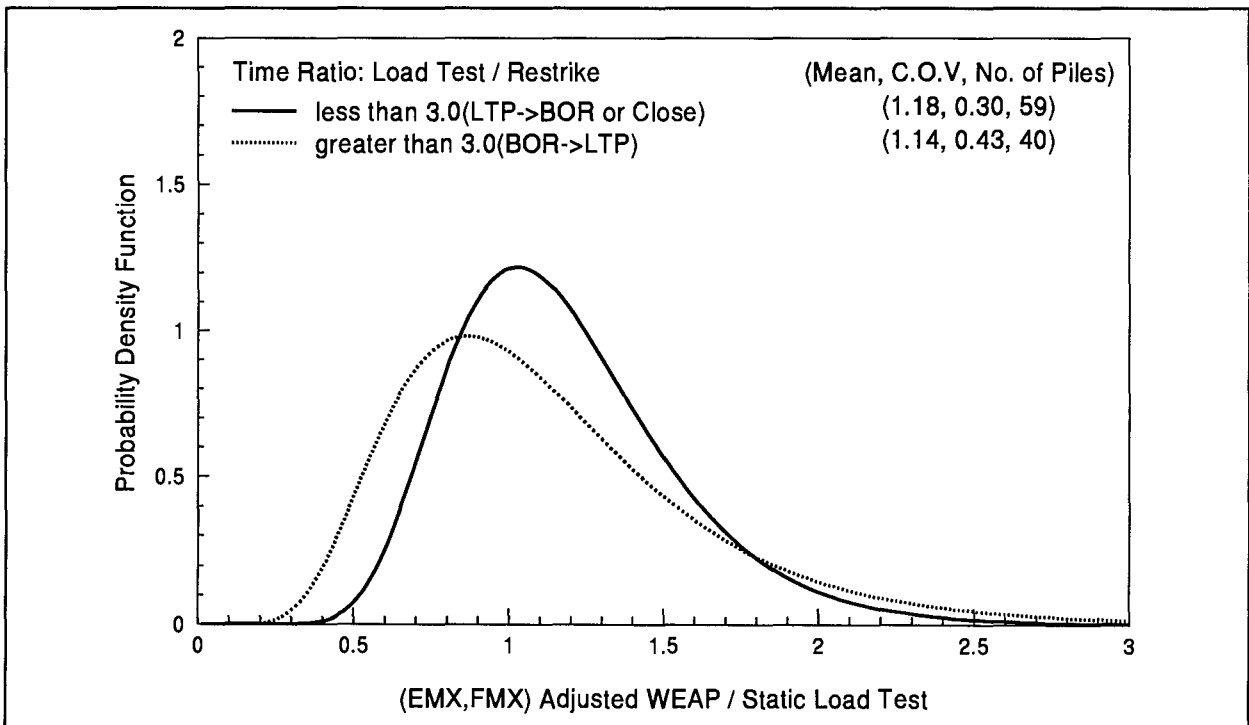


Figure 2.13: Log Normal Probability Density for Adjusted GRLWEAP BOR Capacity with Two Different Time Ratios

than 10 s/m). The variability of calculated factors is in part attributed to the uncertainty of BOR blow count and energy levels.

It is surprising how much greater the average damping factors are when compared with normal recommendations. Again, this fact might be attributed to the restrike situation. Reasons for this high magnitude and the scatter have been investigated. Comment (f) in section 2.5 pointed out the potential effect of low velocities. Among other possibilities is the influence of time or a "setup of the shaft damping factor" (Svinkin and Teferra, 1994). Indeed, several cases were studied for sites where restrikes were performed at various time intervals, and an increasing tendency of damping factor with time could be observed. Figure 2.16 indicates trends thus established.

For the shaft damping, it appears that silts and fine sands should have damping factors of 0.1 s/ft (0.33 s/m); gravels would yield satisfactory results with 0.05 s/ft (0.17 s/m). These three, relatively uniform soil types indicated the least variability in damping factor. Mixtures of soils, non-fine sands and clays seem to behave much more erratic; average damping factors typically vary between 0.2 and 0.3 s/ft (0.66 and 1.0 s/m) for sands and mixed soils and 0.8 s/ft (2.6 s/m) for clay.

The calculated average toe damping values were not as variable as the shaft values ranging from 0.1 to 0.2 s/ft (0.33 to 0.66 s/m) with the exception for sand and gravel for which 10 times lower factors seemed satisfactory. The surprisingly large rock damping value of nearly 0.2 s/ft (0.66 s/m) might be attributed to cases with piles driven into weathered rock or shale where relaxation often occurs. Cases of piles driven into hard rock would yield excessive blow counts and/or non-failing static load tests and therefore are not included in the data base.

Again, it should be emphasized that the values summarized in this study pertain to restrike situations with sometimes very low pile toe velocities (near refusal); this situation makes capacity predictions rather insensitive to toe damping factor variations. Results from SPT measurements (discussed in chapter 6) actually suggest that end of driving toe damping factors are much smaller than calculated from this correlation study. Furthermore, no differentiation has been made between pile types (e.g., displacement and non-displacement piles), geology, time of testing relative to the load test, and soil conditions such as soft, hard, saturated, non-saturated, underconsolidated, or overconsolidated materials among other important conditions. For example, it is possible that the low shaft damping values in clay occur primarily in hard clays. With a data base in existence, hopefully further enlarged in the future, more meaningful studies can and should be performed which check these effects.

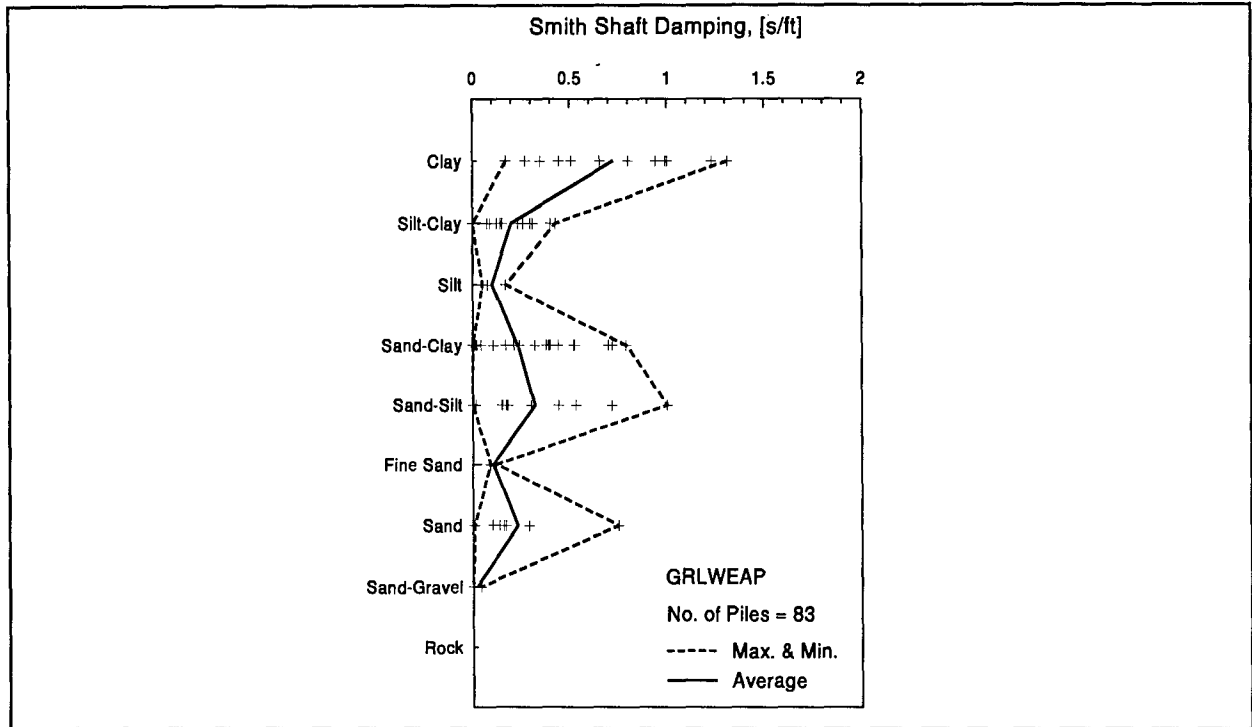


Figure 2.14: Smith Shaft Damping Factors Back-Calculated for Piles with More Than 30 Percent Shaft Resistance

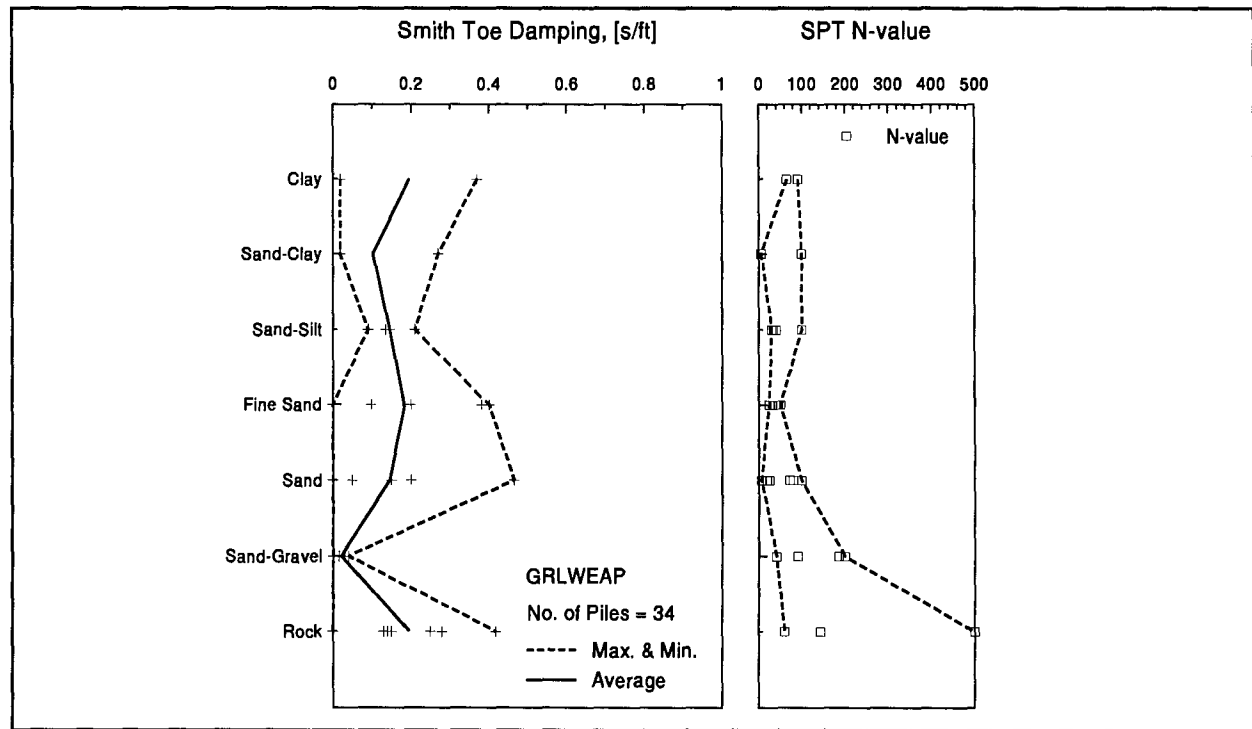


Figure 2.15: Smith Toe Damping Factor Back-calculated For Piles with Less Than 70 Percent Shaft Resistance

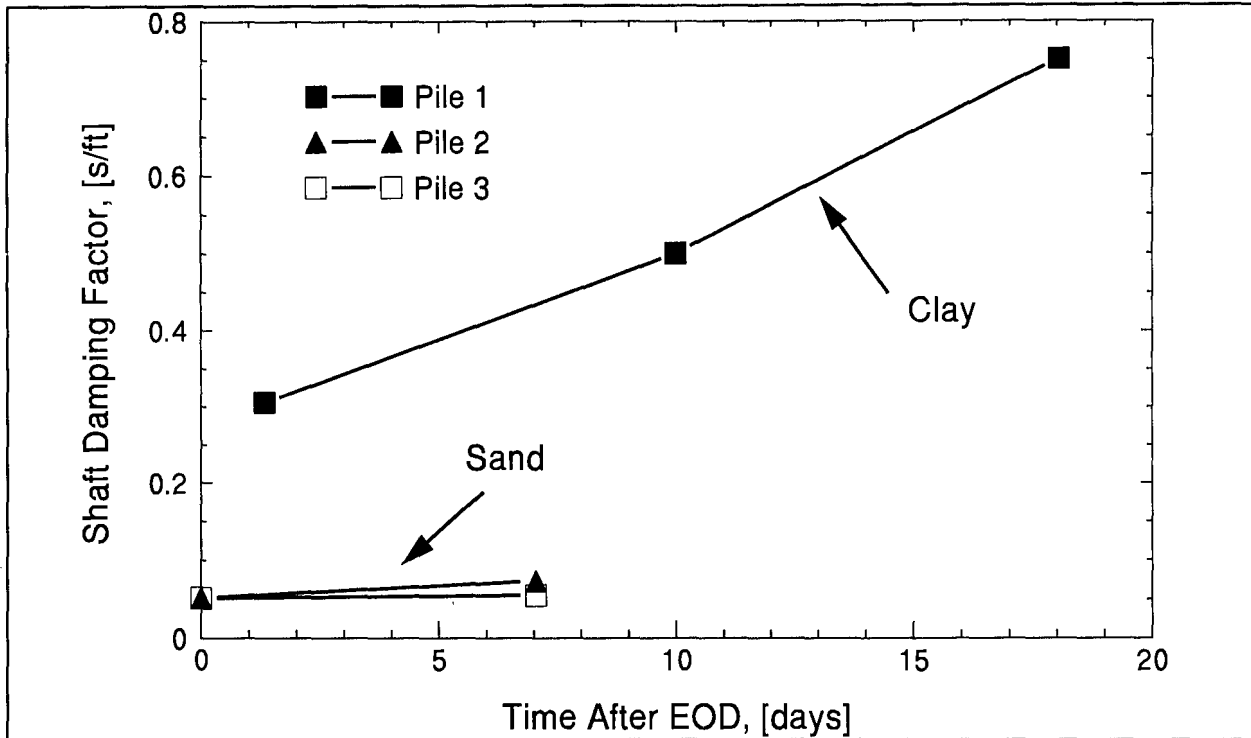


Figure 2.16: Increasing Tendency of Shaft Damping with Time (Svinkin and Teferra, 1994)

2.6.3 Apparent Setup Factors

Ideally, restrike testing would not be routinely necessary for long-term bearing capacity assessment. Setup factors would describe the gain of soil strength during the setup period following pile installation. For setup calculations, the most difficult problem is determining the EOD capacity. In this study, EOD capacities and therefore "apparent" (because they are not exact) setup factors were calculated in two different ways. First, the damping factors and quake values back-calculated from restrike test and load test were used in a wave equation analysis which then, with the EOD blow count, indicated an EOD capacity. The static load test capacity was then divided by this "correlated" EOD capacity to yield the "correlated setup factor." The second method utilized the standard Smith soil parameters for the EOD wave equation analysis and thus yielded a "standard setup factor." The latter approach lends itself to a generally applicable method for situations without any load test or restrike test.

Figure 2.17 shows correlated setup factors organized according to shaft soil type (see also (c) in section 2.5) for all piles of the data base with more than 50 percent shaft resistance. These results are highly variable for clay, silt, and sand-clay. For all other soil types, the setup factors average approximately 1.5.

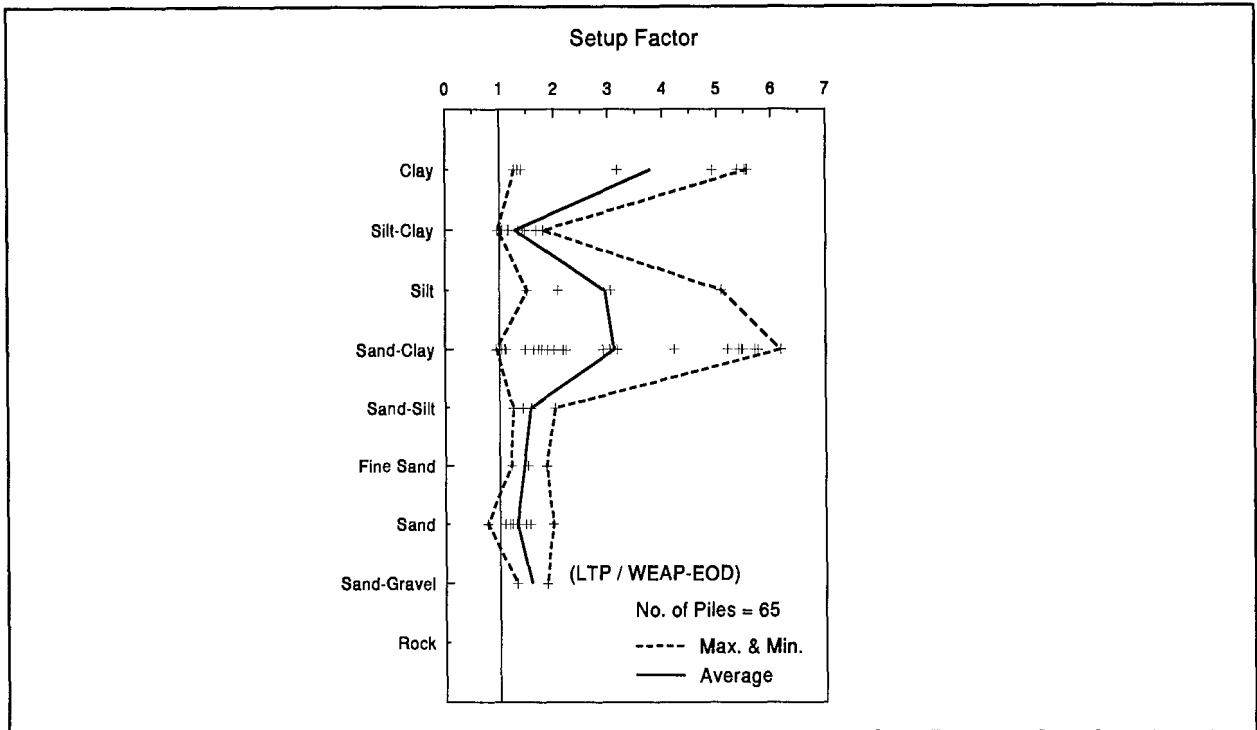


Figure 2.17: Correlated Setup Factors for Piles with More Than 50 Percent Friction

Figure 2.18 is based on EOD analyses with standard Smith parameters; individual sites, not piles, were included. Surprisingly, clays appear to be much less variable than in figure 2.16. The reason is the rather large magnitude of restrike damping factors back-calculated from restrike tests which made the EOD capacities very low and therefore the correlated setup factors high. Sand-clay and sand-silt mixtures indicate a high variability. A number of data points fell below the 1.0 line which means that relaxation was indicated, if the EOD analysis was correct. A reduced variability with less apparent relaxation was formed when the adjusted hammer performance was used for the EOD analysis (figure 2.19).

CAPWAP predictions from EOD measurements were also used to calculate a "CAPWAP" setup factor. Comparing these factors with those from the standard Smith analyses, figure 2.20, a remarkably good agreement between correlated and CAPWAP setup factors, averaged for each soil type, was indicated. Clay was the only exception. Based on these results a table of conservative setup factors was established; these values are both graphically and numerically depicted in figure 2.20. The circle was then closed by recalculating the long-term pile capacity from the adjusted EOD GRLWEAP analysis and multiplication with the apparent setup factor from figure 2.20. The same process was applied to CAPWAP predictions from EOD. Results are shown in figure 2.21. Obviously, the average prediction now better agrees with the load test

average, however, the variability of these predictions is greater than that of the unfactored results.

Since grain size based soil types apparently do not represent a reliable indicator of setup factors, another grouping of apparent setup factors may be of interest. Recognizing that piles in certain states are often driven into similar geologic materials, the setup factors were also organized first by state and secondly according to variability of apparent setup factor as shown in figure 2.22. The variability of the data of the State of Wisconsin and several other states was surprising. As a check, the CAPWAP indicated set-up factors were also plotted in figure 2.23. This graph showed less scatter, except for Louisiana where a great variety of fine grained soils has always made capacity predictions based on EOD information very difficult.

In summary, the concept of using setup factors to supplement or replace restrrike tests is promising. Naturally, it is important that accurate EOD capacities and associated apparent setup factors be reliably established. The setup factor should be considered an additional dynamic soil parameter like damping and quake. Studies with the modified SPT discussed later in this report indicate that a direct in-situ measurement of this quantity is sometimes possible.

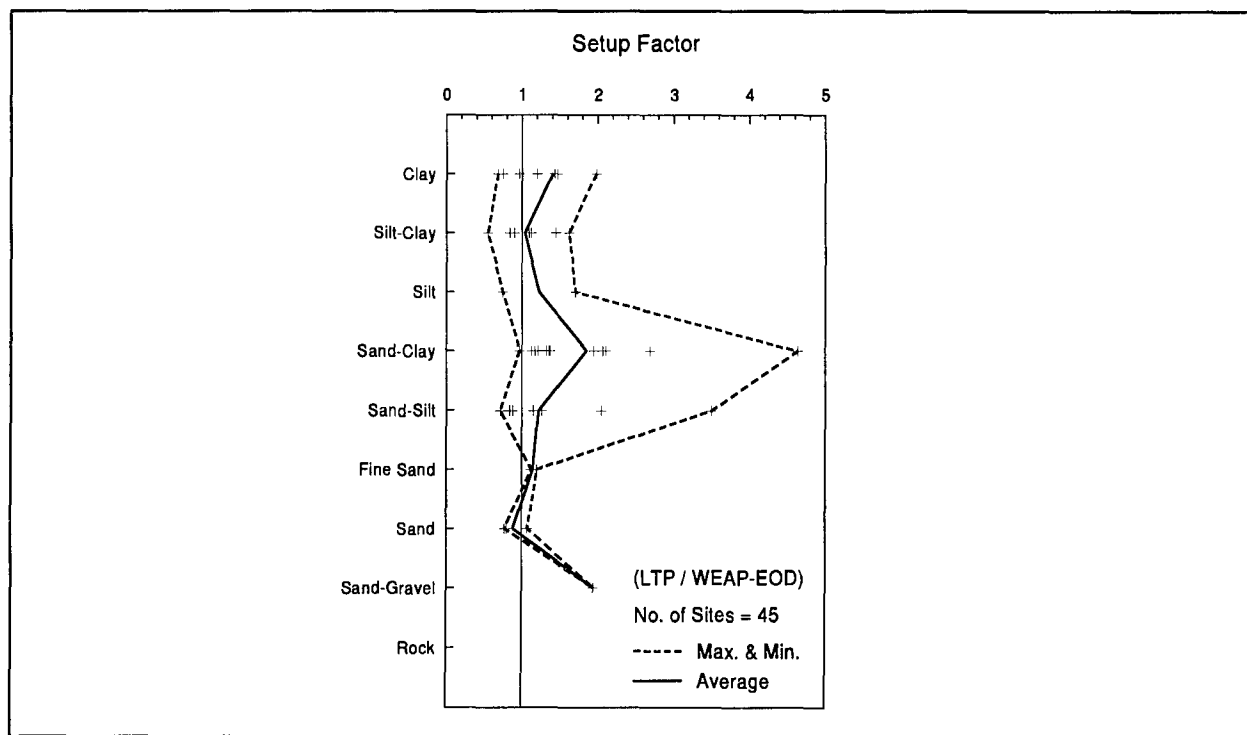


Figure 2.18: Standard Setup Factors from Unadjusted Wave Equation EOD Analysis

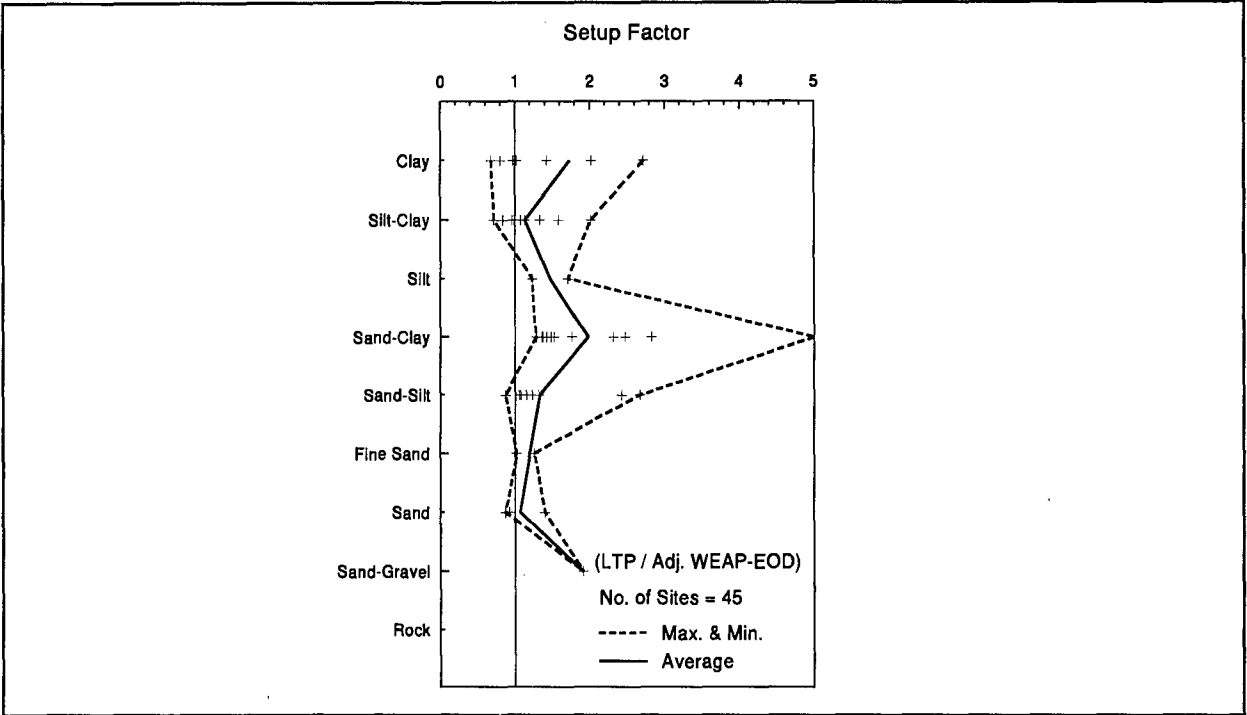


Figure 2.19: Setup Factors Based on Standard Smith EOD Analyses with Adjusted Hammer/Driving System Parameters

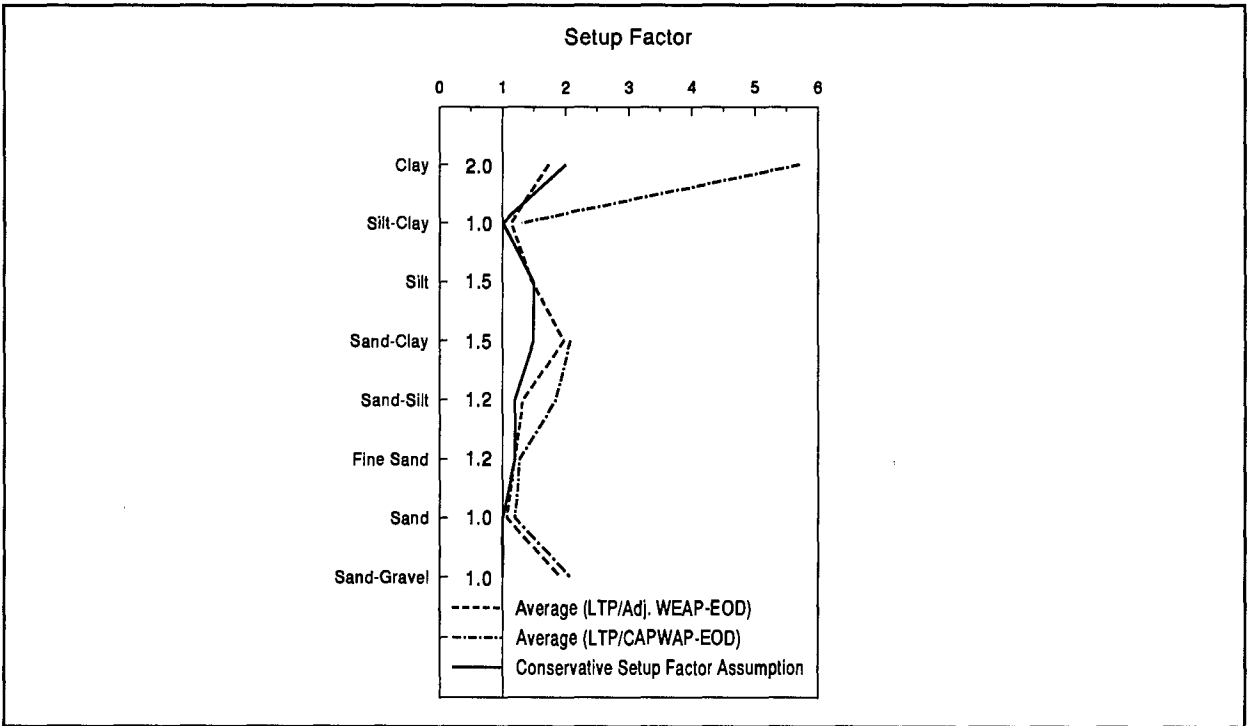


Figure 2.20: Average Standard Setup Factors and Recommended Setup Factors

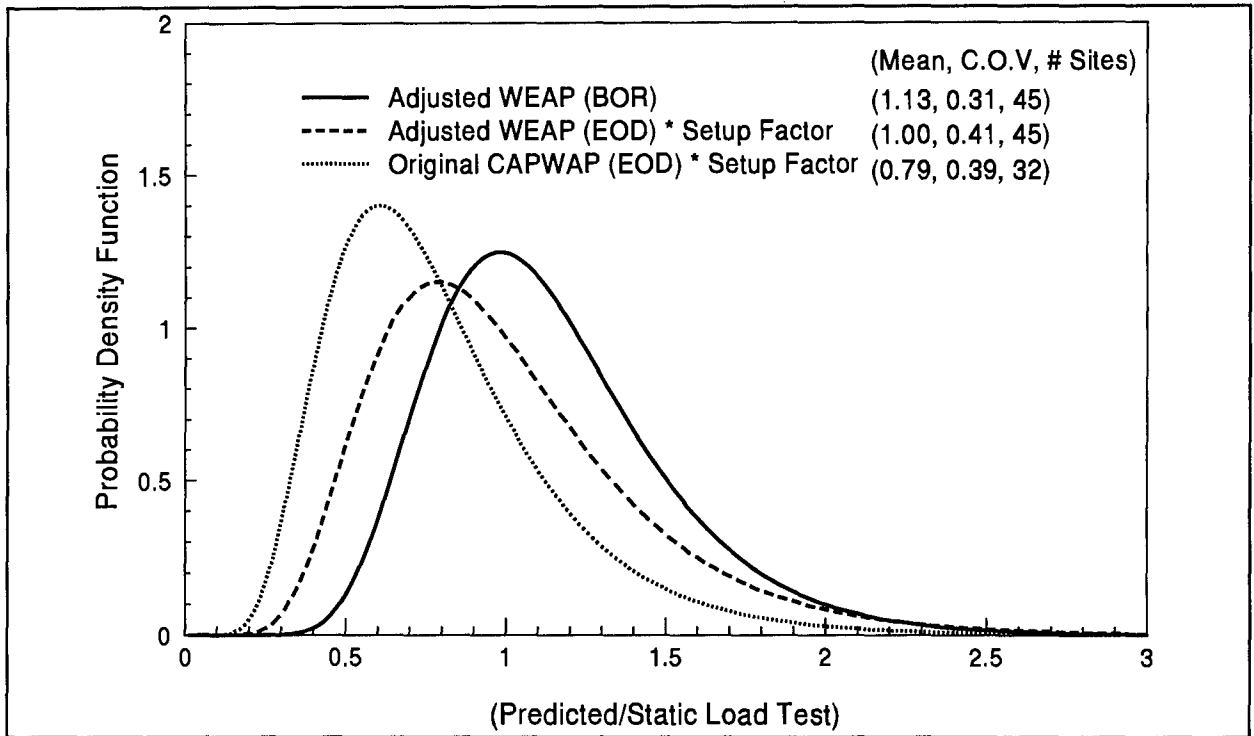


Figure 2.21: Log-Normal Probability Density for Standard EOD and CAPWAP EOD Factored with Conservative Setup Factors (Apply Only to Non End Bearing Pile)

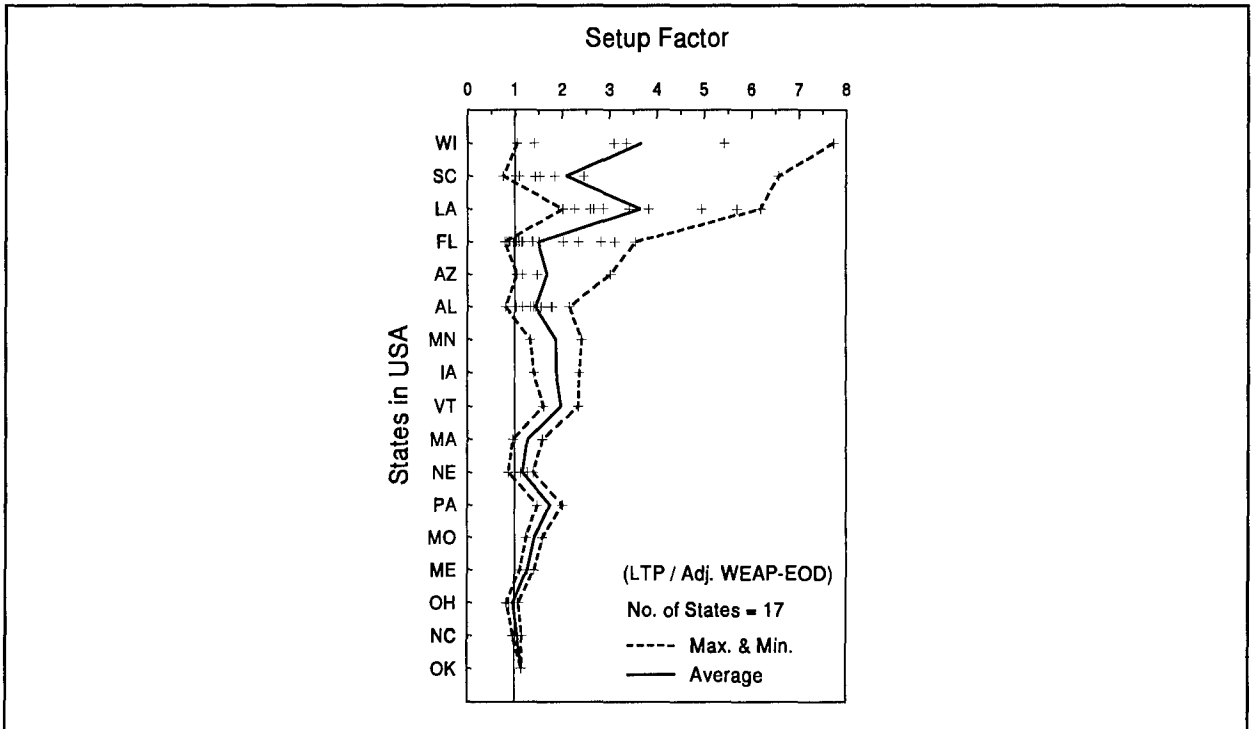


Figure 2.22: Apparent Setup Factors for Various States (Load Test / Adjusted WEAP-EOD)

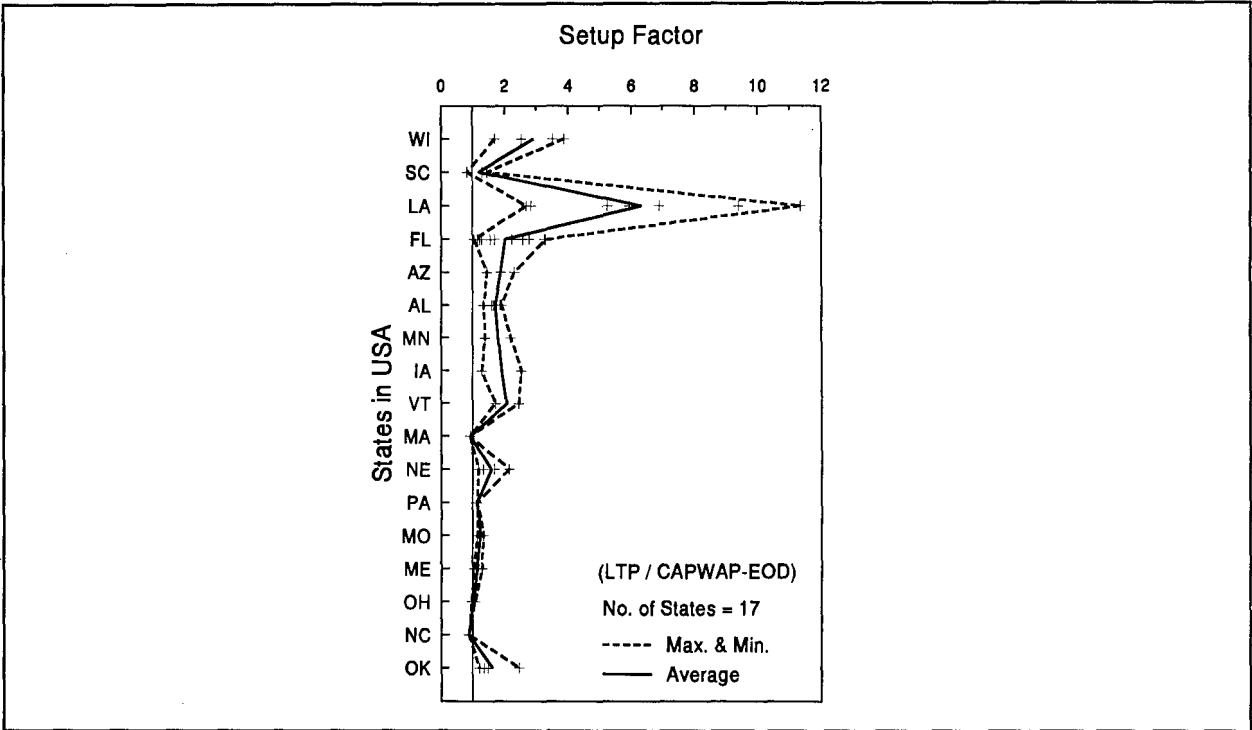


Figure 2.23: Apparent Setup Factors for Various States (Load Test / CAPWAP-EOD)

CHAPTER 3

CAPWAP CORRELATION AND SOIL PARAMETER CALCULATIONS

3.1 INTRODUCTION

One of the criteria for a data set to be accepted into the data base is the availability of dynamic testing results from restrike testing which can be used to establish correlation with a static load test. CAPWAP analysis of the dynamic restrike test data has been a standard procedure for pile capacity prediction (see also volume III). The objectives of this CAPWAP study described herein include:

- (a) to critically re-evaluate the CAPWAP analysis procedures and results;
- (b) to investigate statistically the reliability of CAPWAP capacity prediction;
- (c) to study the soil radiation damping model which has been included in the CAPWAP program and based on the study results, to give some guidelines of how to use radiation damping; and
- (d) to investigate relationships between the dynamic parameters (damping and quake) and soil types surrounding the pile.

The basis for any correlation study is the static load test result. The remarks about the value of the data base, capacity time dependence, and accuracy of static load test evaluation discussed in chapter 2 are again appropriate.

Several CAPWAP capacities are presented in this study. The "*original*" CAPWAP capacities, obtained from an existing CAPWAP result, were presented in chapter 2. These values came from different versions of the CAPWAP program, and were analyzed by different engineers using various computer hardware (newer faster PC's allow a more thorough investigation so more recent results may tend to be more reliable). For consistency of comparison during this study, the dynamic results were reanalyzed with CAPWAP®, Version 1.993-1. This CAPWAP program has a built-in automatic search capability based on about 25 years of experience which will provide a solution using optimal matching of signals with no user interaction. The experienced user can (and should) also interact in a manual operating mode to iteratively seek a best match solution. The CAPWAP reanalyzed results include the "*automatic*," "*best match*," and "*radiation damping*" solution results.

The automatic results were obtained from the CAPWAP automatic matching process and therefore the results were completely independent of an engineer's interpretation or skills. After the CAPWAP automatic matching was completed, the matching was iteratively improved by GRL's engineer to obtain a "best match" with a standard soil model. This process involved, as a minimum, the review and often adjustment of resistance distribution and other dynamic parameters, and almost always resulted in a lower match quality value (less error). After the best match results were obtained, the "radiation damping" model was inserted and analyzed to yield a third CAPWAP capacity results. Each of these CAPWAP capacities were compared with the static load test capacities in figures 3.1(a), 3.2(a) and 3.3(a) for automatic, best match, and radiation damping match, respectively.

In addition, for an easier comparison, the ratios of CAPWAP capacity to static load test capacity were also computed for each pile, and the statistical mean, coefficient of variation (standard deviation divided by the mean), number of piles and the log-normal probability density function were presented for each sample population. Probability density functions are presented in figures 3.1(b), 3.2(b) and 3.3(b) to allow for a qualitative assessment of different CAPWAP capacities or an assessment of different criteria. The means and coefficients of variation from each result are also summarized in table 3.1.

Time Ratio ¹	Number of Piles	Mean			Coefficient of Variation		
		Auto-matic	Best Match	Radiation	Auto-matic	Best Match	Radiation Damping
less than 0.8	11	0.97	0.96	1.04	0.20	0.16	0.13
0.8-3.0	41	0.98	0.95	1.03	0.18	0.15	0.09
greater than 3.0	30	0.94	0.89	1.00	0.29	0.17	0.21

Note: 1 - Time Ratio = (Time of Static Load Test Capacity / Time of BOR CAPWAP Capacity)
 < 1 when Static Load Test is performed before Restrike
 > 1 when Static Load Test is performed after Restrike.

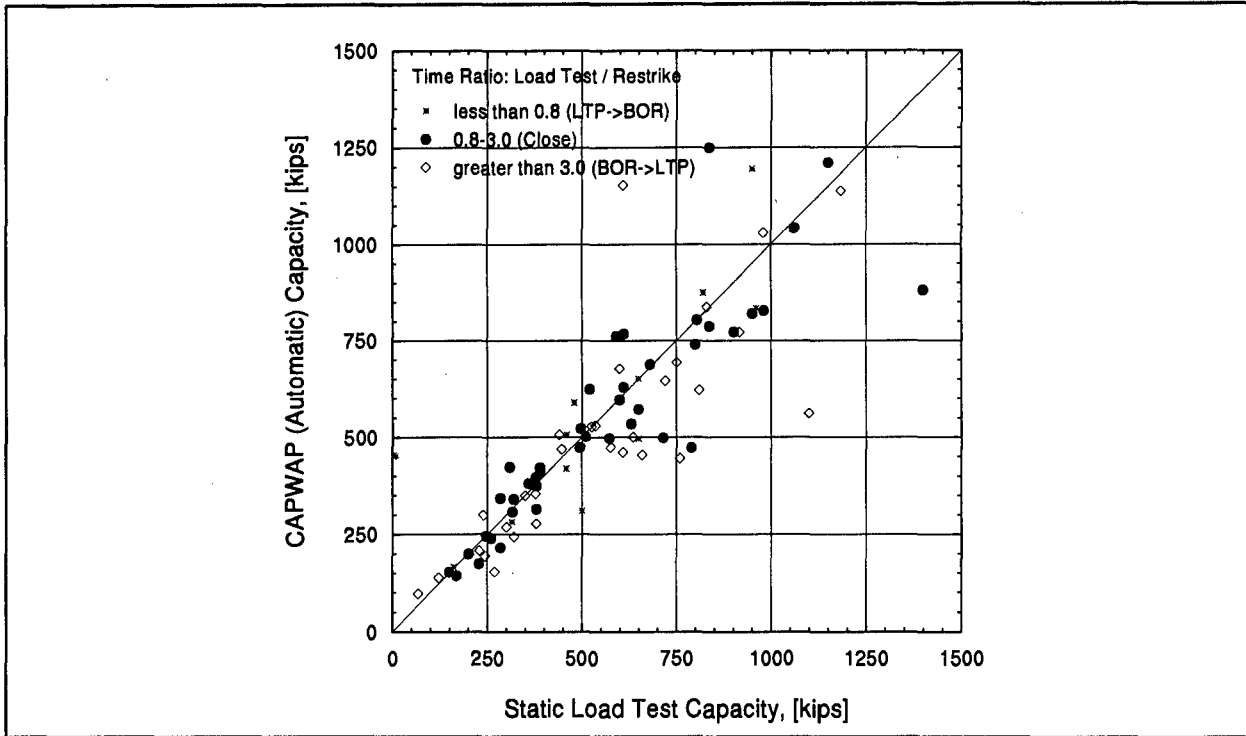


Figure 3.1(a): CAPWAP (Automatic) Capacity versus Static Load Test Capacity Showing Different Time Ratios

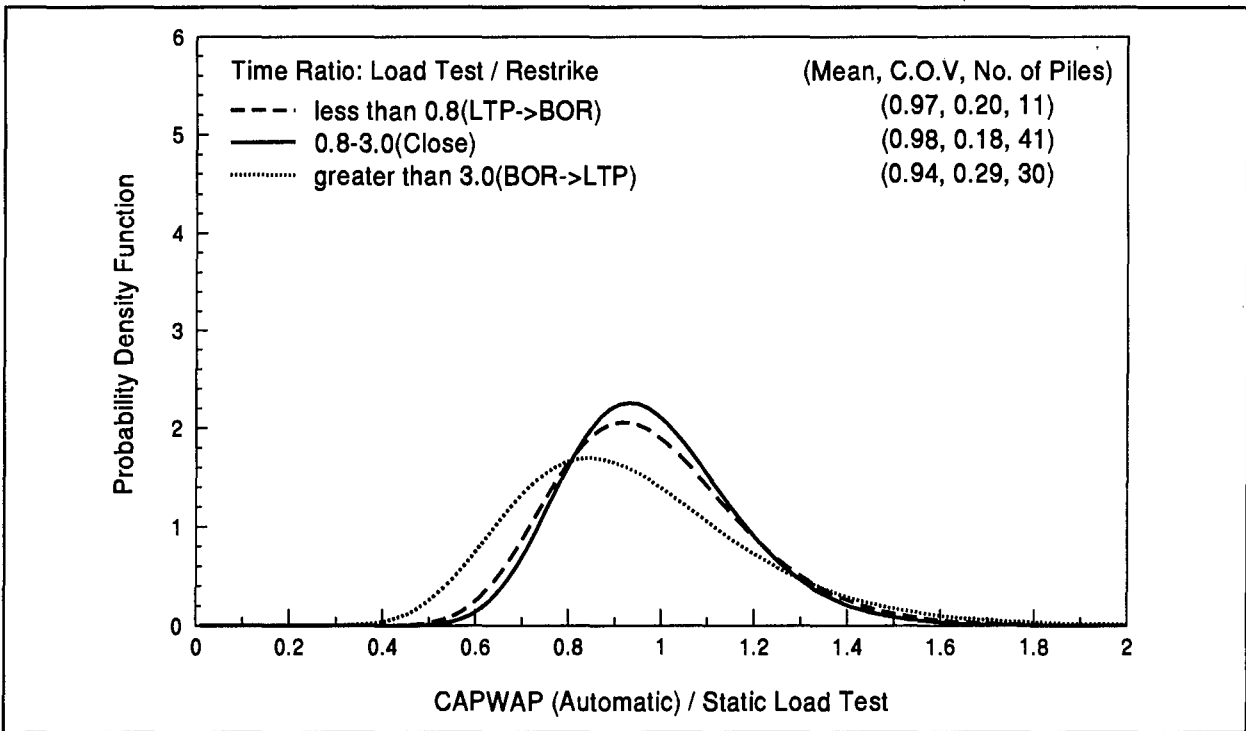


Figure 3.1(b): Log-Normal Probability Density Function for CAPWAP (Automatic) Capacity Prediction at Different Time Ratios

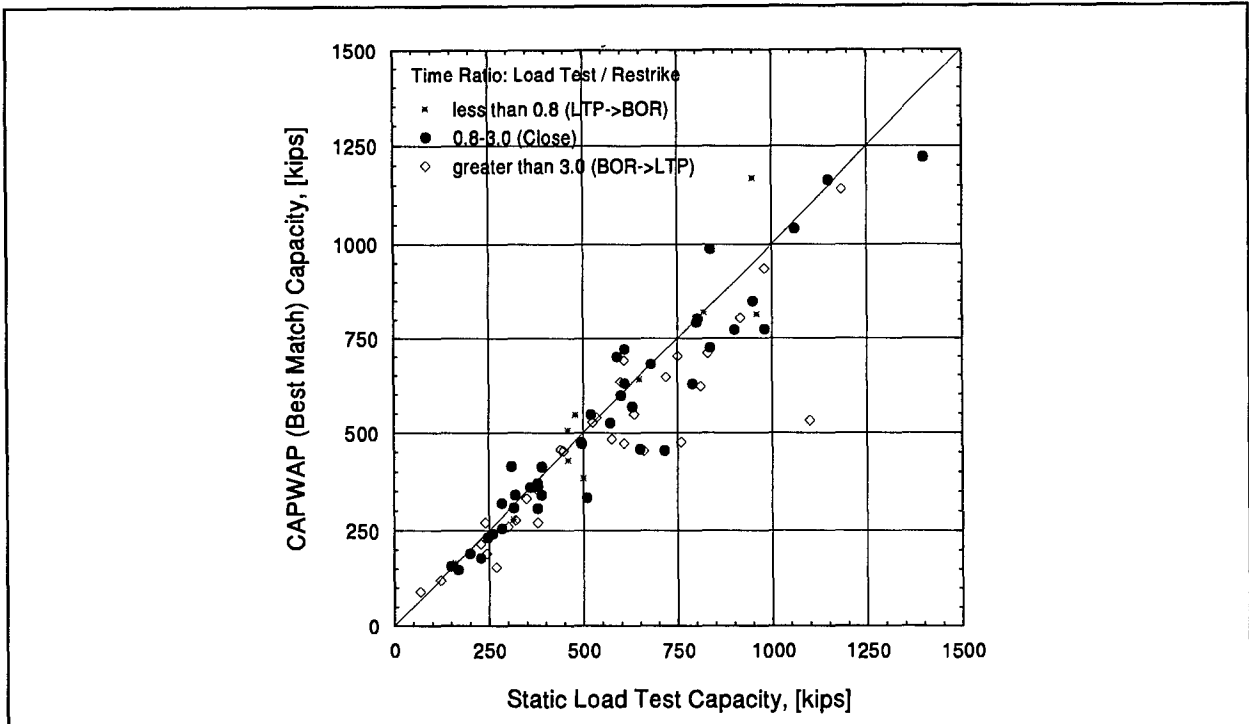


Figure 3.2(a): CAPWAP (Best Match) Capacity versus Static Load Test Capacity Showing Different Time Ratios

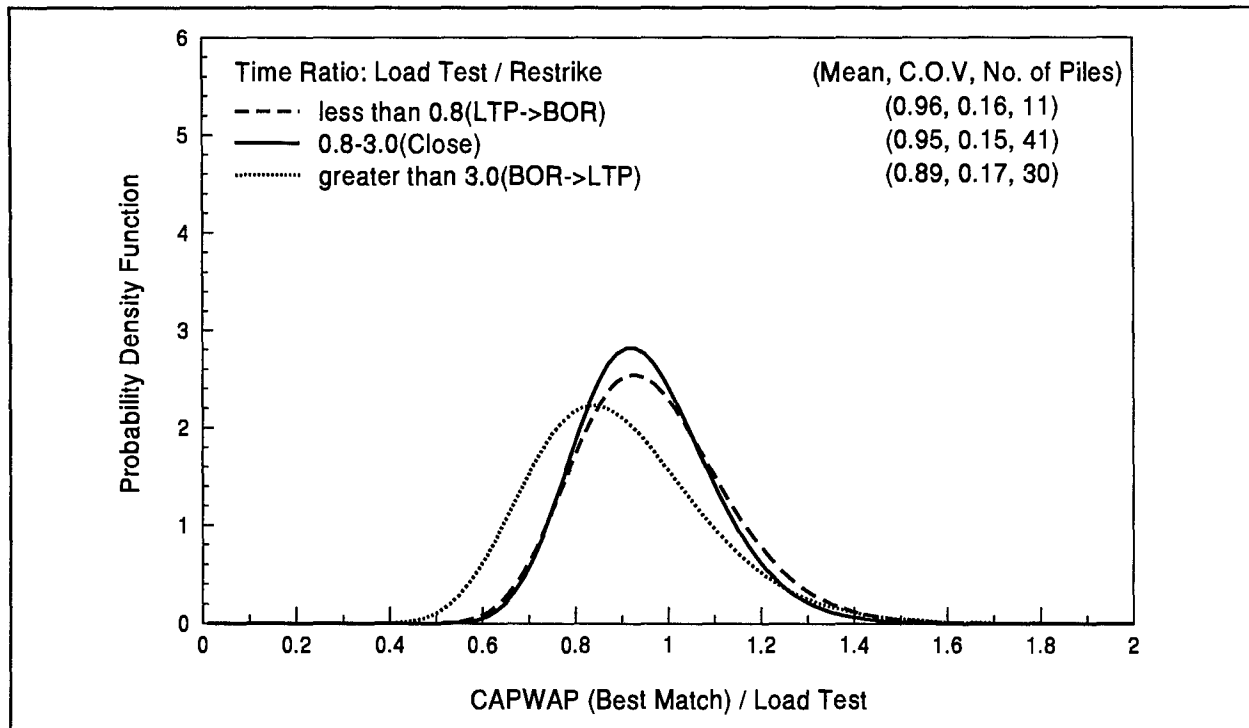


Figure 3.2(b): Log-Normal Probability Density Function for CAPWAP (Best Match) Capacity Prediction at Different Time Ratios

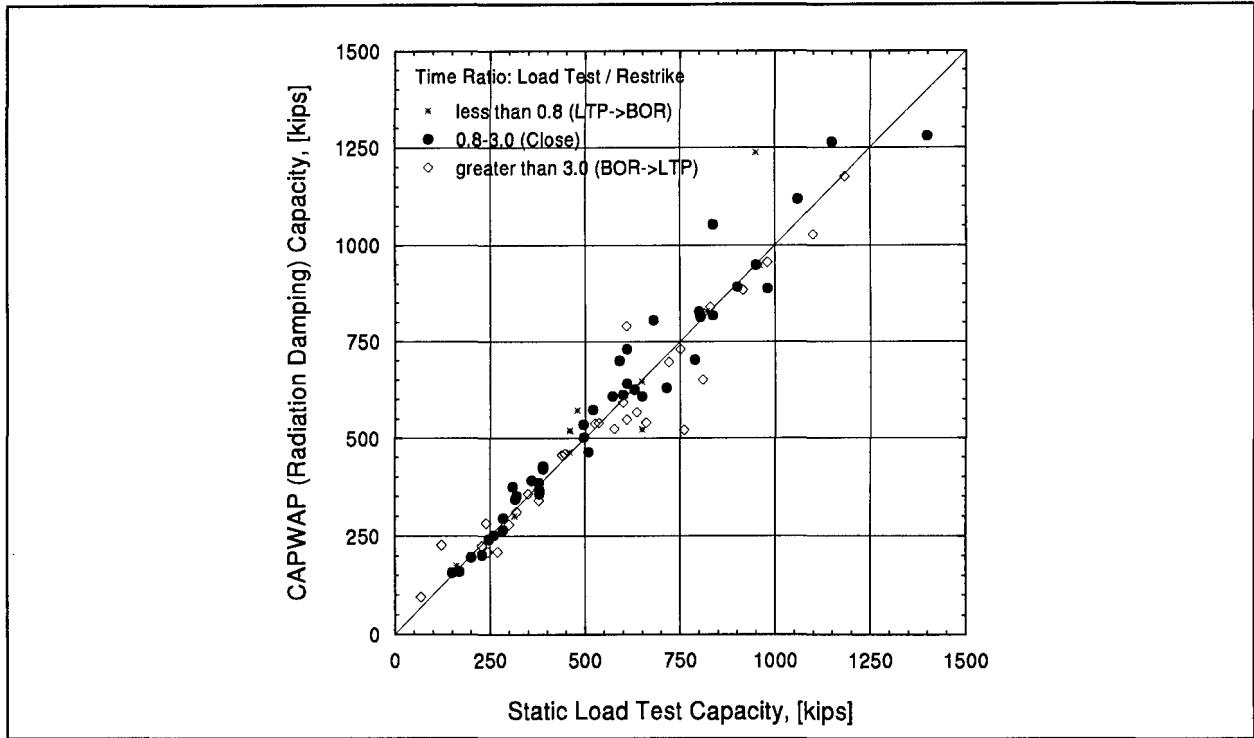


Figure 3.3(a): CAPWAP (Radiation Damping) Capacity versus Static Load Test Capacity Showing Different Time Ratios

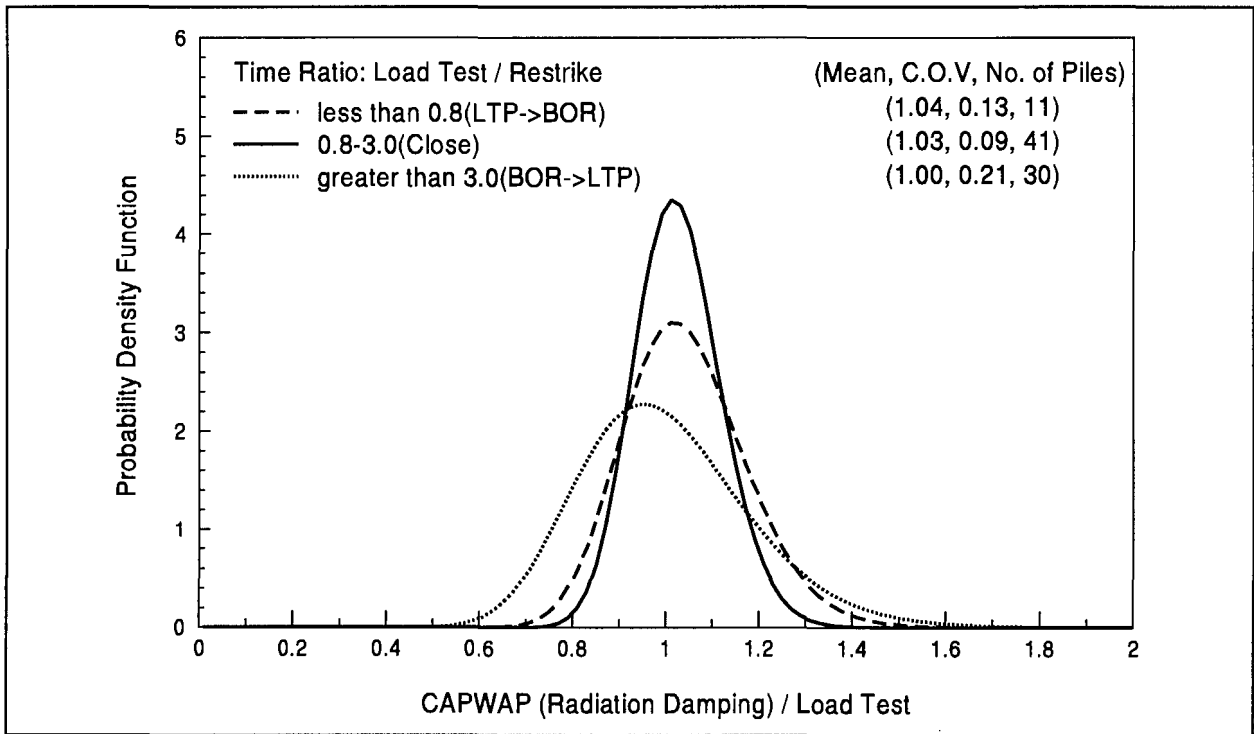


Figure 3.3(b): Log-Normal Probability Density Function for CAPWAP (Radiation Damping) Capacity Prediction at Different Time Ratios

3.2 TIME RATIO

Since the pile capacity is usually a function of time after installation, one very important factor that must be considered when comparing the static load test capacity with the restrike CAPWAP capacity is the time comparison between the static load test and dynamic restrike test. In this study, the time difference between the static load test and the dynamic restrike test is expressed as a ratio of the number of days between the end of driving and static load test (T_1), and the number of days between end of driving and dynamic restrike test (T_2), or (T_1/T_2). Thus, a time ratio (T_1/T_2) less than one means that the static load test was performed before the dynamic restrike test. A ratio of 3.0 means that the static load test was performed three times later than the restrike test.

Figures 3.1 to 3.3 demonstrate the importance of performing both the static load test and dynamic restrike test within a very short time, as in every case the coefficient of variation of the CAPWAP to static load test ratio is smallest when the time ratio is between 0.8 and 3.0. For the purpose of this study, and since many studies show that setup increases linearly with the log of time, the time difference is considered acceptably small when the ratio of (T_1/T_2) is between 0.8 and 3.0. Most of this data had time ratios between 0.8 and 1.5. Relatively little data (11 cases in all) was obtained for time ratios less than 0.8, or in other words where the static test is performed much earlier than the restrike test.

Figures 3.1 to 3.3 also show that the largest capacity prediction variability occurs when the static load test is performed significantly later than the dynamic restrike test such that the time ratio is greater than 3.0. The data base contained 30 such cases. In general practice, the dynamic restrike test is performed within the first 2 days following pile installation as a matter of compromise or convenience to minimize costs and speed determination of driving criteria to facilitate production. However, the static load testing often is done a week or more after the installation due to code requirements. For clean sands, the capacity is generally thought to not change significantly after driving. However, in the more usual case of piles installed into layered soils or in soils with fine grain content, additional soil setup often occurs after the dynamic restrike test and before the static load test, and therefore the early restrike capacity will underpredict the static capacity. This underprediction is indicated by the smallest mean values of CAPWAP capacity to static load test capacity ratios for time ratios greater than 3.

It should be apparent that to obtain better capacity predictions, the dynamic test should be performed at a time after installation comparable to the static load test. Recent trends in practice have recognized this and as a result many specifications for dynamic testing now require longer wait times after pile installation before the restrike test. If a dynamic test with many blows is performed shortly before the static test, in sensitive soils, the capacity may decrease (temporarily) blow by blow and the soil strength will not have sufficient time to recover

resulting in a static test with a reduced failure load. Thus, restrike tests with many blows shortly before a static load tests are to be discouraged. In some cases, the restrike test turns into a redrive, perhaps advancing the pile into a new bearing layer or adding several feet to the penetration and thus increasing shaft resistance; in such cases, the dynamic restrike test can then no longer be directly compared with the static load test and several potential data sets were excluded from consideration on this basis. In summary, for good correlations, the dynamic restrike test should be performed as soon as possible after the static load test. As it is impossible to perform both test simultaneously, some of the difference between the two test results must be attributed to time factor differences.

3.3 PILE TYPE

Figures 3.4 through 3.6 distinguish pile types, material types, and shapes (a), and displacement/nondisplacement piles (b). Generally, the CAPWAP capacity predictions are equally good for all pile types.

3.4 COMPARISON BETWEEN AUTOMATIC, BEST MATCH, RADIATION DAMPING RESULTS

Table 3.2 summarizes the mean and coefficient of variation (C.O.V.) of the ratio of CAPWAP capacity and static load test capacity for the automatic, best match, and radiation damping CAPWAP predictions, and for cases with time ratios between 0.8 and 3.0. For ease of visual qualitative comparison, the log-normal probability distribution function for each of the three prediction methods are presented in figure 3.7.

Matching Type	Number of Piles	Mean	C.O.V.
Automatic	41	0.98	0.18
Best Match	41	0.95	0.15
Radiation	41	1.03	0.09

The automatic and best match CAPWAP capacity prediction to static load test capacity are, on average, slightly below unity, or in other words "conservative." The average CAPWAP capacity predictions utilizing radiation damping, on the other hand, are slightly higher than the static load test capacity. However, the mean ratio is only 1.03 meaning that on the average CAPWAP overpredicts by approximately 3 percent. For those cases for which the dynamic test followed

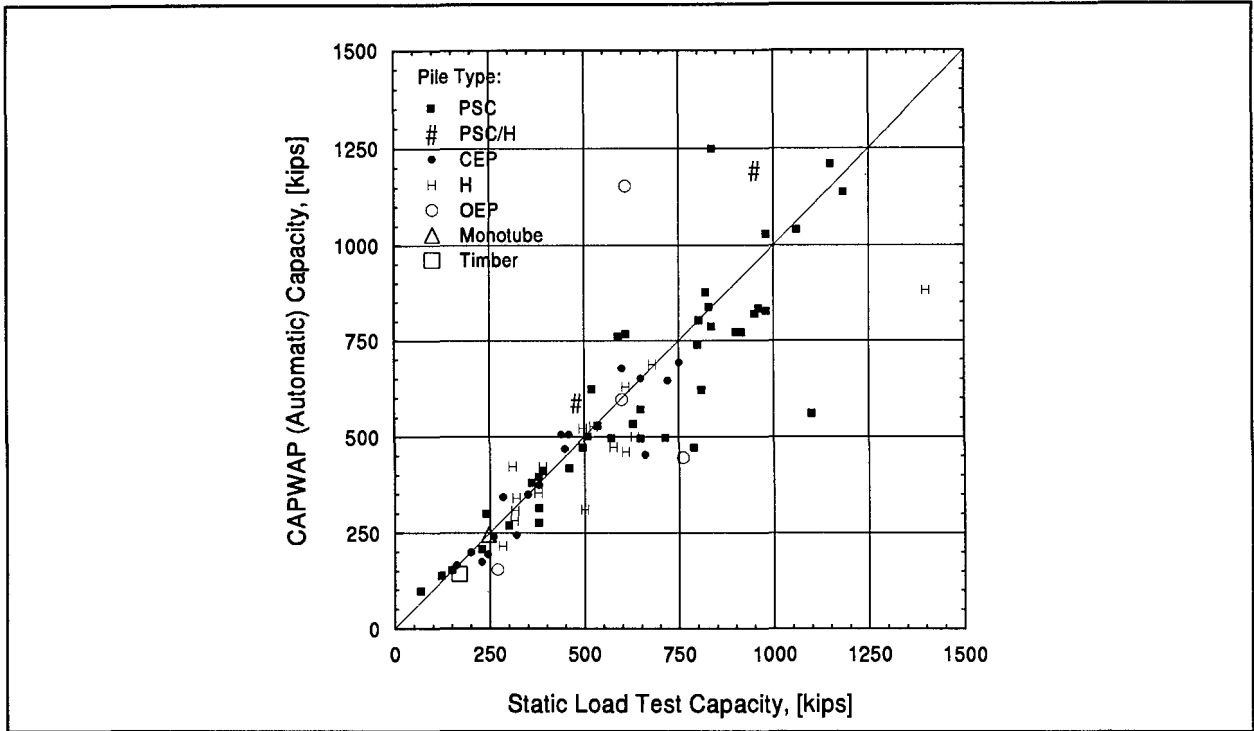


Figure 3.4(a): CAPWAP (Automatic) Capacity versus Static Load Test Capacity Showing Different Pile Types

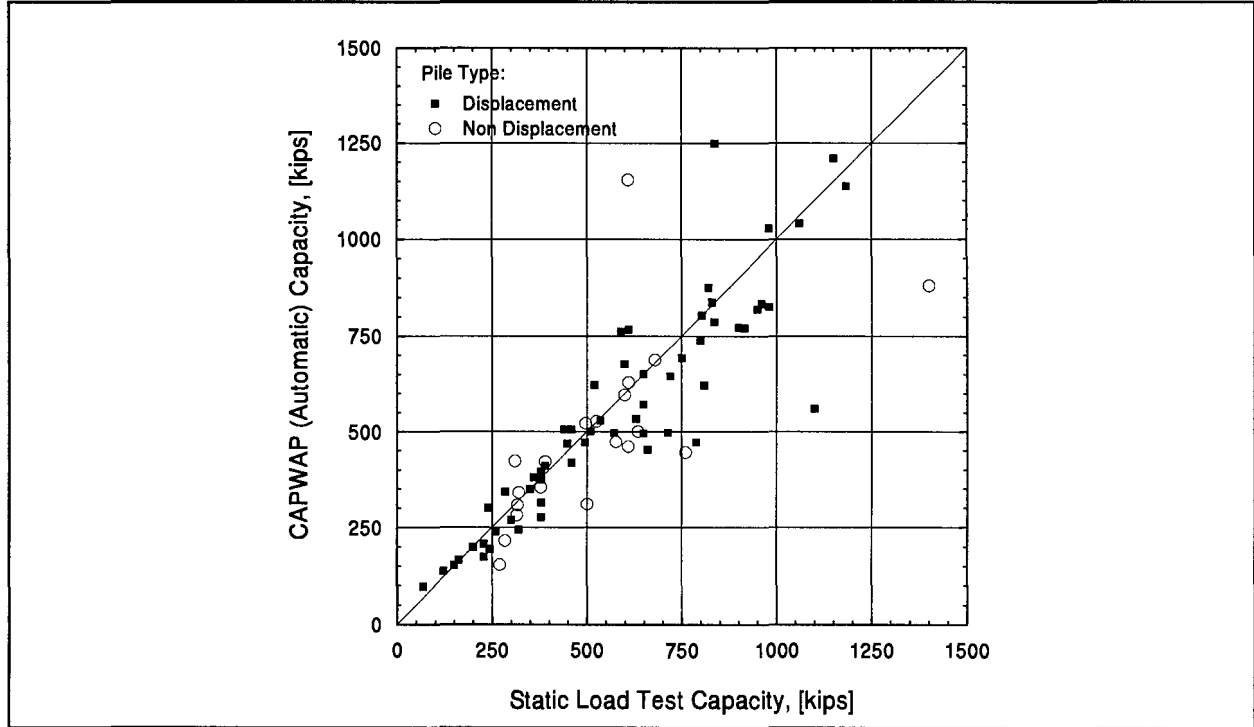


Figure 3.4(b): CAPWAP (Automatic) Capacity versus Static Load Test Capacity Showing Displacement and Nondisplacement Piles

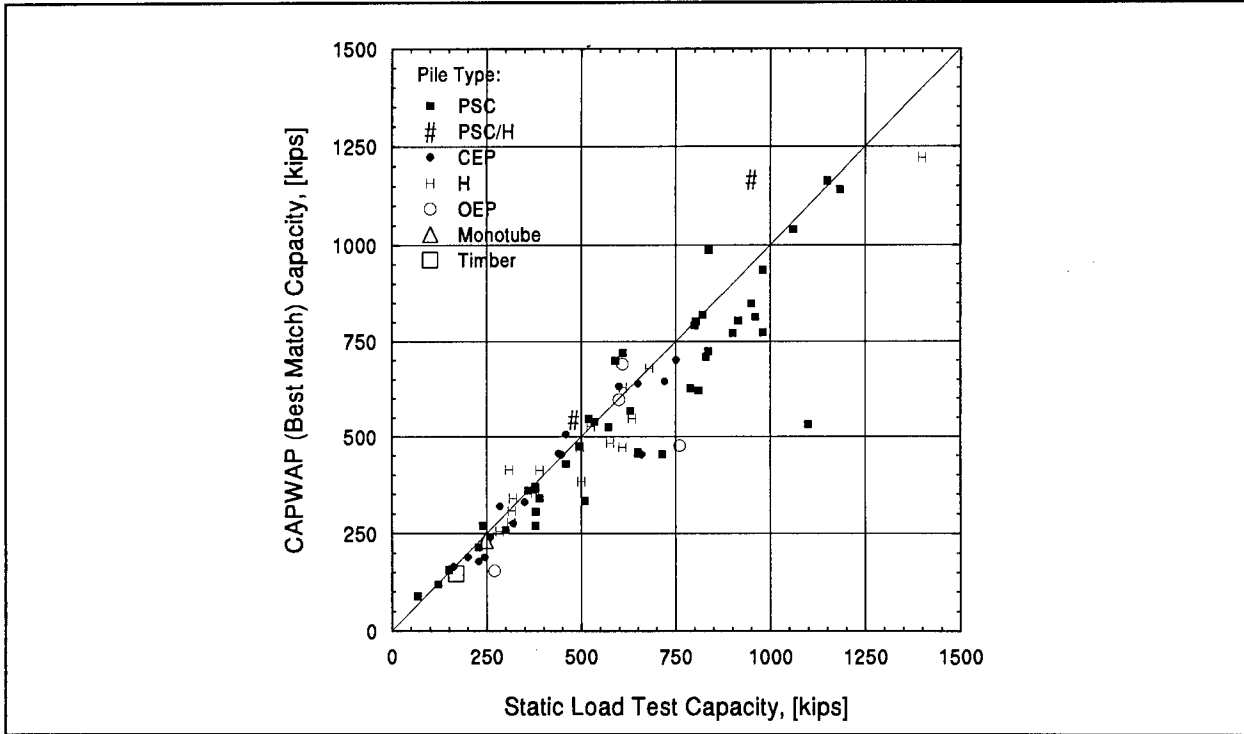


Figure 3.5(a): CAPWAP (Best Match) Capacity versus Static Load Test Capacity Showing Different Pile Types

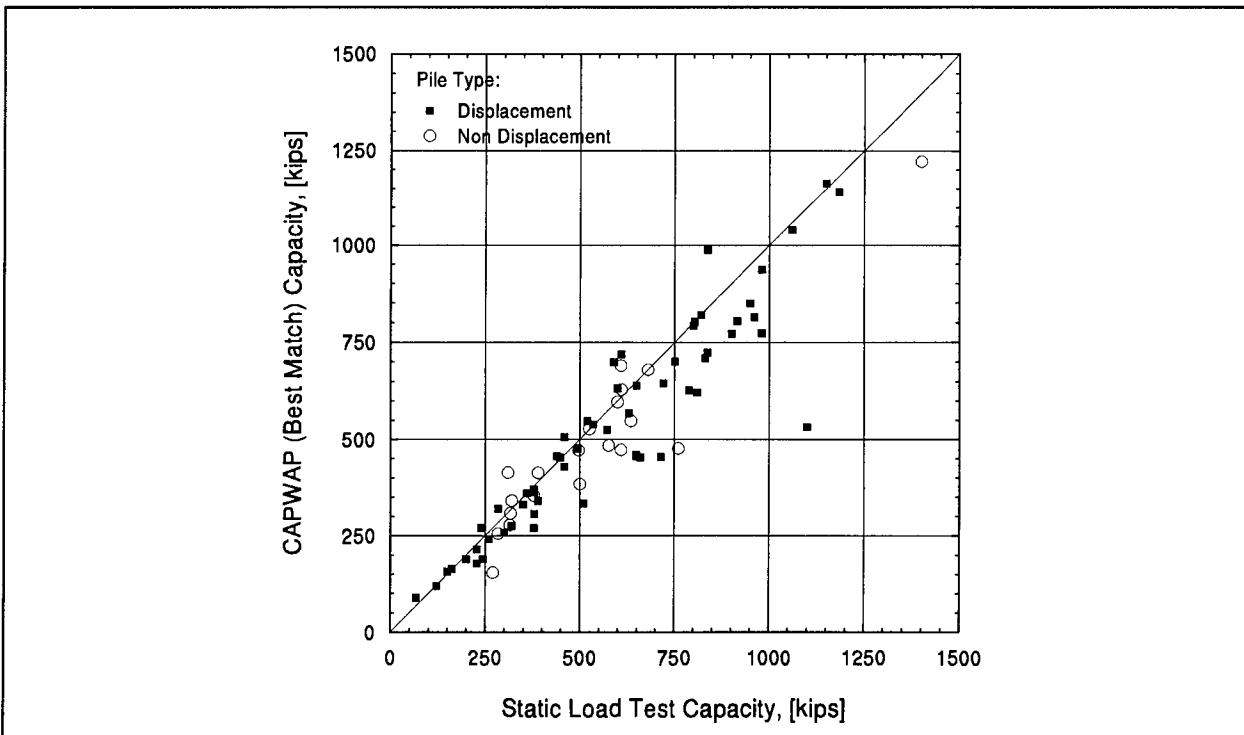


Figure 3.5(b): CAPWAP (Best Match) Capacity versus Static Load Test Capacity Showing Displacement and Nondisplacement Piles

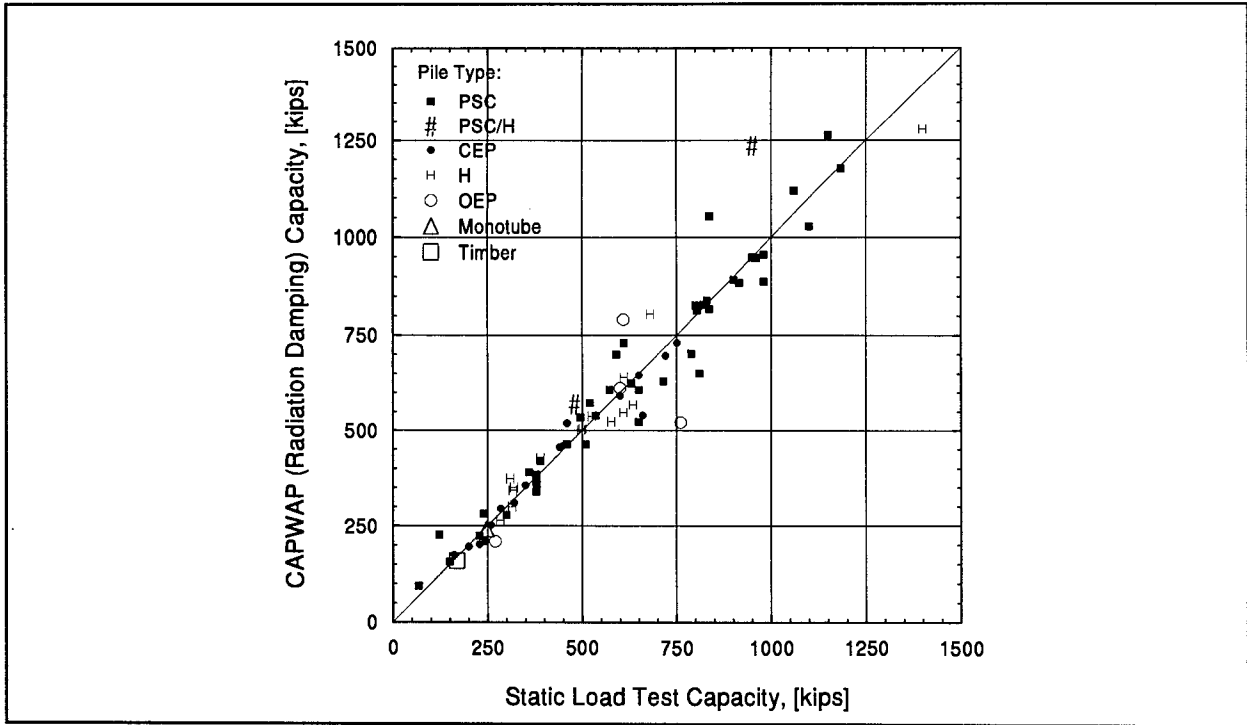


Figure 3.6(a): CAPWAP (Radiation Damping) Capacity versus Static Load Test Capacity Showing Different Pile Types

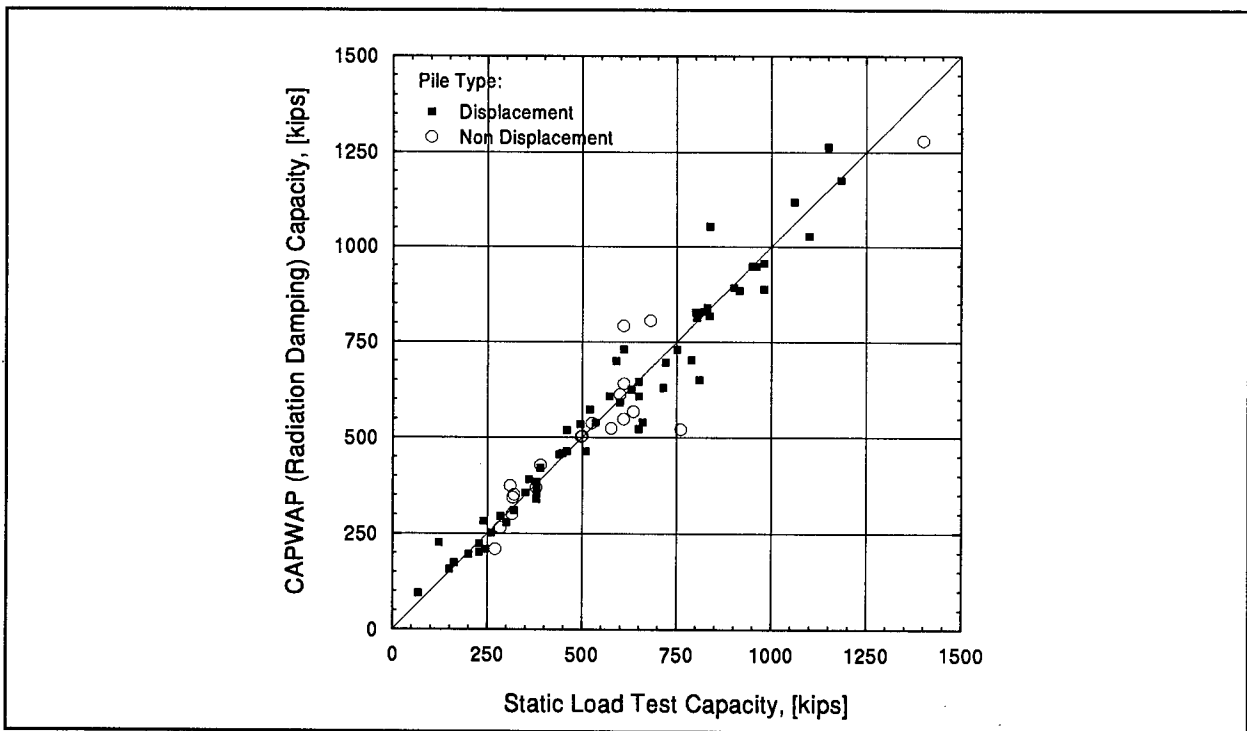


Figure 3.6(b): CAPWAP (Radiation Damping) Capacity versus Static Load Test Capacity Showing Displacement and Nondisplacement Piles

the static load test, this might simply reflect additional setup. The data for the radiation damping model has a coefficient of variation of only 9 percent meaning that it has a very high precision of prediction. Statistically, with a mean of 103 percent and a standard deviation of 9 percent, 95 percent of all predictions should be within two standard deviations of the mean, or in other words within 85 and 121 percent of the static load test value. Guidelines for choosing the radiation damping model parameters are presented in section 3.6.

The above compares the CAPWAP results with the Davisson's failure criterion limit load evaluation of the static load test. Davisson's criterion is a consistent mathematical procedure. It is based on the premise that the pile is basically end bearing and that settlements should be limited to a small value. For end bearing piles in sand, for example, the full end bearing resistance may not be activated at this small displacement. In the data base cases, most piles had a significant percentage of shaft resistance. Further, the Davisson procedure requires evaluation of the pile stiffness for concrete piles or concrete filled pipe piles which requires knowing the modulus of the concrete. Thus the Davisson evaluation procedure is not entirely without some problems. However, it is readily acknowledged that the method is generally conservative and relatively easily applied and that it is probably among the best methods available for capacity evaluation purposes.

In some cases, the static test curve abruptly plunged and thus any load evaluation method would yield a similar result to the Davisson load. However, in other cases, the slope of the static curve more gradually changed and different evaluation methods could lead to vastly different failure loads. Such variability is not easily reflected in the above statistical comparisons. If one were to visually inspect each static load test curve, a lowest possible failure load could be assigned. Similarly, the maximum applied load or a load calculated by Chin's extrapolation method could be considered an upper bound solution. In every data correlation case analyzed, the visually selected lowest possible failure load from the static load test was below the CAPWAP result, while the maximum applied load was above the CAPWAP result. The selection of the Davisson limit load as the correct static test result does lead to a good correlation. In summary, although the Davisson limit value is assumed to be the correct answer and results in a good correlation with the dynamic restrike test, there is potential error in both the static measurements and the Davisson evaluation process. The dispersion in the probability density function shown in figure 3.7 can be attributed (a) to a combination of dispersion in both the dynamic and static test results and (b) to the time factor, *i.e.*, the fact that the two tests were not performed with the same wait time after installation.

For comparison purposes, the CAPWAP radiation damping results for the time ratios between 0.8 and 3.0 are presented together with the original CAPWAP results from the same data set in figure 3.8.

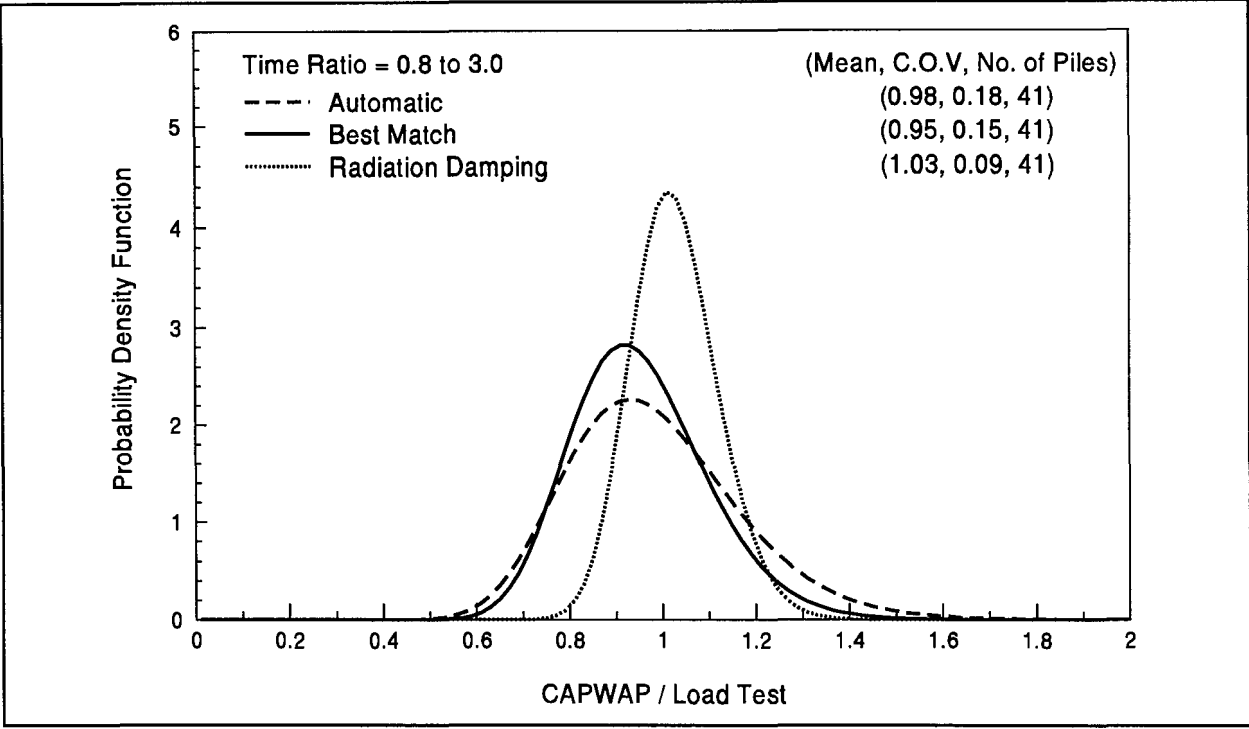


Figure 3.7: Log-Normal Probability Density Function for Automatic, Best Match, and Radiation Damping CAPWAP Capacity Prediction

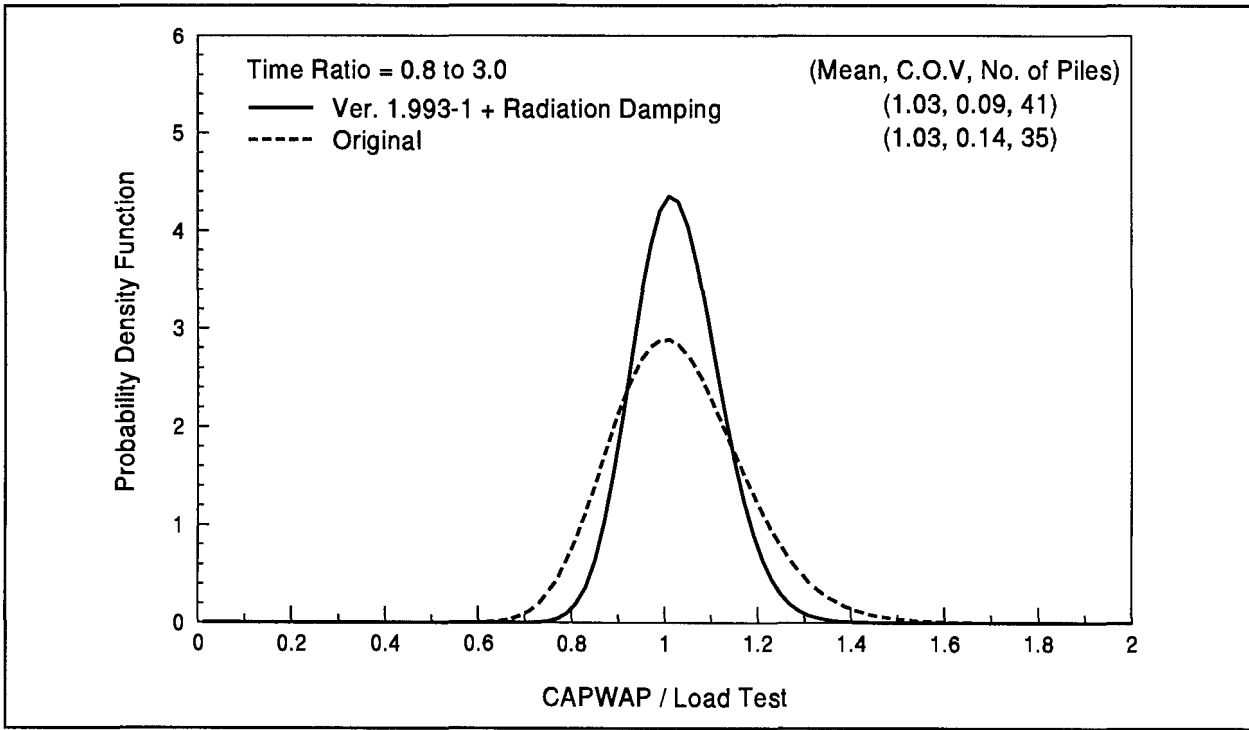


Figure 3.8: Log-Normal Probability Density Function for Original and Version 1.993-1 + Radiation Damping CAPWAP Capacity Prediction

3.5 DYNAMIC SOIL PARAMETERS

Figures 3.9 to 3.12 present the soil damping factors and quake values calculated by CAPWAP plotted against dominant soil type at the pile shaft or the soil at the pile toe. The dominant soil type at the pile shaft was determined based on the soil layer which provided most of the pile shaft resistance. The (a) figures show the soil parameters determined from best match CAPWAP while the (b) figures from the radiation damping CAPWAP. For the toe soil parameters, the SPT N-value at the pile toe is also presented.

As for the wave equation back calculations of chapter 2, no absolutely clear trend can be established from these plots. However, the average Smith damping constants generally reduce for both shaft and toe as the soil grain size increases. The average shaft quake seems to be always about 0.1 in. However, large toe quakes seem to occur in soils of clay, and in silty, fine and coarse sands. Previous studies (Likins, 1983) have shown large quakes can occur in any saturated soil. There are not enough piles with predominately silt on the pile shaft in the data base to allow for conclusions on this soil type.

It should be noted that the results summarized from figures 3.9 to 3.12 are from analyses of restrrike data. The restrikes were selected for analyses since they are better correlated with the static load tests which was initially thought to provide the best proof for the correctness of the solution, and indeed that the correlations are as good as described above does lend credibility to the CAPWAP method. However, it has been observed that the damping constants are generally higher for restrrike than for the same pile in the same soil at the end of driving. Toe quakes are also often higher in driving than during restrrike. Thus, these results should probably not be used as a general guide for the parameters applicable at the end of driving. Unfortunately, dynamic restrrike test data is not available for all piles in the data base. Further, time and cost limitations prevented CAPWAP analysis of both end of drive and restrrike tests.

3.6 GUIDELINES FOR USING RADIATION DAMPING

The CAPWAP study described here only considered radiation damping along the pile shaft. From the result of this correlation study with the radiation damping model, the following guidelines can be formulated to help CAPWAP users select the shaft radiation damping parameters (MS and SK). MS represents a soil mass which is put into motion by the reaction of the standard Smith soil parameters in the pile soil interface. SK represents a dashpot which supports this soil mass, MS. The CAPWAP radiation damping model has been described in appendix D of volume III. The following rules were established:

$$\text{Shaft support soil mass, } MS \text{ [kips]} = (\text{NFac}) (0.34) CI \text{ [ft]} \quad (3.1a)$$

$$\text{or, } MS \text{ [kN]} = (\text{NFac}) (5.0) CI \text{ [m]} \quad (3.1b)$$

$$\text{Shaft radiation damper, } SK = (A3) (\text{NFac}) (\phi_a)/Z1 \quad (3.2)$$

where A3 is the average of the three highest friction per unit length results in the shaft friction distribution (kips/ft or kN/m, and obtained from the CAPWAP Final Results Table), NFac is the ratio of number of pile segments to soil segments in the embedded portion of the pile (usually 2.0), C1 is the pile circumference, ϕ_a is a value between 4 and 8 (usually about 6), and Z1 is the impedance of the very top pile segment (kip/ft/s or kN/m/s).

It is logical to assume that the mass of soil set in motion (MS) is related to pile soil interface and hence the circumference of the pile (CI). The strength of the damper, SK, must be carefully selected as above. If the damper is too stiff (high value) then it will have little effect and the solution results will hardly differ from the normal best match and thus no advantage achieved. Selection of a high value will tend to produce conservative predictions. However, if the damper value is set too low, then the resulting solution may overpredict the capacity (the capacity generally increases as the SK value is reduced), providing a solution which may become non-conservative. Thus, the SK value should never be set below the minimum value recommended above. The solution should further have a Smith shaft damping factor of less than 0.4 s/ft (1.3 s/m).

It is suggested that for driving resistances of less than 24 blows/ft (80 blows/m), the radiation damping model should not be employed as it tends to increase the predicted capacity which may not be justified in weak soils.

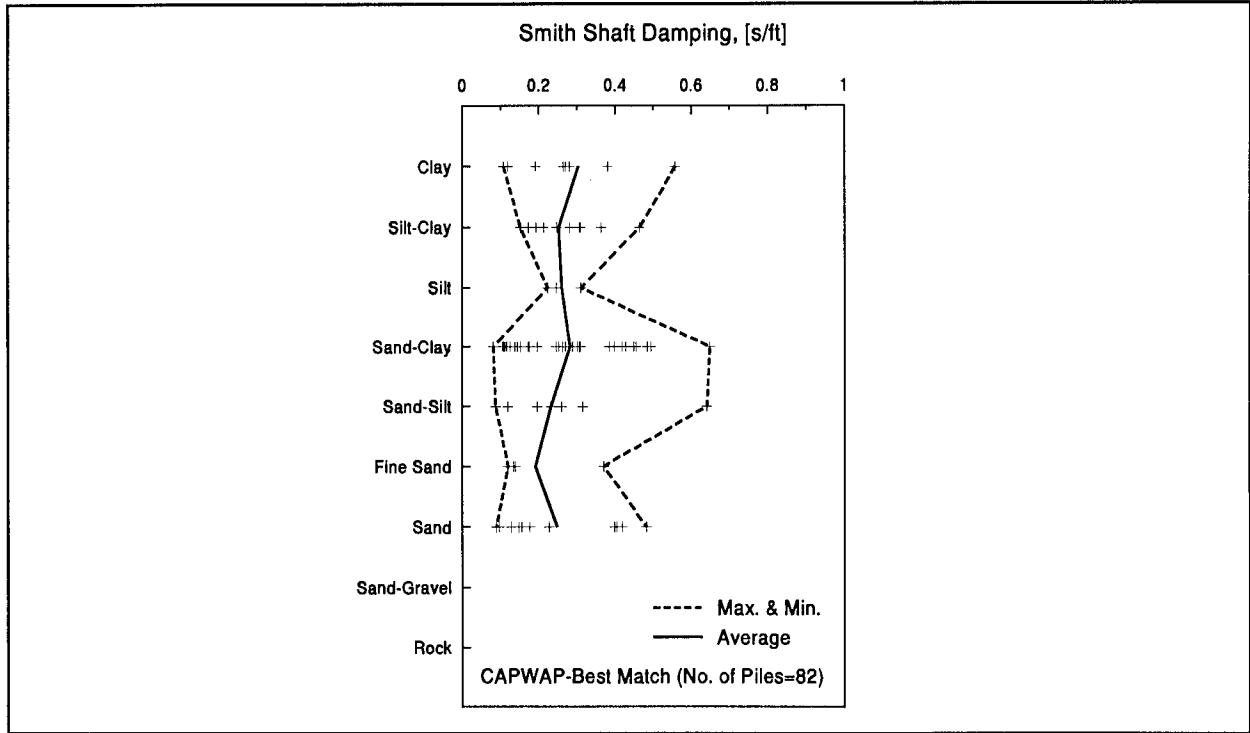


Figure 3.9(a): Smith Shaft Damping versus Soil Types from Best Match CAPWAP

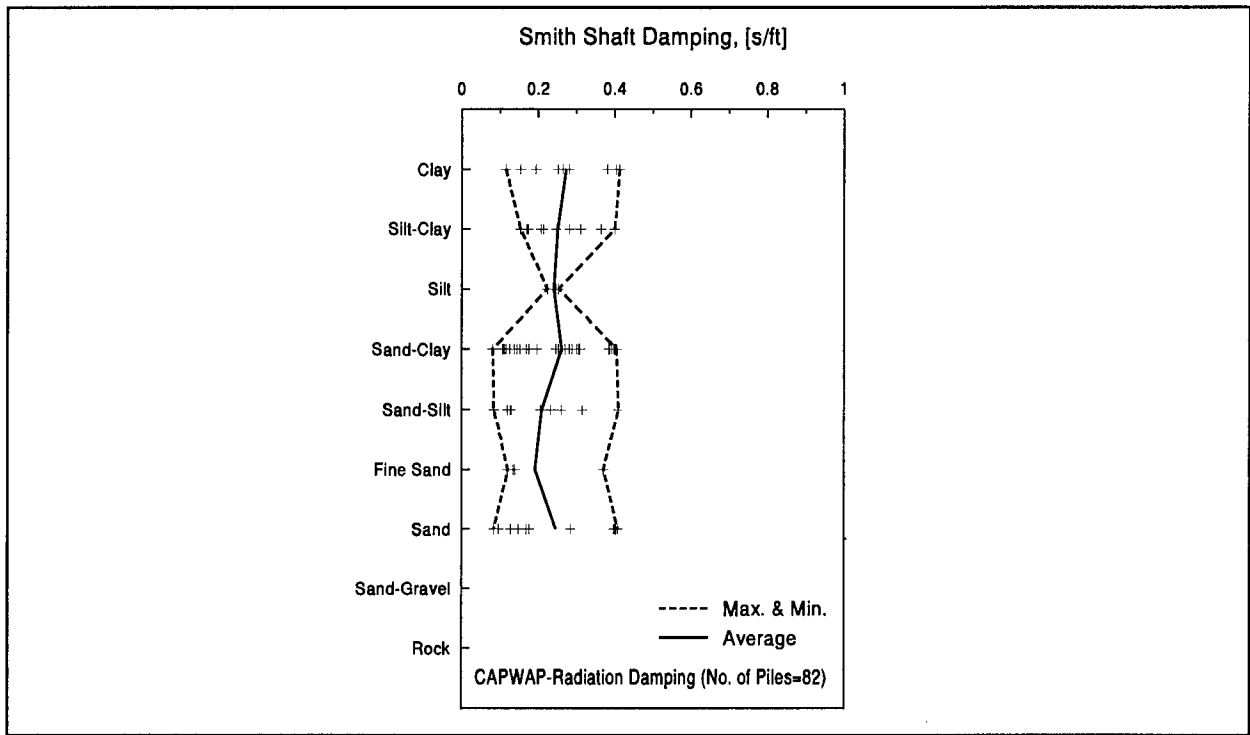


Figure 3.9(b): Smith Shaft Damping versus Soil Types from Radiation Damping CAPWAP

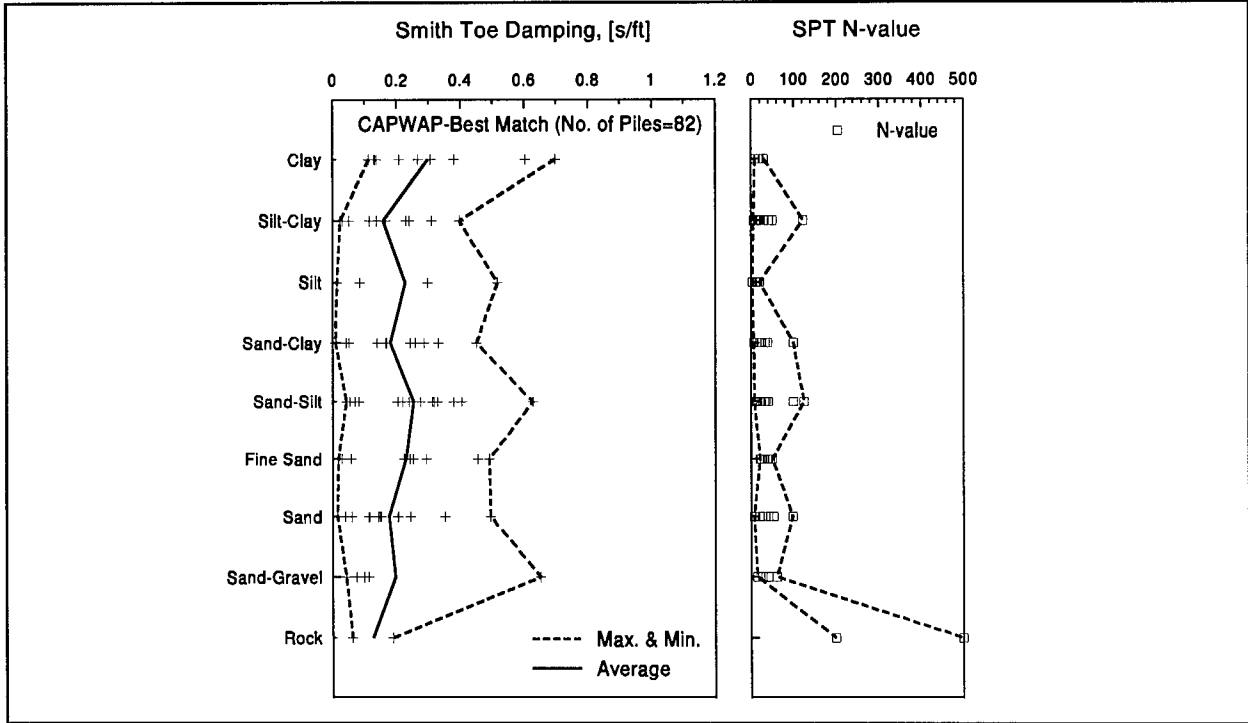


Figure 3.10(a): Smith Toe Damping versus Soil Types from Best Match CAPWAP

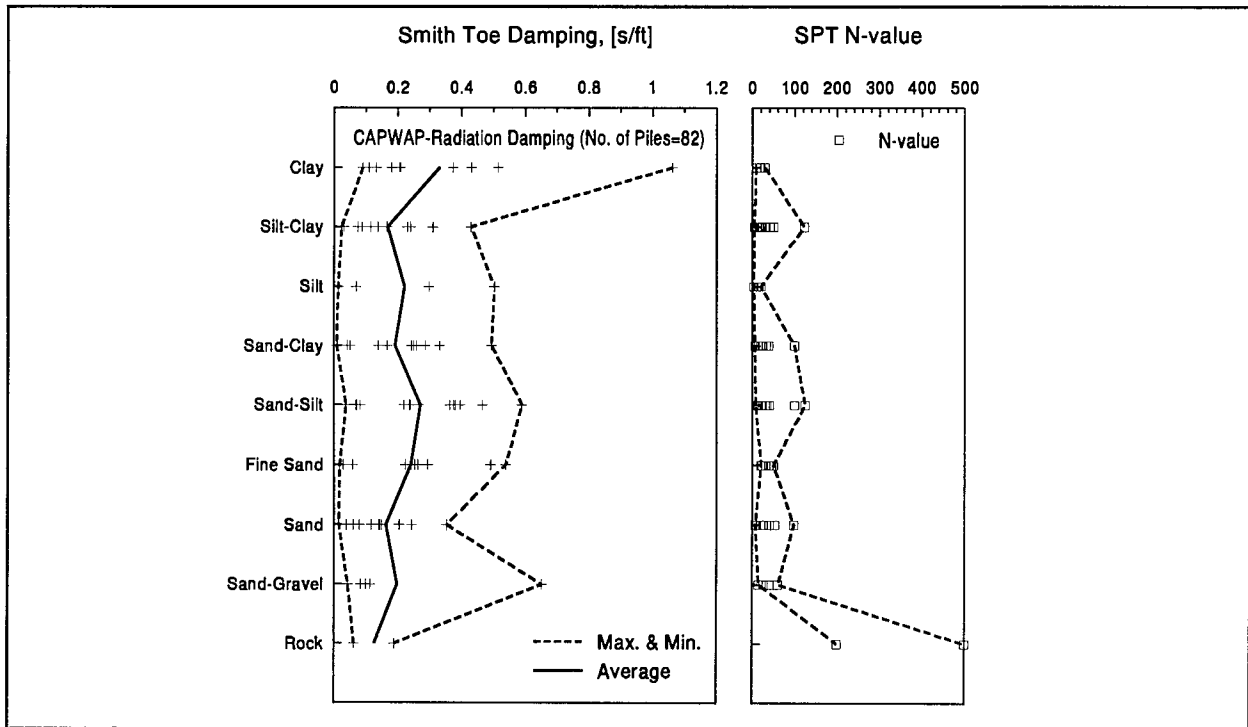


Figure 3.10(b): Smith Toe Damping versus Soil Types from Radiation Damping CAPWAP

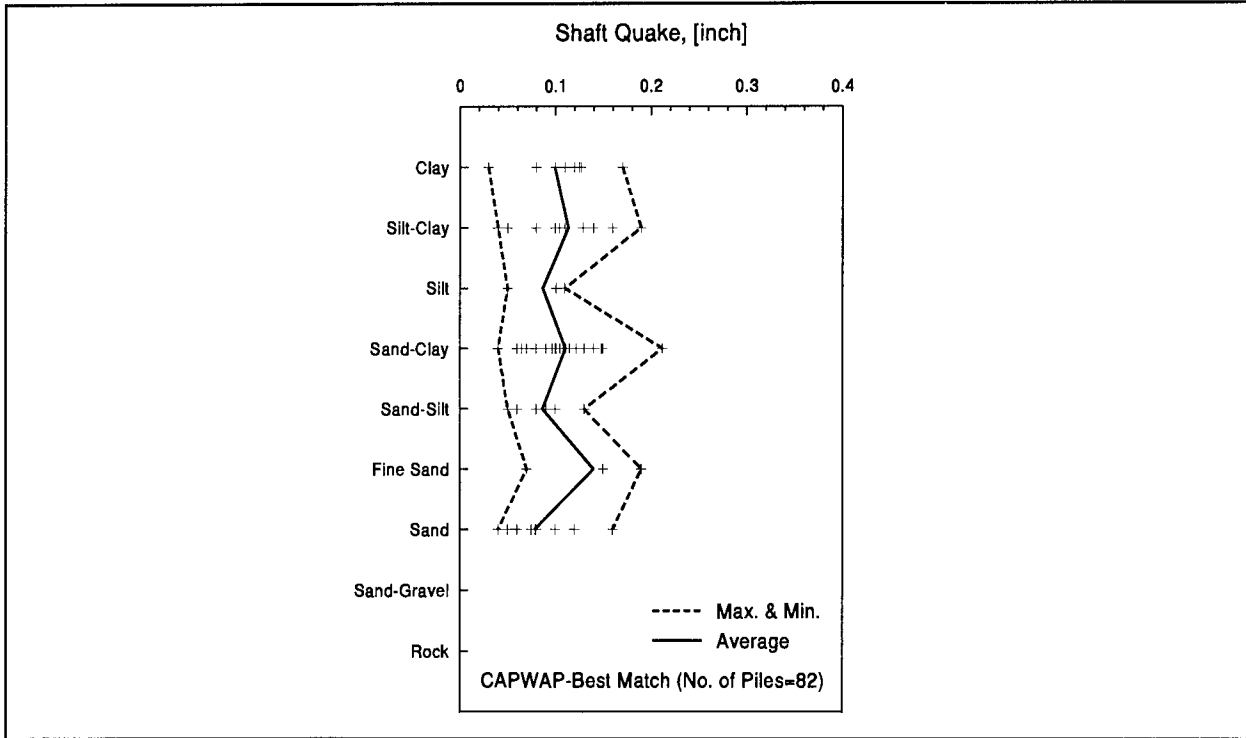


Figure 3.11(a): Shaft Quake versus Soil Types from Best Match CAPWAP

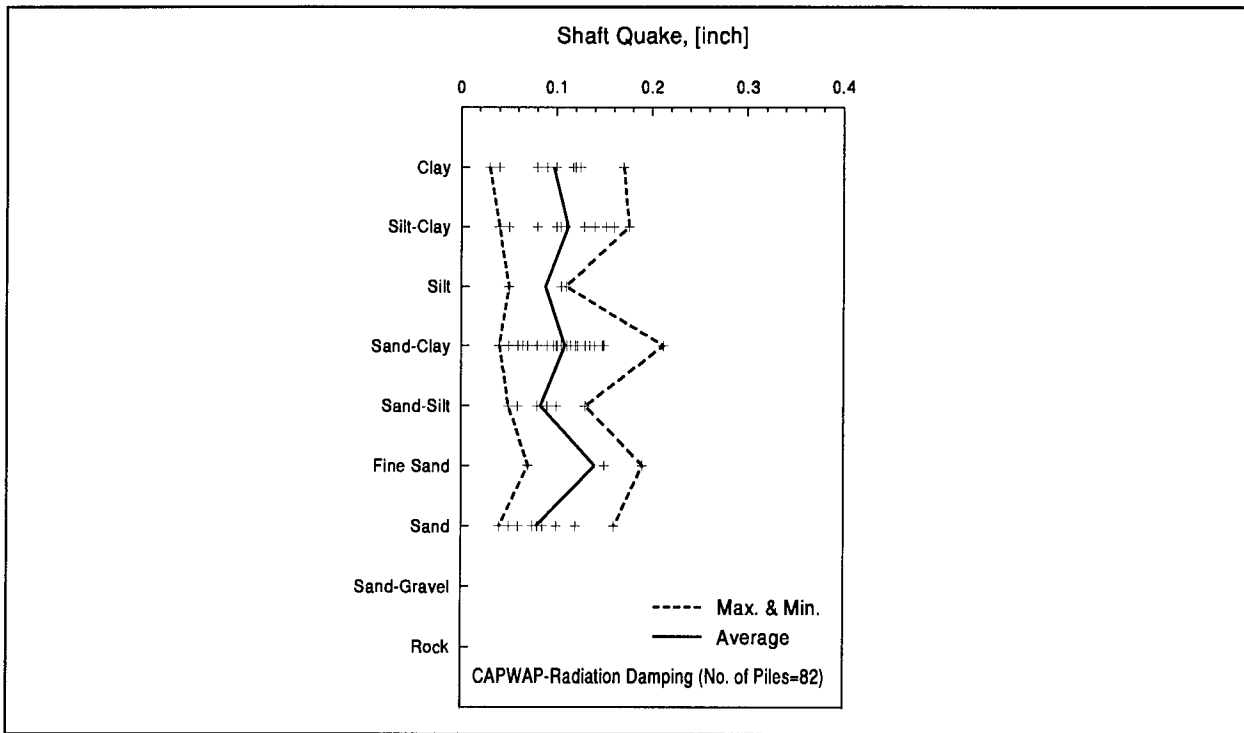


Figure 3.11(b): Shaft Quake versus Soil Types from Radiation Damping CAPWAP

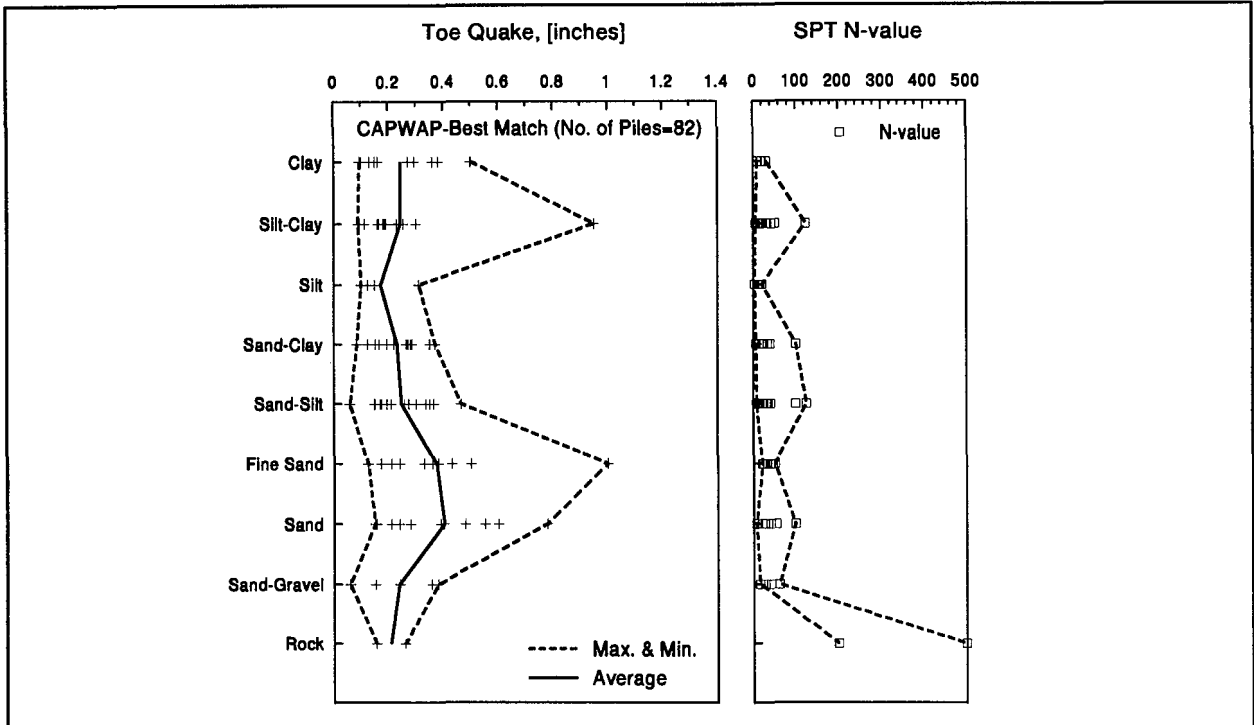


Figure 3.12(a): Toe Quake versus Soil Types from Best Match CAPWAP

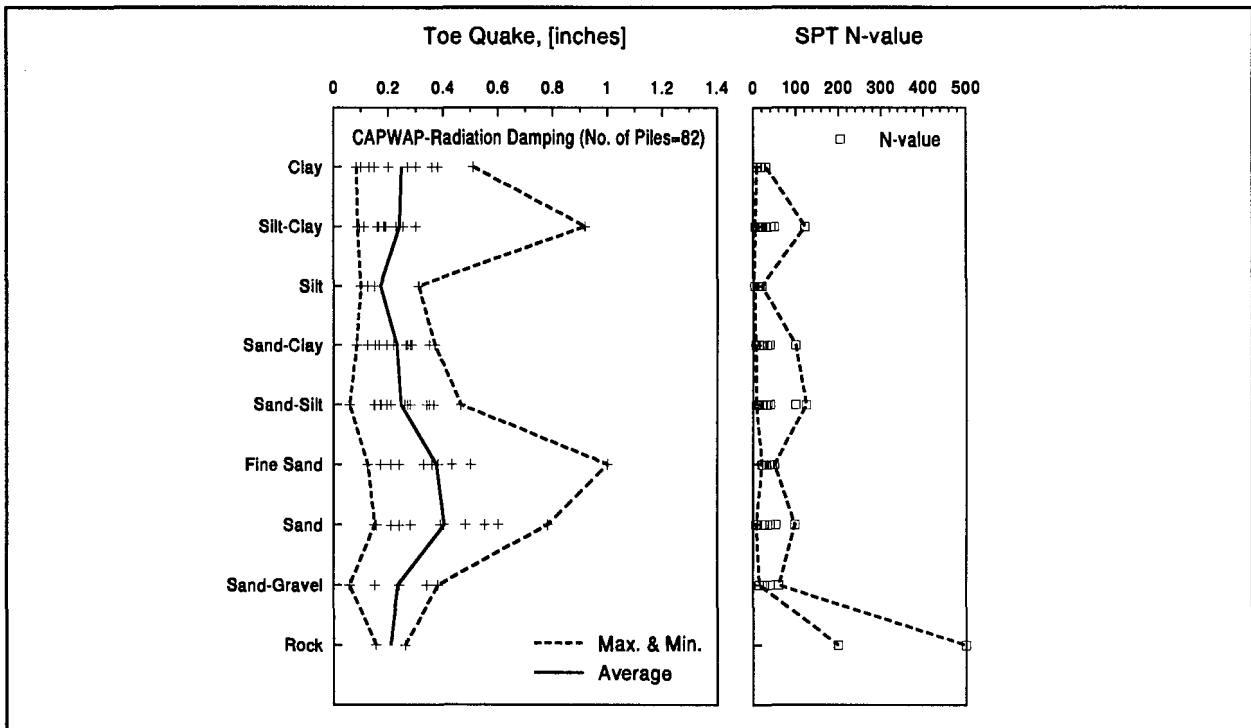


Figure 3.12(b): Toe Quake versus Soil Types from Radiation Damping CAPWAP

CHAPTER 4

THE MODIFIED SPT PROCEDURE

4.1 INTRODUCTION

The Standard Penetration Test (SPT) procedure is a soil investigation technique commonly used in the United States and many other countries. The SPT procedure consists of driving a 2-in O.D. with 1.375-in I.D. (51-mm O.D., 35-mm I.D.) split-spoon sampler 18 in (457 mm) into the soil with a 140-lb (625-N) hammer free falling from 30 in (760 mm) height (Vanikar, 1986). The number of blows for every 6 in (152 mm) of sampler penetration is recorded. The total number of blows for the last 12-in (305-mm) sampler penetration is used as the penetration resistance and is the well-known SPT N-value. For many driving projects, the SPT N-values are used in predicting the bearing capacity of piles as well as the pile driveability. However, using the SPT N-value alone does not always yield satisfactory quantitative results.

With the recent advances in transducer and data acquisition technology, additional measurements can be performed during the SPT procedure; a series of such measurements during and after SPT driving had been proposed (Interim Report, 1992) and will be referred to as the Modified SPT procedure. Simply taking dynamic measurements during the SPT procedure had been used on several projects in an almost routine fashion to assess the transferred energy of various SPT driving systems. The present study will make use of the additional information obtained from the Modified SPT procedure to determine the static and dynamic soil parameters which will be used for predictions of both pile bearing capacity and pile driveability using the wave equation analysis.

4.2 THE MODIFIED SPT PROCEDURE CONCEPT

After careful evaluation (GRL, 1992) of various proposed measurement techniques for dynamic soil parameter determination, including direct and indirect methods for both laboratory and in-situ measurements, the Modified SPT procedure was considered most advantageous for the following reasons. First, the SPT procedure is widely used due to its applicability in many soil types and its possibility for actual sample retrieval. Second, the SPT procedure involves impact driving of the sampler and the sampler experiences both static and dynamic (damping) resistance forces which are related to those encountered in pile driving. Therefore, the main concentration of effort in this study is directed toward the Modified SPT procedure. The objectives of the Modified SPT measurement include the determination of:

- Static soil strength parameters including the time dependent strength change factor.
- Damping effects.
- Soil stiffness (practically the inverse of the quake).
- The rate dependent soil-pile interface shear strength.

The Modified SPT procedure was designed such that existing test equipment could be used. It was also considered important that the standard procedure for N-value measurement would be unaffected. Furthermore, the additional test components were made conceptually simple considering the typical drilling environment. The Modified SPT procedure was also designed to work with all drilling methods. Since the drilling method depended on the local soil condition, the choice of drilling method was selected based on the experience of local drilling crews.

4.3 SPT EQUIPMENT MODIFICATIONS

4.3.1 Dynamic Force and Velocity Measurements

The Modified SPT procedure requires the measurement of dynamic force and velocity near the top of the SPT drill rod during sampler driving, and N-value counting. The force and velocity measurements are very similar to the routine measurements performed during dynamic testing of piles with the Pile Driving Analyzer® (PDA). The top force and velocity measurements are accomplished with strain gauges and accelerometers, respectively, mounted at the midpoint of a 2-ft (0.61-m) long AW type SPT drill rod section. For the SPT drill rod other than AW type, a sub can be used to connect the two different rod sizes. An NW type drill rod, or any other rod type, can also be instrumented should this type of drill rod be driven. The instrumented section (figure 4.1), manufactured by Pile Dynamics, Inc. (PDI), is attached to the top of the drill string beneath the anvil, and the details are shown in figure 4.1.

For strain measurements, the instrumented section consisted of foil type strain gauges which were attached to the sub such that they cancelled bending effects and wired to form a full Wheatstone bridge. Calibrations of several instrumented sections are presented in appendix G.

Two accelerometers were mounted on blocks and then bolted to the instrumented section. Two different types of newly developed accelerometers were used; the first, a piezoresistive type and the second, a shear mounted piezoelectric type. Both types of accelerometer showed adequate performance. The improved selection, testing, calibration, and use of these accelerometers

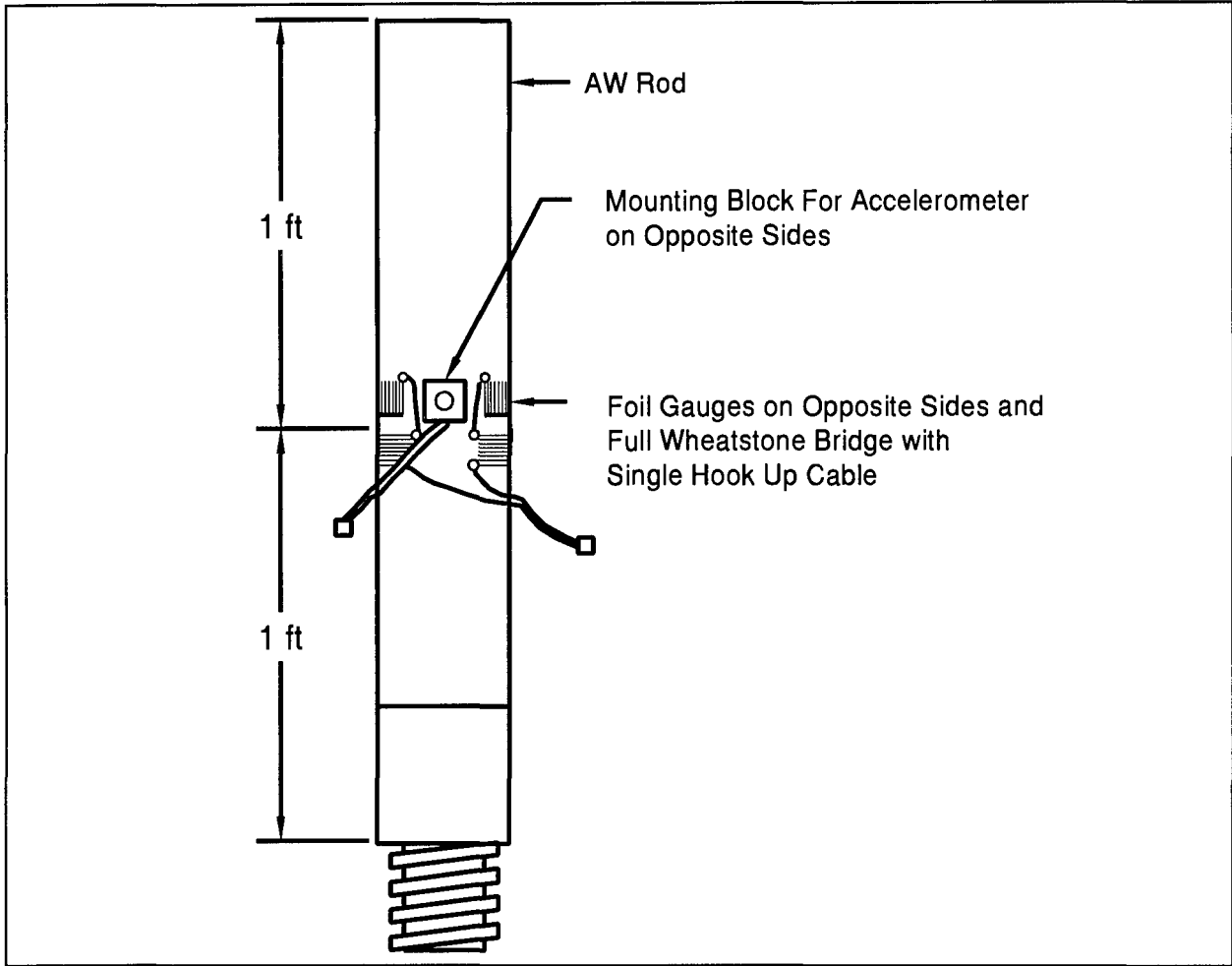


Figure 4.1: Instrumented SPT Rod

were a direct outcome of the present research. It was found that the actual acceleration levels induced in an SPT rod are of a magnitude which make their accurate measurement a highly advanced technology. In fact, a special calibration procedure had to be developed by the manufacturer which, for the SPT application, appears to be better than anything else in existence. The accelerometer calibration results are presented in appendix G.

Analog signals from strain gauges and accelerometers were conditioned, digitized, and processed with a PDA, Model PAK, manufactured by PDI. Due to high frequency signals generated by the steel to steel impact between the hammer and anvil, a high sampling rate of 20 kHz was required when converting the signals to digital form. The PDA recorded the strain and acceleration signals from each hammer impact and converted them to force and velocity, respectively, before saving the records as functions of time to the PDA's hard disk. The force and velocity records were also displayed on the PDA's liquid crystal display (LCD) screen for data quality evaluation. Stored force and velocity records were used in this investigation to determine the dynamic soil parameters.

4.3.2 Oversized Tips

When the SPT N-value and the recovered sample suggested that the layer could have potential for significant end bearing or refusal pile driving, a special investigation of the soil's end bearing capacity was performed. For this special test, the sampler was replaced by an oversized solid tip for better prediction of unit end bearing. The advantage of the oversized tip is a reasonable simulation of the pile end bearing condition without friction effects, since the tip is larger than the AW drill rod.

Two types of tip were investigated in this study; the flat end and the cone tip, shown in figure 4.2. The flat end tip was chosen since most displacement piles have flat bottoms and therefore the flat end tip would simulate the real pile behavior. The cone tip was also investigated because of the widespread experience with cone penetration test (CPT) in soil investigation and because some closed end pipes are driven with conical point. Both types of oversized tip have an outside diameter of 2.5 in (64 mm). This diameter gives the oversized tip an area of approximately 3 times the area of the standard CPT tip. Comparison of results from both tip types will be presented in section 5.1.3.

4.3.3 Hammer Performance Analyzer™

The Hammer Performance Analyzer (HPA) uses radar technology to determine the ram speed. The hammer velocity during SPT sampler driving can be easily measured with the HPA which continuously plots hammer velocity as a function of time on a strip chart. The hammer velocity just prior to impact (hammer impact velocity, V_i) can then be determined from the strip chart and hence the hammer kinetic energy (prior to impact) can be calculated. The hammer impact energy provides additional information for SPT performance evaluation and for N-value correction. Together with PDA transferred energy results, HPA data allows for identifying the reasons for low or variable energy output. The average hammer impact velocity at each test depth is presented and discussed in appendix E. Figure 4.3 shows the Modified SPT procedure being performed by a normal drill rig. Also shown in the photograph is the instrumented SPT rod and the HPA.

4.4 ADDITIONAL VERIFICATION TESTS

4.4.1 General Remarks

For a most complete and meaningful set of results from this study, several additional tests were included in the Modified SPT procedure. Some of these tests were very simple, took little time, and provided additional useful information. Therefore, they might be considered for permanent

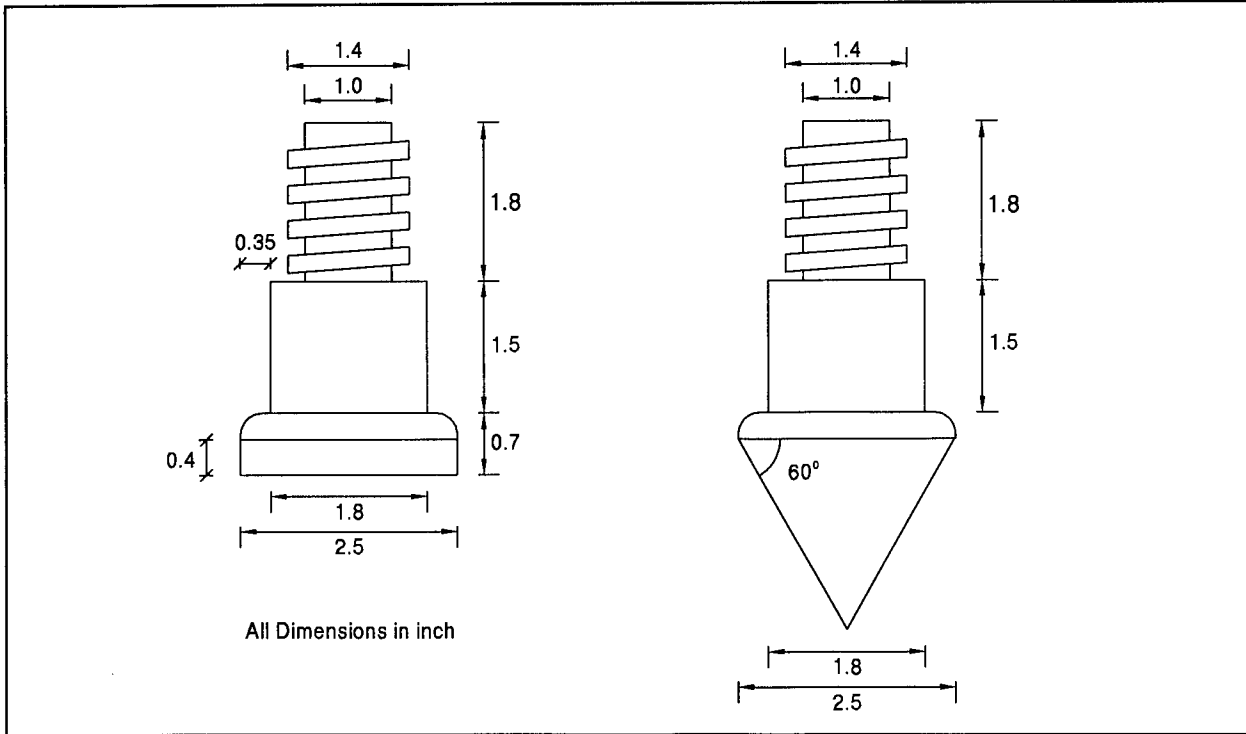


Figure 4.2: Oversized Tips - Flat End and Cone



Figure 4.3: The Modified SPT Procedure with HPA Measurement.

inclusion in the routine Modified SPT practice. Some other tests were quite time consuming but were extremely useful for establishing correlations between static and dynamic results. These extensive tests are not needed in routine practice.

4.4.2 Axial Static Load Test

The static load test was performed at the end of sampler or oversized tip driving. The main purpose of performing the load test was to determine directly the static soil resistance or end bearing from the uplift and compression test, respectively. In this study, the static load test was primarily performed for verification purposes. In practice, the static soil resistance and end bearing will be determined with less effort by other, simpler procedures.

4.4.2.1 Reaction Frame

To perform the static tests, a reaction frame was set up centered over the drill hole for both compressive and tensile reaction forces. The frame was set on and connected to a pair of hollow stem augers which had been screwed into the ground, one on each side of the drill hole. A center hole, 60-ton (533-kN) hydraulic jack provided uplift or compression loads by pushing against the top or bottom of the reaction beam. Of course, the depth of penetration required for the auger was governed by the maximum compressive test load. During this study, two different sizes of hollow stem augers were used, the 2¼-in and 4¼-in (57-mm and 108-mm) inside diameter; each auger section was 5 ft (1.5 m) long. The deepest auger penetration drilled was 26.5 ft (8.1 m) and the maximum compression load applied without failing the augers was 11.6 kips (52 kN). Typically, the tops of the augers were left about 2.5 to 3.0 ft (0.76 to 0.91 m) above the ground. Figure 4.4 shows the schematic reaction frame setup for the uplift and compression tests. The top and middle figures show the hollow stem augers, reaction frame, and hydraulic jack setup for uplift and compression test, respectively. The bottom figure shows the hollow stem augers and reaction frame setup with respect to the drilling truck.

The main component of the reaction beam was constructed from two C8x11.5 channel sections, each of 4 ft (1.2 m) long, assembled together by means of lateral stiffeners at four locations along the beam. The beam was seated on each auger through W8x10 sections and a 2-in (50-mm) outside diameter pipe for alignment. Figure 4.4 (top and middle) presents further details of the reaction load system. Figures 4.5a and 4.5b shows the actual setup of the reaction frame for static uplift and compression test, respectively, at the White City, FL sites.

4.4.2.2 Load Transducers

For load measurement, the instrumented SPT rod for dynamic monitoring was again employed. A strain gauge signal conditioner manufactured by Daytronic, Model 3170 balanced and

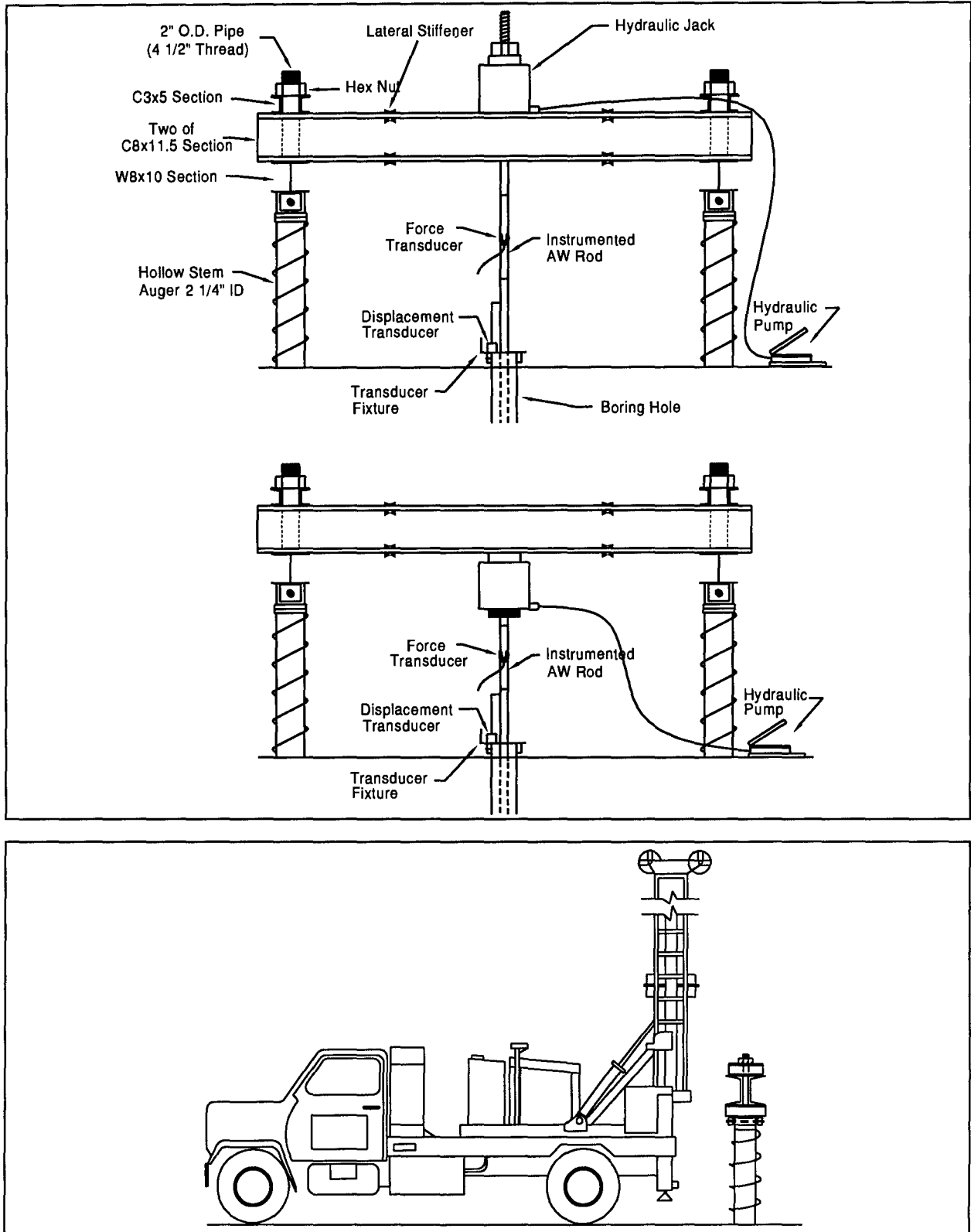


Figure 4.4: Schematic Static Uplift and Compression Test Setup

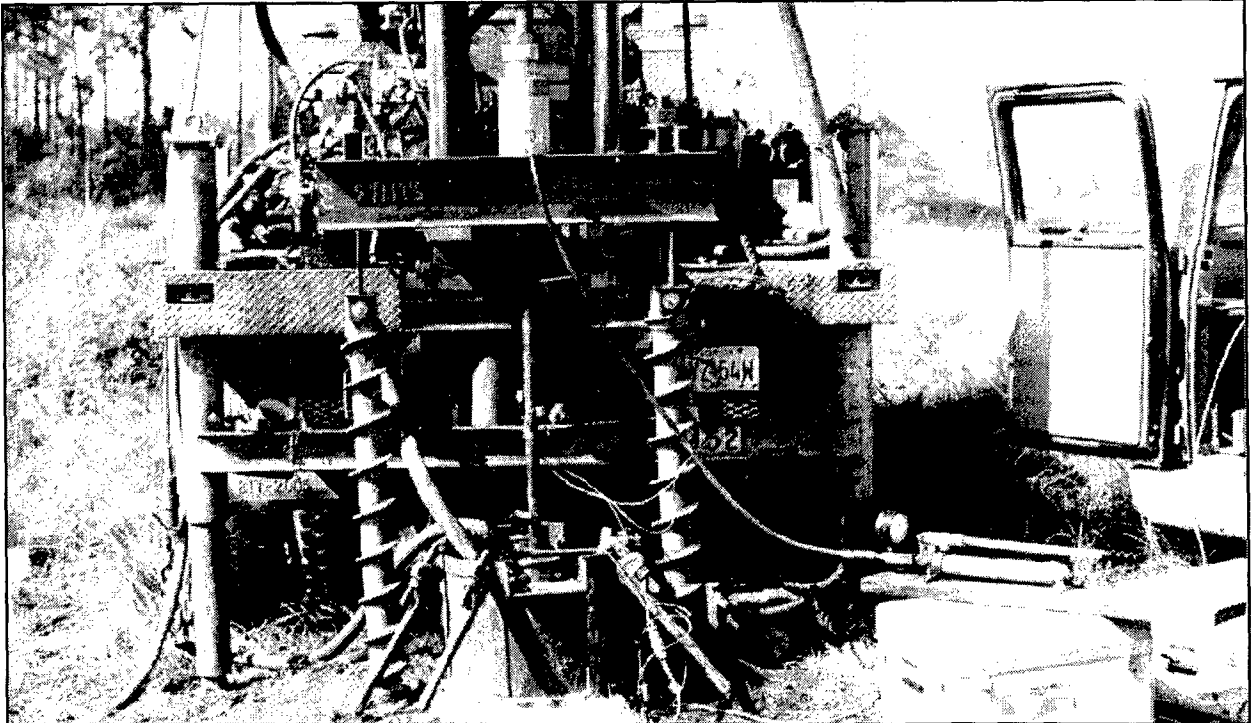


Figure 4.5(a): Static Uplift Test Setup at White City, TP3, FL Site

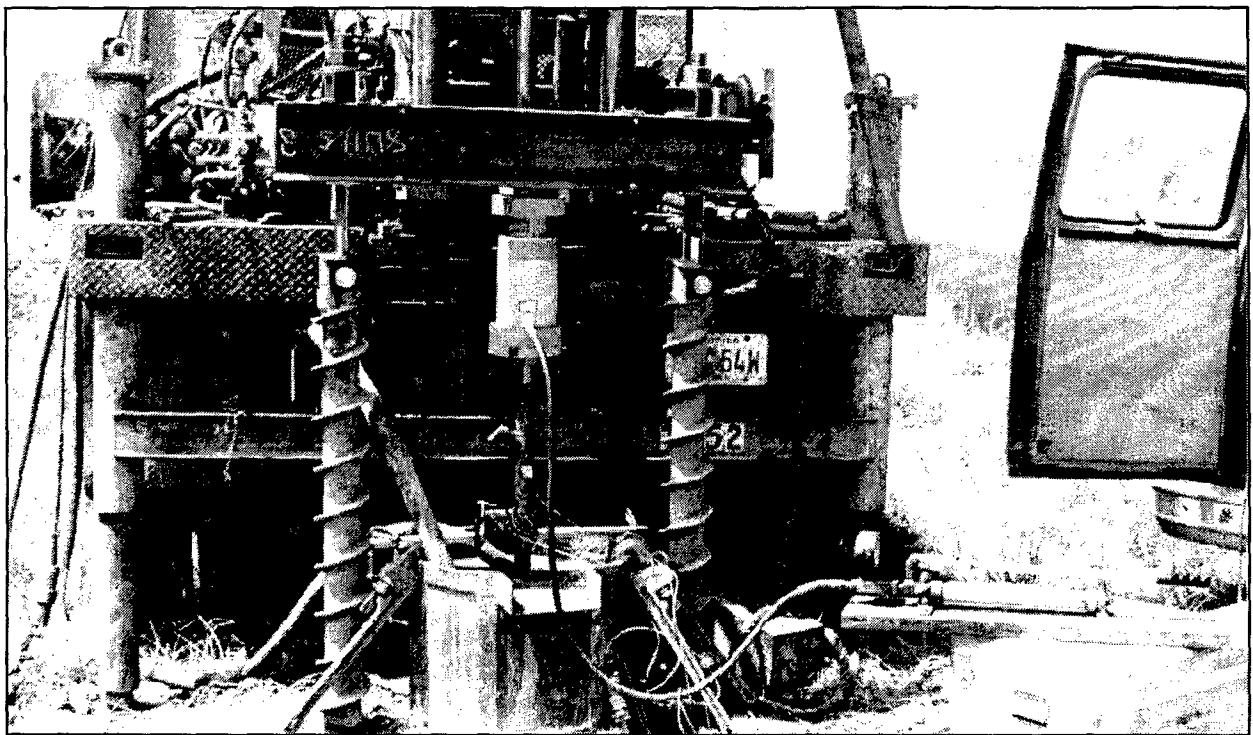


Figure 4.5(b): Static Compression Test Setup at White City, TP6, FL Site

amplified the strain gauge signals from the instrumented SPT rod, before the signal was fed into the data acquisition system.

4.4.2.3 Displacement Transducers

For displacement measurement, a wooden reference beam was initially used and was set up near the drill hole just before the static load test. The reference beam was supported approximately 3 ft (1 m) away from the drill hole. Later in this study, the reference beam was replaced by a fixture mounted on the casing or hollow stem auger at the drill hole, depending on the drilling method used. This fixture was designed to be used for both uplift and compression tests, as well as the torque test discussed below. Based on the field experience gained in this study, the casing or hollow stem auger at the drill hole should provide an adequate reference for the displacement measurements.

The displacement transducers used in this study were a cable extension type, obtained from Psitronix, Model DT-10-A, having a range of 10 in (254 mm). The transducer was mounted on the fixture and the cable was attached to the drill rod. An internal spring maintained a constant tension on the cable and also served as the retraction mechanism. When displacement occurred, the cable extended from the transducer while rotating a sensing element connected to the internal drum. The displacement was measured from the cable extension or retraction during uplift or compression test, respectively. The displacement transducers were recalibrated by the contractor. The calibration results are presented in appendix G.

4.4.2.4 Spacers

During some compression tests, depending on the drilling method, spacers were inserted in the drill rod connections at 10 ft (3 m) intervals to prevent drill string buckling. The spacers were effective when hollow stem augers or continuous casings were used in advancing the drill hole. However, in some cases, only drilling mud was used without casing and for those cases, the spacers were not considered useful and therefore disregarded. A simple calculation was performed to check the significance of buckling to the measured displacement near the top of the drill string. The calculation indicated that even without the spacers, the top displacement due to buckling (if it occurred) would be insignificant in comparison with the magnitude of displacements measured in this study.

Since the Modified SPT was designed to work with all drilling methods, no particular drilling method was prescribed. Several drilling methods were used in this study including hollow stem auger, continuous casing with water only, continuous casing with drilling mud, partial casing with drilling mud, and drilling mud only without casing.

4.4.2.5 Data Acquisition and Software

The static load test was also monitored with the PDA, Model PAK. A special load test program called Automatic Load Test Program™ (ALTP) was developed which used the data acquisition capability in the PDA to record data. The program can be used for up to eight measurement channels. During a static load test, the program recorded the force and displacement data continuously and saved results into the PDA's hard disk at a user specified frequency. The program displays the load vs displacement curve, the load and displacement time history, and the displacement rate on the PDA's screen during the in progress static load test. Other optional features available in the program include the display of the Davisson's failure criterion, a transducer zero offset correction, and a pile weight correction. The displacement rate display in this program provided assistance for maintaining a constant penetration rate. The pile weight option added the weight of the drill rod to the measured compressive load or subtracted from the measured uplift load. This adjustment is important for this study since the weight of the rod can be significant in comparison with the measured soil resistance load. The weight adjustment will be discussed further in chapter 5.

4.4.3 Torque Static Test

Using torque loads to determine the soil shear strength has been adopted by the in-situ vane shear test to determine the undrained shear strength of soft clays. The Swedish Dynamic Cone Penetration Test (DCPT) practice has also included torque measurements for a rough evaluation of the soil shear strength (Ericksson, 1990). Torque testing after SPT sampler driving was considered particularly valuable in this study, since it could be correlated with results from both static uplift tests and dynamic tests.

The torque tests were initially performed with a torque wrench manufactured by APCO Mossberg, Model 8096A, which was capable of measuring torques up to 300 lb-ft (406 N-m) with an accuracy of 5 lb-ft (7 N-m). The results obtained from the torque wrench were promising and therefore an instrumented torque rod was designed and manufactured by PDI. The instrumented torque rod was designed similar to the instrumented SPT rod. Foil type strain gauges were again glued onto two directly opposite sides of a 2-ft (0.6-m) AW rod and were wired to form a full Wheatstone bridge. The calibration results of the instrumented torque rod are presented in appendix G.

An adaptor, consisting of an AW sub and a 2½-in (64-mm) nut, was attached to the top of the instrumented torque drill rod application. A 2½-in (64-mm) socket with a 1-in (25-mm) "T" drive adaptor was mounted on top of the nut. The torque was manually applied by using a 4-ft (1.2-m) rod inserted into the "T" drive adaptor. The instrumented torque rod setup is presented in

figure 4.6. A photograph in figure 4.7 shows an engineer performing the torque test at the White City, FL site.

The rotation due to torque was measured with the same displacement transducer and mounted on the same fixture for uplift and compression test. The displacement transducer was positioned such that when the torque was applied, the transducer cable wrapped around the drill rod and measured the circumferential displacement. This displacement was later converted to angle of rotation. Both torque and rotation were automatically recorded by the PDA-ALTP program described in section 4.4.2.5 above.

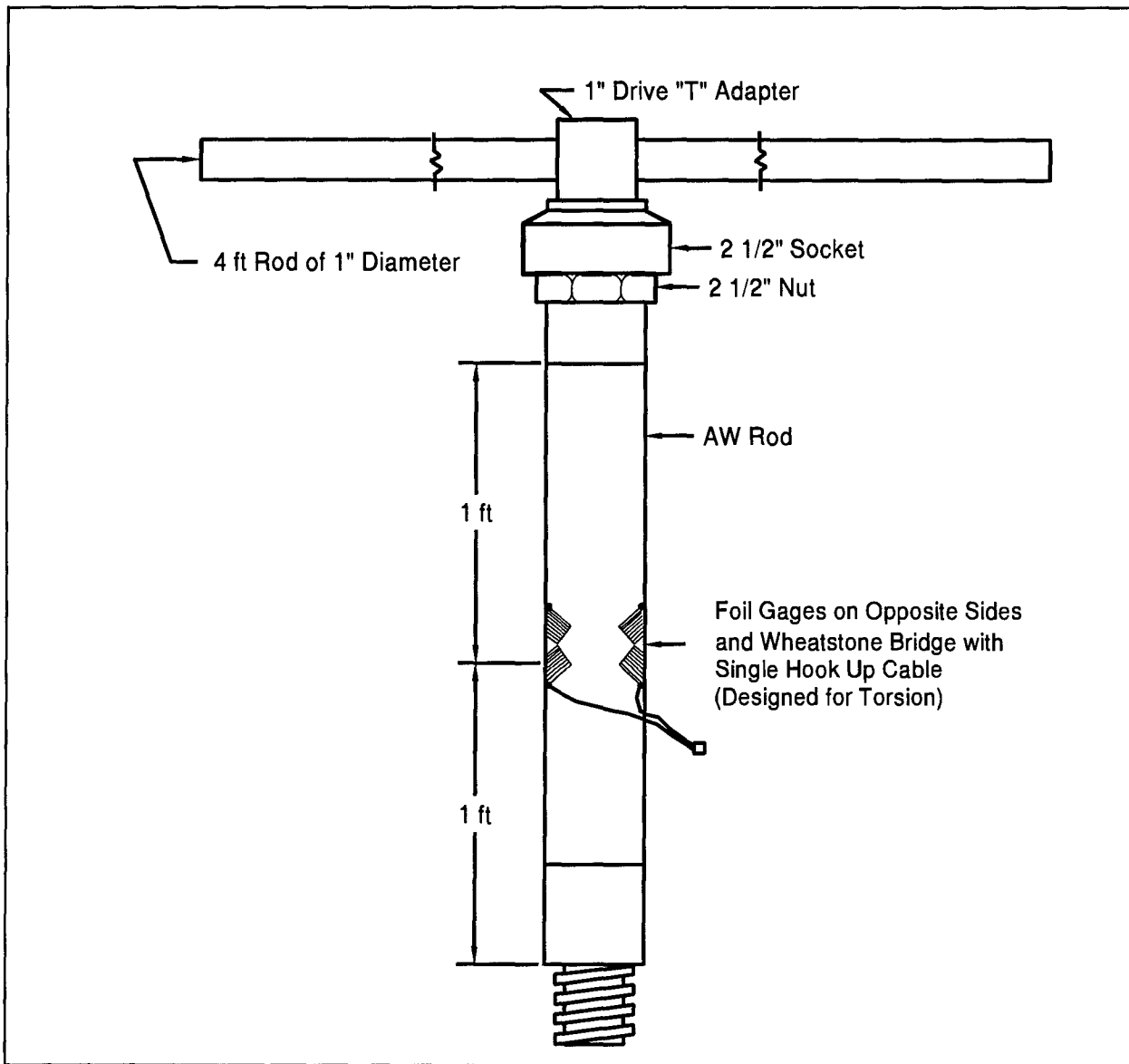


Figure 4.6: Instrumented Torque Rod

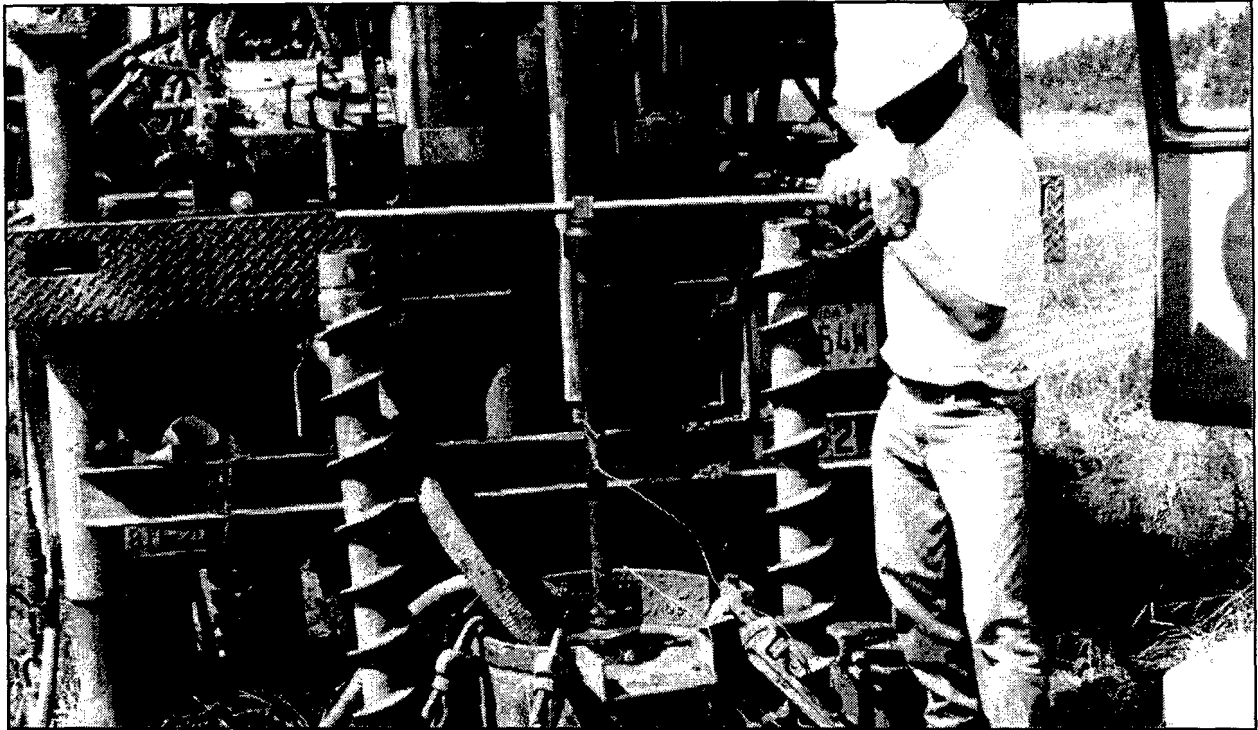


Figure 4.7: Torque Test Being Performed

4.4.4 Instrumented Sampler

Force and velocity records measured during SPT driving formed the basis for the calculation of dynamic soil parameters. Before these parameters can be determined, the bottom force and velocity at the sampler location must be calculated from the top measurements. To confirm that this calculation is correct, a split spoon sampler was instrumented with strain gauges and an accelerometer to directly measure sampler force and velocity, respectively. Instrumentation added to the sampler was the same as that used for the rod top. Due to the time consuming and complicated nature of the test (e.g., wire feeding through the rod and gauge protection), sampler instrumentation was only attempted once. This one test proved the validity of the theoretically correct top measurement approach. The instrumented sampler results are discussed in chapter 5.

4.4.5 Cone Penetration Test

The Cone Penetration Test (CPT) was not performed specifically in this study. However, four CPT results were available at one correlation and three verification test sites to independently estimate the static capacity of the piles. The CPT results are also compared with the unit shear resistance and end bearing obtained from uplift and/or compression test in section 5.1.8. At the correlation test site, the CPT was performed near the test pile location; at all three

verification sites, the CPT was performed immediately at the test pile location. The CPT results are presented in appendix F.

4.5 THE MODIFIED SPT TEST PROCEDURE

A summary of the Modified SPT test procedure is presented in table 4.1. The normal SPT driving operation is strictly adhered to during sampler driving for 18 in (457 mm), so that the N-value is not affected. Furthermore, the dynamic measurements do not affect the N-value measurements. These measurements include the hammer impact energy measurements by HPA, and the rod top force and velocity measurements by PDA.

After the normal SPT procedure is completed, if the N-value is less than 40, a few additional hammer drops using at least two different reduced heights are applied such that the rod penetration is about 0.2 in (5 mm) per blow which corresponds to 60 to 120 blows/ft (197 to 394 blows/m). Different drop heights are useful for studies of soil damping and static resistance. If the soil layer has a potential for setup, then a restrike test (with at least two different hammer drops) is performed after a 5-min wait. If the restrike test indicates an increase of blow count by more than 20 percent, a 15-min, 1-h, or possibly overnight wait restrike is also attempted with again at least two hammer drops. The waiting times allow the pore water pressure to dissipate; the restrike tests will allow for an assessment of soil strength changes with time and therefore a better estimate of the long-term soil strength.

Next, uplift tests are performed to determine the shear resistance between the soil and sampler. The uplift test is performed with three different pulling rates ranging between 0.01 and 1.8 in/min (0.25 and 45.7 mm/min) to investigate rate effects on soil resistance. The uplift test is performed with different wait times ranging between 15 min and 15 h. In addition, at some sites, torque tests were performed after the uplift tests and just before sampler extraction.

If the N-value and the extracted sample indicates that the soil layer has the potential for significant end bearing; the sampler is replaced with the oversized tip. When the oversized tip is used, the tip is then driven at least 6 in (152 mm) or 50 blows whichever occurs earlier. Dynamic force and velocity data are also recorded during driving with the oversized tip. At the end of tip driving, several different additional hammer drops (at least two) are applied such that the penetration per blow is about 0.2 in (5 mm) per blow. Where relaxation is expected such as when the tip soil is a very dense silty sand, decomposed shale, or shale, a 30-min to 12-h restrike should be attempted.

Table 4.1: The Modified SPT Procedure

Items in *italics* were performed only for this study

1.	Advance drill hole to the required test depth and insert the split spoon sampler.
2.	Attached the instrumented rod to the top of the drill string just before mounting the hammer.
3.	Perform a normal SPT procedure (18 in or 457 mm of sampler driving) while measuring force and velocity with the PDA, and the hammer impact velocity with the HPA.
4.	If N-value is less than 40: reduce the hammer drop height such that equivalent N-value is around 60 to 120, (i.e., rod penetration of 0.1 to 0.2 in or 2.5 to 5.0 mm per blow).
5.	If the soil layer has a potential for setup: wait for 5 min and then restrike with at least two different hammer drop heights.
6.	If restrike in step 5 yields more than 20 percent set / blow: wait for 15 min, 1 h, or possibly overnight and then restrike again with at least two different hammer drop heights.
7.	<i>Remove the hammer and perform static uplift tests at three different rates. Repeat the test after some wait period.</i>
8.	<i>Perform torque test after the static uplift test and before sampler extraction.</i>
9.	Extract sampler from drill hole, inspect, mark and save the sample.
10.	If N-value, extracted sample and uplift test suggest that the soil layer is significant for end bearing: Replace sampler with a special tip and re-insert the rod in the drill hole.
11.	Attach the instrumented rod, mount the hammer, and drive the tip at least 6 in or 50 hammer blows whichever is achieved first; while taking the force velocity measurement.
12.	If the tip penetration is more than 0.2 in (5 mm) per hammer blow: reduce the hammer drop height such that the above tip penetration is achieved.
13.	When relaxation is expected such that in a very dense silty sand, decomposed shale, or shale, a 30-min to 12-h restrike should be performed.
14.	<i>Remove the hammer and performed a static compression test with at least three different loading rates. If relaxation is expected then repeat the static and dynamic test after some wait period.</i>
15.	Advance to the next sampling depth.

In this study, compression load tests were performed after tip driving to determine the bearing capacity of the soil. During static loading with the special tip, three different loading rates were also investigated. Restrike tests were not performed with the special tip because relaxation was not suspected in the soils encountered during this study.

4.6 LOCATION OF TEST SITES

A total of 11 sites were investigated in this study. Seven of these sites were used for a *correlation study* and method improvement, 3 sites were used in *Class-A verification* of the improved method, and one site, the "Sunshine Skyway Bridge, FL" originally planned for verification tests had to be aborted because the original pile driving plan was cancelled. At each of these 10 sites, both static and dynamic load tests had been or were later performed. Information about soil, pile driving system, and pile driving conditions for each site are presented in appendix F.

The name of each site, abbreviated name, test type, and the dominant soil type at the pile shaft and toe are summarized in table 4.2. The abbreviated name will be used in this report for convenience.

4.6.1 Correlation Study Sites

The first seven sites listed in table 4.2 were used in the correlation study to improve the method. Both pile driving and static load test had been completed at the time the Modified SPT procedure was performed. The correlation study sites were selected because of the particularly interesting soil conditions previously encountered at these sites. Each of these sites will be discussed briefly. The subsurface conditions presented are based on the existing soil boring (if available) and the laboratory classification using the samples obtained from this study.

St. Mary site is located in the "Flats" area, of downtown Cleveland, OH near the Cuyahoga River. In 1992, H-piles (HP12x53) were installed at this site for the foundation of a cement silo. The soils in this area have been difficult for prediction of both capacity and driveability. Difficulties occurred because pile driving was relatively hard and yet the static bearing capacities were often low. The blow count and static resistance often appeared to be unrelated. The soil consisted of approximately 10 ft (3 m) of fill, underlain by 40 ft (12 m) of mainly sand with a mixture of silt and gravel (SP-SM). Underlying the sand layer, from a depth of 50 to 150 ft (end of boring) or 15 to 46 m, the soil consisted of silty clay with occasional sand layers (SC to CL). The SPT N-values for the silty clay layer ranged between 10 and 50. The ground water depth was at 1 ft (0.3 m). The silty clay soil in this area has been observed to behave in a very "bouncy" manner during pile driving which is partly responsible for the hard driving condition.

Sites	Abbreviated Name	Site Type	Pile Type	Dominant Soil Type	
				Shaft	Toe
1. St. Mary, Cleveland, OH	St. Mary	Correlation	HP12x53	SC	SC
2. Fore River Bridge, Portland, ME	Portland	Correlation	18" Pipe	SP-SM	SP-SM
3. C&D Canal, Pier 17, DE	CD17	Correlation	24" PSC	SM	SM
4. C&D Canal, Pier 21, DE	CD21	Correlation	24" PSC	SM	SM
5. White City Bridge, TP3, FL	WC3	Correlation	24" PSC	SC	SP-SM
6. White City Bridge, TP6, FL	WC6	Correlation	24" PSC	SM	SP-SM
7. Apalachicola River Bridge, FL	AP	Correlation	24" PSC	SC	SC
8. Sunshine Skyway Bridge, FL	Skyway	Aborted	N/A	SP-SM	SP-SM
9. Aucilla River Bridge, FL	Aucilla	Verification	18" PSC	CH	Limerock
10. Vilano Bridge - East, FL	VE	Verification	18" PSC	SP	SW
11. Vilano Bridge - West, FL	VW	Verification	18" PSC	OH	ML

Notes: PSC - Prestressed Concrete Pile.

1 in = 25.4 mm.

According to the existing soil boring (Boring L-4), traces of gravel and rock fragments were encountered near the test pile toe (105 ft or 32 m depth below grade), a condition which probably caused the SPT N-value to increase to 104. The existing soil boring was used in conjunction with the test result obtained from this study. The St. Mary site is included in the data base under ID# 43.

The *Portland site* is located along the Fore River and within the International Ferry Terminal Facility in Portland, ME. During driving of 18 in (457 mm) O.D. pipe piles for the Fore River Bridge Replacement foundation in 1990, an unusually large toe quake was observed at this site. The large toe quake can result in pile capacity overprediction, or blow count and tension stress underprediction when not recognized in a wave equation analysis. The subsurface conditions can be described as approximately 13 ft (4 m) of fill overlying a medium dense to very dense, medium to fine sand with varying amount of gravel and silt to approximately 87 ft or 26 m (SP-SM to GP-GM) or locally known as ablation till, as indicated in Boring B558. The ground water depth varied between 9 and 15 ft (3 to 5 m) depending on the tide in Portland harbor. The test

pile had been driven to a depth of 53 ft (16 m) below grade where the SPT N-value was 32. The SPT N-values of the ablation till layer along the test pile shaft varied between 15 and 39. The ablation till layer is suspected as the cause of the large toe quake. The Portland site data can be retrieved from the data base at ID# 24.

The **CD17 and CD21 sites** are located at Pier 17 and 21, respectively, of the Chesapeake and Delaware Canal Bridge in St. Georges, DE. Wave equation analyses using standard soil parameters had been underpredicting pile capacity of the 24-in (610-mm) square prestressed concrete piles. CAPWAP analysis of the dynamic records indicated that a good matching can only be obtained by using the soil model with radiation damping. The subsurface conditions at both of these sites generally consisted of silty fine sand with a trace of gravel (SM), and some layers of silty clay to clay (CL or CH). The toes of the test piles were at a depth of 66 and 72 ft (20 and 22 m) and were seated on the silty fine sand (SM) with the SPT N-values of 56 and 15, for Pier 17 and 21, respectively. Ground water depths were at 19 and 30 ft (6 and 9 m) according to borings SB#424 and SB#428 for Pier 17 and 21, respectively. The CD17 and CD21 sites have been included in the data base under ID# 204 and 203, respectively.

WC3 and WC6 designate the Piers 5 and 8, respectively, of the White City Bridge which is located on State Road 71 across the Intercoastal Waterway, northeast of Port St. Joe, in South Central Gulf County, FL. A large toe quake behavior, similar to that at the Portland site, had been encountered during driving of 24-in (610-mm) square prestressed concrete piles at these two sites. The soil generally consisted of silty sand (SM) with alternating layers of silty sandy clay to silty clayey sand to depths of approximately 30 and 20 ft (9 and 6 m) for WC3 and WC6, respectively. The SPT N-values for this silty sand layer varied between 1 and 12. A 10 to 15 ft (3 to 5 m) layer of dense sand (SP) found below the silty sand layer had the SPT N-values ranging between 14 and 55 where the toes of both test piles were seated. The ground water level was very close to the surface. The similarity between the Portland and WC sites can be attributed to the fully saturated dense sand which probably contributed to the large toe quake behavior. The data base contains complete information about the test piles at ID# 62 and 63.

The **AP site** is situated at Pier 3 of Apalachicola River Bridge, Franklin County, FL. The wave equation correlation study performed for this project indicated an unusually high shaft or toe damping factor, up to 0.7 s/ft (2.29 s/m) for the 24-in (610-mm) square prestressed concrete piles. When a standard wave equation damping factor was used in the restrrike analysis, the pile capacity was overpredicted in comparison with the static load test capacity based on Davisson's criterion. The soil boring near the test pile indicated approximately 40 ft (12.2 m) of very loose to loose clayey sand (SC) with SPT N-values ranging between 1 to 14, overlying approximately 10 ft (3.1 m) of stiff clay with SPT N-values between 9 to 11. Below the clay layer, from a depth of 50 ft (15 m) to the end of the boring, a dense clayey sand was encountered with SPT N-values between 12 and 33. The test pile was driven to a depth of approximately 89 ft (27.1 m)

into this dense clayey sand. Ground water was encountered near the surface. Several soil borings around the site indicated the presence of high piezometric pressures which, in conjunction with the clayey sand, were probably responsible for the high damping factor. CPT results in the proximity of the test pile are available and presented in appendix F. The AP site is presented in the data base under ID# 1.

4.6.2 Verification Sites

The last three sites listed in table 4.2 were used for Class-A verification of the improved method and were designated as verification sites. The University of Florida at Gainesville is also conducting research at these three sites to study soil setup on concrete piles. These researchers are responsible for conducting the static tests of the full-scale piles. CPT results at the test pile locations for all three sites are presented in appendix F.

The **Aucilla site** is located at the west end of Aucilla River Bridge (Eastbound) on State Road 20, Jefferson and Madison County, FL. The soil condition at this site generally can be described as silty clay to clay (CL to CH) with alternating layers of clayey sand to sand, overlying sandy limestone. The ground water depth was at 4 ft (1.2 m). The test pile, an 18-in (457 mm) square prestressed concrete section, was apparently driven to the limestone at depth of 63 ft (19.2 m).

VE and VW sites are located at the east and west embankment, respectively, of the Vilano Bridge on State Road A1A at St. Johns County, FL. CPT results are available for both Vilano Bridge sites and included in appendix F.

At the VE site, the soil basically consisted of loose sand (SP) with SPT N-values between 2 (near the top) and 20, at the design depth 35 ft (10.7 m). The SPT N-values were 28 at 40 ft (12.2 m) depth.

The top 30-ft (9 m) layer of the VW site consisted of sand to silty sand which is not expected to contribute significant shaft resistance to the test pile due to jetting. From 30 to 63 ft (9 to 19 m), the soil consisted mainly of clay (CH and OH) based on the soil samples obtained for this study. The SPT N-values were less than 5. The test pile toe is to be driven to a silty sand layer with an SPT N-value of 20.

CHAPTER 5

DATA REDUCTION, ANALYSES, AND RESULTS

5.1 STATIC RESULTS

5.1.1 Background

A load test was performed on the Modified SPT at the end of both sampler and tip driving to determine the static shaft resistance strength and end bearing, respectively. During the test, rod top load and displacement were monitored with the PDA's data acquisition system which was controlled with the Automatic Load Test Program (ALTP) program. The load was measured with the same instrumented SPT rod which was used for dynamic monitoring during sampler driving. The displacement was measured with a cable extension displacement transducer. Both the load and displacement were recorded by the ALTP and stored on the PDA's hard disk. Similar instrumentation was also used for monitoring the torque and circumferential displacement during the torque test. Descriptions of this equipment have been given in chapter 4.

Since the load and displacement were measured near the top of the drill string during the static load tests, corrections had to be made to determine the actual load and displacement experienced by the soil at sampler or special tip. These corrections included the weight of drill rod and an estimate of the elastic compression or elongation of the drill rod. For an uplift test, the weight of the drill rod was subtracted from the measured load, and the elastic elongation was subtracted from the measured displacement; for a compression test, the weight of the drill rod was added to the measured load, and the elastic compression was subtracted from the measured displacement. The corrected load *versus* displacement plots presented in appendix B, therefore, represent the actual soil response.

During a torque test, torque and circumferential displacement were measured near the top of the drill string. Corrections of the measured top circumferential displacements to account for drive rod twist were not attempted because of the unknown connector slack and the insignificance of the elastic twist in comparison to the magnitude of the circumferential displacement measurement. The amount of elastic twist in the SPT rod is a function of torque and the length of the torque rod. To demonstrate the insignificance of this elastic twist, it was calculated for both maximum length (105 ft or 32 m) and maximum torque (350 lb-ft or 475 N-m) encountered in this study and was found to be approximately six degrees, corresponding to a circumferential displacement of approximately 0.10 in (2.5 mm). Compared to the typically applied total angle of twist of 90 degrees, this value was insignificant.

5.1.2 Uplift and Compression

The static load test results are presented as load *versus* displacement plots and are included in appendix B. The static load test results were used in determining the unit soil strength (shaft resistance and end bearing) and the quake. The load *versus* displacement of most soils in uplift (shaft shear resistance) conformed to an "elasto-plastic" behavior which agreed with the Smith model assumption used in the wave equation analysis. However, unlike the shaft shear resistance, the compressive (end bearing) load *versus* displacement did not always behave ideally elasto-plastic, but rather indicated some degree of strain hardening. As expected, this strain hardening effect was more clearly indicated in granular soils. Figure 5.1 shows load *versus* displacement curves from both a clay site and a sand site. The curves were obtained from the static compression tests performed at St. Mary and Portland, respectively, using the flat end tip. As shown in figure 5.1, the load *versus* displacement curves for the clayey soil (CL) is elasto-plastic with only a very slight strain hardening effect. In contrast, the load *versus* displacement for the sandy soil (SP-SM) shows a significant strain hardening effect. In this case, the load increases from 3.0 to 5.5 kips (13.3 to 24.4 kN) from the point of the Davisson's failure load to 4 in (102 mm) of tip displacement. The measured capacity of the sandy soil, therefore, strongly increased with tip displacement.

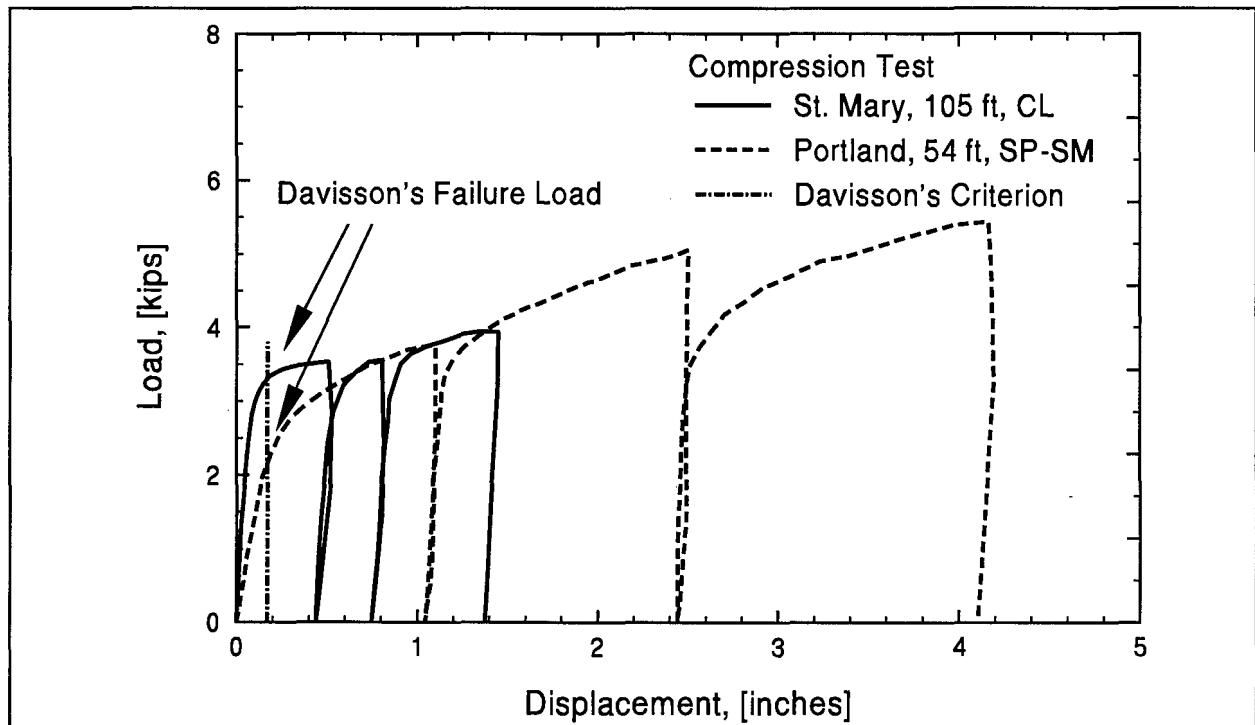


Figure 5.1: Typical Load *versus* Displacement for Clay and Sand

Since the uplift load *versus* displacement of the SPT sampler in most soils behaves elasto-plastically, the unit shaft resistance was determined from the *pullout load* which was the same as Davisson's failure load. The unit end bearing was calculated from Davisson's failure load.

The soil shaft quake was determined from the intersection of the initial tangent of the load *versus* displacement curve with the horizontal line through the pullout load. The shaft quake values obtained from most uplift tests generally ranged from 0.03 to 0.06 in (0.76 to 1.52 mm). Soil toe quake values from the compression load *versus* displacement curves were not as clearly defined because of the strain hardening effect. For consistency, the toe quake was determined by taking the intersection between the initial tangent line through the origin and the horizontal line passing through Davisson's failure load.

5.1.3 Comparison of Flat and Cone Tip

Bearing behavior on two types of oversized SPT tips (one having a flat end and one a cone shaped tip; see chapter 4) was investigated. Comparison tests of the performance of these two tips were conducted at the Portland and CD21 sites. At both sites, the tips were tested within 2-ft (0.61-m) depths for a meaningful comparison. At the Portland site, the flat end tip was used first followed by the cone tip; at the CD21 site, the sequence was reversed to reduce the possibility of an incorrect conclusion due to loading history effects.

At the Portland site, rotary drilling with water stabilization was used in advancing the hole to the sampling depth. The drill hole location was within 10 ft (3.1 m) of the full-scale test pile. Compression tests were conducted at depths of 54 and 56 ft (16.5 and 17.1 m) using first the flat end tip and then the cone tip. The full-scale pile toe was seated at a depth of 54 ft (16.5 m) below grade. The soil, between the test depths was described as dense, silty medium to fine sand with coarse gravel, or SP-SM based on the USCS classification using the sample obtained from this study. The SPT N-values ranged from 34 to 39 between depths of 45 and 60 ft (13.7 and 18.3 m). The flat end tip was tested first at a depth of 54 ft (16.5 m), exhibiting a driving resistance of 40 blows for 6 in (152 mm) of tip penetration and a Davisson's tip capacity of 2.3 kips (10.2 kN). The drill hole was then advanced to 56 ft (17.1 m) to test the cone tip. The driving resistance of the cone tip was an equivalent of 21 blows for 6 in (152 mm) of tip penetration and a Davisson's tip capacity of 1.5 kips (6.7 kN). Both driving resistances occurred under an average donut hammer transfer efficiency (energy measured in rod divided by SPT potential energy) of 17 percent, with the driving resistance of the cone tip prorated for an equivalent driving resistance at an equal transfer efficiency. The load *versus* displacement plots for both tips are superimposed in figure 5.2. Both the driving resistance and tip capacity of the cone tip indicated a lower value than the flat end tip, even though the SPT N-values from an existing soil boring did not indicate any reduction between 54 and 56 ft (16.5 and 17.1 m). Both the static load test and the dynamic test results for the full-scale pile indicated a soil type

with large quake behavior. The static load *versus* displacement plots of both tips, presented in figure 5.2, indicated such a large quake on the flat end tip but not on the cone tip. Based on the CAPWAP analysis results, the unit end bearing of the full-scale pile was 147 ksf (7.1 MPa) compared to 110 and 56 ksf (5.3 and 2.7 MPa) for the flat end and cone tip, respectively. These tip resistance values were taken at the same tip displacement as those of the full-scale pile's maximum CAPWAP toe displacement.

At the CD21 site, drill holes were advanced with hollow stem augers to the sampling depth. The drill hole was located within 20 ft (6.1 m) of the full-scale pile. The full-scale pile tip depth was 72 ft (21.9 m) below grade. According to an existing boring, the soil consisted of a medium dense silty fine sand, with some mica, and a trace of coarse sand, gravel, and organic material, *i.e.*, SM based on the USCS classification using the sample recovered from this study. The SPT N-values at this depth varied between 13 and 19. The compression tests were conducted at a depth of 70 ft (21.3 m) with the cone tip and then at 71 ft (21.6 m) with the flat end tip. The driving resistance of both tips was 9 blows for 6 in (152 mm) of tip penetration and at an average safety hammer transfer efficiency of 54 percent. The Davisson's tip capacities were 1.3 and 1.5 kips (5.8 and 6.7 kN) for the cone and flat end tips, respectively. The corresponding load *versus* displacement plots are presented in figure 5.3. Beginning of restrike CAPWAP analyses of the full-scale pile indicated a unit end bearing of 88 ksf (4.2 MPa) compared to 37 and 48 ksf (1.8 and 2.3 MPa) for the cone and flat end tip, respectively, at both tip displacements equal to the full-scale pile's maximum CAPWAP toe displacement.

Based on these two test results summarized in table 5.1, the flat end tip indicated higher unit end bearings than the cone tip. The unit end bearing predictions of the flat end tip at the Portland site (for which telltale measurements were made) appeared to agree better with the full-scale test results than the cone tip. In addition, it appeared that the flat end tip was more likely to detect soil with "large quake" behavior as observed on the full-scale pile. It was, therefore, decided to use the flat end tip exclusively at both the remaining correlation sites and at the method verification sites.

5.1.4 Scale Factor for Unit End Bearing Prediction

To evaluate the accuracy of unit end bearing predictions from flat end tip measurements, comparison calculations were made using unit end bearing from either a full-scale pile static load test or from CAPWAP. The unit end bearing of the full-scale pile can be calculated from the static load test results only when telltales or other load transfer measurements were made during the static load test. The load and displacement measured at the pile top, in addition to the telltale results, can be converted into the load and displacement transferred to the pile toe using the method discussed by Fellenius (1980). The main objective of this evaluation was to

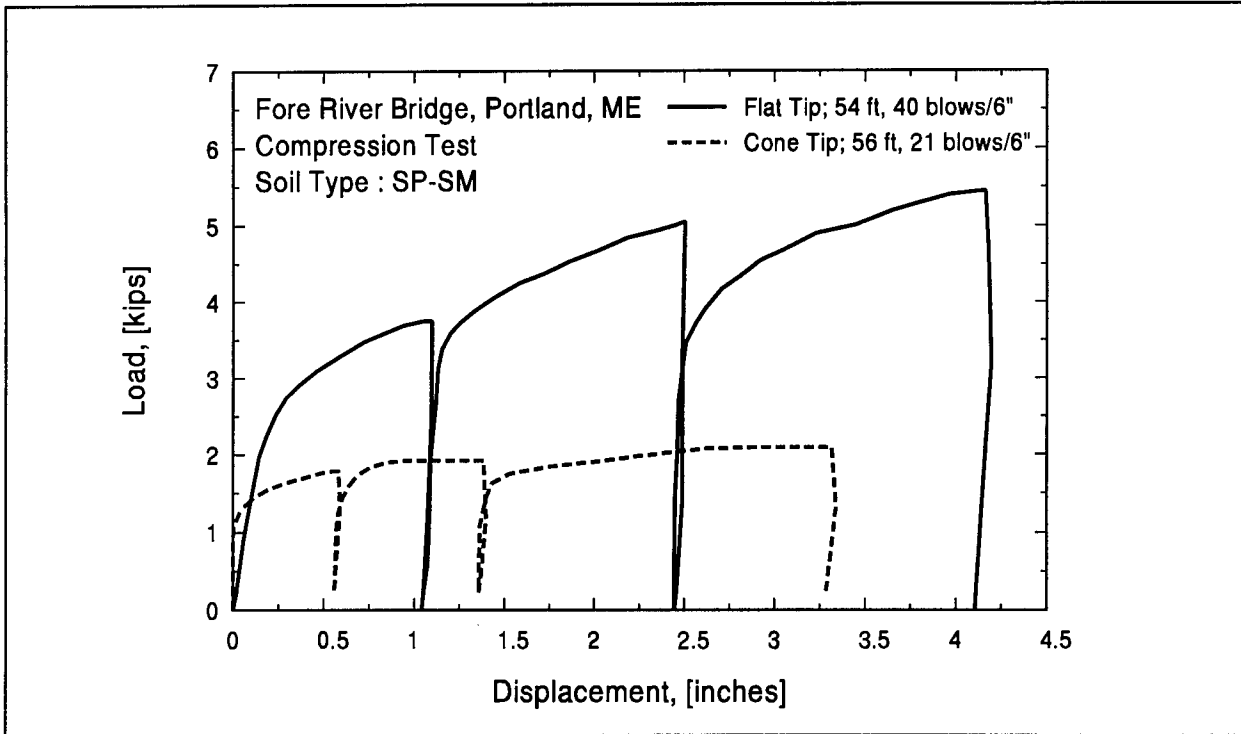


Figure 5.2: Load versus Displacement for Flat End and Cone Tip at Portland Site

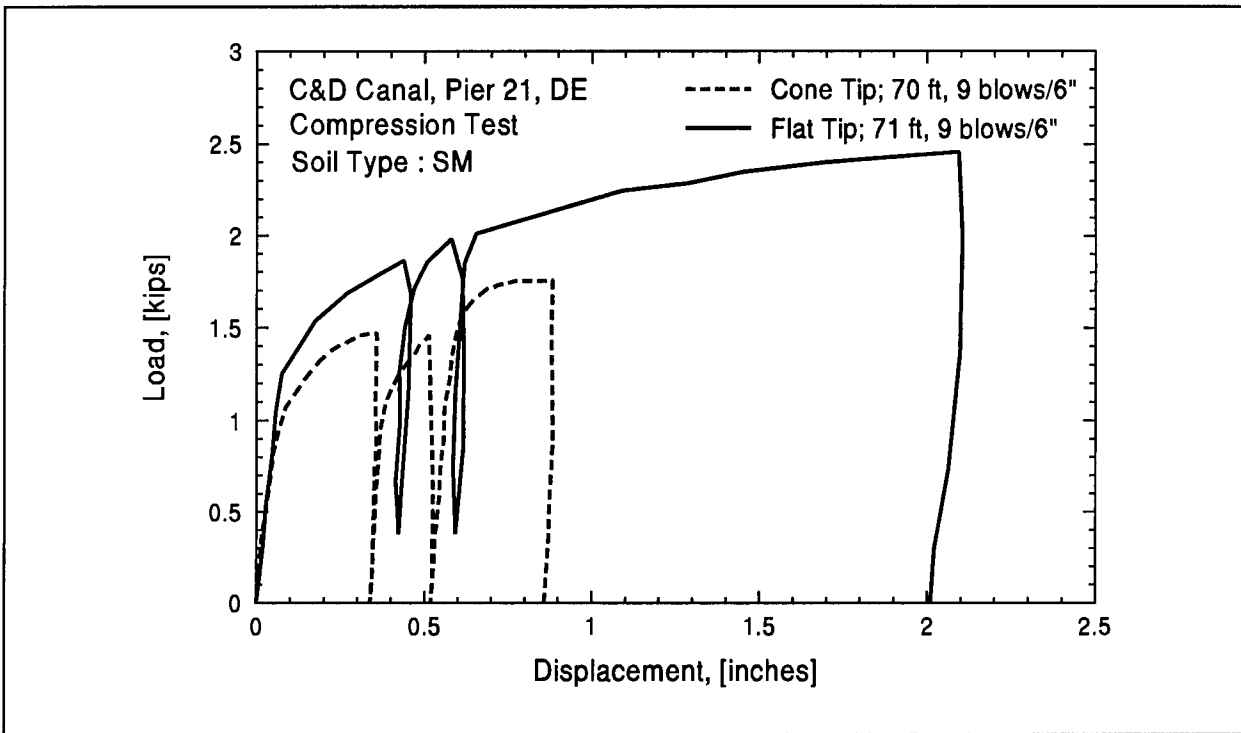


Figure 5.3: Load versus Displacement for Flat End and Cone Tip at CD21 Site

Site	Tip Type	Driving Resistance [blows/6"]	Hammer Transfer Efficiency [%]	Unit End Bearing		Soil Type
				Tip* [ksf]	Full-scale Pile [ksf]	
Portland	FLAT END	40	17	80	147	SP-SM
	CONE	21	17	56		SP-SM
C&D 21	FLAT END	9	54	48	88	SM
	CONE	9	54	37		SM

Notes: (*) On the Modified SPT the unit end bearing is taken at the maximum calculated tip displacement of the full-scale pile.
 1 in = 25.4 mm; 1 ksf = 48 kPa.

establish whether or not a scaling factor would be required for the calculation of full-scale pile end bearing from the flat end tip measurements.

At two of the six correlation sites (Portland and Apalachicola), the static load tests of the full-scale pile were instrumented with telltales. Therefore, the load transferred to the pile toe and the toe displacement are approximately known. The unit end bearing was calculated by dividing the load at the pile toe by the bearing area of the pile; this result was plotted *versus* displacement of the full-scale pile in figures 5.4 and 5.5, respectively. The unit end bearing *versus* displacement curve of the flat end tip was depicted on the same plot for comparison. In addition, a scale factor was calculated for agreement between the full-scale pile curve and the flat end tip curve and the resulting scaled unit end bearing *versus* displacement curve of the flat end tip was also displayed in these figures.

The flat end tip results from all six correlation sites were compared with the unit end bearing from full-scale piles. At each of the correlation sites, a flat end tip compression test was performed at the toe depth of the full-scale pile. The unit end bearing predictions from flat end tip measurements were compared with those determined from either CAPWAP or static load test results of the full-scale pile, and summarized in table 5.2. The ratios presented in table 5.2 were determined from the unit end bearing calculated by CAPWAP divided by the unit end bearing predicted by the flat end tip based on Davisson's criteria. Exceptions were Portland and Apalachicola for which telltale results were divided by the flat end tip unit end bearing.

Site	Pile Toe Area [ft ²]	Ratio of		Unit End Bearing, [ksf]			Ratio
		Pile&Tip Diameter	Pile&Tip Toe Area	CAPWAP	Telltale	Flat End Tip ¹	
St. Mary	0.99	4.8	28.2	112	--	104	1.08
Portland	1.76	7.2	50.3	147	165	80	2.06
CD17	4.00	9.6	114.3	74	--	71*	1.04
CD21	4.00	9.6	114.3	88	--	48	1.83
WC	4.00	9.6	114.3	77	--	155	0.50
AP	4.00	9.6	114.3	100	86	94*	0.91

Note: (1) Based on Davisson's Failure Criteria.

* Depth was adjusted as discussed in sections 6.2.3 and 6.2.6.

1 ft² = 0.09 m²; 1 ksf = 48 kPa.

In summary, the unit end bearing *versus* displacement plots (figures 5.4 and 5.5) of scaled flat end tip and full-scale pile load test with telltales showed good agreement. Unfortunately though, the required scaling factors were quite different. For example, Portland site required a scale factor of 2.06; the White City site required a scale factor 0.50. Investigations into the relationship between soil type and scale factor did not provide any clear tendency. Further investigation is required before any definite conclusion can be drawn. At the present, it may be concluded that the end bearing predictions from flat end tip measurements could be 0.5 to 2 times of the full-scale pile result. Please note that the unit end bearing and ratio in table 5.2 for the Apalachicola site (AP) are different from the 0.56 factor used in figure 5.5. The values in table 5.2 were calculated based on considerations presented in chapter 6.

5.1.5 Rate Effect of Soil

Two types of soil rate effects were investigated in this study, (a) those due to rod tip compression loading, and (b) those due to sampler shaft loading. The investigation of rate effects on compression loading was not successful because of the effects of loading history, *i.e.*, an increased soil unit end bearing with repeated loading cycles. In other words, the effect of increasing loading rate could not be differentiated from strain hardening effects due to repeated loading cycles. Therefore, the rate effect study was concentrated on the shear loading from uplift tests of the sampler.

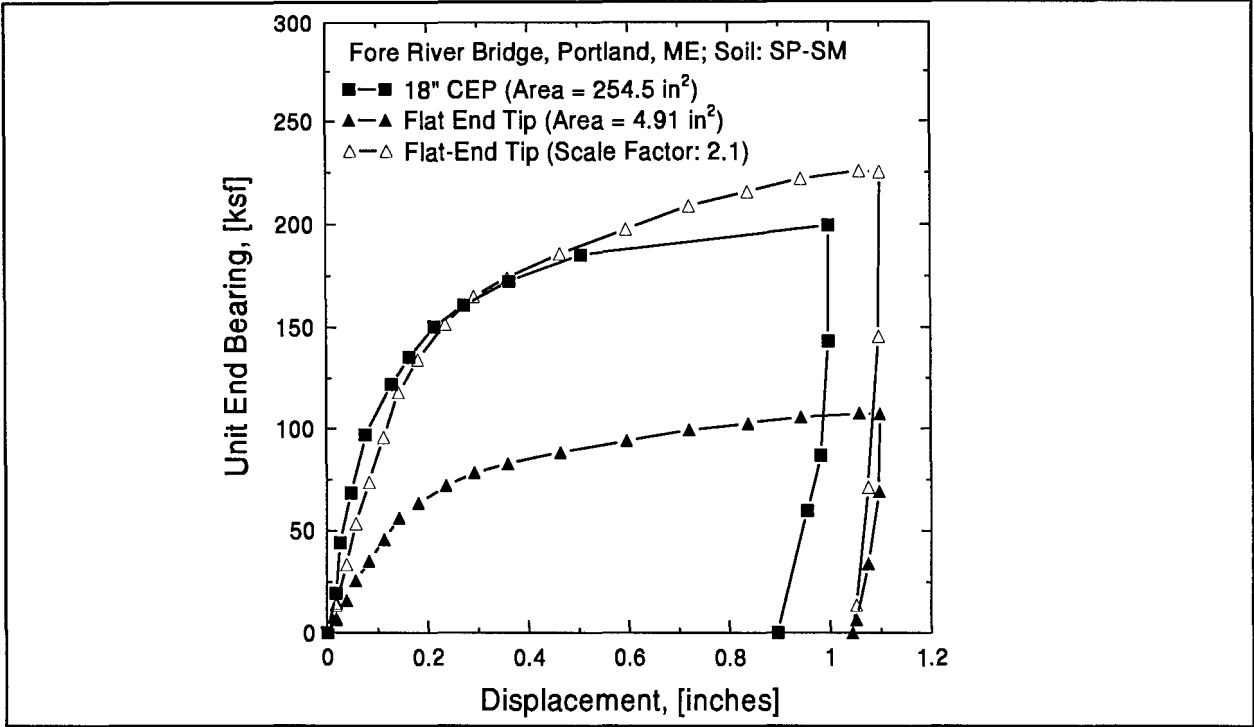


Figure 5.4: Load versus Displacement for Flat End Tip and Full-Scale Pile, Portland Site

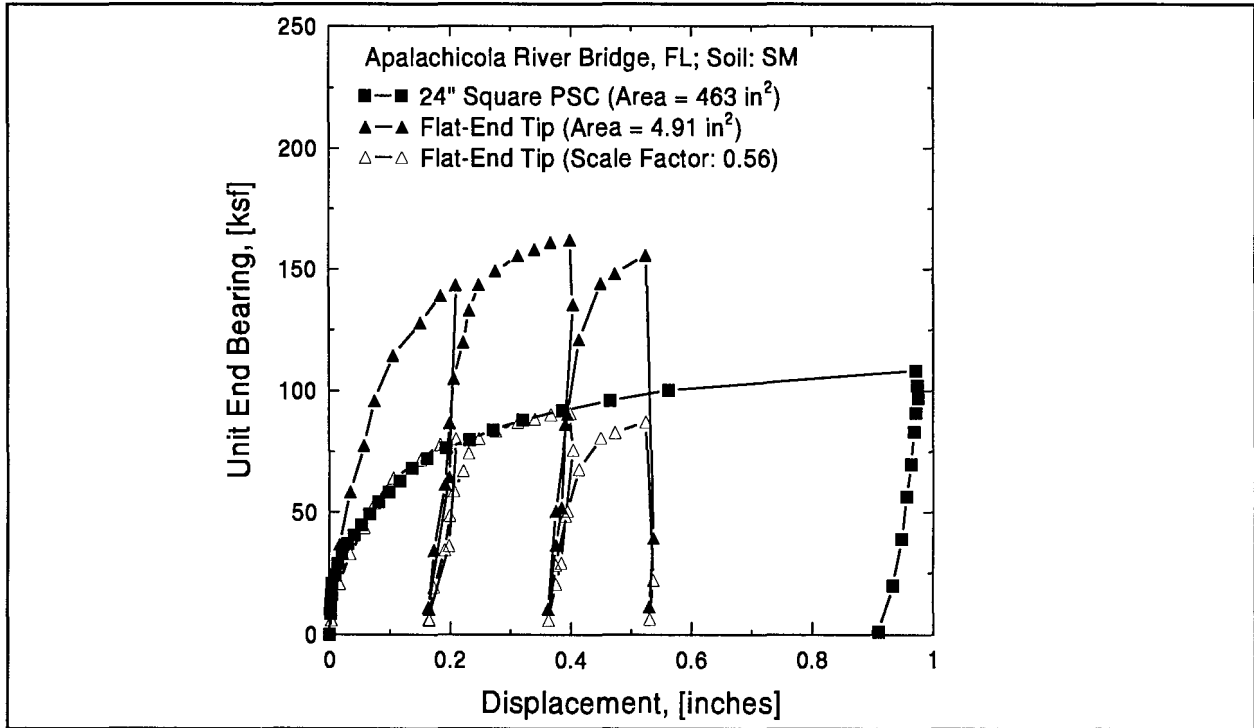


Figure 5.5: Load versus Displacement for Flat End Tip and Full-Scale Pile, AP Site

During uplift testing after sampler driving, several displacement rates were applied to determine the rate effect of the soil. Due to the limits of hydraulic jack and pump, the highest displacement rate was 1.8 in/min or 0.0025 ft/s (45 mm/min or $(7.5) \cdot 10^{-4}$ m/s). The lowest, reasonably accurately applied rate was approximately 0.01 in/min or $(1.4) \cdot 10^{-5}$ ft/s (0.25 mm/min or $(4) \cdot 10^{-6}$ m/s). Thus, three displacement rates, each differing by at least an order of magnitude, could be applied. The results from four different test locations (two from the St. Mary site, and two from CD17 site) are presented in table 5.3. For each test location, soil resistance for three different displacement rates are presented in the table.

Site	Soil Resistance, [kips]				Exponent n	Damping Factor J_c [[s/ft] ⁻ⁿ]	Correlation Coefficient r^2
	Displacement Rate, [in/min]						
	0.01	0.1	1.0	1.6			
St. Mary100	0.68	0.73	0.92	--	1.19	3.12	0.94
St. Mary103.5	0.95	0.95	1.25	--	1.24	2.63	0.75
CD17-50	0.20	0.26	--	0.37	1.16	3.19	0.66
CD17-65	1.80	1.85	--	2.05	1.07	2.17	0.92

Note: 1 kip = 4.45 kN; 1 in/min = 25.4 mm/min; 1 s/ft = 3.28 s/m.

Since higher displacement rates could not be achieved by the static uplift test, a second approach was also attempted. In this case, several different hammer drop heights, varying from 2 to 30 in (51 to 762 mm), were used to generate different displacement rates at the SPT sampler. The sampler was first driven 18 in (457 mm) and the SPT N-value was 2. The sampler was then left in the soil for about 15 h to allow for soil setup, before various hammer drop heights were applied starting with a lowest drop height of 2 in (50 mm) and going up to 30 in (762 mm). The force and velocity time history at the sampler, due to the various hammer drop heights, are presented in figures 5.6 and 5.7, respectively. The 2-in (50-mm) drop indicated setup effects in the later part of the force curve; the other curves apparently had the soil resistance reduced due to re-driving effects. The forces (resistances) at the time of peak velocity, together with the peak velocities from different hammer drop heights were used in the rate effect study discussed below. Note that usually peak force and peak velocity occur at the same time; thus, the peak force occurs when the acceleration is zero and therefore contains no inertia effects. Thus, peak force can be equated to peak resistance. The

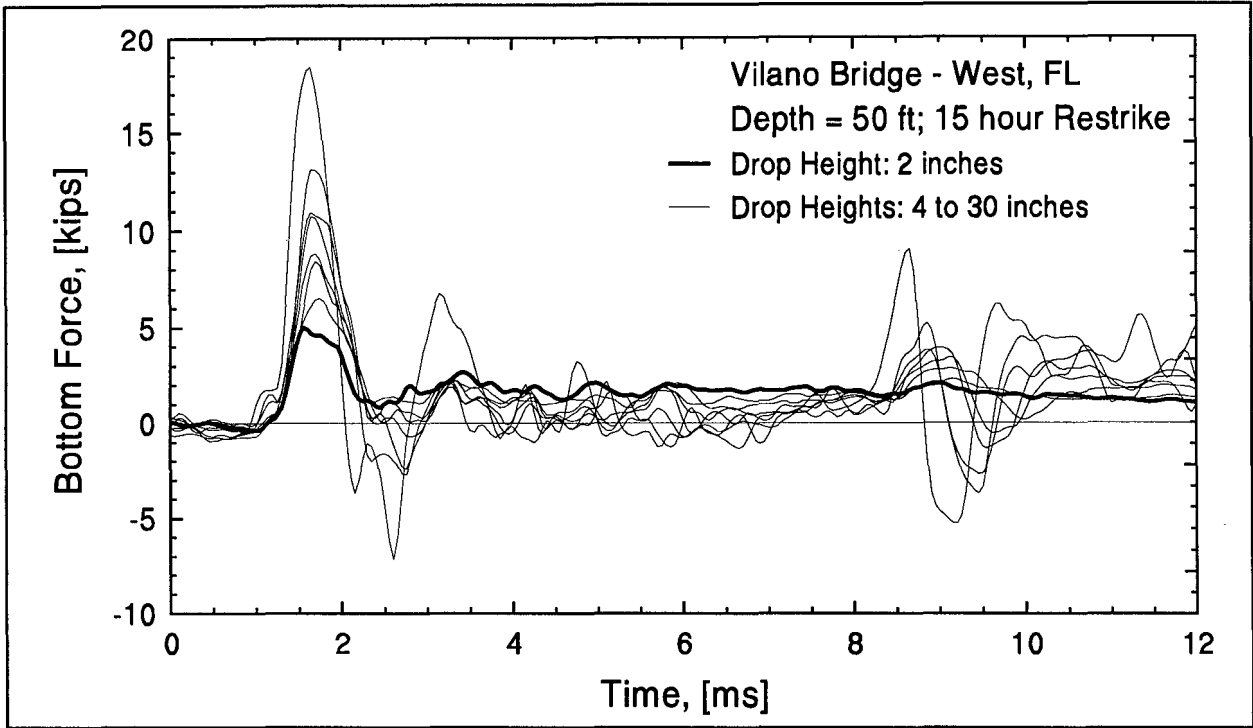


Figure 5.6: Bottom Force from Various Hammer Drop Heights

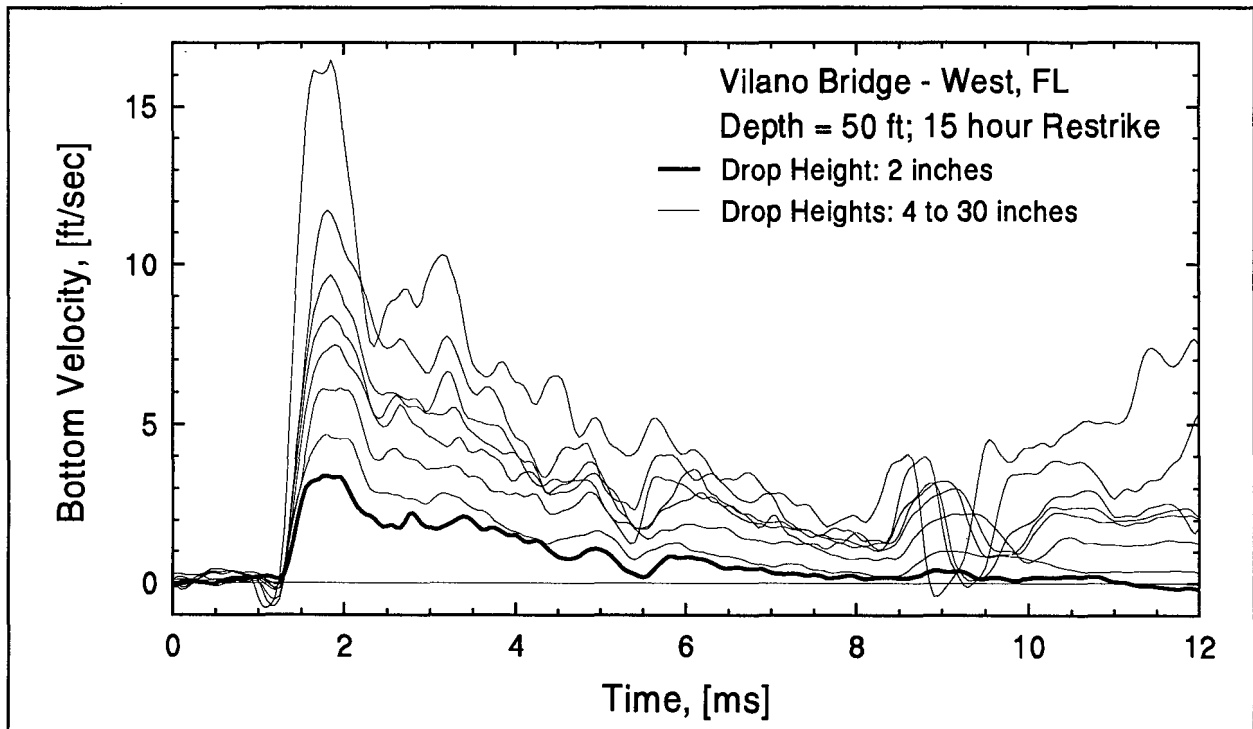


Figure 5.7: Bottom Velocity from Various Hammer Drop Heights

soil recovered from the sampler was classified as clay (CH), with a Liquid Limit of 85 percent and Plasticity Index of 51 percent.

The main objective of the rate effect study was to investigate the exponential law observed by Coyle and Gibson (1970). According to Coyle and Gibson, the Smith soil resistance should follow the relationship:

$$R_d = R_s [1 + J_c \dot{u}^n] \quad (5.1a)$$

where n is approximately 0.2; R_d is the total dynamic resistance; R_s is the static resistance; J_c is the soil damping; and \dot{u} is the velocity of the pile. The objective of this study was to determine the values for n and J_c .

To determine these values, equation (5.1a) was rearranged as

$$\log_{10} \left[\frac{R_d}{R_s} - 1 \right] = \log_{10} (J_c) + n \log_{10} (\dot{u}) \quad (5.1b)$$

By using a regression analysis, J_c and n were determined as shown in table 5.3 first for the static uplift tests with different displacement rates. The resulting n values were between 1.07 and 1.24, and the J_c values were between 2.17 and 3.19 unit $(s/ft)^{-n}$.

In a second regression analysis, eight different velocity maxima were used together with eight force maxima corresponding to eight different hammer drop heights. Again, a best fit straight line was calculated based on peak velocity and ratios of peak resistances as presented in figure 5.8. The resulting n value was 0.916, again very close to unity, and J_c was $1.81 (s/ft)^{-0.916}$.

In summary, the present results could not confirm the $n = 0.2$ exponent which has been suggested in the literature by laboratory tests. It is felt that the Modified SPT is a rather realistic model of pile driving and based on the present study with n values near unity, it appears unnecessary to complicate standard wave equation analysis with the exponential damping approach.

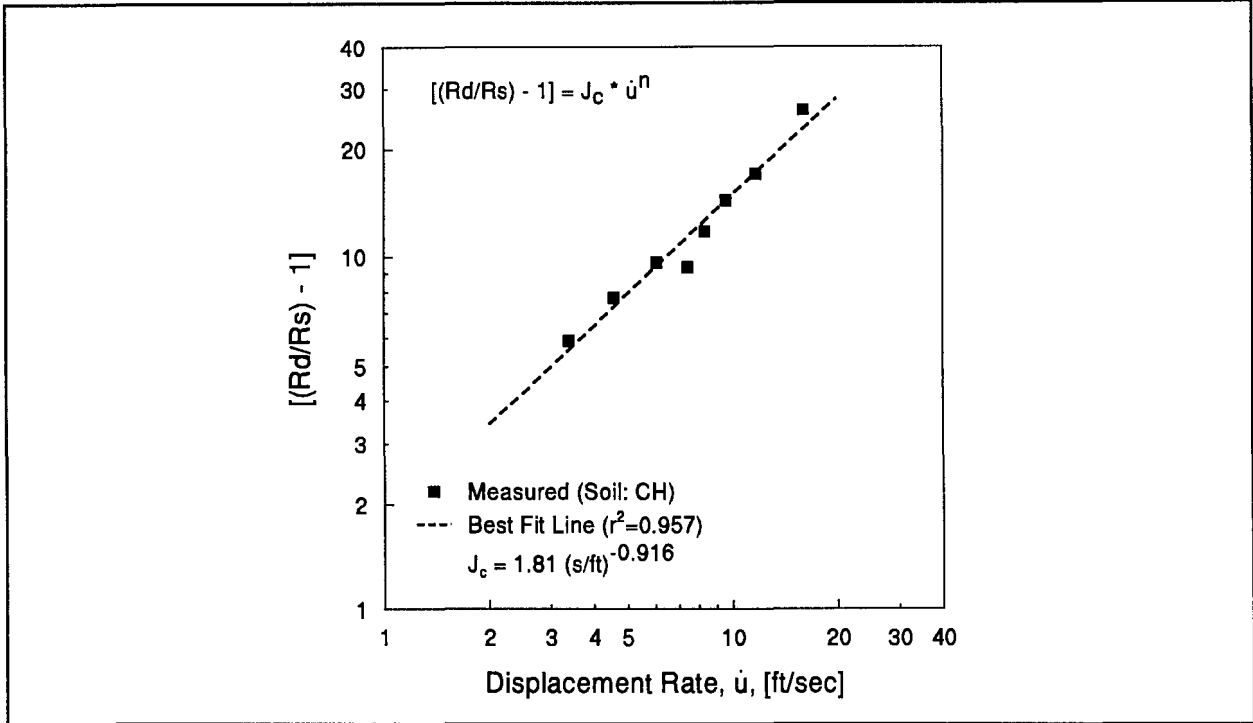


Figure 5.8: Rate Effect Study for CH Type Soil

5.1.6 Soil Setup

Soil strength changes with time after pile driving are a well-recognized phenomenon in the piling industry. In fact, soil setup has also been observed after drilled shaft construction. As discussed in volume III, Skov and Denver (1988) proposed that the pile bearing capacity be calculated as a function of the time ratio (t/t_0) in which t is the elapsed time since the end of installation, and t_0 is a reference time which is also measured from the end of installation. For the present study, this equation was slightly modified to shear strength at time t , $\tau(t)$, instead of the bearing capacity and is expressed as follows.

$$\tau(t) = \tau_0 [1 + A \log_{10} (t/t_0)] \quad (5.2)$$

where τ_0 is the soil shear strength at time t_0 , and A is the soil setup parameter.

Static uplift tests from three different sites were used to study the soil setup. These sites were Apalachicola, Aucilla, and Vilano West. Eight series of uplift tests, performed at various depths, were available. At each test location, uplift tests were performed at least at three times: at the end of sampler driving (elapsed time between driving and this test was usually at least 10 min), after a 15-min wait after the initial test, and after a 1-h wait after the initial test. At two test

locations, 11 and 14-h wait tests were also performed. Each uplift test was only carried to the Davisson failure load. The soil type at these three sites was generally cohesive or between MH and OH according to the USCS Classification system. The SPT N_{60} ¹ values were very low, ranging between 1 and 5. The Atterberg Limit tests indicated that the Liquid Limits of these soils were between 65 and 94 percent, the Plastic Limits were between 28 and 53 percent, which corresponded to Plasticity Indices between 31 and 66 percent. This soil type is considered to be of medium to high plasticity. The uplift test results for end of drive (EOD) and for the indicated waiting times, and the soil properties are summarized in table 5.4.

Table 5.5 summarizes the soil setup evaluation for the above three sites using equation (5.2). For this study, τ_o was defined as the uplift soil shear strength from the first test, the associated wait time t_o was arbitrarily set to 1 min, even though the actual waiting time after driving may have been greater. The data from each test location was plotted in figure 5.9. Two lines representing the average setup behavior of the soils for a low ($N_{60}=1$) and higher ($N_{60}=7$) strength soil, were also included in this figure.

The initial soil shear strength (τ_o) is believed to be related to N_{60} . The ratios of initial test shear strength to N_{60} , (τ_o/N_{60}), for the eight test locations averaged approximately 0.25 as presented in table 5.5. Excluding the unusually high VW59, the ratio for the other seven test locations averaged approximately 0.20. Therefore for $N_{60} = 5$, the shear strength may be estimated to be about 1.0 ksf (48 kPa). According to table 5.3 of Vanikar, (1986), based on $N = 5$ the undrained shear strength can be estimated as 0.63 ksf (30 kPa). Additional strength information for the AP55 site included depth. Two unconfined compression tests performed using Shelby Tube samples for depths of 56.5 to 57.0 ft and 57.0 to 57.5 ft (17.2 to 17.4 m and 17.4 to 17.5 m); the strength values determined were 0.51 ksf and 3.11 ksf (24 and 149 kPa), respectively. The static uplift test performed at 55 ft (16.8 m) on the sampler indicated an initial uplift strength of 0.96 ksf (46 kPa).

At the AP55 site, on the full-scale pile, dynamic testing and CAPWAP analyses were performed for both EOD and BOR records, the later taken immediately after the static load test. The restrike capacity predicted by CAPWAP utilizing the radiation soil model agreed well with the static load test result. CAPWAP also indicated that the end of driving and beginning of restrike pile shaft resistances were 184 and 520 kips (817 and 2309 kN), respectively, yielding a setup factor of 2.83. The time between the end of driving and the beginning of restrike was 12 days or 17,280 min. Based on the Modified SPT data and the setup equation presented in figure 5.9, the setup factor for AP55 at 17,280 min is approximately 2.4. The setup equation shown in figure 5.9 is averaged from the data presented in figure 5.9.

¹For a definition of N_{60} , *i.e.*, an SPT N value corrected for transferred energy variations from the perceived average of 60 percent, see appendix E.

Site Name	Uplift Capacity, [kips]				Soil [Type]	SPT N_{60}	LL [%]	PL [%]	PI [%]
	EOD	15 min	1 hour	(n hours)					
AP55	0.75	1.134	1.134	--	MH	5	84	53	31
Aucilla20	0.65	0.92	--	--	CH	4	72	33	39
Aucilla30	0.81	0.996	1.195	1.549 (11)	CH	4	65	26	39
Aucilla45	0.54	0.61	--	--	CH	4	77	30	47
VW45	0.18	0.24	0.31	--	CH	1	85	34	51
VW50	0.29	0.30	0.52	0.65 (14)	CH	2	92	30	62
VW55	0.27	0.41	0.57	--	OH	2	92	30	62
VW59	0.48	0.60	0.68	--	OH	1	94	28	66
Average					MH to OH		83	33	50

Site Name	Soil Type	Uplift Test Shear Strength, τ_o , [ksf]	SPT N_{60}	(τ_o/N_{60})
AP55	MH	0.96	5	0.19
Aucilla20	CH	0.83	4	0.21
Aucilla30	CH	1.03	4	0.26
Aucilla45	CH	0.69	4	0.17
VW45	CH	0.20	1	0.20
VW50	CH	0.37	2	0.19
VW55	OH	0.34	2	0.17
VW59	OH	0.62	1	0.62
Average				0.25

Notes: Site name is followed by test depth in ft.

LL, PL, and PI are Liquid Limit, Plastic Limit, and Plasticity Index, respectively.

N_{60} is the SPT N-value corrected to 60 percent transfer efficiency.

Soil Type is based on USGS Classification.

$\tau_t = \tau_o + A \log(t/t_o)$ where $\tau_o = 0.17 N_{60}$ [ksf] and $t_o = 1$ min.

1 ksf = 48 kPa.

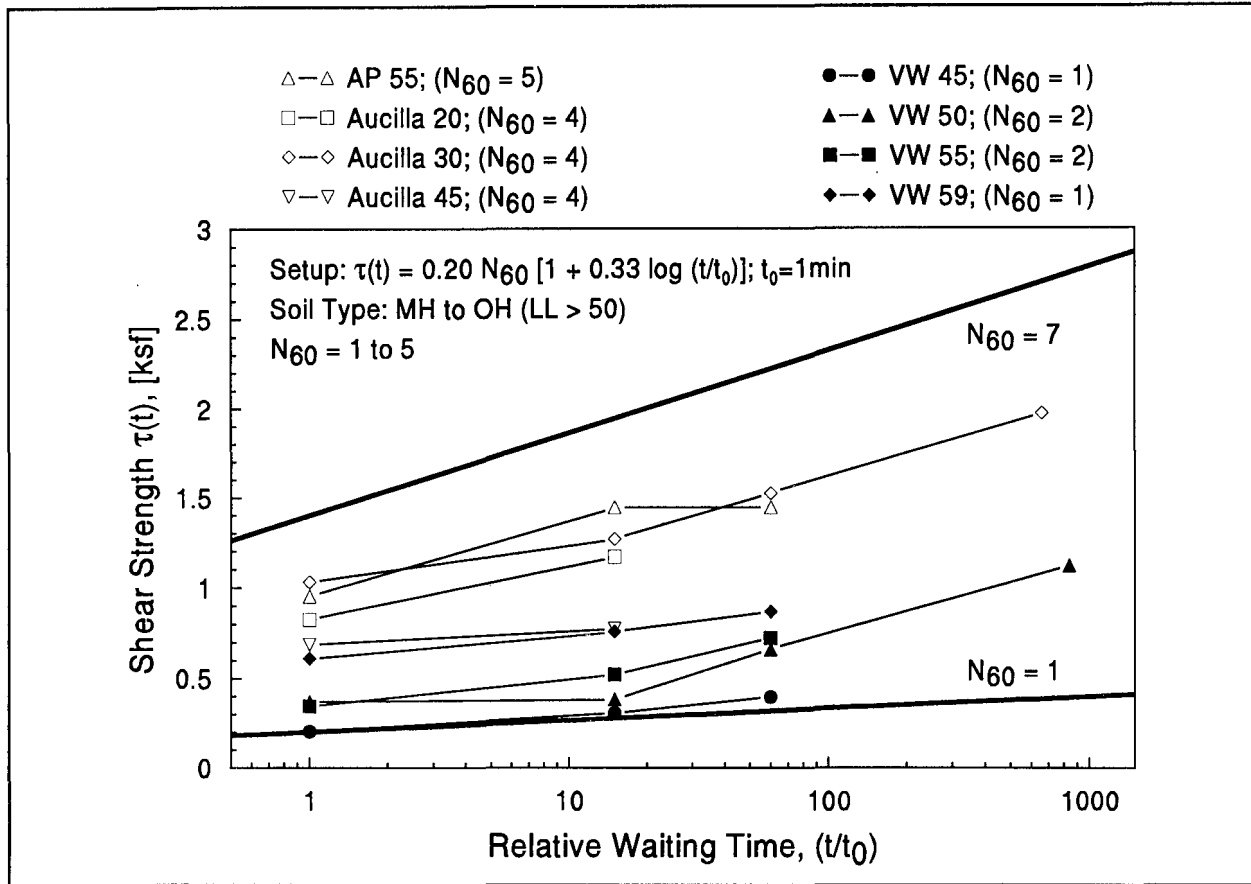


Figure 5.9: Setup Evaluation for Three Sites

Of course, this very limited setup study is not intended for establishing a table of generally applicable setup factors. Instead it is intended to demonstrate that equation (5.2) produces a promising agreement with dynamic field results and that it is applicable to shaft resistance results from SPT sampler. Obviously, further study and correlation of field results are required to establish the setup factor for other soils.

5.1.7 Torque Test

In addition to, and following the uplift test, a static torque test was performed to determine the shear strength of the soil prior to split spoon sampler extraction. The torque generates a horizontal shear loading between the outside perimeter of the split spoon sampler and the soil. The maximum shear strength of the soil, resisting the torque, will be referred to as *torque resistance*. The torque resistance is calculated by dividing the measured torque by the radius of the sampler. The torque resistance divided by the embedded sampler shaft area yields the unit torque resistance. During this investigation, the torque tests were initially performed with

a torque wrench (TW). Preliminary results from the TW were then used for designing the instrumented torque rod (TR). The type of torque device used on each site is presented in table 5.6. Both torque devices were described in chapter 4. When the torque wrench was used, only the peak and residual torque could be measured. With the instrumented torque rod, continuous records of torque *versus* rotation were obtained.

A total of 20 torque tests were performed during this investigation and the results have been summarized in table 5.6. Unit torque resistance values are presented in table 5.6 together with the unit uplift resistance. In some uplift tests, the load-displacement curves indicated both a peak and a residual strength. For these cases, a range of uplift resistances is presented in table 5.6. Also presented in table 5.6, is the "*Remolding Factor*" which is the ratio of residual strength to peak torque resistance. The inverse of this Remolding Factor may be called the "*Soil Sensitivity Factor*" as in the interpretation of the vane shear test results. The Remolding Factor may be a useful quantity for predicting the remolded soil resistance on a pile during pile driving.

Usually, the uplift test was performed prior to the torque test. The uplift test was also repeated approximately 15 min to 2 h after the end of sampler driving. The "*Setup Factor*" presented in table 5.6 is the ratio of the uplift resistances after the longest elapsed time and the uplift resistances at the end of driving. The setup factor is useful in predicting the soil strength gain based on the capacity at the end of pile driving. A setup factor less than unity indicates a loss of soil strength (relaxation).

Comparison of the unit torque and uplift resistance is presented in figure 5.10 together with the soil setup factor. Test location designations are keyed to table 5.6. Figure 5.10 shows both the peak and residual torque resistances and also indicates the range of uplift resistances. At site F (Apalachicola, FL; at 55 ft or 16.8 m), a Shelby tube sample was extracted and an unconfined compression test was performed. The unconfined compression strength is also presented in figure 5.10 for comparison with the torque and uplift resistance. The unconfined compression test curves are presented in appendix H. A general description of the soil type at the torque test sites is also presented in figure 5.10. Note, the order of test locations in figure 5.10 follows the magnitude of the Remolding Factor (as apparent from the difference between torque peak and torque residual) while table 5.6 is chronologically organized.

In general, the results in figure 5.10 show good agreement between torque and uplift resistance. The uplift resistance generally falls between peak and residual torque, indicating that the uplift resistance may be determined by factoring either one of these two values. Note that the only available result from an unconfined compression strength test happened to fall below both torque and uplift test results. Figure 5.11 is a scattergram of uplift resistance *versus* peak torque and includes the best fit regression line. The regression analysis indicates that uplift

Table 5.6: Summary of Torque Resistance and Uplift Resistance									
	Test Location	Depth [ft]	Torque Device	Unit Resistance, [ksf]			Remolding Factor	Setup Factor	Torque Factor
				Peak	Residual	Uplift			
A	CD17	60	TW	1.07	1.07	0.74-0.92	--	0.75	0.69-0.86
B	CD17	65	TW	3.36	2.29	2.68-2.99	--	1.26	0.80-0.89
C	CD21	40	TW	0.23	0.23	0.52-0.75	--	0.80	2.26-3.26
D	CD21	55	TW	1.99	1.99	1.03-1.13	--	0.78	0.52-0.57
E	CD21	65	TW	2.29	2.29	1.38-1.69	--	--	0.60-0.74
F	AP	55	TR	1.17	0.70	0.83	0.60	1.51	0.71
G	AP	75	TR	0.89	0.89	0.53	1.00	1.00	0.60
H	Skyway	45.5	TR	1.90	1.04	0.87-1.55	0.55	1.53	0.46-0.82
I	Skyway	50	TR	1.36	0.84	0.80	0.62	--	0.59
J	Aucilla	10	TR	1.07	0.33	1.17-1.68	0.31	--	1.09-1.57
K	Aucilla	20	TR	1.53	0.62	1.13	0.41	1.31	0.74
L	Aucilla	30	TR	1.38	0.69	1.13-1.34	0.50	1.37	0.82-0.97
M	Aucilla	45	TR	0.94	0.78	0.76	0.82	1.13	0.81
N	VE	30	TR	0.46	0.41	0.23	0.93	0.40	0.50
O	VW	30	TR	0.85	0.56	0.48-0.66	0.66	--	0.56-0.78
P	VW	35	TR	0.98	0.64	0.54-0.64	0.77	1.19	0.55-0.65
Q	VW	45	TR	0.87	0.51	0.45	0.58	1.94	0.52
R	VW	50	TR	0.90	0.41	0.83-1.12	0.46	1.86	0.92-1.24
S	VW	55	TR	1.12	0.47	0.72	0.43	2.07	0.64
T	VW	59	TR	0.93	0.56	0.63	0.61	1.48	0.68

Notes: TW - Torque Wrench; TR - Instrumented Torque Rod.

Peak and Residual Unit Strengths were determined from torque tests.

Uplift Unit Strengths were determined from uplift tests.

Remolding Factor is residual divided by peak strength from torque tests.

Setup Factor is strength gain over a period of 15 min to 2 h.

Torque Factor is the ratio of uplift resistance and peak torque resistance.

1 ft = 0.305 m; 1 ksf = 48 kPa.

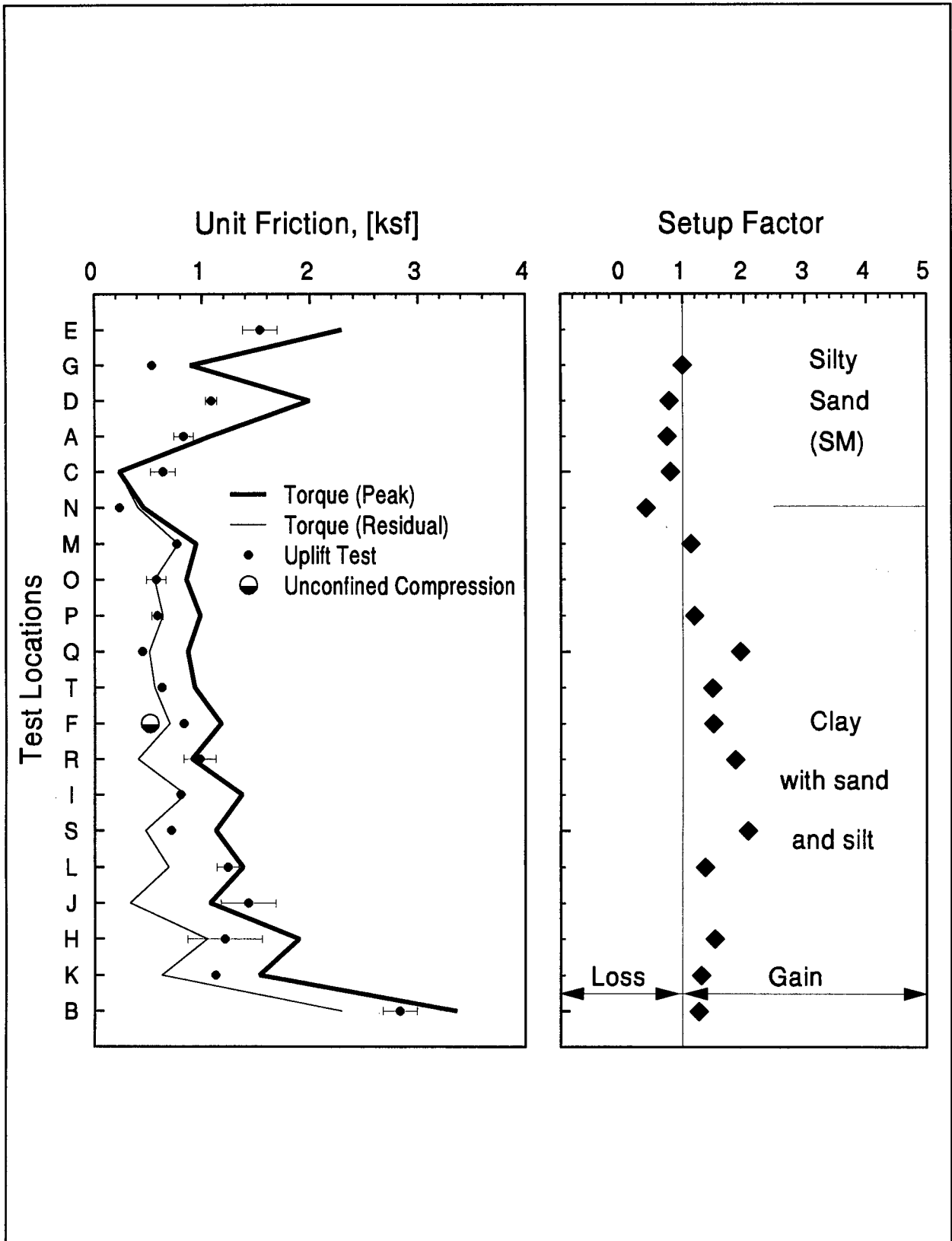


Figure 5.10: Summary of Torque Test Results from 20 Sites

resistance (including setup) averages 69 percent of the peak torque resistance with a correlation coefficient $r^2 = 0.75$.

The torque test generally yielded consistent and repeatable results. Figure 5.12 demonstrates this by showing four torque test results from Vilano Bridge - West from depths of 45 to 59 ft (13.7 to 18.0 m). The SPT N-values and the soil type are about the same between these depths.

5.1.8 Pile Capacity Determination Using CPT Results

CPT results were available for four test sites. The capacity of the test piles at these four test sites was calculated from the CPT data utilizing the method discuss below. The calculated capacities are presented in chapter 6 for Apalachicola site, and chapter 7 for Aucilla, Vilano - East, and Vilano - West sites. The computed unit shaft resistance and end bearing from the CPT data are compared with those measured from static test (uplift test of SPT sampler and compression test of flat end tip), and the unit shear resistance from the torque test in figures 5.13(a), (b), (c), and (d). The unit shaft resistance and end bearing from the static SPT uplift and compression flat tip tests were based on Davisson's failure load.

The method used to calculate pile capacity from the CPT data is similar to that recommended by Vanikar (1986). The unit shaft resistance was determined from the unit sleeve friction of the cone. The unit sleeve friction was limited to 2 ksf (100 kPa). The total shaft friction of the pile, Q_s , was computed using the following equation:

$$Q_s = K \left[\frac{(\bar{f}_s A_s)_{0 \text{ to } 8B}}{2} + (\bar{f}_s A_s)_{8B \text{ to } L} \right] \quad (5.3)$$

where K is the ratio of unit pile friction to unit sleeve friction of a mechanical penetrometer, and has a value of 0.48 for piles with (length, L, to width, B, ratios) greater than 20; \bar{f}_s is the average unit sleeve friction over the depth interval (*i.e.*, 0 to 8B or 8B to L); A_s is the pile soil contact area; [0 to 8B] refers to distance from pile top to a depth equal to 8B; [8B to L] refers to the distance from 8B depths to the pile tip.

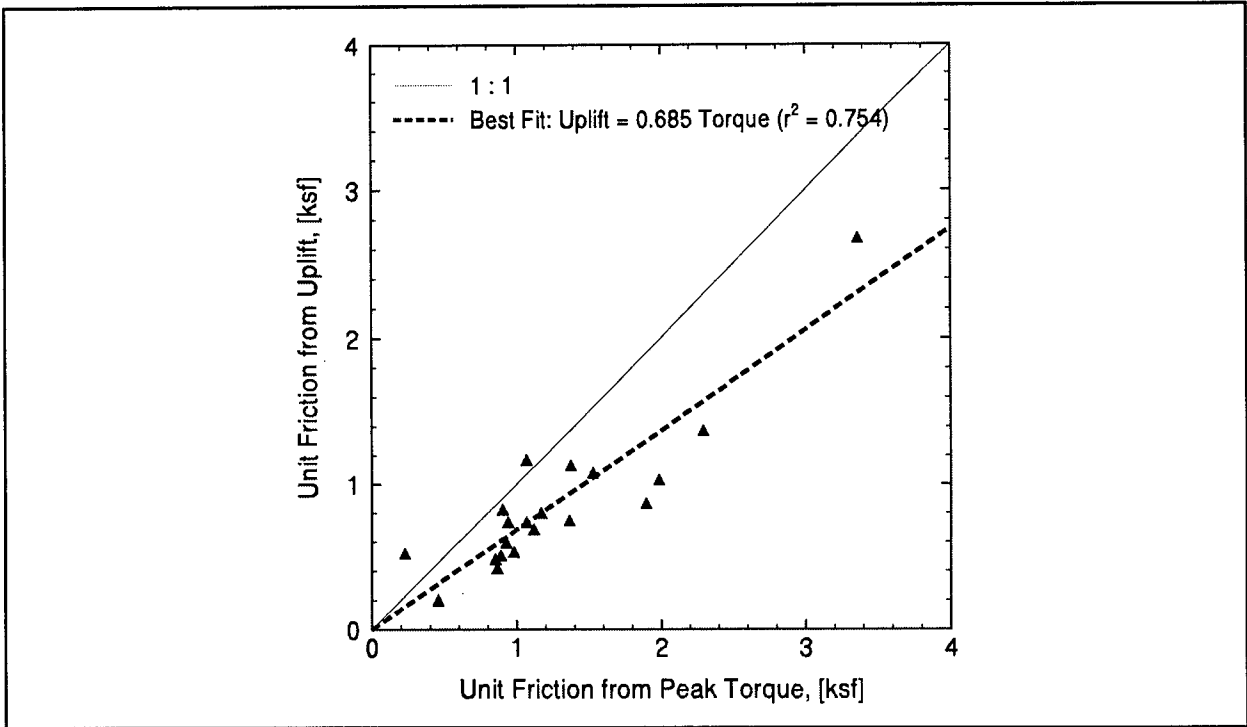


Figure 5.11: Torque Resistance versus Uplift Resistance

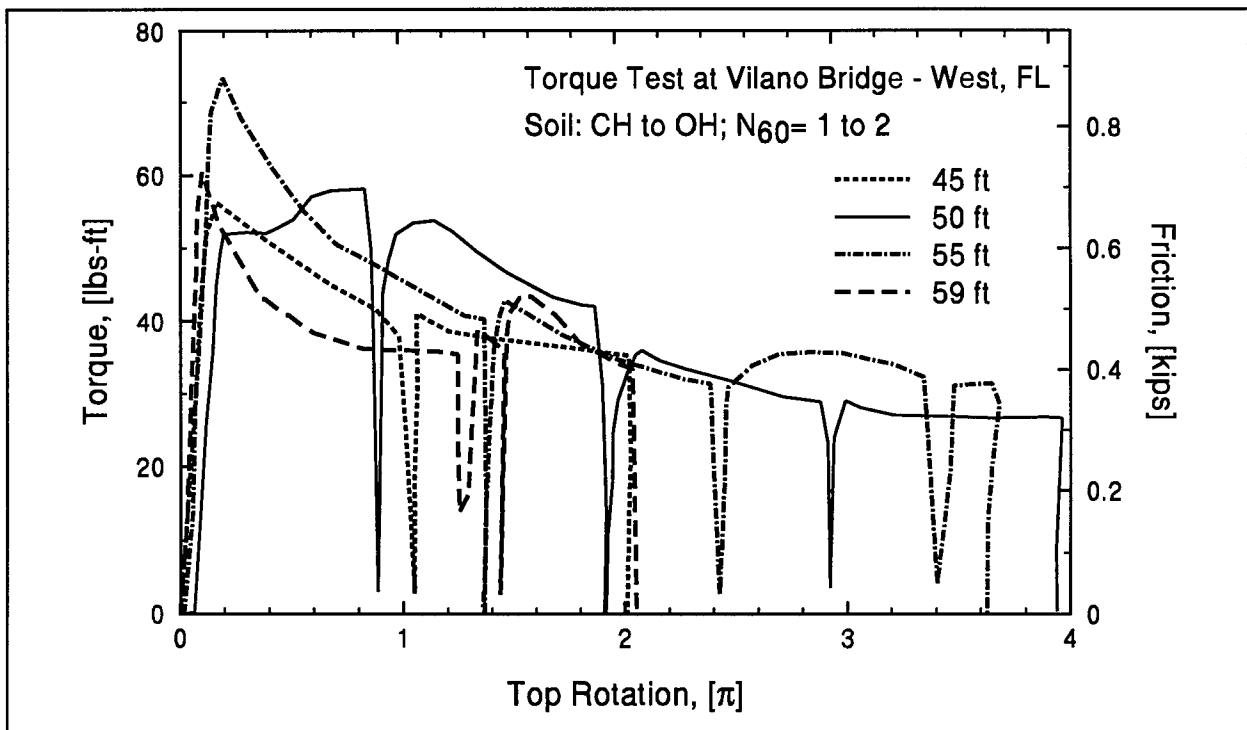


Figure 5.12: Torque Test Results from Vilano Bridge - West, FL

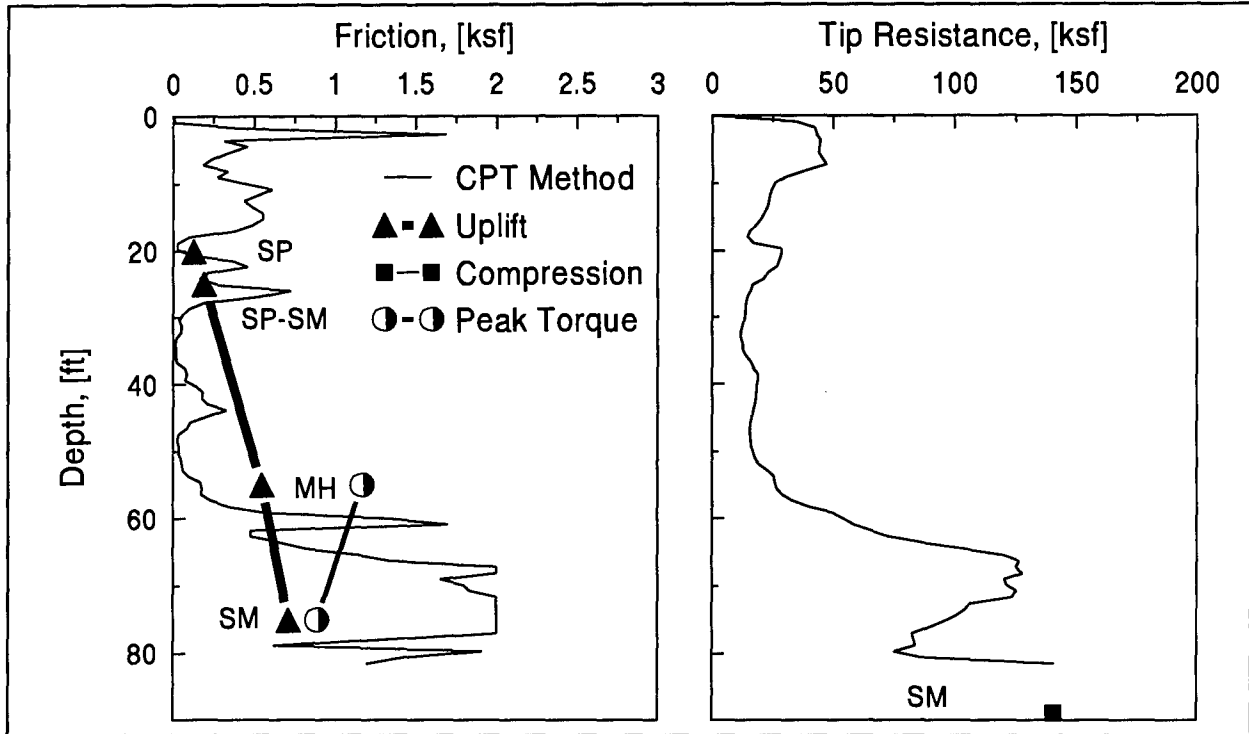


Figure 5.13(a): Comparison of CPT and Modified SPT Data for AP Site

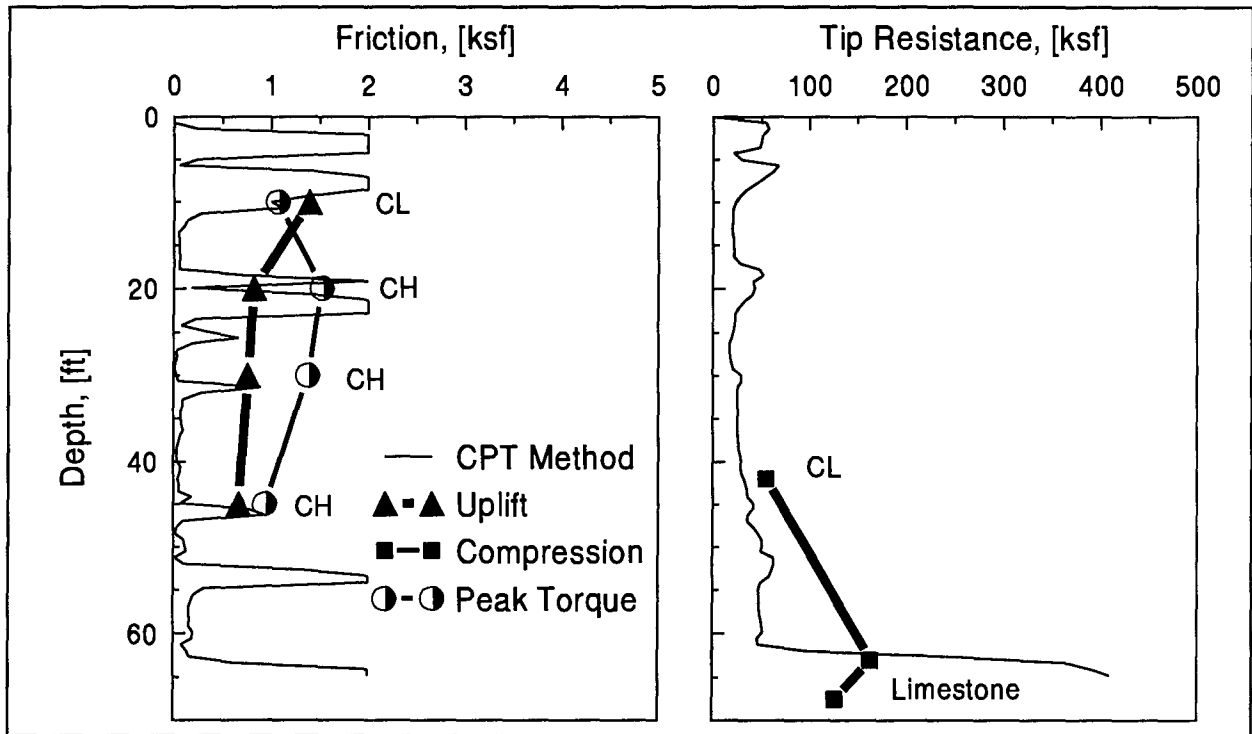


Figure 5.13(b): Comparison of CPT and Modified SPT Data for Aucilla Site

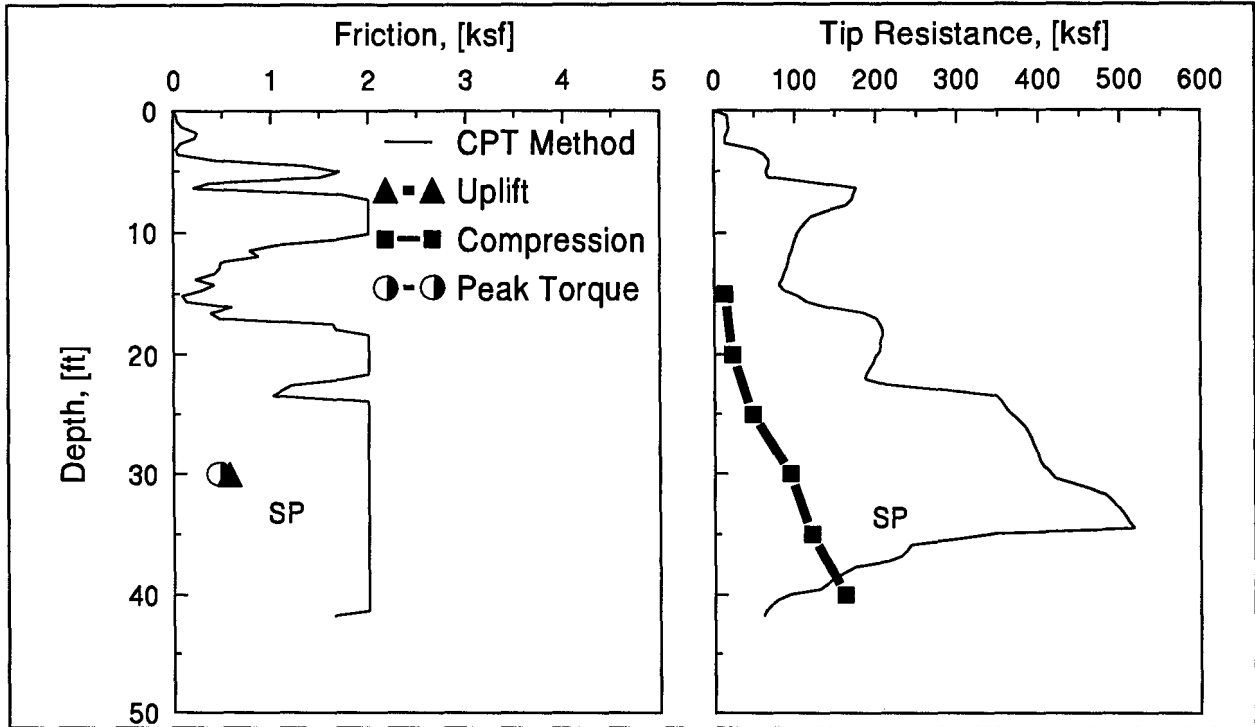


Figure 5.13(c): Comparison of CPT and Modified SPT Data for VE Site

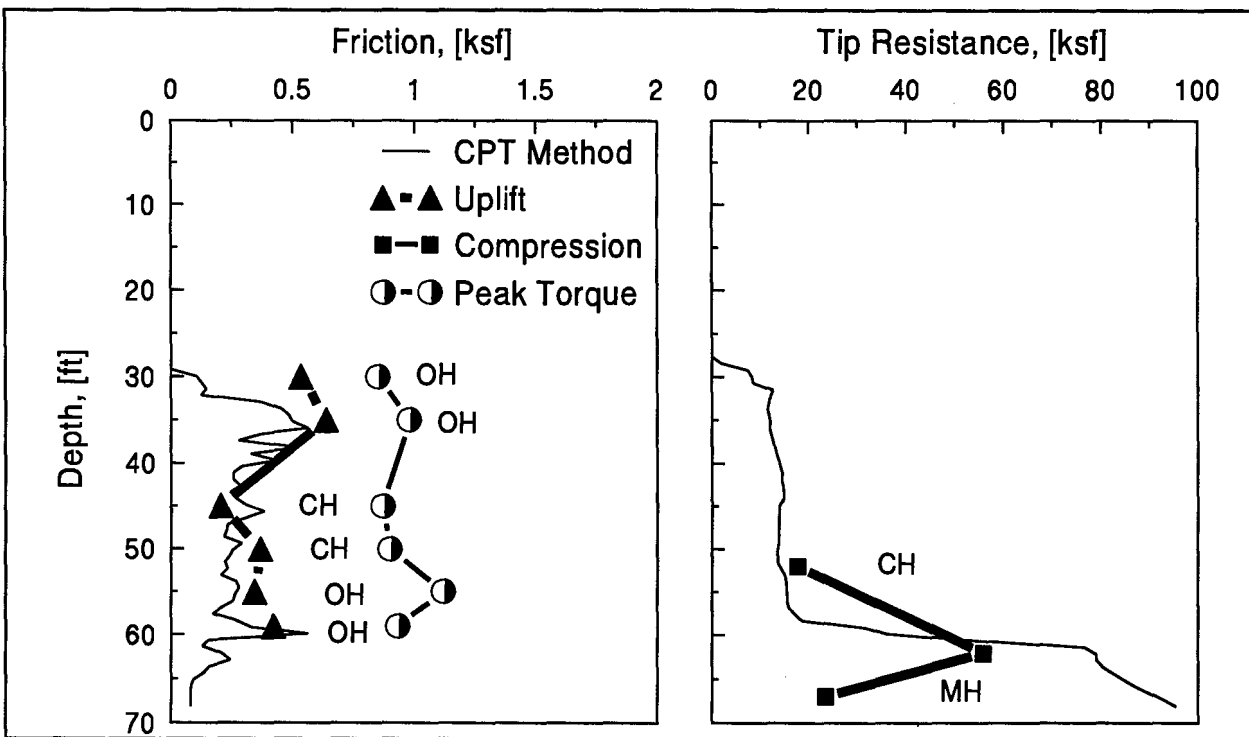


Figure 5.13(d): Comparison of CPT and Modified SPT Data for VW Site

For unit end bearing calculations, a slightly different technique for averaging the unit cone tip resistance, was utilized. This averaging technique, called Koppejan Method (Bowles, 1988), was introduced by a Dutch firm and reportedly performs quite well. The pile toe resistance, Q_p , is determined from the following equation:

$$Q_p = \min. \left\{ \frac{\left[\frac{q_{c1} + q_{c2}}{2} \right] + q_{c3}}{2} \right\} A_{toe} \quad (5.4)$$

where A_{toe} is the pile toe area and is multiplied by the minimum of average unit cone tip resistance values calculated over certain distances xB . The quantities q_{c1} , q_{c2} , and q_{c3} , are averaged; for the averaging procedure, reference is made to figure 5.14. The first parameter, q_{c1} , is determined by averaging the unit cone tip resistance (q_c) over a distance xB below the pile tip (path a-b), with x ranging between 0.7 and 4.0. The actual q_c values along path a-b are averaged. The second parameter, q_{c2} , is calculated using the *minimum upward path rule* along path b-c. The minimum upward path rule chooses the q_c value for averaging by following the upward path, and the q_c selected for averaging is only that value which is less than or equal to the previous q_c . The third parameter, q_{c3} , is the average of q_c selected over a distance $8B$ above the pile tip (along the path c-d), also using the minimum upward path rule.

The results of figures 13(a) through 13(d) indicate both good and poor agreement between Modified SPT and CPT results. Of course, the CPT methods provide for a continuous strength vs. depth plot while the SPT only yields results at a few discrete locations. The lines connecting the SPT results were plotted for purposes of identification. They sometimes produce the impression of a poor correlation even where it is relatively good at points where measurements were taken. An exception with a very poor correlation was Vilano East, figure 13(c). Reasons for this poor correlation are not clear.

5.2 DYNAMIC RESULTS

5.2.1 Analytical Background

Consider the forces acting on the SPT rod during sampling. The drill rod extends down the drill hole with no resistance forces acting on the shaft during an impact by the ram. The penetration of the sampler is impeded by the resistance of the soil at the bottom of the drill hole. Thus, the only forces acting on the drill string are the impact forces and the sampler resistance forces. At the top of the rod, the force and velocity (actually obtained from measured acceleration) are

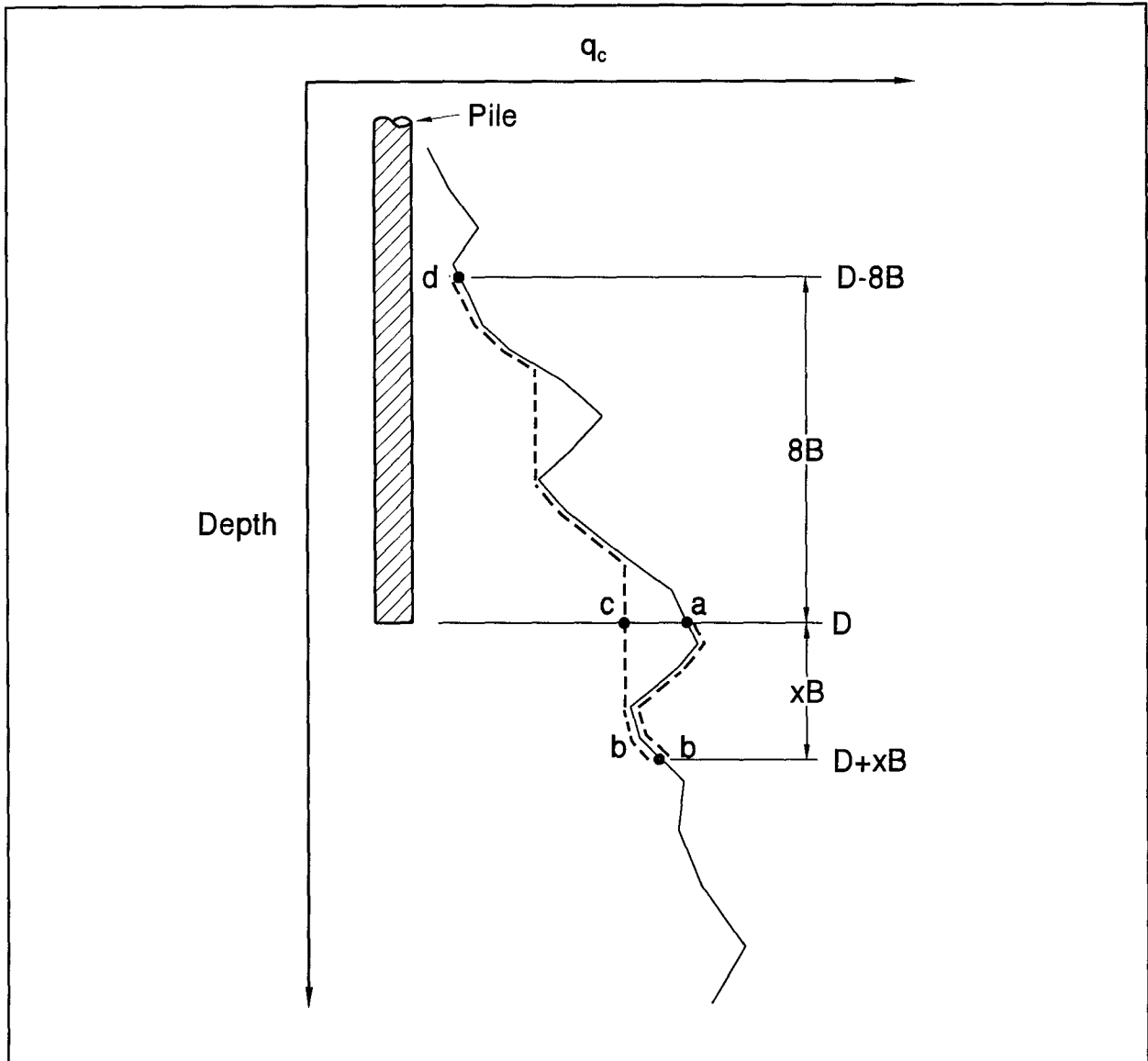


Figure 5.14: Procedure for Estimating Pile Tip Bearing Capacity from the Measured Cone Resistance (After Vanikar, FHWA-DP-66-1, 1986)

measured. It will be shown that the force and motion at the bottom of the rod can be determined from the measured quantities at the top.

During an impact event, the force in the rod at the measurement point can be divided into a downward and an upward traveling wave. The downward traveling force is (see also appendix A, volume III):

$$F^{\downarrow}(t) = \frac{1}{2} \left[F_m(t) + \frac{EA}{c} \dot{u}_m(t) \right] \quad (5.5)$$

where $F_m(t)$ is the force measured at the top and $\dot{u}_m(t)$ is the velocity measured at the same location as the force, both as a function of time, E is the modulus of elasticity of the rod material, A is the area of the rod, and c is the velocity of wave propagation in the rod. The upward traveling force wave is similarly calculated as:

$$F^\uparrow(t) = \frac{1}{2} \left[F_m(t) - \frac{EA}{c} \dot{u}_m(t) \right] \quad (5.6)$$

When the sampler is driven into the soil, the hammer impact induces a force and motion at the top of the rod and therefore, a downward traveling wave. This wave propagates down the rod essentially unchanged since there are no resistance forces along the shaft, and cross sectional variations are minor as discussed below. When the impact wave arrives at the toe, it is reflected and an upward wave travels back up the rod. Due to the motion associated with the downward wave, resistance forces are generated at the sampler and these forces also generate waves that travel up the rod. When they arrive at the top, these reflected waves affect the measurements.

Now consider these effects in a more quantitative manner. The upward traveling wave arriving at the measurement point had been generated by the effect of both the downward traveling wave at the measurement point at a time $2L/c$ earlier and the toe resistance force L/c earlier. The rod can be considered as an impacted rod with a free bottom end with the resistance force superimposed on the other forces acting on the rod. When the downward traveling wave reaches the toe end, it is reflected back up the rod with the opposite sign. Thus, the upward traveling force at the measurement point is equal to the negative of the downward traveling force at a time $2L/c$ earlier plus the toe resistance force at time L/c earlier. This can be expressed:

$$F^\uparrow(t+2L/c) = R(t+L/c) - F^\downarrow(t) \quad (5.7)$$

If the expressions of equations (5.5) and (5.6) are substituted into equation (5.7), the resulting expression can be solved for the toe resistance force:

$$R(t+L/c) = \frac{1}{2} [F_m(t) + F_m(t+2L/c)] + \frac{1}{2} \frac{EA}{c} [\dot{u}_m(t) - \dot{u}_m(t+2L/c)] \quad (5.8)$$

This relationship (also called the Case Method formula) was derived based on the assumption of a uniform rod cross section with no shaft resistances. However, the same expression can be used for rods with shaft resistance in addition to the toe resistance as shown by (Rausche et al., 1985) to calculate the total resistance. If the rod is of variable cross section, the same basic

approach could be used, but from a practical point of view, it could best be calculated from wave propagation considerations using a discrete representation of the rod.

It is also useful to determine the velocity of motion at the toe. With the availability of velocity, both displacement and acceleration can be calculated. At the end of a free rod, the particle velocity reflects with the same sign. During the reflection process, the velocity at the free end doubles. For a rod with toe resistance, this velocity is reduced by the effect of the resistance force (proportional to the velocity effect). Therefore, in the case of a pile with only end bearing, such as the SPT, the velocity at the toe is:

$$\dot{u}(t+L/c) = 2\dot{u}(t) - \frac{c}{EA}R(t+L/c) \quad (5.9)$$

where $\dot{u}(t)$ is the downward traveling velocity wave. If the expression for the downward traveling velocity wave at the measurement point is substituted into equation (5.9)

$$\dot{u}(t+L/c) = \left[\frac{c}{EA}F_m(t) + \dot{u}_m(t) \right] - \frac{c}{EA}R(t+L/c) \quad (5.10)$$

This expression can be integrated or differentiated to obtain the toe displacement or acceleration, respectively. This approach had been used by Teferra (1977) in the derivation of the so-called Pile End Bearing Wave Analysis Program (PEBWAP) method for calculation of the soil stiffness at the pile toe.

5.2.2 Verification of the Method

The method presented above assumes a uniform rod. In fact, the drill string used in the SPT procedure is not really uniform. The connectors, between 5 or 10 ft (1.52 or 3.05 m) long sections, have a larger mass than an equivalent length of plain rod. More seriously, a loose connector might exist in the drill string making the rod non-uniform. The effect of the connectors and the existence of a loose connection on the calculation of bottom force and velocity will be discussed.

To verify the above discussed approach, force and velocity were actually measured at the sampler during a regular SPT operation. An accelerometer was mounted inside the sampler for velocity measurements and two sets of strain gauges were mounted on opposite sides of the split spoon sampler to measure the force. Also, force and velocity were measured near the top of the drill string. A Pile Driving Analyzer simultaneously recorded the force and velocity at the top and the force and velocity at the bottom. The bottom force was from only one set of strain gauges.

Force and velocity measurements taken near the top of the drill string during the Modified SPT are shown in figure 5.15(a). Force and velocity at the bottom were calculated from these top measurements according to the method presented above; they will be referred to as the *calculated* bottom force and velocity. The calculated bottom force and velocity is compared with the measured bottom force and velocity in figures 5.15(b) and 5.15(c), respectively. Figure 5.15(c) shows a very good agreement between the measured and calculated velocities. The discrepancy between the forces in figure 5.15(b) were probably due to the fact that force measurements were taken on only one side of the sampler. Any bending that may have occurred at the strain gauge locations is not accounted for in the measurements. However, the two signals follow a similar path. Also, as discussed below, there is evidence of a connector reflection which might have affected some of the peaks of the very rapidly changing force record.

Another condition that violates the assumption of a uniform rod cross section is the existence of a loose connection in the drill string. Consider the measurements shown in figure 5.15. Since there is no cross sectional or shaft resistance variation in the SPT rod, force and velocity measured near the top should be proportional until a reflected wave returns from the pile toe (approximately 4 ms after impact in figure 5.15(a)). The loss of proportionality between force and velocity approximately 1 ms after impact in the record of figure 5.15(a), was due to the existence of a loose connection approximately 10 ft (3.05 m) below the gauge location. In fact, this was the location of a connector between the first and second 10 ft (3.05 m) section. The very good agreement between the velocities in figure 5.15(b) shows that the existence of a loose connection in the drill string may not be a major problem for the simple calculation of bottom force and velocity.

In summary, it may be concluded that the bottom force and velocity calculated from the top measurements are sufficiently reliable. The mass effect of connectors or loose connections apparently have some effect on the bottom variables which can be evaluated by inspecting the top records. These conclusions are made for uniform AW rods; other rod types (and especially rods composed of different rod types with subs) might violate the uniform rod assumption, and the method shown above will not be applicable.

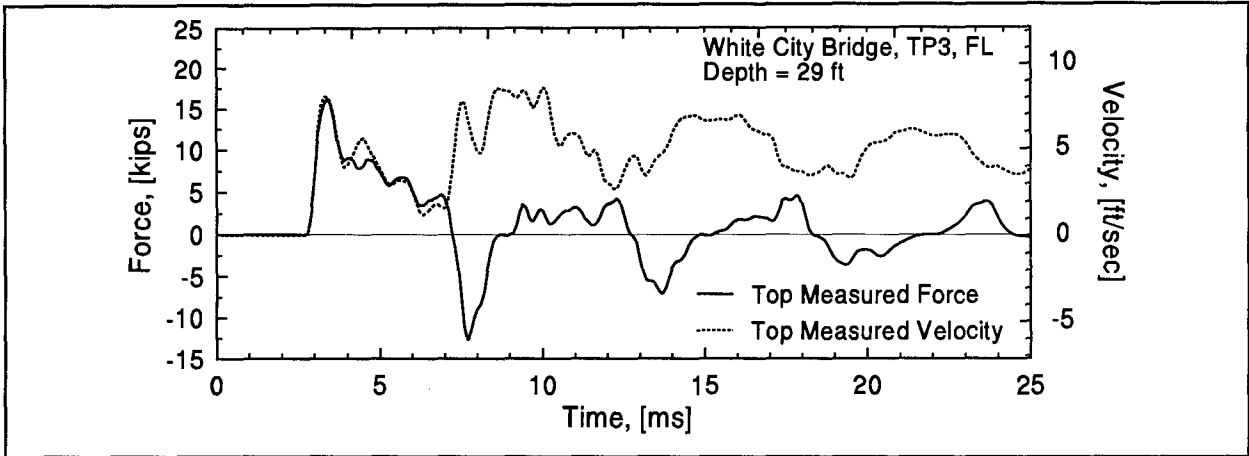


Figure 5.15(a): Force and Velocity Measured at the Top

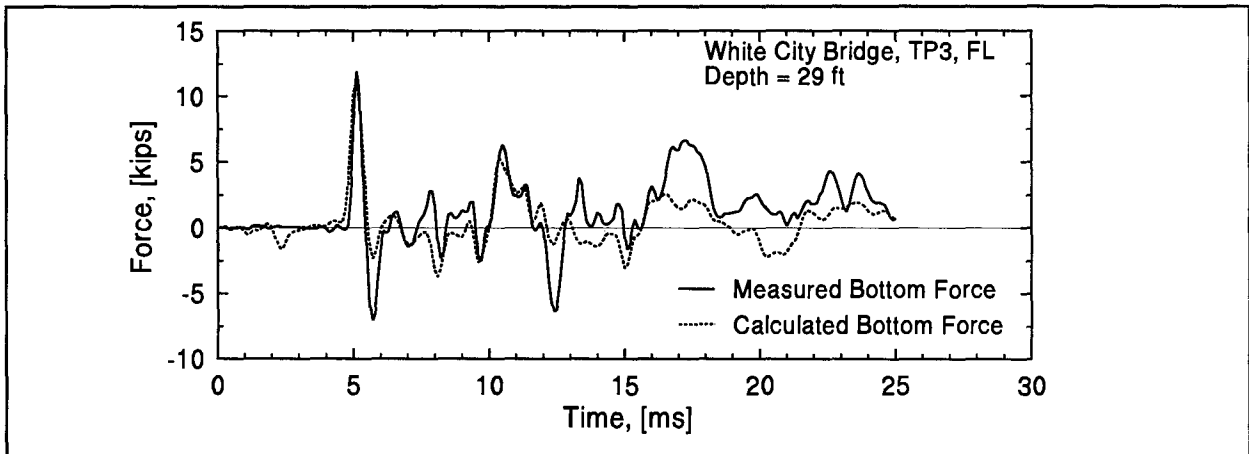


Figure 5.15(b): Comparison Between Measured and Calculated Bottom Force

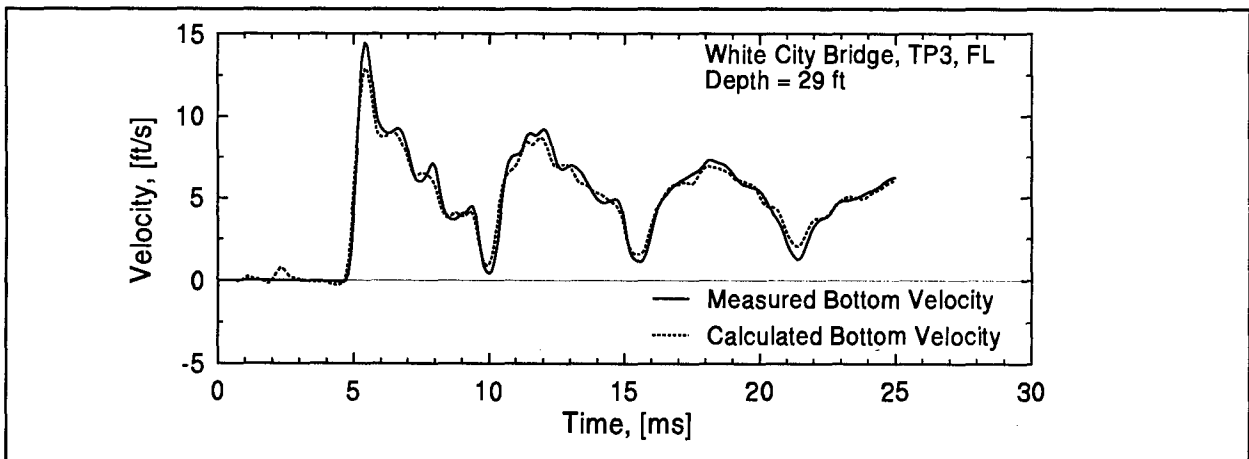


Figure 5.15(c): Comparison between Measured and Calculated Bottom Velocity

5.2.3 Determination of Wave Equation Soil Constants

In this section, a systematic signal matching approach will be presented to determine Smith soil parameters for wave equation analyses. According to Smith, the toe resistance force can be represented analytically as the sum of three separate resistance forces:

$$R_{cT} = R_a + R_d + R_s \quad (5.11)$$

where R_a is the inertia or acceleration dependent resistance, R_d is the dynamic or velocity dependent resistance, and R_s is the static or displacement dependent resistance. The subscript cT denotes that the resistance force is calculated from the acceleration, velocity, and displacement determined at the toe from the top measurements. The acceleration dependent component can be written as:

$$R_a(t) = m\ddot{u}(t) \quad (5.12)$$

where m is the additional mass of the sampler plus the mass of the soil inside the sampler and in the zone around it. The dynamic portion is given by:

$$R_d(t) = R_s J \dot{u}(t) \quad (5.13)$$

where J is the Smith damping constant and $\dot{u}(t)$ is the bottom velocity. As long as no rebound occurs, the static portion of the resistance can be expressed as:

$$R_s(t) = \begin{cases} \frac{R_u}{q} u(t) & \text{if } u < q \\ R_u & \text{if } u \geq q \end{cases} \quad (5.14)$$

where R_u is the ultimate static capacity, q is the quake, and $u(t)$ is the bottom displacement. Thus, for given values of m , J , R_u , and q together with the values of the bottom acceleration, velocity, and displacement all obtained from SPT rod top measurements, R_{cT} can be calculated. If the proper values of the constants have been selected then R_{cT} should match the bottom force calculated from the top measurements which can be considered the measured resistance, R . The problem to be solved is then:

$$\text{Find } (m, J, R_u, q)$$

$$\text{such that:} \quad (5.15)$$

$$\int |R - R_{cT}| dt \quad \text{is a minimum}$$

In the present case, the problem of finding four unknowns could be reduced to two unknowns since a static uplift or compression test was performed at certain test locations. These static tests yielded the ultimate static capacity, R_u , and the quake, q . The unknowns to be determined by the signal matching search were therefore damping factor, J , and the mass, m . This method was called the "static" analysis. All four quantities (R_u , q , J , m) were also determined solely by record matching. This procedure was called the "dynamic" analysis.

5.2.4 GRLWEAP Analysis

The soil parameter values from "static" and "dynamic" methods were examined using the wave equation analysis program, GRLWEAP, modeling the SPT sampler driving conditions. The analysis was also performed on the SPT driving system using the standard GRLWEAP Smith soil parameter values. The objective of the study was the comparison of blow counts calculated by GRLWEAP with field measured blow counts (SPT N-value) for an assessment of each method's accuracy.

Before such comparison could be made, it was necessary to ensure that the SPT driving system was properly modeled for the wave equation analysis. Due to the steel-to-steel impact in the SPT system, rod forces had a high frequency content and a very short rod segment had to be used in modeling the drill string. The "round-out"¹ at the top of drill string and the efficiency were varied to match the measured maximum impact force and maximum energy. This was done by comparing the force and velocity curves generated by GRLWEAP with the measured quantities. Such comparison was made for each test location either for shaft or oversized tip. Typical force and velocity comparisons are shown in figures 5.16 and 5.17. The (a) figures compare the measured and GRLWEAP generated top force and velocity, the (b) figures compare the calculated and GRLWEAP generated bottom force and velocity. It was concluded that good agreement between measurement and GRLWEAP calculated SPT top and bottom quantities can be achieved.

5.2.5 SPT Result Summary

The Modified SPT measurements were performed at 11 sites, but only 10 sites (seven correlation sites and three verification sites) were analyzed, for reasons discussed in section 4.6. A total of 82 individual tests from these 10 sites were analyzed, and, on average, eight tests were

¹The round-out is a term used in GRLWEAP to describe a compression value over which a spring's stiffness increases linearly from 0 to nominal. This round-out is only used for springs which represent component interfaces.

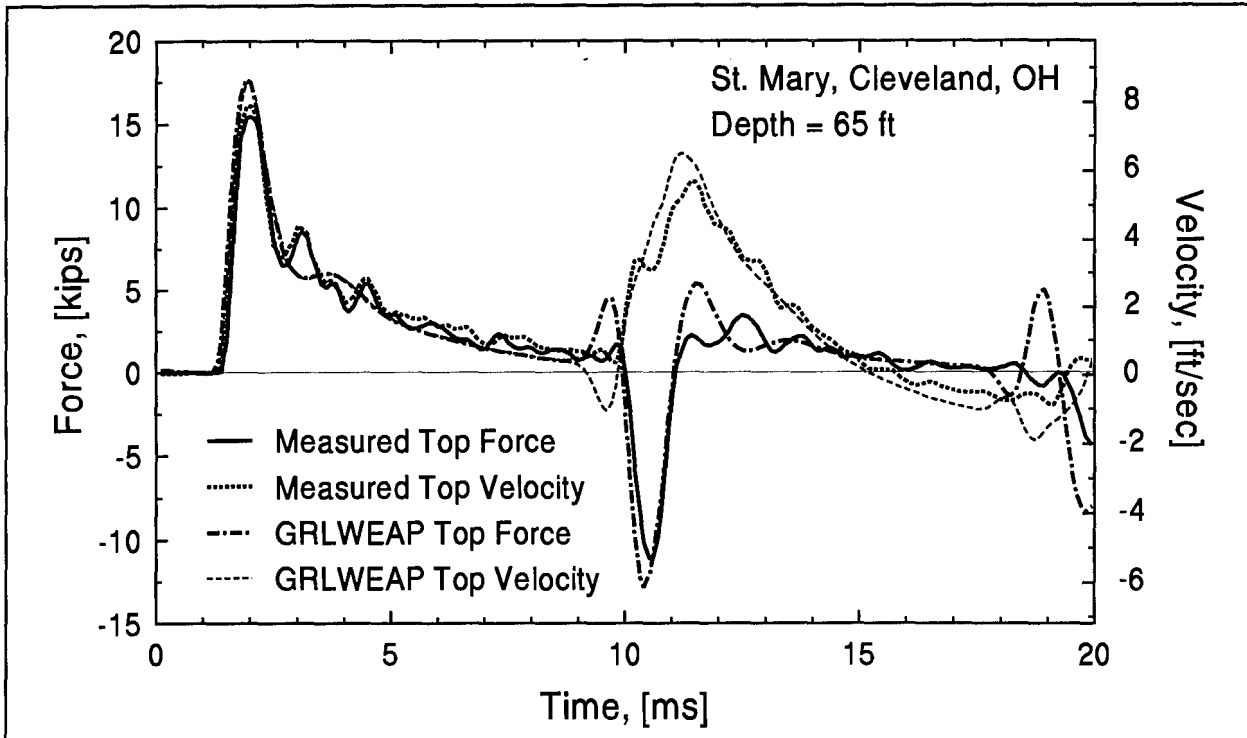


Figure 5.16(a): Comparison Between GRLWEAP and Measured Top Force and Velocity from St. Mary Site

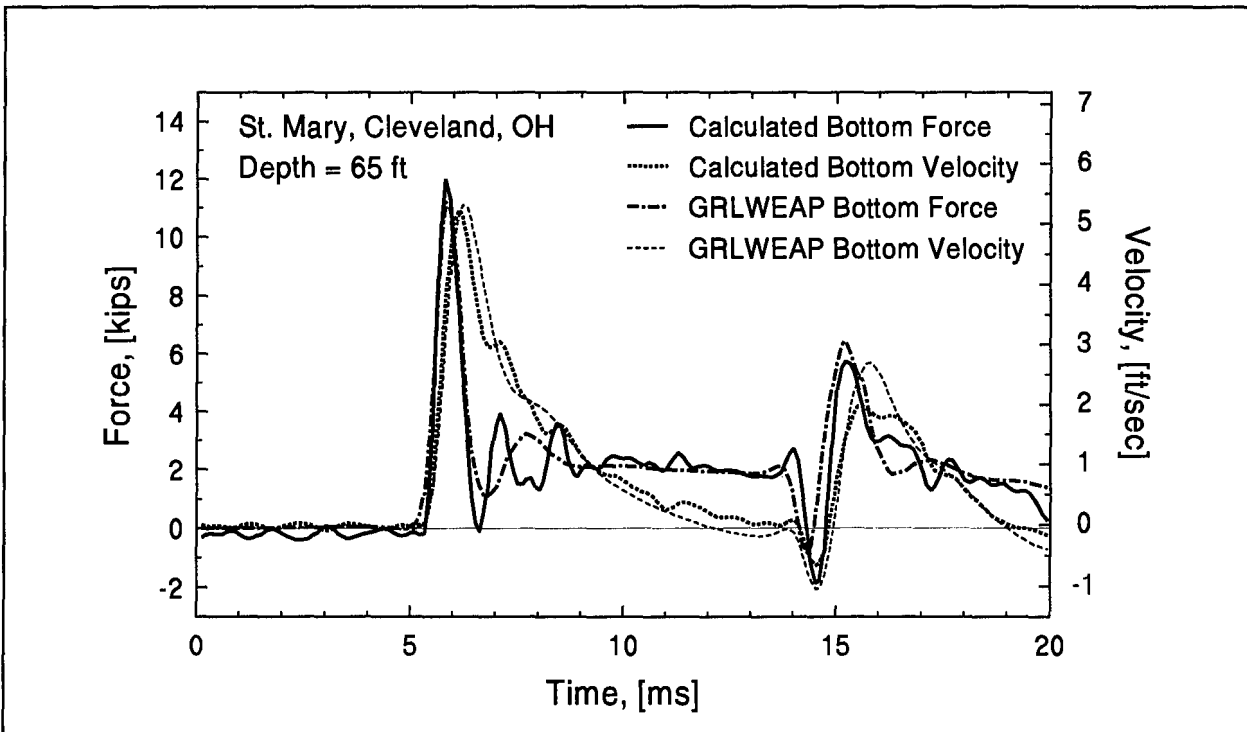


Figure 5.16(b): Comparison Between GRLWEAP and Measured Bottom Force and Velocity from St. Mary Site

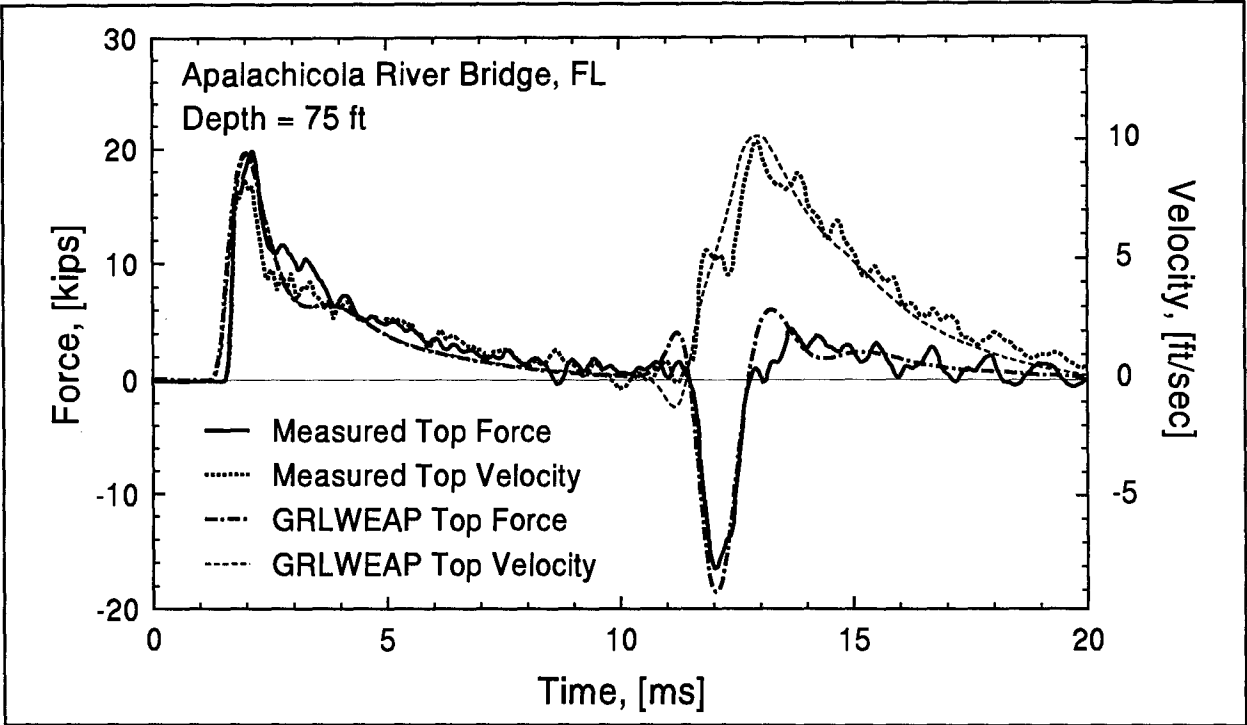


Figure 5.17(a): Comparison Between GRLWEAP and Measured Top Force and Velocity from Apalachicola Site

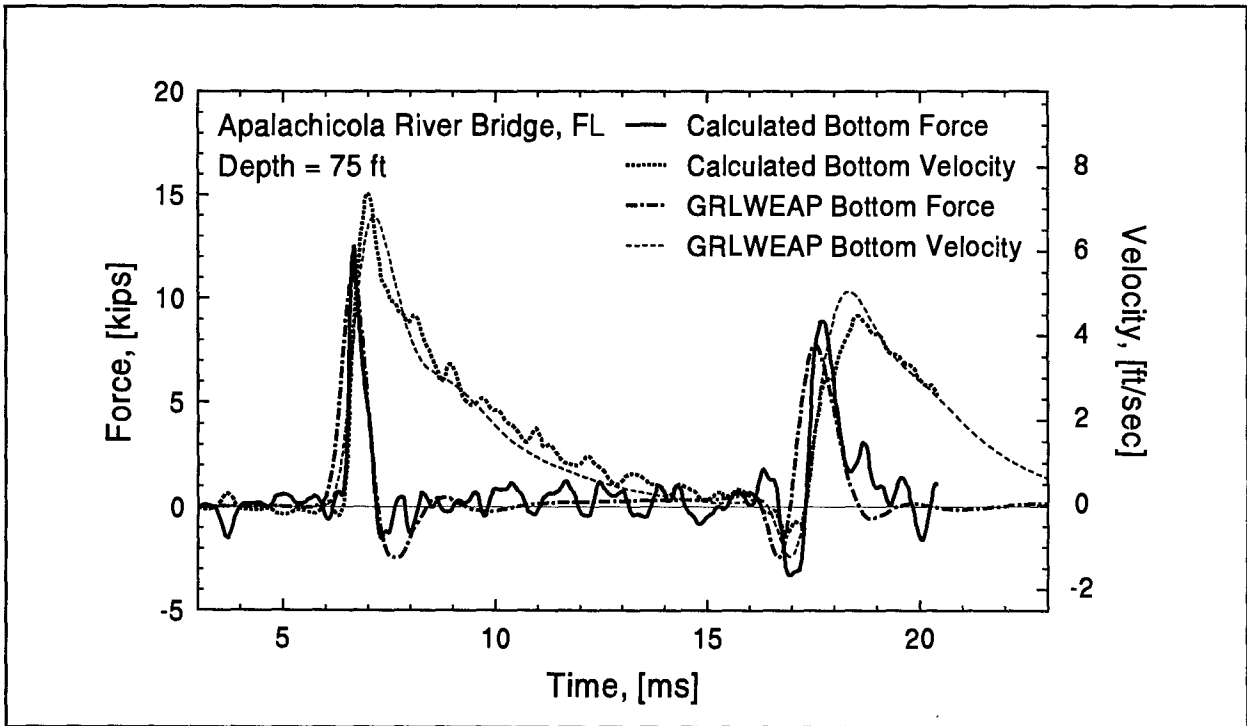


Figure 5.17(b): Comparison Between GRLWEAP and Measured Bottom Force and Velocity from Apalachicola Site

analyzed for each site. From each test, the average peak force and velocity, and the maximum energy transferred to the drill string were calculated by the PDA and presented in table E.1 in appendix E together with a complete summary of the SPT top measurements. In addition to the force and velocity measurements, the hammer impact velocity was also measured using the Hammer Performance Analyzer (HPA) and the results are also presented in table E.1. Also included in table E.1 are the SPT N-values and the transfer efficiency (transferred energy divided by ram weight times specified drop height).

5.2.6 Dynamic Data Collection

At the six correlation sites, the test piles had already been driven. Both the static load tests, and dynamic tests with the PDA had also been performed on these full-scale piles prior to the Modified SPT test. Existing soil borings with SPT N-values were also available. Since the standard SPT results were available, there was no need to perform the Modified SPT continuously or at short depth intervals. Instead, the test was performed at depths (a) where previous SPT results indicated a particularly important soil layer, (b) where a considerable amount of resistance was anticipated, or (c) where a potential soil setup layer was encountered. At the verification sites (see chapter 7), the Modified SPT procedure was performed at 5-ft (1.5 -m) increments.

For pile shaft resistance determination, the Modified SPT procedure consisted of (a) a standard SPT procedure with force and velocity measurement near the top of the drill string; (b) a static uplift test with continuous monitoring of force and displacement; and (c) a redrive of the sampler after the uplift test or after a waiting period, again with force and velocity measurements. The redrive tests were generally performed with a lower than 30 in (762 mm) hammer drop height. Additional uplift tests followed by subsequent redrive tests were performed only if the soil showed a potential for setup. Uplift tests and re-driving were typically done after a waiting period of 15 min, 1 h, or in a few cases overnight (approximately 12 to 16 h).

Near the toe of the test piles, a compression test was performed to measure the end bearing. For the compression test, the sampler was removed and replaced with an oversized tip (see section 4.3.2 for description). The oversized tip allows the study of toe resistance parameters without the interference of the shaft resistance parameters. This tip was first driven 6 in (152 mm) with the standard SPT hammer before the static compression test was performed. The force and velocity measurement was also performed during tip driving. At some sites, where hollow stem augers or casing were used, spacers were placed at 10-ft (3.05-m) intervals (at the connectors between the drill rods) to reduce the likelihood of buckling during the static compression test. Further descriptions of the Modified SPT procedure have been presented in chapter 4.

5.2.7 Dynamic Data Analysis and Results of SPT

At each test depth where the Modified SPT was performed, a representative force and velocity record from the end of driving (EOD) of sampler or oversized tip was chosen for analysis. When a redrive test was performed on the SPT after the static uplift test or a waiting period, a representative force and velocity record from the first hammer blow was also selected and analyzed. The analysis involved determination of soil parameters (R_u , q , J , m) using the method discussed in section 5.2.3. The selected top force and velocity records, the calculated bottom force and velocity and the force matching curves are presented in appendix D.

Because of the existence of some loose connections in the drill string, the overall wave speed was lower than that of steel (normally 16,800 ft/s or 5,140 m/s) and therefore the actual wave travel time was longer than the theoretical one. To calculate the bottom force and velocity from the top measured quantities, the actual wave travel time had to be used. As mentioned earlier, two types of analyses were performed: the "static" analysis utilized the ultimate resistance, R_u , and the quake, q , both obtained from the static test and then only solved for the damping factor, J , and the mass, m . The second, "dynamic" analysis considered all four soil parameters (R_u , q , J , m) unknown and determined them by signal matching of the bottom force.

In addition to the two analyses discussed above, wave equation analyses (GRLWEAP) were also performed on the SPT driving system using the above calculated soil parameters (static and dynamic), and the standard GRLWEAP soil parameter values (standard). The blow counts computed by the wave equation analyses (GRLWEAP N-value) were compared with the field measured SPT N-values; both results are presented in equivalent blows per foot (blows/ft).

Tables 5.7 through 5.12 present the results obtained from both "static" and "dynamic" methods. The tables include the depths where the tests were performed, the soil type and the test type; "shaft" indicates regular SPT sampler driving and uplift tests, and "toe" indicates a compression test. The fourth through seventh columns list the four soil parameters explained above. The eighth and ninth columns are the respective measured SPT N-value and the GRLWEAP computed blow count with dynamic soil parameters determined by either the "static" or "dynamic" method as indicated in the 10th column. The last two columns indicate a figure reference in appendix D and some additional information, such as whether the records are taken before or after the uplift test, the hammer drop height, the type of oversized tip for compression test, and for the redriving cases, the waiting period given in parenthesis.

Depth [ft]	Soil Type	Test Type	Ultimate Resistance R_u [kips]	Quake q [in]	Damping Constant J [s/ft]	Acceleration Constant m [lbs]	Measured N-Value [blows/ft]	GRLWEAP N-Value [blows/ft]	Analysis Type	Figure Ref.	Remarks		
40	SP-SM	Shaft	0.90	0.070	0.130	0.26	8	13	Dynamic	D.1c	Before Uplift. 30" Drop		
			0.80	0.070	0.200	0.26	8	14	Static	D.1d	Before Uplift. 30" Drop		
65	SC	Shaft	2.10	0.030	0.180	0.45	35	35	Static	D.2c	Before Uplift. 24" Drop		
			2.35	0.030	0.150	0.48	35	36	Dynamic	D.2d	Before Uplift. 24" Drop		
			2.10 kips on the shaft (from dynamic matching)										
			2.10	0.030	0.120	0.40	32	31	Static	D.4c	After Uplift. 24" Drop (2hrs BOR)		
			2.10	0.033	0.120	0.40	32	31	Dynamic	D.4d	After Uplift. 24" Drop (2hrs BOR)		
100	CL	Shaft	0.75	0.023	0.800	0.28	62	31	Static	D.5c	Before Uplift. 24" Drop		
			3.00*	0.020	0.150	0.25	62	47	Dynamic	D.5d	Before Uplift. 24" Drop		
			1.50 kips on the shaft (from dynamic matching)										
			1.25	0.012	0.400	0.28	96**	32	Static	D.6c	After Uplift. 30" Drop (15hrs BOR)		
			2.50	0.012	0.150	0.30	96**	38	Dynamic	D.6d	After Uplift. 30" Drop (15hrs BOR)		
103.5	CL	Shaft	0.98	0.035	0.860	0.20	101	45	Static	D.7c	Before Uplift. 30" Drop		
			2.90*	0.033	0.260	0.22	101	69	Dynamic	D.7d	Before Uplift. 30" Drop		
			2.2 kips on the shaft (from dynamic matching)										
105	CL	Toe	3.50	0.086	0.005	0.48	66	72	Static	D.8c	Flat End tip. 30" Drop		
			2.12	0.025	0.120	0.38	66	43	Dynamic	D.8d	Flat End tip. 30" Drop		

Notes: * Total resistance on the sampler (Shaft+Toe). The shaft resistance is presented on the following row.

** Blow count is calculated from the final set ($\frac{1}{8}$ in). The blow count calculated from the final displacement (obtained from the measured top velocity) was 42 blows/ft.

BOR stands for beginning of restrike

1 ft = 0.305 m; 1 in = 25.4 mm; 1 kip = 4.45 kN; 1 s/ft = 3.28 s/m; 1 lb = 4.45 N; 1 blows/ft = 3.28 blows/m.

Depth [ft]	Soil Type	Test Type	Ultimate Resistance R_u [kips]	Quake q [in]	Damping Constant J [s/ft]	Acceleration Constant m [lbs]	Measured N-Value [blows/ft]	GRLWEAP N-Value [blows/ft]	Analysis Type	Figure Ref.	Remarks
20	Fill	Shaft	0.03	0.011	5.000	0.21	14	9	Static		Before Uplift. 30'' Drop
			0.55*	0.030	0.200	0.22	14	18	Dynamic	D.9c	Before Uplift. 30'' Drop
30	SP-SM	Shaft	0.06	0.012	5.000	0.20	19	16	Static		Before Uplift. 30'' Drop
			1.17*	0.090	0.002	0.24	19	25	Dynamic	D.10c	Before Uplift. 30'' Drop
40	GP-GM	Shaft	0.09	0.030	5.000	0.30	165	25	Static		Before Uplift. 30'' Drop
			3.20*	0.130	0.200	0.33	165	319/162**	Dynamic	D.11c	Before Uplift. 30'' Drop (Sampler Overdriven)
42	GP-GM	Toe	4.00	0.160	0.150	0.6	300	411	Static	D.12c	Cone Tip. 30'' Drop
			4.50	0.120	0.150	0.6	300	338	Dynamic	D.12d	Cone Tip. 30'' Drop
54	SP-SM	Toe	2.50	0.174	0.300	0.50	80	182/76**	Static	D.13c	Flat End Tip. 30'' Drop
			2.64	0.186	0.300	0.50	80	238/82**	Dynamic	D.13d	Flat End Tip. 30'' Drop
56	SP-SM	Toe	1.50	0.028	0.200	0.44	50	49	Static	D.14c	Cone Tip. 30'' Drop
			1.90	0.023	0.080	0.40	50	49	Dynamic	D.14d	Cone Tip. 30'' Drop

Notes: * Total resistance on the sampler (Shaft+Toe). The shaft resistance is that determined from the static uplift test.

** These blow counts were calculated using a toe damping factor of 0.03 s/ft.

1 ft = 0.305 m; 1 in = 25.4 mm; 1 kip = 4.45 kN; 1 s/ft = 3.28 s/m; 1 lb = 4.45 N; 1 blows/ft = 3.28 blows/m.

Depth [ft]	Soil Type	Test Type	Ultimate Resistance R_u [kips]	Quake q [in]	Damping Constant J [s/ft]	Acceleration Constant m [lbs]	Measured N-Value [blows/ft]	GRLWEAP N-Value [blows/ft]	Analysis Type	Figure Ref.	Remarks
14	SM	Shaft	0.42	0.010	0.170	0.28	6	6	Static	D.15c	Before Uplift. 30" Drop
			0.43	0.027	0.150	0.27	6	6	Dynamic	D.15d	Before Uplift. 30" Drop
40	CL	Shaft	0.24	0.015	0.400	0.35	5	6	Dynamic		No Uplift. Standard SPT, 30" Drop
50	SM	Shaft	0.27	0.013	0.080	0.43	10	6	Static		Before Uplift. 30" Drop
			No useful match from the dynamic analysis								
55	CH	Shaft	0.45	0.030	0.400	0.5	12	10	Static	D.18c	Before Uplift. 30" Drop
			0.45	0.010	0.600	0.47	12	12	Dynamic	D.18d	Before Uplift. 30" Drop
			0.39	0.013	0.800	0.25	12	12	Static	D.20c	After Uplift. 30" Drop.(14 hrs BOR)
			0.68	0.014	0.450	0.21	12	14	Dynamic	D.20d	After Uplift. 30" Drop.(14 hrs BOR)
60	SM	Shaft	0.72	0.080	0.800	0.33	38	25	Static	D.21c	Before Uplift. 30" Drop
			1.80*	0.200	0.250	0.3	38	41	Dynamic	D.21d	Before Uplift. 30" Drop
			0.58	0.035	0.570	0.3	16	31	Static	D.22c	After Uplift. 10" Drop.(1 hr BOR)
			0.58	0.030	0.570	0.3	16	30	Dynamic	D.22d	After Uplift. 10" Drop.(1 hr BOR)
65	SM	Shaft	1.90	0.040	0.370	0.23	34	32	Static	D.23c	Before Uplift. 30" Drop
			3.00*	0.040	0.200	0.32	34	36	Dynamic	D.23d	Before Uplift. 30" Drop
			2.20	0.030	0.080	0.3	16	51	Static	D.24c	After Uplift. 10" Drop.(2 hrs BOR)
			1.20	0.030	0.150	0.35	16	35	Dynamic	D.24d	After Uplift. 10" Drop.(2 hrs BOR)
70		Toe	3.20	0.070	0.037	0.34	24	30	Static	D.25c	Cone tip. 30" Drop
			2.76	0.050	0.080	0.33	24	29	Dynamic	D.25d	Cone tip. 30" Drop

Notes: * Total resistance on the sampler (Shaft+Toe). The shaft resistance is determined from the static uplift test.
BOR stands for beginning of restrike.
1 ft = 0.305 m; 1 in = 25.4 mm; 1 kip = 4.45 kN; 1 s/ft = 3.28 s/m; 1 lb = 4.45 N; 1 blow/ft = 3.28 blows/m.

Table 5.10: Summary of the Smith Soil Constants for the C&D Canal Site, Pier 21, Delaware												
Depth	Soil Type	Test Type	Ultimate Resistance R_u [kips]	Quake q [in]	Damping Constant J [s/ft]	Acceleration Constant m [lbs]	Measured N-Value [blows/ft]	GRLWEAP N-Value [blows/ft]	Analysis Type	Figure Ref.	Remarks	
40	SM	Shaft	0.67	0.030	0.010	0.40	7	7	Static	D.26c	Before Uplift. 30" Drop	
			No useful match from the dynamic analysis									
55	SM	Shaft	1.05	0.060	0.200	0.27	17	16	Static	D.28c	Before Uplift. 30" Drop	
			1.10	0.087	0.270	0.27	17	19	Dynamic	D.28d	Before Uplift. 30" Drop	
			0.81	0.020	0.150	0.30	48	27	Static	D.29c	After Uplift. 10" Drop. (No Waiting)	
			0.88	0.033	0.050	0.30	48	25	Dynamic	D.29d	After Uplift. 10" Drop. (No Waiting)	
65	SM	Shaft	1.26	0.033	0.001	0.37	20	13	Static	D.30c	Before Uplift. 30" Drop	
			1.20	0.040	0.002	0.40	20	12	Dynamic	D.30d	Before Uplift. 30" Drop	
71		Toe	1.54	0.080	0.070	0.27	18	26	Static	D.32c	Flat End tip. 30" Drop	
			1.25	0.023	0.060	0.23	18	18	Dynamic	D.32d	Flat End tip. 30" Drop	

Notes: 1 ft = 0.305 m; 1 in = 25.4 mm; 1 kip = 4.45 kN; 1 s/ft = 3.28 s/m; 1 lb = 4.45 N; 1 blow/ft = 3.28 blows/m.

Table 5.11: Summary of the Smith Soil Constants for the White City Bridge Site, Florida											
Depth	Soil Type	Test Type	Ultimate Resistance R_u [kips]	Quake q [in]	Damping Constant J [s/ft]	Acceleration Constant m [lbs]	Measured N-Value [blows/ft]	GRLWEAP N-Value [blows/ft]	Analysis Status	Figure Ref.	Remarks
TP3											
20	SM	Shaft	0.10*	0.050	0.07	0.30	3	4	Dynamic		Before Uplift. 30" drop
29	SM	Shaft	0.32*	0.005	0.15	0.35	3	5	Dynamic	D.34c	Before Uplift. 30" drop
31	SM	Shaft	0.74*	0.016	0.17	0.47	6	9	Dynamic		Before Uplift. 30" drop
32	SM	Toe	3.35	0.150	0.33	0.52	30	95/34**	Static	D.36c	Flat End Tip. 30" drop
			4.00	0.27	0.15	0.43	30	125/60**	Dynamic	D.36d	Flat End Tip. 30" drop
35	SM	Toe	4.60	0.160	0.01	0.65	50	46	Static	D.37c	Flat End Tip. 30" drop
			4.00	0.270	0.08	0.45	50	78	Dynamic	D.37d	Flat End Tip. 30" drop
TP6											
16	SP	Shaft	0.55	0.180	0.39	0.41	11	11	Dynamic		No uplift
32	N/A	Toe	6.80	0.230	0.08	0.50	70	248	Dynamic	D.39c	Flat End tip. 30" drop
33	N/A	Toe	8.80	0.200	0.05	0.65	100	588	Dynamic		Flat End tip. 30" drop

Notes: * Resistance at the sampler toe only.

** These blow counts were calculated using a toe damping factor of 0.01 s/ft.

1 ft = 0.305 m; 1 in = 25.4 mm; 1 kip = 4.45 kN; 1 s/ft = 3.28 s/m; 1 lb = 4.45 N; 1 blow/ft = 3.28 blows/m.

Table 5.12: Summary of the Smith Soil Constants for the Apalachicola River Bridge Site, Florida												
Depth	Soil Type	Test Type	Ultimate Resistance R_u [kips]	Quake q [in]	Damping Constant J [s/ft]	Acceleration Constant m [lbs]	Measured N-Value [blows/ft]	GRLWEAP N-Value [blows/ft]	Analysis Status	Figure Ref.	Remarks	
20	SP	Shaft	0.90	0.058	0.100	0.25	8	9	Dynamic	D.41	Before Uplift. 30" drop	
			0.15*	No useful match from static analysis						Static		Before Uplift. 30" drop
25	SP-SM	Shaft	0.62	0.050	0.180	0.35	4	7	Dynamic	D.42	Before Uplift. 30" drop	
			0.15*	No useful match from static analysis						Static		Before Uplift. 30" drop
			0.97	0.022	0.050	0.5	24	22	Dynamic	D.43	After Uplift. 10" drop. (14 hrs BOR)	
			0.22*	No useful match from static analysis						Static		After Uplift. 10" drop. (14 hrs BOR)
55	MH	Shaft	0.45	0.010	0.200	0.4	6	8	Static	D.44	Before Uplift. 30" drop	
			0.40	0.023	0.250	0.4	6	8	Dynamic		Before Uplift. 30" drop	
			0.65	0.015	1.000	0.44	48	51	Static	D.45	After Uplift. 10" drop. (1 hr BOR)	
			1.80	0.015	0.200	0.5	48	63	Dynamic		After Uplift. 10" drop. (1 hr BOR)	
75	SM	Shaft	0.42	0.030	0.200	0.25	7	8	Static	D.46	Before Uplift. 30" drop	
			0.40	0.008	0.250	0.25	7	8	Dynamic		Before Uplift. 30" drop	
			0.42	0.054	1.000	0.3	48	38	Static	D.47	After Uplift. 10" drop. (1 hr BOR)	
			1.00	0.020	0.180	0.25	48	38	Dynamic		After Uplift. 10" drop. (1 hr BOR)	
89	N/A	Toe	5.70	0.065	0.010	0.3	16	50	Static	D.48	Flat End tip. 30" drop	
			5.00	0.100	0.010	0.25	16	44	Dynamic		Flat End tip. 30" drop	

Notes: * Used in the calculation of shaft resistance of the full-scale pile.

BOR stands for beginning of restrike.

1 ft = 0.305 m; 1 in = 25.4 mm; 1 kip = 4.45 kN; 1 s/ft = 3.28 s/m; 1 lb = 4.45 N; 1 blow/ft = 3.28 blows/m.

Comparisons between GRLWEAP calculated and measured blow counts for all sites and test depths at EOD are also graphically presented in figure 5.18 and tabulated in table 5.13. Cases with high blow count (greater than 100 blows/ft, or 300 blows/m) were not included in the comparison. With a few exceptions, the blow counts calculated using Smith's soil model obtained from the matching analysis showed a relatively good agreement with the measured blow counts. The blow counts obtained by utilizing the soil constants determined from both "static" and "dynamic" analyses produced correlations with greater scatter. Four cases, marked "1" through "4" in table 5.13, are discussed in the following.

Case 1 - (Apalachicola, toe test at 89 ft or 27 m): the field measured blow count was 16 blows/ft (53 blows/m) while the GRLWEAP computed blow counts ranged from 44 to 55 blows/ft (144 to 182 blows/m). At this location, the SPT tip driving was suspected to be completed at the top of a strong bearing layer and therefore the blow count did not reflect that of the pile bearing layer. Since the static compression test was performed at the end of tip driving, the tip resistance measured by the compression test was that of the bearing layer, which could explain the discrepancy between the measured and computed blow count. The existing soil boring also indicated a sudden increase in SPT N-value at this location.

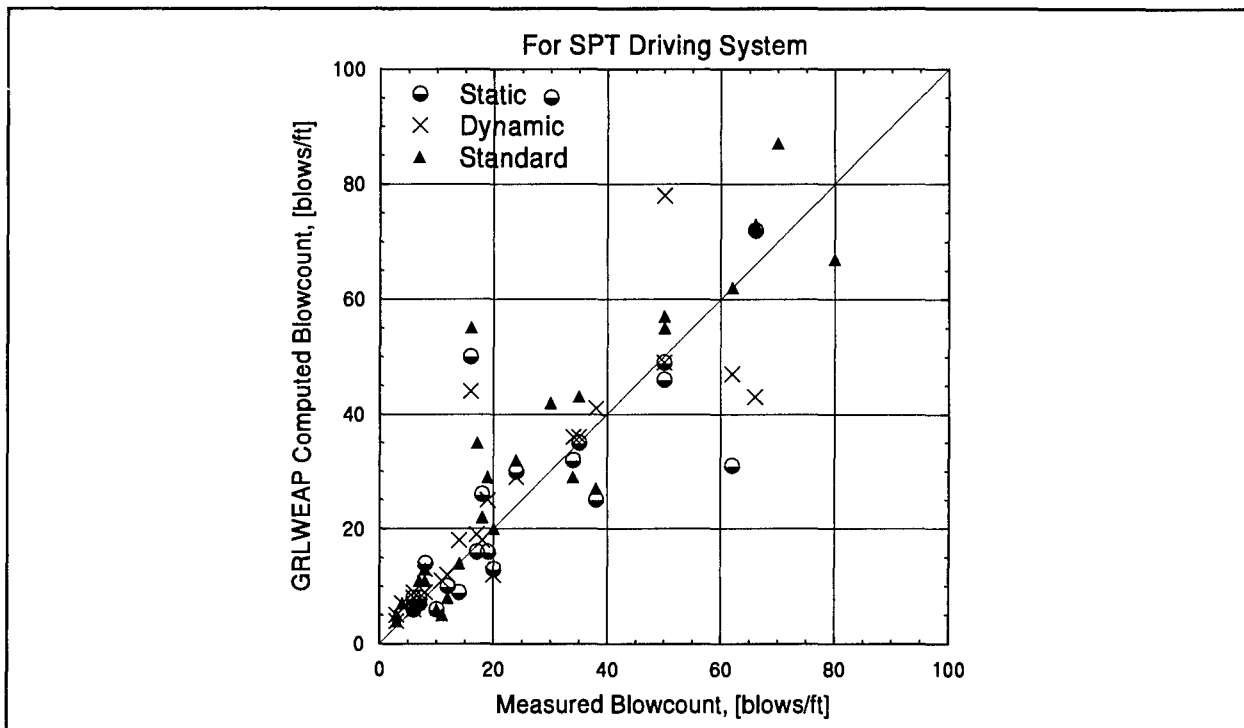


Figure 5.18: Comparison Between GRLWEAP and Measured Blow Count from SPT Driving System

Sites	Depth [ft]	Blow Count [blows/ft]			
		Measured	GRLWEAP		
			Static	Dynamic	Standard
St. Mary	40	8	14	13	13
	65	35	35	36	43
	100	62	(31) ³	47	62
	103	101	45	69	92
	105	66	72	43	73
Portland	20	14	9	18	14
	30	19	16	25	29
	40	165	25	319	107
	42	300	411	338	118
	54	80	(182) ⁴	238	67
	56	50	49	49	55
CD 17	14	6	6	6	6
	50	10	6	--	6
	55	12	10	12	8
	60	38	25	41	27
	65	34	32	36	29
	70	24	30	29	32
CD 21	40	7	7	--	11
	55	17	16	19	35
	65	20	13	12	20
	71	18	26	18	22
White City, TP3	20	3	--	4	4
	29	3	--	5	5
	31	6	--	9	7
	32	30	(95) ²	125	42
	35	50	46	78	57
White City, TP6	16	11	--	11	5
	32	70	--	248	87
	33	100	--	588	119
Apalachicola	20	8	--	9	11
	25	4	--	7	7
	55	6	8	8	7
	75	7	8	8	7
	89	16	(50) ¹	44	55

Note: 1, 2, 3 and 4 are explained in section 5.2.7.

Numbered results, in parentheses, are discussed in section 5.2.7.

1 blow/ft = 3.28 blows/m; 1 ft = 0.305 m.

Case 2 - (White City, toe test 32 ft or 9.8 m): the field measured blow count was 30 blows/ft (100 blows/m) while the blow count calculated by GRLWEAP using the soil constants from the "static" analysis was 95 blows/ft (314 blows/m). If a low toe damping factor, $J = 0.01$ s/ft (0.03 s/m) had been used the blow count would have agreed better (34 blows/ft or 113 blows/m). The measured and computed blow counts also agreed better when the hyperbolic soil model was used (see section 5.2.11).

Case 3 - (St Mary, sampler driving at 100 ft or 30.5 m): good "dynamic" matching could not be obtained for the Modified SPT data at this location;

Case 4 - (Portland, toe test at 54 ft or 16.5 m): the computed blow counts were very high (182 blows/ft static and 284 blows/ft dynamic vs. 80 blows/ft measured). Again for a low damping factor of $J = 0.01$ s/ft (0.03 s/m) the computed blow count would have been a more reasonable 72 blows/ft. A reasonable computed blow count was also obtained with the hyperbolic soil model as discussed in section 5.2.11.

In general, blow counts calculated with soil constants from the Modified SPT data produced a slightly better correlation with the measured blow counts than those recommended by standard GRLWEAP. However, the static resistance of the SPT is relatively small, and thus the effect of the soil parameters on the blow count calculation is not as significant as for full-scale piles (see chapter 6).

5.2.8 Discussion of Shaft Results

To eliminate the effect of the tip resistance, sampler shaft resistance was calculated from uplift tests, assuming that the soil's shaft resistance would behave similarly in compression and uplift. A redrive of the sampler was not always done immediately following the uplift test, especially for those soils which indicated a potential for setup. There, the redrive was performed following the last uplift test which occurred some time after initial driving. Performing dynamic restrrike tests after each static test would have been prohibitively time consuming. Also, it was assumed that the sampler tip resistance in soils where shaft resistance and thus set-up effects are dominant (typically clays) would be relatively small. Therefore, it seemed to be a realistic assumption that the static resistance component for driving the sampler was approximately the same as that for the uplift. This argument applies to cases designated as "before uplift" in tables 5.7 through 5.12.

Wave equation calculated forces and velocities generally agreed well with measured ones. However, for some locations where the soil was mostly sand, such as the Portland and White City sites, the uplift test capacities were very low compared to the relatively high SPT blow count. Apparently, in these cases, the driving resistance occurred mostly at the tip. Analyses

with only static uplift resistance yielded a poor match quality. On the other hand, dynamic matching was successful. Of course, the calculated ultimate resistance was then a combination of both shaft and tip resistances. A significant difference between ultimate resistance values obtained from static and dynamic analyses was commonly observed for sandy materials. The difference is reasonably attributed to end bearing on the bottom of the sampler.

In some cases, it was possible to identify the tip resistance as the static resistance from dynamic analysis (assuming all four soil constants as variables) using a record taken before uplift minus the uplift static resistance, or by comparing the static resistance calculated dynamically from records taken both before and after the uplift test. For example, at depth 65 ft (20 m) at the St. Mary site, the static uplift test showed an ultimate resistance of 2.10 kips (9.3 kN), the "dynamic" analysis from a blow taken before uplift yielded a resistance of 2.35 kips (10.7 kN). The difference is the tip resistance which is about 0.25 kips (1.11 kN). This was verified when a blow, recorded after the uplift test was finished, yielded the same ultimate resistance of 2.10 kips (9.3 kN). Unfortunately, results from calculations of sampler tip resistance were not so clear in all cases.

At the Apalachicola site, the ultimate resistance obtained from a blow taken after uplift using the purely "dynamic" analysis was higher than that obtained from the static uplift test. Furthermore, the damping factor calculated from the "static" analysis was much higher than that from the "dynamic" analysis. Probably, the apparent setup in the "dynamic" analysis was actually an increase in damping.

Damping factors obtained at end of driving (before uplift) were in general close to or slightly above standard GRLWEAP recommended values. Restrike test analyses yielded inconsistent damping factors and did not allow for a definite conclusion. However, cases for which restrike tests were performed and analyzed are limited. As for quakes, the results did not show any clear trend. The quake values were in general lower than recommended values which may be attributed to a scale effect. The results generally indicated that the currently used Smith's soil model and the recommended shaft parameter values should yield satisfactory results.

5.2.9 Discussion of Toe Results

The bottom force matches from both "static" and "dynamic" analyses were in most cases good (see appendix D). A comparison between ultimate resistance determined from "dynamic" matching and from static compression testing is presented in figure 5.19(a) and tabulated in table 5.14. This comparison also includes the toe results obtained from the three verification sites (see chapter 7). The results show that most of the dynamically determined ultimate resistance values are less than those from static compression tests.

Table 5.14: Ultimate Resistance and Toe Damping Factor Calculated by "Static" and "Dynamic" Analyses for Static $R_u >$ Dynamic R_u						
Site	Soil Type	Static R_u [kips]	Dynamic R_u [kips]	Static J [s/ft]	Dynamic J [s/ft]	Tip Type
St. Mary	CL	3.50	2.12	0.01	0.12	Flat End
Portland	GP-GM	4.00	4.50	0.15	0.15	Cone
	SP-SM	2.50	2.64	0.30	0.30	Flat End
	SP-SM	1.50	1.90	0.20	0.08	Cone
CD 17	N/A	3.20	2.76	0.04	0.08	Cone
CD 21	N/A	1.54	1.25	0.07	0.06	Flat End
White City, TP3	SM	3.35	4.00	0.33	0.15	Flat End
	SM	4.60	4.00	0.01	0.08	Flat End
Apalachicola	N/A	5.70	5.00	0.01	0.01	Flat End
Aucilla	CL	1.90	1.10	0.01	0.12	Flat End
	Limerock	3.70	2.50	0.12	0.30	Flat End
	Limerock	2.80	2.00	0.05	0.10	Flat End
Vilano-East	SP	0.45	0.33	0.03	0.01	Flat End
	SP	0.72	0.10	0.01	0.01	Flat End
	SP	1.60	1.50	0.16	0.15	Flat End
	SP	4.20	3.50	0.12	0.25	Flat End
	SP	7.30	6.00	0.12	0.12	Flat End
	SP	8.70	12.00	0.28	0.13	Flat End
Vilano-West	OH	0.60	0.20	0.01	0.50	Flat End
	OH	1.95	2.30	0.20	0.15	Flat End

Notes: 1 kip = 4.45 kN; 1 s/ft = 3.28 s/m.

Damping factors determined from both "static" and "dynamic" analyses, for sites with cohesive soils at the toe, were relatively small ranging between 0.01 to 0.08 s/ft (0.03 to 0.26 s/m). In non-cohesive soils, the damping factors ranged from 0.15 to 0.33 s/ft (0.49 to 1.08 s/m). Not unexpected was the fact that for low resistance values with relatively large differences between "static" and "dynamic" capacity results (e.g., Vilano West with 0.6 and 0.2 kips, respectively), differences between damping factors were also very large (0.01 and 0.50 s/ft). To further investigate this point, figure 5.19(b) depicts all of those toe damping factors for which the "statically" determined R_u values exceeded the "dynamic" ones. In these cases, it would be expected that "dynamic" damping factors would be greater than "static" ones since the sum of static resistance and damping resistance should be approximately the same, regardless of the signal matching method. However, with the exception of the very poor Vilano-West agreement, the scattergram of figure 5.19(b) is remarkably symmetric to the 45° line. These results clearly point out the uncertainty associated with toe damping factors.

The GRLWEAP recommended toe quake value depends on the pile diameter, D , and is $D/120$. Since the oversized tip of the Modified SPT has a 2.5-in (64-mm) diameter, the recommended quake value would be $(2.5/120) = 0.02$ in or 0.53 mm. Observed values were larger, particularly for the flat end tip. The SPT determined average quakes were compared with the GRLWEAP recommended values in table 5.15. For comparison with GRLWEAP recommended values, the SPT toe quakes were normalized with $(D/120)$ indicating large quakes, particularly Portland and White City. To further identify these sites, the quakes were also normalized with the average quakes of all sites (0.119 and 0.146 in, or 3.02 and 3.71 mm for static and dynamic, respectively, as shown at the bottom of table 5.15). Clearly, Portland and White City produced much greater quakes than the average; these sites have also been identified as large quake sites from full-scale pile CAPWAP analyses.

A similar study was also performed on the quakes determined from CAPWAP analysis of the full-scale piles for end of driving (EOD) and beginning of restrike (BOR). The results are presented in table 5.16. The quakes were again normalized with the recommended values, $D/120$. Significantly, if the EOD data are to be used for the classification, all sites (except perhaps Apalachicola) would be classified as large quake sites. For all except the Portland site, the BOR toe quakes were smaller than the EOD toe quake; this had been observed in other dynamic test results by the authors.

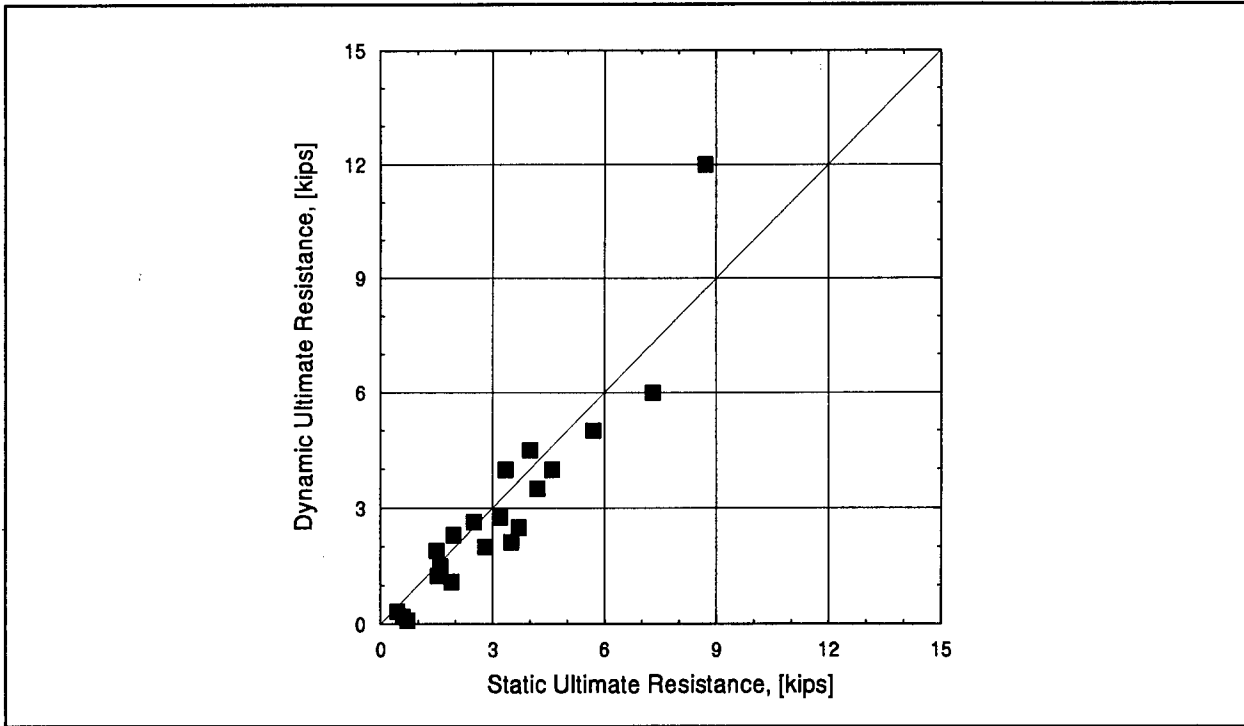


Figure 5.19(a): Comparison Between Ultimate Toe Resistance from Static Compression Tests and Dynamic Analyses

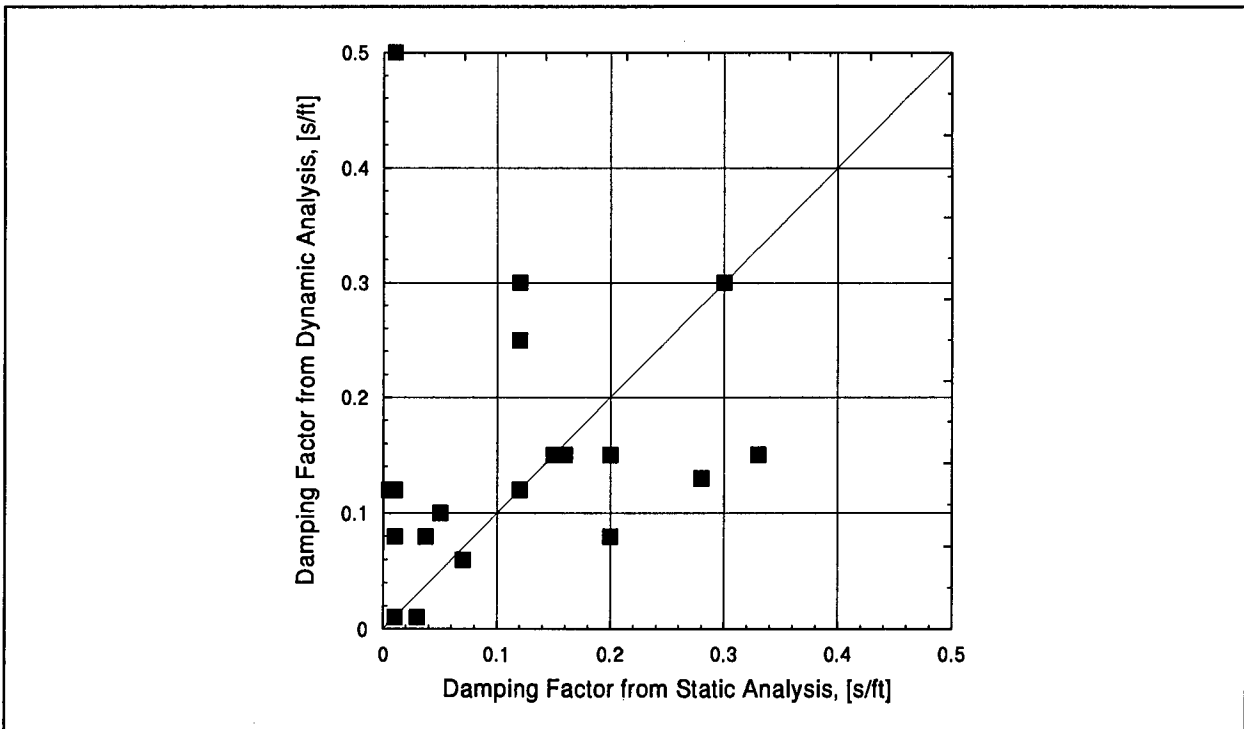


Figure 5.19(b): Comparison of Toe Damping Factors from "Static" and "Dynamic" Analyses for Static $R_u >$ Dynamic R_u

Table 5.15: Comparison of Toe Quakes from Modified SPT Compression Tests (Flat End Tip)							
Site	Depth [ft]	SPT Toe Quake		Normalized with D/120		Normalized with Average Quake	
		Static [in]	Dynamic [in]	Static	Dynamic	Static	Dynamic
	St. Mary	105	0.086	0.025	4.13	1.20	0.72
Portland	54	0.174	0.186	8.37	8.94	1.46	1.27
CD 21	71	0.080	0.023	3.85	1.11	0.67	0.16
White City, TP3	32	0.150	0.270	7.21	12.98	1.26	1.85
	35	0.160	0.270	7.69	12.98	1.34	1.85
Apalachicola	89	0.065	0.100	3.13	4.81	0.55	0.68
Average:		0.119	0.146				

Notes: 1 in = 25.4 mm; 1 ft = 0.305 m; D = 2.5 in (64 mm) = diameter of an oversized tip.

Table 5.16: Comparison of Full-Scale Pile Toe Quakes from CAPWAP Results				
Site	Pile Toe Quake, [in]		Normalized with D/120	
	EOD	BOR	EOD	BOR
St. Mary	0.51	0.16	5.10	1.60
Portland	0.40	1.00	2.67	6.67
CD 17	0.41	0.20	2.05	1.00
CD 21	0.42	0.20	2.10	1.00
White City, TP3	0.40	0.30	2.00	1.50
Apalachicola	0.25	0.17	1.25	0.85

Note: 1 in = 25.4 mm; D = diameter of the full-scale pile.

5.2.10 Shaft Soil Model Studies

The GRLWEAP study demonstrated good agreement between measured and calculated velocities and forces using Smith's shaft resistance model. The measured and computed blow counts were also in good agreement when soil parameters from the so-called "static" analysis were used. For example, the measured and computed blow counts for St. Mary at 65 ft (19.8 m) presented in figure 5.16, were both 35 blows/ft (115 blows/m). For the Apalachicola site at 75 ft (22.9 m) presented in figure 5.17, the measured and computed blow counts were 7 and 8 blows/ft (23 and 26 blows/m), respectively. The calculated soil damping factors for the St. Mary and Apalachicola sites were 0.18 and 0.20 s/ft (0.59 and 0.66 s/m) for clayey sand, which were close to the recommendations in the GRLWEAP manual. The adequacy of the Smith shaft soil model can be further demonstrated by plotting the dynamic force *versus* the dynamic displacement records together with the static load *versus* displacement curve as shown in figure 5.20. Obviously, after the major dynamic effect dies out, the static portion follows the static load *versus* displacement curve. These comparisons are extremely instructive and indicate how dynamic records can be very simply evaluated for static and dynamic model parameters.

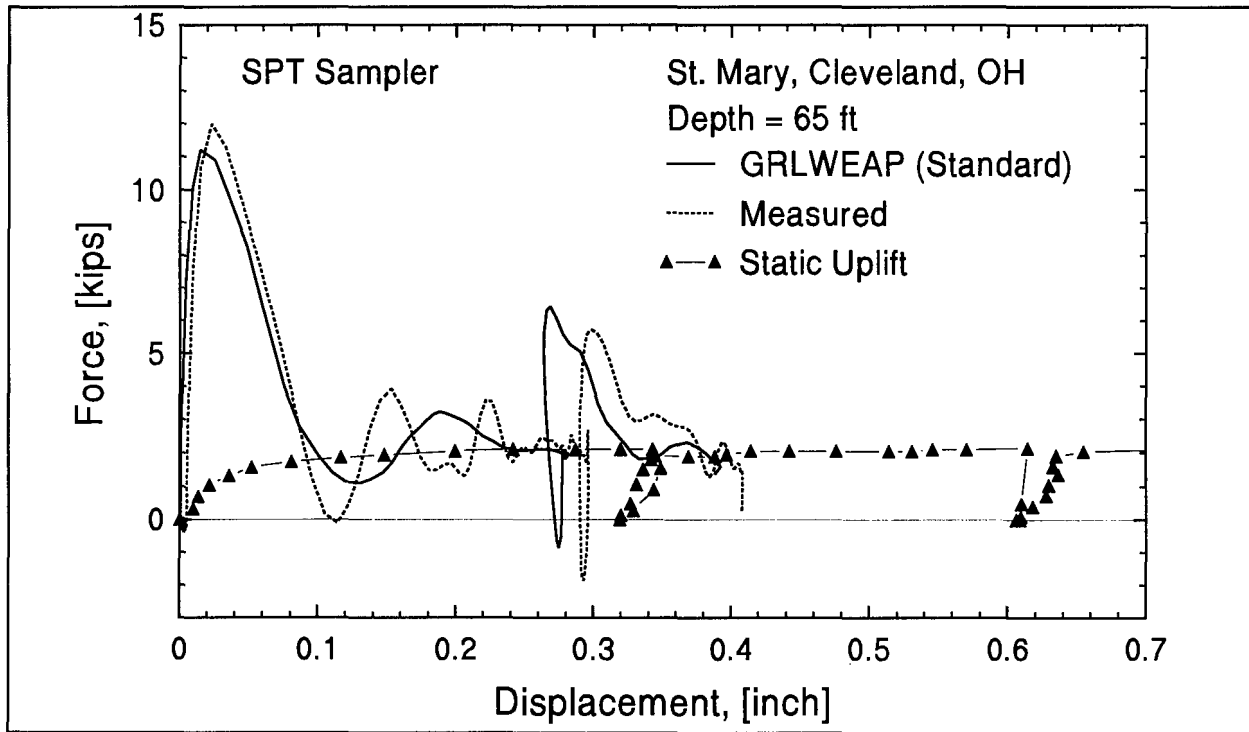


Figure 5.20: Measured and GRLWEAP Computed Dynamic Force vs Dynamic Displacement, and Static Force vs Displacement; (For SPT Sampler at St. Mary 65 ft or 19.8 m)

5.2.11 Toe Soil Model Studies

The results from the above study suggest that some modification to Smith's toe soil model should be further investigated. For example, from the SPT compression test results, especially for those identified as large quake sites, the soil resistance indicated significant strain hardening which was not represented by Smith's elastic, perfectly plastic model. Such elasto-plastic behavior was successfully modeled by a hyperbola defined by two quake parameters, one defining the initial slope of the load-set curve and one the point of failure. The unloading stiffness followed the initial slope. In addition to the modification of the static resistance model, a one directional plug and a gap were also included in the soil model. This new soil model was included in GRLWEAP and used for matching the Modified SPT records.

GRLWEAP analyses with the new soil model were performed for all the cases where SPT compression tests were performed with the flat end tip. Table 5.17 presents comparisons between the measured blow counts and the calculated blow counts from standard GRLWEAP, GRLWEAP with Smith's soil constant from "static" analysis (see section 5.2.7), and GRLWEAP with new soil models. The results presented in table 5.17 indicate that the standard GRLWEAP gives an adequate prediction at the St. Mary and C&D 21 sites. At the Apalachicola site, the disagreement between measured and computed blow count is believed to be caused by a sudden change in soil layer as discussed in section 5.2.7. Disagreement between blow counts had been anticipated for Portland and White City which had been identified as large quake sites. The static and dynamic Modified SPT data indicated that the soil showed a significant strain hardening effects which were not modeled by the standard GRLWEAP.

The above observations were also supported by the comparison between the measured and GRLWEAP calculated dynamic force *versus* dynamic displacement plots, and also with the static load *versus* displacement plot, as shown in figures 5.21 and 5.22 for St. Mary and White City, respectively. Figure 5.21 shows that Smith's toe soil model is adequate for the St. Mary site. However, for the large toe quake site at White City, the hyperbolic behavior is clearly evident and, if modeled, leads to a very good match in figure 5.22.

Table 5.17: GRLWEAP Study of New Toe Soil Models on SPT Flat End Tip						
Site	Depth [ft]	Blow Counts, [blows/ft]				Soil Type
		Measured	Standard GRLWEAP	GRLWEAP "static" *	New Models	
St. Mary	105	66	73	72	72	CL
Portland	54	80	67	182	97	SP-SM
C&D 21	71	18	22	26	19	SM
White City, TP3	32	30	42	95	48	Sand to SM
White City, TP3	35	50	57	46	54	Sand to SM
Apalachicola	89	16	55	50	40	SC to SM

Notes: * Based on soil constants from "static" analysis.
 1 ft = 0.305 m; 1 blow/ft = 3.28 blows/m.

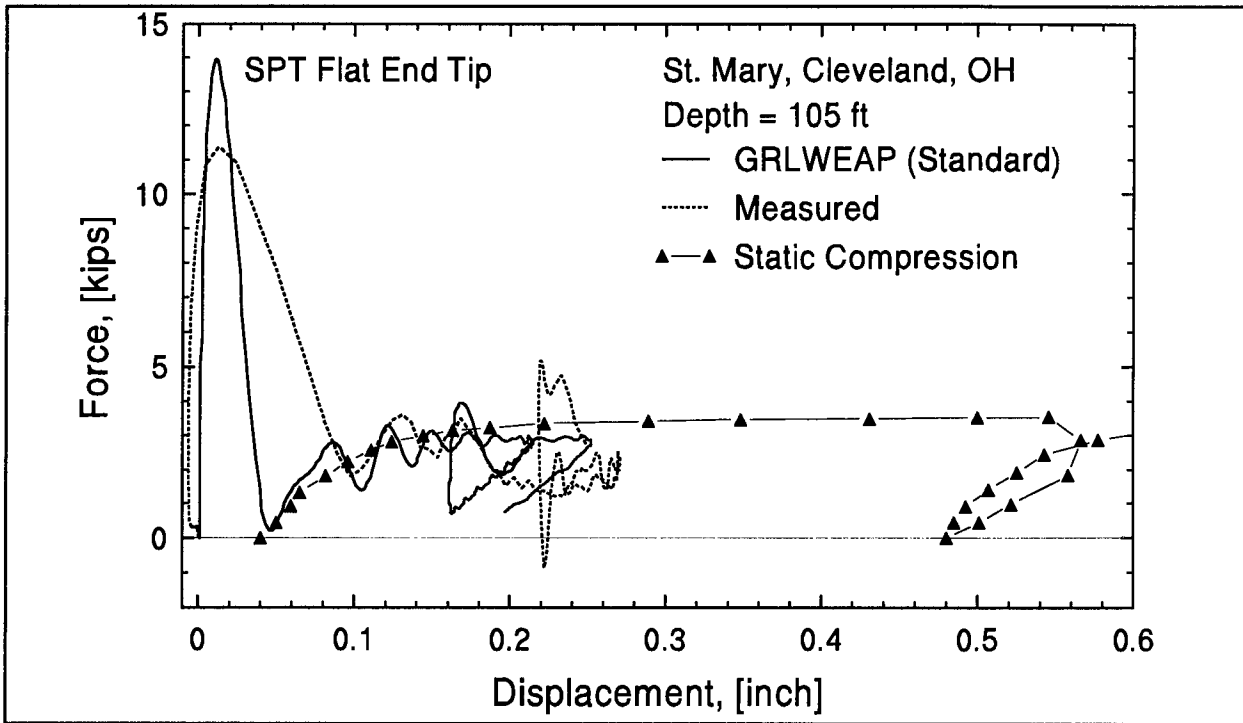


Figure 5.21: Measured and GRLWEAP Computed Dynamic Force vs Dynamic Displacement, and Static Force vs Displacement for Flat End Tip at St. Mary 105 ft or 32 m

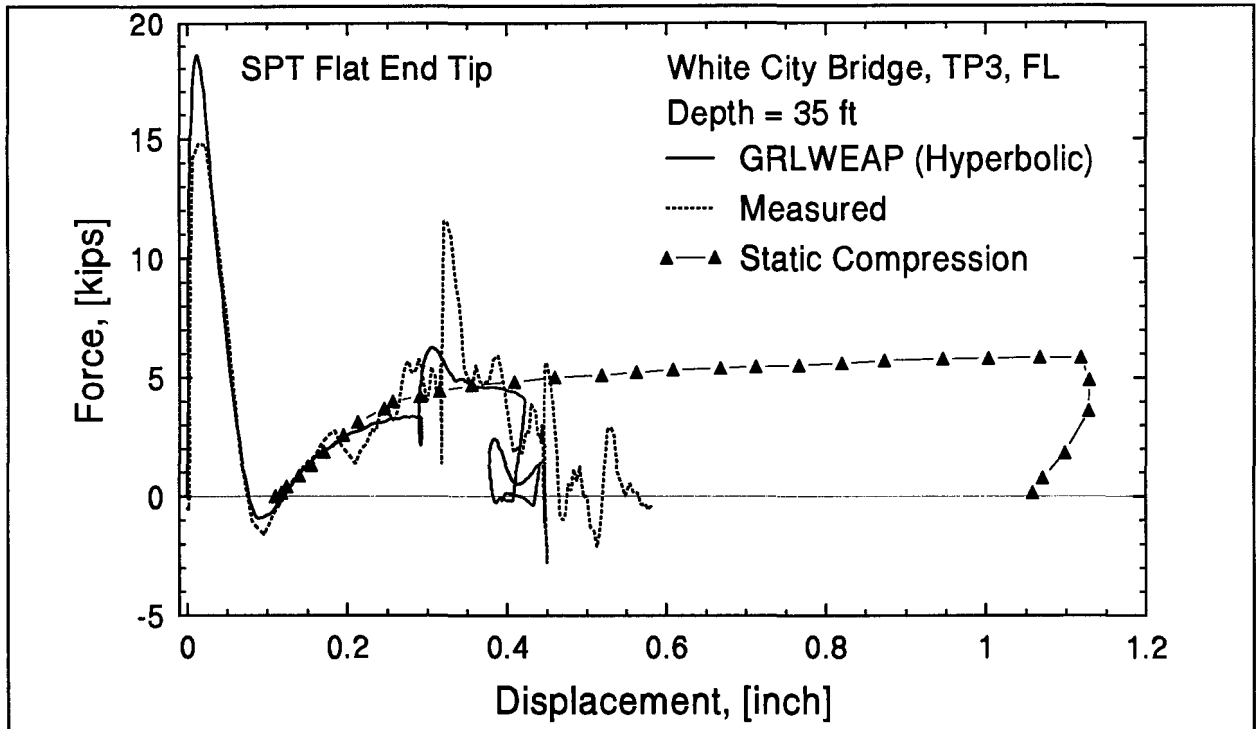


Figure 5.22: Measured and GRLWEAP Computed Dynamic Force vs Dynamic Displacement, and Static Force vs Displacement for Flat End Tip at White City 35 ft or 10.7 m

CHAPTER 6

WAVE EQUATION ANALYSIS OF FULL-SCALE PILES

6.1 INTRODUCTION

As a check on the feasibility and accuracy of the methods developed in chapter 5, wave equation analyses were performed for the full-scale load test piles installed and tested at 6 correlation test sites using GRLWEAP 1993-1. Two types of analyses were conducted.

- (a) Driveability analyses with static capacity values and dynamic soil parameters from the Modified SPT leading to a prediction of blow counts vs depth. These blow counts were compared with the actual driving logs.
- (b) Bearing graph analyses with dynamic soil parameters from the Modified SPT yielding capacity vs blow count. With observed blow counts from end of driving (EOD) and beginning of restriking (BOR), the corresponding EOD and BOR bearing capacities were calculated and compared with static load test results and other bearing capacity predictions.

For driveability analyses by the wave equation, the ultimate bearing capacity must be calculated prior to performing the dynamic analysis. Based on standard geotechnical methods, *e.g.*, SPT N-values, these "static formula calculations" yield unit shaft and toe resistance values, and after introducing pile geometry, the shaft and toe resistances, and the ultimate bearing capacity are resulted.

In the present studies, static measurements on both SPT sampler (uplift, torque) and oversized tip (compression test) allowed for the so-called "Modified SPT STATIC" calculations of unit shaft resistance and end bearing, and then the total Modified SPT STATIC pile capacity. Furthermore, ignoring the Modified SPT STATIC results, the dynamic measurements on the SPT alone were also evaluated for static unit resistance values by the so-called "Modified SPT DYNAMIC" method.

Both Modified SPT capacity calculations, being direct methods for the calculation of unit resistance and then full-scale pile capacity, are described in section 6.2, summarized in tables 6.1 through 6.6, and compared with other full-scale pile capacity prediction methods in table 6.7. These other full-scale pile capacity prediction methods are, of course, the static load test, the static formula calculation, CAPWAP (based on load test pile dynamic measurements), and

standard GRLWEAP (based on standard procedures and parameters plus observed EOD and BOR load test pile blow counts).

For GRLWEAP driveability input, the results from Modified SPT STATIC or DYNAMIC methods were compiled as shown in tables 6.8 through 6.13 for the six correlation sites. Tables 6.14 through 6.19 summarize the respective blow counts calculated by the GRLWEAP driveability analyses.

Tables 6.20 through 6.25 list the calculated bearing graphs for the six sites based on four different methods of soil parameter calculation. Again using load test pile observed blow counts, capacity predictions from these bearing graphs were calculated and compared with load test results in table 6.26. Note that this procedure is an indirect manner in which the Modified SPT results are used to yield capacity values. However, using the wave equation approach together with Modified SPT parameters and including the field observation of blow count make the capacity prediction more realistic than the direct methods described above.

Another study summarized in this chapter was an investigation of the enlarged soil model introduced into GRLWEAP. The results of this study are presented in table 6.27.

6.2 DIRECT PILE CAPACITY CALCULATION FROM MODIFIED SPT

Pile capacities for six correlation sites were evaluated based on the results obtained (a) from the analyses of the Modified SPT data and (b) from SPT N-values of existing soil borings ("existing" soil borings had been performed prior to the full-scale pile installation.) The results from these calculations are presented in tables 6.1 through 6.6. The first column contains the soil types classified from samples collected by the Modified SPT. The next three columns show depth, existing SPT N-values and the N-values from the Modified SPT ("New"). The remaining columns list first the capacity results from the Modified SPT's uplift and compression tests and then capacity values calculated from the Modified SPT's dynamic records. These calculation methods were explained in chapter 5. Pile capacity values calculated in this way are presented as shaft resistance per unit length for both EOD and BOR conditions (the latter from uplift or retaps after setup), and as total toe resistance.

To compute the capacity values in tables 6.1 through 6.6, the soil along the pile shaft was divided into several layers as indicated by existing SPT results. In general, at least one Modified SPT tests was performed in each layer. Shaft capacity values of EOD and BOR were calculated according to Davisson's criterion from the earliest and latest Modified SPT uplift test after sampler driving, respectively. If the soil type did not suggest a potential for setup then no tests after waiting were performed, and BOR capacity values were taken equal to the EOD values.

Capacity values in parentheses in tables 6.1 through 6.6 were directly calculated from the Modified SPT uplift (shaft) or compression (toe) tests, or from the Modified SPT dynamic records. For those penetration for which no Modified SPT results were available, the values in parentheses were prorated based on the ratios of N-values of existing SPT logs. The row at the bottom shows total shaft resistance (from shaft resistance per unit length times depth interval) and bottom toe resistance for full pile penetration.

The toe resistance was calculated from the unit end bearing obtained from the Modified SPT static compression test with the oversized tip using Davisson's failure criterion. At other depths, the unit end bearing was prorated using existing and newly measured SPT N-values. Exceptions were indicated in the footnotes of each table. At some locations, it was also possible to calculate the toe resistance of the sampler and therefore the unit end bearing. The sampler toe resistance was obtained from the difference between static capacity values calculated by dynamic signal matching analyses from blows taken before and after the Modified SPT uplift test. (The test before uplift indicated shaft resistance plus end bearing; the test after uplift only experienced shaft resistance.)

The same procedure for pile capacity calculation was followed for the "Modified SPT DYNAMIC" analysis, except that the ultimate resistance, R_u , was obtained from "dynamic" matching (see chapter 5.2.4) instead of the Modified SPT uplift or compression tests.

The new SPT N-values were, in general, lower than the existing values; and the reason could be attributed to the operator performance. Almost all the SPT driving systems used in this project were operated by Cathead and rope. During the performance of the Modified SPT, the regular SPT sampling was done at a relatively long time intervals allowing the operator to rest and therefore perform better than during the continuous sampling. Of course, it is equally possible that the nature of an instrumented and closely observed test compelled the operator to do as good a job as possible.

A more detailed discussion on the pile capacity evaluation for each site is presented below. Also, comparison between the static load test, static formula calculations, Cone Penetration Test (CPT) if available, GRLWEAP and CAPWAP capacities with the "Modified SPT STATIC" and "Modified SPT DYNAMIC" capacities are presented and summarized in table 6.7. Again, the static pile load test capacity was based on the Davisson's failure criterion. The static calculation was performed according to Vanikar (1986) and using the SPT N-value from either the existing soil borings or the Modified SPT. The CPT capacities were computed using the Koppejan Method described in chapter 5.1.8. The GRLWEAP capacities were based on the standard recommended soil parameters and the field recorded blow counts. CAPWAP capacities were obtained from the original CAPWAP results. Detailed descriptions of the results obtained for the six correlation sites follow.

Table 6.1: Pile Capacity Prediction for St. Mary Site, Cleveland, Ohio; (12x53 H Pile; Static Load Test Capacity 315 kips)									
Soil Type	Depth [ft]	Existing SPT N-Value	New SPT N-Value	Modified SPT STATIC			Modified SPT DYNAMIC		
				Shaft, [kips/ft]		Toe	Shaft, [kips/ft]		Toe
				EOD	BOR	[kips]	EOD	BOR	[kips]
SP-SM	10	3		0.47	0.47	3	0.42	0.42	3
	15	3		0.47	0.47	3	0.47	0.47	3
	20	4		0.63	0.63	4	0.63	0.63	4
	25	8		1.26	1.26	7	1.25	1.25	7
	30	10		1.60	1.60	9	1.60	1.60	9
	35	11		1.73	1.73	10	1.73	1.73	10
	40	6	8	0.94*	0.94	5	0.94	0.94	5
SC	45	30		4.71	4.71	27	4.71	4.71	27
	50	34		5.35	5.35	31	5.35	5.35	31
	55	25		3.93	3.93	23	3.93	3.93	23
	60	42		6.61	6.61	38	6.61	6.61	38
	65	34	35	(5.35)	(5.35)	(31)**	(5.35)	(5.35)	(31)**
CL	70	28		1.27	2.12	29	2.54	4.20	17
	75	26		1.18	1.97	27	2.36	3.90	16
	80	39		1.77	2.96	40	3.54	5.90	23
	85	27		1.23	2.05	28	2.46	4.10	16
	90	10		0.45	0.76	10	0.90	1.50	6
	95	10		0.45	0.76	10	0.90	1.50	6
	100	42	62	(1.91)	(3.18)	43	(3.80)	(6.37)	26
	105	104	101	(2.50)	(4.17)	(103)	(5.56)	(10.60)	(62)
Total:	Pile toe at 105 ft			212	244	103	260	342	62

Notes: * @40 ft, sand blew into the casing. Shaft & toe resistance were calculated from 65 ft using ratio of N-values.
 ** Obtained from dynamic measurements performed before and after static uplift test.
 1 ft = 0.305 m; 1 kip = 4.45 kN; 1 kip/ft = 14.6 kN/m.

Table 6.2: Pile Capacity Prediction for Fore River Bridge, Portland, Maine (Closed End Pipe Pile 18 in by 0.5 in, Concrete Filled; Static Load Test Capacity 350 kips)									
Soil Type	Depth [ft]	Existing SPT N-Value	New SPT N-Value	Modified SPT STATIC			Modified SPT DYNAMIC		
				Shaft, [kips/ft]		Toe	Shaft, [kips/ft]		Toe
				EOD	BOR	[kips]	EOD	BOR	[kips]
	5	18		0.00	--	9	0.00	--	0
	10	3		0.00	--	12	0.00	--	0
	15	18		0.09*	--	15	0.09*	--	22
Fill	20	33	14	(0.18)	--	18	(0.18)	--	(45)
	25	29		0.27	--	21	0.27	--	67
SP-SM	30	34	19	(0.36)	--	24	(0.36)	--	(89)
	35	23		0.45	--	116	0.45	--	170
GP-GM	40	15	165	(0.54)	--	208	(0.54)	--	(252)
	42	23	300**	0.58	--	(208)	0.58	--	(234)
	45	34		0.63	--	191	0.63	--	218
SP-SM	50	32	129	0.72	--	163	0.72	--	183
	51	33		0.74	--	155	0.74	--	172
	53	36		0.77	--	138	0.77	--	148
	54	38	80**	0.79	--	(130)	0.79	--	(137)
	55	39		0.81	--	104	0.81	--	118
	56	39	50**	0.83	--	(78)	0.83	--	(99)
Total:	Pile toe at 51 ft			19		155	19		172
	Pile toe at 53 ft			21		138	21		148

Notes: * From the uplift capacities at 20 ft, 30 ft, and 40 ft and the shaft resistance distribution appeared to be triangular.

** Using the oversized tip instead of the sampler.
1 ft = 0.305 m; 1 kip = 4.45 kN; 1 kip/ft = 14.6 kN/m.

Table 6.3: Pile Capacity Prediction for C&D Canal, Pier 17, Delaware (PSC Pile 24 in Square; Static Load Test Capacity 1146 kips)									
Soil Type	Depth [ft]	Existing SPT N-Value	New SPT N-Value	Modified SPT STATIC			Modified SPT DYNAMIC		
				Shaft, [kips/ft]		Toe	Shaft, [kips/ft]		Toe
				EOD	BOR	[kips]	EOD	BOR	[kips]
SM	4	14	6	(4.28)	7.66	117	(4.38)	6.61	101
	10	6		1.83	3.30	50	1.88	2.84	43
	15	4		1.22	2.20	33	1.25	1.88	29
	20	3		0.92	1.65	25	0.94	1.42	22
	25	0		0.00	0.00	0	0.00	0.00	0
CL	30	11	5	3.16	3.62	92	(2.44)	3.68	79
	35	8		2.30	2.63	67	1.77	2.67	58
SM	40	15	10	(2.75)	4.92	125	3.33	5.03	108
CH	45	16	12	(4.59)	(8.25)	134	(4.59)	(6.93)	115
SM	50	67	38	(7.34)	(5.91)	560	(7.34)	(5.91)	(376)
SM	55	56	34	(19.36)	(22.42)	468	(19.36)	(12.23)	(383)
	60	45	24*	15.56	18.02	(376)	15.56	9.83	(324)
	65	36		12.45	14.42	301	12.45	7.86	259
	66	34		11.75	13.61	284	11.75	7.43	245
Total:	Pile toe at 66 ft			350	453	284	357	323	245

Notes: * Using the cone tip instead of the sampler.
1 ft = 0.305 m; 1 kip = 4.45 kN; 1 kip/ft = 14.6 kN/m.

Table 6.4: Pile Capacity Prediction for C&D Canal, Pier 21, Delaware (PSC Pile 24 in Square; Static Load Test Capacity 1300 kips)									
Soil Type	Depth [ft]	Existing SPT N-Value	New SPT N-Value	Modified SPT STATIC			Modified SPT DYNAMIC		
				Shaft, [kips/ft]		Toe [kips]	Shaft, [kips/ft]		Toe [kips]
				EOD	BOR		EOD	BOR	
	5	0		0.00	0.00	0	0.00	0.00	0
	10	0		0.00	0.00	0	0.00	0.00	0
	15	1		0.83*	0.83	10	0.86	0.86	8
	20	9		7.41*	7.41	90	7.76	7.76	73
	25	6		4.94*	4.94	60	5.17	5.17	49
	30	11		9.05*	9.05	111	9.48	9.48	90
	35	5		4.12*	4.12	50	4.31	4.31	41
SM	40	18	7	(6.83)	(6.83)	181	15.52	15.52	147
	45	19		15.64	15.64	191	16.38	16.38	155
	50	24		19.75	19.75	241	20.70	20.70	196
SM	55	13	17	(10.70)	(10.70)	131	(11.21)	(11.21)	106
	60	15		12.35	12.35	151	12.93	12.93	122
SM	65	13	20	(12.84)	(12.84)	131	(12.23)	(12.23)	106
	70	17		16.80	16.80	171	16.00	16.00	139
	72	19	18**	18.77	18.77	(191)	17.87	17.87	(155)
Total:	Pile toe at 72 ft			600	600	191	657	657	155

Notes: * Calculated from the results obtained at 55 ft.
 ** Using the special tip instead of the sampler.
 1 ft = 0.305 m; 1 kip = 4.45 kN; 1 kip/ft = 14.6 kN/m.

Table 6.5: Pile Capacity Prediction for White City Bridge, TP3, Florida (PSC Pile 24 in Square; Static Load Test Capacity 630 kips)									
Soil Type	Depth [ft]	Existing SPT N-Value	New SPT N-Value	Modified SPT STATIC			Modified SPT DYNAMIC		
				Shaft, [kips/ft]		Toe	Shaft, [kips/ft]		Toe
				EOD	BOR	[kips]	EOD	BOR	[kips]
	3	10		0.00	--	159	0.00	--	138
	6	9		0.00	--	143	0.00	--	124
	9	8		0.00	--	127	0.00	--	111
	12	10		0.00	--	159	0.00	--	138
	15	11		0.00	--	175	0.00	--	152
	18	4		0.00	--	64	0.00	--	55
SM	21	3	3	0.00	--	48	(0.00)*	--	41
	24	12		0.00	--	191	0.00	--	166
	27	7		0.00	--	111	0.00	--	97
SM	29	8	3	0.00	--	127	0.00	--	111
	30	8		0.51	--	127	0.53	--	111
SM	31	16	6	(1.02)	--	255	(1.06)*	--	221
	32	24	30**	1.53	--	(394)	1.59	--	(470)
	33	32		2.04	--	509	2.12	--	470
	35	34	50**	2.17	--	(541)	2.18	--	(470)
	36	35		2.23	--	557	2.32	--	484
SM	37.2	39		2.48	--	621	2.58	--	539
	39	46		2.93	--	732	3.04	--	637
Total:	Pile toe at 37.2 ft			18		621	19		539

Notes: * Dynamic matching gave total capacity. Shaft Resistance was obtained by subtracting the calculated sampler toe resistance from the total capacity.

** Using the special tip instead of the sampler.

1 ft = 0.305 m; 1 kip = 4.45 kN; 1 kip/ft = 14.6 kN/m.

Table 6.6: Pile Capacity Prediction for Apalachicola River Bridge, Florida (PSC Pile 24 in Square; Static Load Test Capacity 960 kips)									
Soil Type	Depth [ft]	Existing SPT N-Value	New SPT N-Value	Modified SPT STATIC			Modified SPT DYNAMIC		
				Shaft, [kips/ft]		Toe [kips]	Shaft, [kips/ft]		Toe [kips]
				EOD	BOR		EOD	BOR	
	8	14		4.28	6.28	278	5.71	23.14	249
	11	14		4.28	6.28	278	5.71	23.14	249
	14	9		2.75	4.03	179	3.67	14.87	160
	17	11		3.36	4.93	219	4.49	18.16	195
SP	20	5	8	(1.53)	(2.24)	99	(2.04)	8.23	89
	23	3		0.92	1.35	60	1.23	4.97	53
SP-SM	26	6	4	1.83	2.69	119	2.44	(9.88)	107
	29	7		2.14	3.14	139	2.86	11.57	124
	32	4		1.22	1.80	80	1.63	6.60	71
	35	3		0.92	1.35	60	1.23	4.97	53
	38	3		0.92	1.35	60	1.23	4.97	53
	41	2		0.61	0.90	40	0.81	3.30	36
	44	4		1.22	1.80	80	1.63	6.60	71
	47	1		0.31	0.45	20	0.41	1.68	18
	50	6		1.83	2.69	119	2.44	9.89	107
	53	7		4.01	5.80	139	3.56	16.00	124
MH	55	8	6	(4.58)	(6.62)	159	(4.07)	(18.3)	142
	59	9		5.16	7.45	179	4.60	20.60	160
	62	9		5.16	7.45	179	4.60	20.60	160
	65	11		6.31	9.10	219	5.60	25.10	195
	68	16		6.85	6.85	318	6.51	16.30	284
	71	16		6.85	6.85	318	6.51	16.30	284
	74	15		6.42	6.42	298	6.11	15.30	266
SM	75	10	7	(4.28)	(4.28)	199	(4.07)	(10.2)	178
	77	6		2.57	2.57	119	2.44	6.10	107
	80	12		5.14	5.14	239	4.88	12.20	213
	83	19		8.13	8.13	378	7.73	7.73	337
	86	14		6.00	6.00	278	5.70	5.70	249
	89	19	16**	8.13	8.13	378	7.73	7.73	337
	90.5	33		14.10	14.10	(656)	13.43	13.43	(586)
Total:	Pile tip at 89 ft			295	372	378	342	1110	337

Notes: ** Using the special tip instead of the sampler.
1 ft = 0.305 m; 1 kip = 4.45 kN; 1 kip/ft = 14.6 kN/m.

Table 6.7: Comparison of Capacity Values from Different Methods								
Site & Pile Type	Method	Status	Shaft [kips]	Toe [kips]	Total [kips]	Total/Davisson	Remarks	
St. Mary TP 5 ID #43 HP12x53	Load Test	--	N/A	N/A	315	--	Davisson	
		--	--	--	330	1.05	Maximum	
	Static Calc.	--	173	41	214	0.68		
		GRLWEAP	EOD	--	--	392	1.24	
	CAPWAP	BOR	--	--	370	1.17		
		EOD	170	124	294	0.93		
		BOR	189	111	300	0.95		
		Modified SPT	EOD	212	103	315	1.00	STATIC
			BOR	244	103	347	1.10	STATIC
		EOD	260	62	322	1.02	DYNAMIC	
BOR	342	62	404	1.28	DYNAMIC			
Portland ID # 24 Closed end Pipe 18 in by 0.5 in (Filled with Concrete)	Load Test	--	60	290	350	--	Davisson	
		--	--	--	400	1.14	Maximum	
	Static Calc.	--	453	194	647	1.85		
		GRLWEAP	EOD	--	--	390	1.11	
	CAPWAP	BOR	--	--	470	1.34		
		EOD	63	260	323	0.92		
		BOR	120	220	340	0.97		
	Modified SPT	EOD	21	138	159	0.45	STATIC	
		BOR	--	--	--	--	STATIC	
		EOD	21	148	169	0.48	DYNAMIC	
BOR		--	--	--	--	DYNAMIC		
C&D Canal Pier 17 ID # 204 PSC 24 in Square	Load Test	--	N/A	N/A	1,150	--	Davisson	
		--	--	--	1,200	1.04	Maximum	
	Static Calc.	--	684	1570	2,254	1.96		
		GRLWEAP	EOD	--	--	635	0.55	
	CAPWAP	BOR	--	--	1,420	1.23		
		EOD	N/A	N/A	N/A	--		
	Modified SPT	BOR	751	294	1,045	0.91		
		EOD	350	284	634	0.55	STATIC	
		BOR	453	284	737	0.64	STATIC	
		EOD	357	245	602	0.52	DYNAMIC	
BOR	323	245	568	0.49	DYNAMIC			

Table 6.7: Comparison of Capacity Values from Different Methods (continued)							
Site & Pile Type	Method	Status	Shaft [kips]	Toe [kips]	Total [kips]	Total/Davisson	Remarks
C&D Canal Pier 21 ID # 203 PSC 24 in Square	Load Test	--	N/A	N/A	1,300	--	Davisson Maximum
		--	--	--	1,340	1.03	
	Static Calc. GRLWEAP	--	882	120	1,002	0.77	
		EOD	--	--	575	0.44	
	CAPWAP	BOR	--	--	1,700	1.31	
		EOD	N/A	N/A	N/A	--	
	Modified SPT	BOR	755	352	1,107	0.85	STATIC STATIC DYNAMIC DYNAMIC
		EOD	600	191	791	0.61	
		BOR	600	191	791	0.61	
		EOD	657	155	812	0.62	
White City TP3 ID # 62 PSC 24 in Square	Load Test	--	N/A	N/A	630	--	Davisson Maximum
		--	--	--	690	1.10	
	Static Calc. GRLWEAP	--	218	479	697	1.11	
		EOD	--	--	650	1.03	
	CAPWAP	BOR	--	--	680	1.08	
		EOD	202	306	508	0.81	
	Modified SPT	BOR	189	346	535	0.85	STATIC STATIC DYNAMIC DYNAMIC
		EOD	18	620	638	1.01	
		BOR	--	--	--	--	
		EOD	19	539	558	0.89	
Apalachicola ID # 1 PSC 24 in Square	Load Test	--	616	344	958	--	Davisson Maximum
		--	--	--	964	1.01	
	Static Calc. GRLWEAP	--	789	490	1,279	1.34	
		EOD	--	--	1,015	1.06	
	CAPWAP	BOR	--	--	1,320	1.38	
		EOD	183	183	368	0.38	
	CPT Modified SPT	BOR	523	402	925	0.97	STATIC STATIC DYNAMIC DYNAMIC
		--	303	904	1,207	1.26	
		EOD	295	378	673	0.70	
		BOR	372	378	750	0.78	
EOD	342	337	679	0.71			
	BOR	1,110	337	1,447		1.51	

Note: 1 kip = 4.45 kN; 1 in = 25.4 mm.

6.2.1 St. Mary, Cleveland, Ohio

The shaft resistance per unit length, the toe resistance at different depths, the existing and new SPT N-values are presented in table 6.1. The soil was divided into three layers: from the top to 40 ft (12.2 m), from 40 to 65 ft (12.2 to 19.8 m), and from 65 to 105 ft (19.8 to 32.0 m). The Modified SPT test performed at depth 40 ft (12.2 m) would have represented the first layer, but during testing sand blew into the casing rendering the Modified SPT uplift test results at this depth unreliable. Therefore, the shaft resistances for both first and second layer were based on the test results obtained at 65 ft (19.8 m). The shaft resistance for the third layer was based on the test results performed at 100 ft (30.5 m). Since the pile was an H-section, the shaft resistance was assumed to be acting along the flanges only, *i.e.*, only 2 ft² (0.61 m²) area per foot (per m) pile length was considered.

At this site, only one Modified SPT compression test was performed near the pile toe at depth of 105 ft (32 m). The compression test results from this depth was used to calculate the unit end bearing at depth 105 ft and, by prorating based on the existing SPT N-values, at other depths in the third layer. From the Modified SPT test performed at 65 ft (19.8 m), it was possible to calculate the unit end bearing from the sampler dynamic capacities by analyzing the dynamic records taken before and after the Modified SPT uplift test. This unit end bearing was then used to calculate the toe resistance at different depths in the top two layers.

The "Modified SPT STATIC" capacity at EOD was 315 kips (1,399 kN) which consisted of 211 kips (937 kN) shaft resistance and 104 kips (462 kN) toe resistance. If the Modified SPT uplift test result taken after a waiting period was used, the "Modified SPT STATIC" capacity at BOR would be 347 kips (1,541 kN) with 244 kips (1,083 kN) shaft resistance and 103 kips (457 kN) toe resistance. The "Modified SPT STATIC" capacity at BOR was 10 percent higher than the static load test result, which might be due to the fact that the setup factor, obtained from the test at 100 ft (30.5 m), was used throughout the third layer. Applying this setup factor to the entire third layer may probably not have been correct, particularly since CAPWAP showed very little gain of capacity due to soil setup.

6.2.2 Fore River Bridge, Portland, Maine

The unit toe resistance from the Modified SPT compression tests at depths of 42, 54, and 56 ft (12.8, 16.5, and 17.1 m) showed a decreasing trend while the existing SPT N-values were increasing. This contradiction leads to the conclusion that the existing SPT N-value could not be used to calculate reliably the shaft resistance distribution. Therefore, the shaft resistance distribution was based on the new SPT N-values, and the results from the Modified SPT uplift and compression tests. The calculated capacity values are shown in table 6.2.

The Modified SPT uplift tests performed at depths 20, 30, and 40 ft (6.1, 9.1, and 12.2 m) indicated a triangular shaft resistance distribution. The shaft resistances from the uplift tests were generally very low. The Modified SPT compression tests were performed at three locations only, therefore the toe resistance at other depths were calculated by prorating according to the new SPT N-values. Only one soil layer was used for pile capacity calculation.

Dynamic matching gave much higher ultimate resistances than the uplift resistances. The differences were attributed to the toe resistance of the sampler. Therefore, for the "Modified SPT DYNAMIC" analysis, the shaft resistance was assumed to be the same as that measured from uplift tests, and the toe resistance calculation was based on the unit end bearing obtained from the sampler toe resistance.

Modified SPT uplift testing after a waiting period was attempted at this site, but no apparent setup was measured. Restrike tests were not performed on the SPT sampler at this essentially sandy site. The calculated shaft resistance based on the uplift test results was 21 kips (93 kN); the toe resistance was 138 kips (613 kN) and 148 kips (657 kN) using the "Modified SPT STATIC" and "Modified SPT DYNAMIC" analysis, respectively.

6.2.3 C&D Canal, Pier 17, Delaware

At this site, a total of five Modified SPT uplift tests and one compression test were performed. The uplift tests were performed at depths of 14, 50, 55, 60, and 65 ft (4.3, 15.2, 16.8, 18.3, and 19.8 m) and the cone tip compression test at 70 ft (21.3 m). In addition, a Modified SPT was also performed at 40 ft (12.2 m) but without an uplift test. The ground surface elevation at the time when the Modified SPT tests were conducted was reportedly about 10 ft (3.05 m) higher than the original ground surface elevation. Therefore, the depths where the Modified SPT tests were performed corresponded to pile penetration depths of 4, 40, 45, 50, 55, and 60 ft (1.2, 12.2, 13.7, 15.2, 16.8, and 18.3 m), respectively. These depths will be used in the following discussion. For analysis (table 6.3), the soil along the pile shaft was divided into three layers. The first layer extended from grade to 25 ft (7.6 m), the second layer ended at 45 ft (13.7 m), and the last layer stops at 66 ft (20.1 m).

The EOD "Modified SPT STATIC" shaft resistance calculation was based on the uplift results at 4 ft (1.2 m) penetration in the first layer, 40 ft (12.2 m) in the second layer, and 55 ft (16.8 m) in the third layer. The toe resistance at different depths were calculated from the compression test results at 60 ft (18.3 m). The EOD "Modified SPT STATIC" shaft and toe resistances were 350 kips (1,554 kN) and 284 kips (1,261 kN), respectively.

Setup tests were performed at 45, 50 and 55 ft (13.7, 15.2 and 16.8 m) depths. The setup test (14 h waiting period) at 45 ft (13.7 m) gave a gain factor of 1.8. This factor was then applied

to the top two layers because their uplift load curves behaved similarly. The test at 50 ft (15.2 m) showed a loss rather than gain over a 1-h waiting period. The setup factor from 55 ft (16.8 m) was 1.16 after a waiting period of 2 h. This factor was then applied to the rest of the third layer. Therefore, the BOR "Modified SPT STATIC" shaft resistance amounted to 453 kips (2,016 kN).

For "Modified SPT DYNAMIC" analysis, the shaft resistance distribution was calculated based on the dynamic results at 4, 30, 45, 50 and 55 ft (1.2, 9.1, 13.7, 15.2 and 16.8 m). At depths 50 and 55 ft (15.2 and 16.8 m), the ultimate resistances, R_u , calculated from "dynamic" analysis using the sampler end of driving records were higher than the uplift resistances. These differences were attributed to the sampler toe resistance. The toe resistances at these two depths were, therefore, calculated from these sampler records. At depths 4 and 45 ft (1.2 and 13.7 m), the R_u values from "dynamic" analysis showed a good agreement with the uplift results. Thus, the sampler toe resistance at these depths might have been negligible, and the toe resistance was, therefore, calculated from the "dynamic" analysis results at 60 ft (18.3 m) using the records from end of tip driving, and before the Modified SPT compression test was performed. The shaft resistance calculated using "Modified SPT DYNAMIC" analysis at EOD and BOR was 357 kips (1,585 kN) and 323 kips (1,434 kN), respectively. The reduction in calculated shaft resistance was due to a loss of resistance (19 percent) at 50 ft (15.2 m) and (37 percent) at 55 ft (16.8 m). Both the "dynamic" analysis and the static uplift test indicated a loss of resistance at 50 ft. The "dynamic" analysis showed a loss of resistance even though the static uplift test indicated setup at 55 ft. This loss may be due to the large uplift displacement or soil disturbance during dismantling of the static SPT load reaction frame.

6.2.4 C&D Canal, Pier 21, Delaware

The soil was divided into two layers, with the interface at 60 ft (18.3 m). Two uplift tests were conducted in the first layer and one test in the second layer. The compression test was performed near the load test pile toe at a depth of 71 ft (21.6 m). The shaft resistance distribution in the first layer was calculated based on the results obtained at 55 ft (16.8 m), except for the 40-ft (12.2-m) location where another uplift result was available. The results obtained at 40 ft (12.2 m) were not used in the shaft resistance distribution because of the big difference between the existing (SPT N-value=18) and new (SPT N-value=7) at that depth. Since the calculated distribution was based on the existing SPT N-values, the results would have been greatly affected. The results are presented in table 6.4.

The capacity obtained from the "Modified SPT STATIC" analysis at EOD included 600 kips (2,664 kN) shaft and 191 kips (848 kN) toe resistance. Tests with waiting times at this site did not indicate soil setup gains. Therefore, EOD and BOR capacity values are identical.

The "Modified SPT DYNAMIC" analysis indicated a somewhat higher shaft resistance than the "Modified SPT STATIC" analysis, but a lower toe resistance. Furthermore, unlike at the previous site, the estimated CAPWAP toe resistance (352 kips or 1,563 kN) is much higher than that calculated from the static compression test results.

6.2.5 White City Bridge, TP3, Florida

Two uplift tests and two compression tests were performed at this site. The first uplift test at 21 ft (6.4 m) indicated no measurable resistance; the second uplift test, conducted at 31 ft (9.5 m), was therefore used to calculate the shaft resistance distribution throughout the shaft length (table 6.3). The soil was divided into two layers; the top layer was 29 ft or 8.8 m (no shaft resistance), and the second layer from 30 to 39 ft (9.1 to 11.9 m). The compression tests were performed at 32 and 35 ft (9.8 and 10.7 m). The pile toe resistance calculated from these compression tests were proportionally related to the corresponding SPT N-values. The compression test results at 35 ft (10.7 m) were used as presented in table 6.5. No setup tests were performed at this site as the soil type did not indicate any potential for setup. The "Modified SPT STATIC" analysis yielded 18 kips (80 kN) shaft resistance and 621 kips (2,757 kN) toe resistance.

For the "Modified SPT DYNAMIC" analysis, the toe resistance at different depths was calculated based on the compression test at 35 ft (10.7 m). The shaft resistance in the top layer was found to be negligibly small by uplift testing; and thus, the ultimate resistance, R_u , from dynamic matching before uplift was all toe resistance. The results from the "dynamic" analysis at 31 ft (9.5 m) was used to calculate the shaft resistance distribution in the bottom layer. The unit toe resistance calculated from "dynamic" analysis at 35 ft (10.7 m) was used to calculate, by prorating according to the existing SPT N-values, the unit toe resistance at other depths. The "Modified SPT DYNAMIC" capacity amounted to approximately 19 kips (84.4 kN) shaft resistance and 539 kips (2,393 kN) toe resistance. The total predicted capacity of 558 kips (2,478 kN) is lower than both the "Modified SPT STATIC" capacity (639 kips or 2,837 kN) and the static load test capacity (630 kips or 2,797 kN). However, it compares very well with the capacity calculated by CAPWAP (535 kips or 2,375 kN).

6.2.6 Apalachicola River Bridge, Florida

At this site, four uplift tests including three setup tests were performed, in addition to a compression test near the pile toe. The soil was divided into three layers; from grade to 50 ft (15.2 m), from 50 to 65 ft (15.2 to 19.8 m) and below 65 ft (19.8 m). Calculations for the shaft resistance distribution in the first layer were based on the results obtained at 20 ft (6.1 m), for the second layer at 55 ft (16.8 m), and for the third layer at 75 ft (22.9 m). Calculations for toe resistance at different depths were based on the results obtained at 89 ft (27.1 m). The static

compression test conducted at 89 ft (27.2 m) showed a high ultimate resistance, (5.7 kips or 25 kN) considering the low SPT N-value of 19. However, the existing SPT N-values showed an increase to 33 which occurred just below the 89 ft (27.1 m) depth. It was, therefore, assumed that the compression test was conducted in the harder layer with N-value of 33.

The capacity calculations are presented in table 6.6. The capacity calculated by the "Modified SPT STATIC" analysis at EOD was 295 kips (1,310 kN) shaft resistance and 378 kips (1,678 kN) toe resistance. The "Modified SPT DYNAMIC" capacity at EOD included 342 kips (1,522 kN) shaft resistance and 337 kips (1,500 kN) toe resistance. The "Modified SPT DYNAMIC" analysis at BOR yielded a rather high setup factor of 3.25. As discussed in chapter 5, this apparent increase in resistance could have been caused by an increase in damping rather than static resistance.

6.2.7 Correlation of Directly Calculated Capacity Values

Table 6.7 summarizes capacity predictions from a variety of methods. The static formula calculations and the Modified SPT methods are both direct methods using in-situ test results to first calculate unit resistance and then pile capacity. CAPWAP and standard GRLWEAP predictions rely on dynamic information taken on the test piles themselves and therefore fall into a different category of capacity prediction method.

The total calculated capacity was divided by the associated Davisson capacity yielding the Total/Davisson ratio of table 6.7. Modified STATIC SPT predicted capacities roughly vary between 0.45 and 1.10 times the Davisson load test capacity. For the Modified SPT DYNAMIC results these ratios are generally higher (0.48 to 1.51). Both methods yielded more conservative capacity ratios than static formula calculations (0.68 to 1.96). In part, the relatively large variations can be attributed to the fact that Modified SPT measurements were taken only on a few points and that prorating of existing N-values was used for interpolation.

Compared with the static load test, the Modified SPT STATIC method (BOR if available) predicted total capacity well (within 10 percent) for St. Mary and White City. It underpredicted by up to 55 percent for all other sites. Shaft and toe resistance values from telltales, available for two cases, indicate that the Modified SPT underpredicted toe capacity for Portland and shaft capacity for Apalachicola. For the remaining four sites, CAPWAP analyses may be used for shaft and toe resistance correlations. However, no clear pattern could be established.

The Modified SPT DYNAMIC methods generally performed similar to and with similar accuracy as the STATIC one. However, because of the limited amount of data available, no clear assessment of the accuracy of these direct capacity calculation methods can be made. Scaling or other empirical factors should reasonably be expected when predicting the full-scale pile

capacity from a small sampler or pile tip. However, the trends indicated by the present data do not allow for any generally applicable conclusions.

6.3 DYNAMIC SOIL PARAMETER CALCULATION

For wave equation analyses, dynamic soil resistance parameters (damping and quake) must be assigned for pile shaft and toe. The assessment of these dynamic soil parameters by the Modified SPT method was one of the main reasons for performing the research presented here. As pointed out in chapter 5, a variety of approaches were conceived for the calculation of quake and damping values from Modified SPT results. Each of these methods must be paired with a direct or indirect approach for the calculation of static resistance distribution (required for bearing graph analysis) or resistance forces (for driveability analysis). In summary, the following three STATIC Methods were tried. A summary of these methods is also presented at the end of this chapter together with results in table 6.26b.

The SPT-ST (SPT static) method utilized the uplift or compression test static capacity values for resistance distribution or resistance forces. Its damping factors were determined by signal matching with fixed static resistance values, quake and ultimate resistance, from associated uplift or compression tests. Quakes were also determined from the Modified SPT static tests.

The MDF-ST (modified static) method was identical to SPT-ST except that shaft damping factors were chosen according to GRLWEAP recommendations. With an exception of Portland, a low toe damping factor was used because the toe damping factor from dynamic signal matching was unusually low.

The STD-ST (standard and static) method was identical to SPT-ST except that all damping and quake values were set according to standard GRLWEAP recommendations.

The SPT-DYN (SPT dynamic) method determined all static and dynamic parameters from signal matching. Neither uplift, compression test, or any other static information was used.

For St. Mary and White City, the directly determined capacity values (section 6.2) agreed reasonably well with the pile load tests. Thus, no further input parameter combinations were tried for these two sites. However, for the other four sites, the knowledge of the pile load test results was utilized in an attempt of improving the wave equation predictions and/or dynamic parameters leading to the following additional two methods.

The **MDF-Cap SPT** method used dynamic parameters (damping and quake) as in SPT-ST (utilizing Modified SPT static results plus signal matching) except that the static resistance forces/distributions were factored based on pile load test information.

The **MDF-Cap STD** method was identical to STD-ST (standard GRLWEAP dynamic parameters) except that the static resistance forces/distributions were factored using pile load test information as for MDF-Cap SPT.

A discussion of driveability analyses and bearing graph generation for the six correlation sites follows in the next two sections.

6.4 DRIVEABILITY ANALYSES

For all driveability analyses, the hammer efficiency input for GRLWEAP was adjusted such that the calculated transferred energy matched the measured transferred energy recorded in the field by the PDA during pile installation. The soil resistance distribution and the Smith soil constants for each site have been presented in tables 6.8 to 6.13. The STATIC tables, (a), correspond to SPT-ST, the DYNAMIC tables, (b), represent SPT-DYN. The GRLWEAP "Sens." input value at the last column of each table was left at the 1.0 default for all analyses.

The complete information about each correlation site, including the pile description, pile driving record, the existing soil information, hammer and driving systems, and the static load test results are presented in appendix F. The driveability graph and the summary tables generated by GRLWEAP for each site are presented in appendix A.

6.4.1 St. Mary, Cleveland, Ohio

The test pile driven at the St. Mary site was an HP12x53, H section pile with a total length of 121 ft (37 m). It was driven to a final penetration of 105 ft (32 m). The hammer was a Vulcan 506 which had a manufacturer rated maximum energy of 32.5 kip-ft (44.04 kN-m). The helmet weight was 0.75 kip (3.34 kN), and the hammer cushion type was not available but was assumed to be 3 in (76 mm) of Hamortex. The soil resistance distribution values and the Smith soil constants are presented in table 6.8.

Comparison between the measured blow counts and the computed blow counts from four analysis are presented in figure 6.1; also these blow counts are tabulated in table 6.14. The four methods (STD-ST, MDF-ST, SPT-ST, and SPT-DYN) gave reasonable and similar blow count predictions to 100 ft (30.5 m) penetration. A significant difference in blow count was indicated

Table 6.8: Soil Resistance Distribution and Smith Soil Constants for St. Mary, OH

Depth (ft)	Skin Friction (k/ft)	End Bearing (kips)	Skin Quake (in)	Toe Quake (in)	Skin Damping (s/ft)	Toe Damping (s/ft)	Sens.
10.00	.470	3.000	.070	.070	.130	.005	1.000
15.00	.470	3.000	.070	.070	.130	.005	1.000
20.00	.630	4.000	.070	.070	.130	.005	1.000
25.00	1.260	7.000	.070	.070	.130	.005	1.000
30.00	1.600	9.000	.070	.070	.130	.005	1.000
35.00	1.730	10.000	.070	.070	.130	.005	1.000
40.00	.940	5.000	.070	.070	.130	.005	1.000
45.00	4.710	27.000	.030	.030	.120	.005	1.000
50.00	5.340	31.000	.030	.030	.120	.005	1.000
55.00	3.930	23.000	.030	.030	.120	.005	1.000
60.00	6.600	38.000	.030	.030	.120	.005	1.000
65.00	5.340	31.000	.030	.030	.120	.005	1.000
70.00	1.270	29.000	.023	.023	.150	.005	1.000
75.00	1.180	27.000	.023	.023	.150	.005	1.000
80.00	1.770	40.000	.023	.023	.150	.005	1.000
85.00	1.230	28.000	.023	.023	.150	.005	1.000
90.00	.450	10.000	.023	.023	.150	.005	1.000
95.00	.450	10.000	.023	.023	.150	.005	1.000
100.00	1.900	43.000	.023	.023	.150	.005	1.000
105.00	2.500	103.000	.035	.100	.150	.005	1.000

a) STATICALLY CALCULATED

Depth (ft)	Skin Friction (k/ft)	End Bearing (kips)	Skin Quake (in)	Toe Quake (in)	Skin Damping (s/ft)	Toe Damping (s/ft)	Sens.
10.00	.470	3.000	.070	.070	.130	.120	1.000
15.00	.470	3.000	.070	.070	.130	.120	1.000
20.00	.630	4.000	.070	.070	.130	.120	1.000
25.00	1.260	7.000	.070	.070	.130	.120	1.000
30.00	1.600	9.000	.070	.070	.130	.120	1.000
35.00	1.730	10.000	.070	.070	.130	.120	1.000
40.00	.940	5.000	.070	.070	.130	.120	1.000
45.00	4.710	27.000	.030	.030	.150	.120	1.000
50.00	5.340	31.000	.030	.030	.150	.120	1.000
55.00	3.930	23.000	.030	.030	.150	.120	1.000
60.00	6.600	38.000	.030	.030	.150	.120	1.000
65.00	5.340	31.000	.030	.030	.150	.120	1.000
70.00	2.540	29.000	.020	.020	.150	.120	1.000
75.00	2.360	27.000	.020	.020	.150	.120	1.000
80.00	3.540	40.000	.020	.020	.150	.120	1.000
85.00	2.460	28.000	.020	.020	.150	.120	1.000
90.00	.900	10.000	.020	.020	.150	.120	1.000
95.00	.900	10.000	.020	.020	.150	.120	1.000
100.00	3.800	43.000	.020	.020	.150	.120	1.000
105.00	5.000	62.000	.033	.025	.150	.120	1.000

b) DYNAMICALLY CALCULATED

Note: 1 ft = 0.305 m; 1 kip/ft = 14.6 kN/m; 1 kip = 4.45 kN; 1 in = 25.4 mm; 1 s/ft = 3.28 s/m.

Table 6.9: Soil Resistance Distribution and Smith Soil Constants for Portland, ME

Depth (ft)	Skin Friction (k/ft)	End Bearing (kips)	Skin Quake (in)	Toe Quake (in)	Skin Damping (s/ft)	Toe Damping (s/ft)	Sens.
15.00	.090	15.000	.011	.150	.050	.150	1.000
20.00	.180	18.000	.011	.150	.050	.150	1.000
25.00	.270	21.000	.012	.150	.050	.150	1.000
30.00	.360	24.000	.012	.150	.050	.150	1.000
35.00	.450	116.000	.012	.150	.050	.150	1.000
40.00	.540	208.000	.030	.160	.050	.150	1.000
42.00	.580	208.000	.030	.160	.050	.150	1.000
45.00	.630	191.000	.030	.160	.050	.150	1.000
50.00	.720	163.000	.030	.174	.050	.200	1.000
51.00	.740	155.000	.030	.174	.050	.200	1.000
53.00	.770	138.000	.030	.174	.050	.300	1.000

a) STATICALLY CALCULATED

Depth (ft)	Skin Friction (k/ft)	End Bearing (kips)	Skin Quake (in)	Toe Quake (in)	Skin Damping (s/ft)	Toe Damping (s/ft)	Sens.
15.00	.090	22.000	.011	.130	.050	.150	1.000
20.00	.180	45.000	.011	.130	.050	.150	1.000
25.00	.270	67.000	.012	.130	.050	.150	1.000
30.00	.360	89.000	.012	.130	.050	.150	1.000
35.00	.450	170.000	.020	.130	.050	.150	1.000
40.00	.540	252.000	.030	.130	.050	.150	1.000
42.00	.580	234.000	.030	.120	.050	.150	1.000
45.00	.630	218.000	.030	.120	.050	.200	1.000
50.00	.720	183.000	.030	.186	.050	.300	1.000
51.00	.740	172.000	.030	.186	.050	.300	1.000
53.00	.770	148.000	.030	.186	.050	.300	1.000

b) DYNAMICALLY CALCULATED

Note: 1 ft = 0.305 m; 1 kip/ft = 14.6 kN/m; 1 kip = 4.45 kN; 1 in = 25.4 mm; 1 s/ft = 3.28 s/m.

Table 6.10: Soil Resistance Distribution and Smith Soil Constants for C&D Pier 17, DE

Depth (ft)	Skin Friction (k/ft)	End Bearing (kips)	Skin Quake (in)	Toe Quake (in)	Skin Damping (s/ft)	Toe Damping (s/ft)	Sens.
5.00	4.280	117.000	.010	.010	.170	.037	1.000
10.00	1.830	50.000	.010	.010	.170	.037	1.000
15.00	1.223	34.000	.010	.010	.170	.037	1.000
20.00	.920	25.000	.010	.010	.170	.037	1.000
30.00	2.450	92.000	.013	.013	.400	.037	1.000
35.00	1.780	67.000	.013	.013	.080	.037	1.000
40.00	2.750	125.000	.013	.013	.080	.037	1.000
45.00	4.586	134.000	.030	.030	.400	.037	1.000
50.00	7.340	560.000	.080	.080	.800	.037	1.000
55.00	19.360	468.000	.040	.040	.370	.037	1.000
60.00	15.560	376.000	.040	.040	.370	.037	1.000
65.00	12.440	301.000	.040	.040	.370	.037	1.000
66.00	11.750	284.000	.040	.070	.370	.037	1.000

a) STATICALLY CALCULATED

Depth (ft)	Skin Friction (k/ft)	End Bearing (kips)	Skin Quake (in)	Toe Quake (in)	Skin Damping (s/ft)	Toe Damping (s/ft)	Sens.
5.00	4.380	101.000	.027	.027	.150	.037	1.000
10.00	1.880	43.000	.027	.027	.150	.037	1.000
15.00	1.250	29.000	.027	.027	.150	.037	1.000
20.00	.940	22.000	.027	.027	.150	.037	1.000
30.00	2.440	79.000	.015	.015	.400	.037	1.000
35.00	1.770	58.000	.015	.015	.400	.037	1.000
40.00	3.330	108.000	.013	.013	.080	.037	1.000
45.00	4.590	115.000	.010	.010	.600	.037	1.000
50.00	7.340	376.000	.030	.030	.570	.037	1.000
55.00	19.360	383.000	.040	.040	.200	.037	1.000
60.00	15.560	324.000	.040	.040	.200	.037	1.000
65.00	12.440	259.000	.040	.040	.200	.037	1.000
66.00	11.750	245.000	.040	.050	.200	.037	1.000

b) DYNAMICALLY CALCULATED

Note: 1 ft = 0.305 m; 1 kip/ft = 14.6 kN/m; 1 kip = 4.45 kN; 1 in = 25.4 mm; 1 s/ft = 3.28 s/m.

Table 6.11: Soil Resistance Distribution and Smith Soil Constants for C&D Pier 21, DE

Depth (ft)	Skin Friction (k/ft)	End Bearing (kips)	Skin Quake (in)	Toe Quake (in)	Skin Damping (s/ft)	Toe Damping (s/ft)	Sens.
15.00	.830	10.000	.030	.030	.010	.070	1.000
20.00	7.410	90.000	.030	.030	.010	.070	1.000
25.00	4.940	60.000	.030	.030	.010	.070	1.000
30.00	9.050	111.000	.030	.030	.010	.070	1.000
35.00	4.120	50.000	.030	.030	.010	.070	1.000
40.00	6.830	181.000	.030	.030	.010	.070	1.000
45.00	15.640	191.000	.060	.060	.200	.070	1.000
50.00	19.750	241.000	.060	.060	.200	.070	1.000
55.00	10.700	131.000	.060	.060	.200	.070	1.000
60.00	12.350	151.000	.060	.060	.200	.070	1.000
65.00	12.840	131.000	.033	.033	.001	.070	1.000
70.00	16.800	171.000	.033	.033	.001	.070	1.000
72.00	18.770	191.000	.033	.080	.001	.070	1.000

a) STATICALLY CALCULATED

Depth (ft)	Skin Friction (k/ft)	End Bearing (kips)	Skin Quake (in)	Toe Quake (in)	Skin Damping (s/ft)	Toe Damping (s/ft)	Sens.
15.00	.860	8.000	.030	.030	.010	.060	1.000
20.00	7.760	73.000	.030	.030	.010	.060	1.000
25.00	5.170	49.000	.030	.030	.010	.060	1.000
30.00	9.480	90.000	.030	.030	.010	.060	1.000
35.00	4.310	41.000	.030	.030	.010	.060	1.000
40.00	15.520	147.000	.030	.030	.010	.060	1.000
45.00	16.380	155.000	.060	.060	.200	.060	1.000
50.00	20.700	196.000	.060	.060	.200	.060	1.000
55.00	11.210	106.000	.060	.060	.200	.060	1.000
60.00	12.930	122.000	.060	.060	.200	.060	1.000
65.00	12.230	106.000	.033	.033	.001	.060	1.000
70.00	16.000	139.000	.033	.033	.001	.060	1.000
72.00	17.870	155.000	.033	.080	.001	.060	1.000

b) DYNAMICALLY CALCULATED

Note: 1 ft = 0.305 m; 1 kip/ft = 14.6 kN/m; 1 kip = 4.45 kN; 1 in = 25.4 mm; 1 s/ft = 3.28 s/m.

Table 6.12: Soil Resistance Distribution and Smith Soil Constants for White City, TP3, FL

Depth (ft)	Skin Friction (k/ft)	End Bearing (kips)	Skin Quake (in)	Toe Quake (in)	Skin Damping (s/ft)	Toe Damping (s/ft)	Sens.
30.00	.510	127.000	.100	.160	.100	.010	1.000
33.00	2.040	509.000	.100	.160	.100	.010	1.000
36.00	2.230	557.000	.100	.160	.100	.010	1.000
37.20	2.480	621.000	.100	.160	.100	.010	1.000

a) STATICALLY CALCULATED

Depth (ft)	Skin Friction (k/ft)	End Bearing (kips)	Skin Quake (in)	Toe Quake (in)	Skin Damping (s/ft)	Toe Damping (s/ft)	Sens.
30.00	.530	111.000	.100	.270	.100	.080	1.000
33.00	2.120	470.000	.100	.270	.100	.080	1.000
36.00	2.320	484.000	.100	.270	.100	.080	1.000
37.20	2.580	539.000	.100	.270	.100	.080	1.000

b) DYNAMICALLY CALCULATED

Note: 1 ft = 0.305 m; 1 kip/ft = 14.6 kN/m; 1 kip = 4.45 kN; 1 in = 25.4 mm; 1 s/ft = 3.28 s/m.

Table 6.13: Soil Resistance Distribution and Smith Soil Constants for Apalachicola, FL

Depth (ft)	Skin Friction (k/ft)	End Bearing (kips)	Skin Quake (in)	Toe Quake (in)	Skin Damping (s/ft)	Toe Damping (s/ft)	Sens.
8.00	4.280	277.000	.050	.048	.150	.010	1.000
11.00	4.280	277.000	.050	.048	.150	.010	1.000
14.00	2.752	178.000	.050	.030	.150	.010	1.000
17.00	3.363	220.000	.050	.038	.150	.010	1.000
20.00	1.528	98.000	.050	.017	.150	.010	1.000
23.00	.917	60.000	.050	.010	.150	.010	1.000
26.00	1.834	120.000	.050	.020	.150	.010	1.000
29.00	2.140	140.000	.050	.024	.150	.010	1.000
32.00	1.223	79.000	.050	.014	.150	.010	1.000
35.00	.917	60.000	.050	.010	.150	.010	1.000
38.00	.917	60.000	.050	.010	.150	.010	1.000
41.00	.611	39.000	.050	.010	.150	.010	1.000
44.00	1.223	79.000	.050	.014	.150	.010	1.000
47.00	.306	20.000	.050	.010	.150	.010	1.000
50.00	1.834	120.000	.050	.020	.150	.010	1.000
53.00	4.013	140.000	.010	.024	.200	.010	1.000
56.00	4.586	159.000	.010	.027	.200	.010	1.000
59.00	5.160	178.000	.010	.030	.200	.010	1.000
62.00	5.160	178.000	.010	.030	.200	.010	1.000
65.00	6.306	220.000	.010	.038	.200	.010	1.000
68.00	6.850	318.000	.030	.055	.200	.010	1.000
71.00	6.850	318.000	.030	.055	.200	.010	1.000
74.00	6.420	298.000	.030	.054	.200	.010	1.000
77.00	2.568	120.000	.030	.020	.200	.010	1.000
80.00	5.136	238.000	.030	.041	.200	.010	1.000

a) STATICALLY CALCULATED

Depth (ft)	Skin Friction (k/ft)	End Bearing (kips)	Skin Quake (in)	Toe Quake (in)	Skin Damping (s/ft)	Toe Damping (s/ft)	Sens.
8.00	5.700	249.000	.050	.076	.150	.010	1.000
11.00	5.700	249.000	.050	.076	.150	.010	1.000
14.00	3.670	160.000	.050	.047	.150	.010	1.000
17.00	4.480	196.000	.050	.060	.150	.010	1.000
20.00	2.040	89.000	.050	.027	.150	.010	1.000
23.00	1.220	53.000	.050	.016	.150	.010	1.000
26.00	2.450	107.000	.050	.032	.150	.010	1.000
29.00	2.850	125.000	.050	.038	.150	.010	1.000
32.00	1.630	71.000	.050	.022	.150	.010	1.000
35.00	1.220	53.000	.050	.016	.150	.010	1.000
38.00	1.220	53.000	.050	.016	.150	.010	1.000
41.00	.820	35.000	.050	.016	.150	.010	1.000
44.00	1.630	71.000	.050	.022	.150	.010	1.000
47.00	.410	18.000	.050	.016	.150	.010	1.000
50.00	2.450	107.000	.050	.030	.150	.010	1.000
53.00	3.560	125.000	.010	.038	.250	.010	1.000
56.00	4.070	143.000	.010	.043	.250	.010	1.000
59.00	4.600	160.000	.010	.047	.250	.010	1.000
62.00	4.600	160.000	.010	.047	.250	.010	1.000
65.00	5.600	196.000	.010	.060	.250	.010	1.000
68.00	6.500	285.000	.030	.087	.250	.010	1.000
71.00	6.500	285.000	.030	.087	.250	.010	1.000
74.00	6.100	267.000	.030	.086	.250	.010	1.000
77.00	2.440	107.000	.030	.032	.250	.010	1.000
80.00	4.880	213.000	.030	.063	.250	.010	1.000

b) DYNAMICALLY CALCULATED

Note: 1 ft = 0.305 m; 1 kip/ft = 14.6 kN/m; 1 kip = 4.45 kN; 1 in = 25.4 mm; 1 s/ft = 3.28 s/m.

Table 6.14: Blow Count Comparison for St. Mary, Cleveland, Ohio

Depth [ft]	Blow Count, [BPF]				
	Measured	STD-ST	MDF-ST	SPT-ST	SPT-DYN
10	0	0	0	0	0
15	0	0	0	0	0
20	0	0	0	0	0
25	0	2	2	2	2
30	2	3	3	3	3
35	3	4	3	3	4
40	4	5	4	4	4
45	4	9	7	6	8
50	6	13	11	9	11
55	10	15	13	11	13
60	17	23	18	15	18
65	21	28	23	19	22
70	23	33	26	21	22
75	24	33	27	22	24
80	28	39	31	25	29
85	24	38	30	24	31
90	27	31	26	21	30
95	28	31	26	21	30
100	34	49	36	28	41
105	52	187	73	55	84

Table 6.15: Blow Count Comparison for Fore River Bridge, Portland, Maine

Depth [ft]	Blow Count, [BPF]						
	Measured	STD-ST	MDF-ST	SPT-ST	SPT-DYN	MDF-Cap SPT	MDF-Cap STD
5	4	0	0	0	0	0	0
10	2	0	0	0	0	0	0
15	8	0	0	0	0	0	0
20	12	0	0	0	0	0	0
25	15	0	0	0	2	0	0
30	18	0	0	0	4	2	0
35	22	5	3	5	9	17	17
40	22	12	6	12	15	42	41
42	16	12	6	12	14	42	42
45	13	11	5	11	15	37	36
51	16	9	5	10	14	31	27
53	--	7	4	11	12	34	23

Note: 1 ft = 0.305 m; 1 blow per foot [BPF] = 3.3 blows per m [BPM].

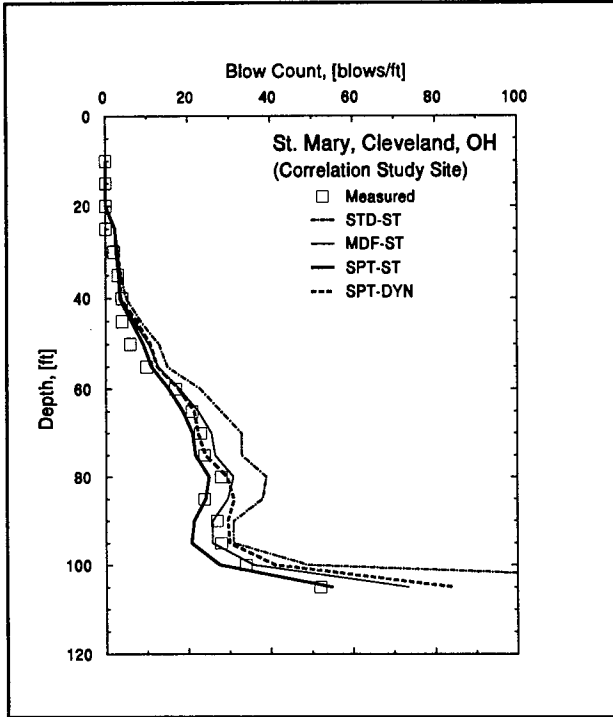


Figure 6.1: Driveability Graphs for St. Mary, Cleveland, OH

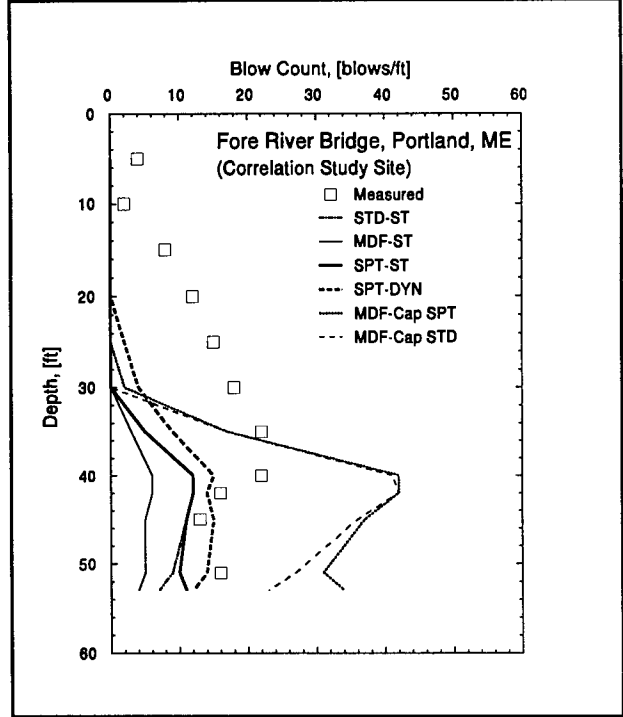


Figure 6.2: Driveability Graphs for Fore River Bridge, Portland, ME

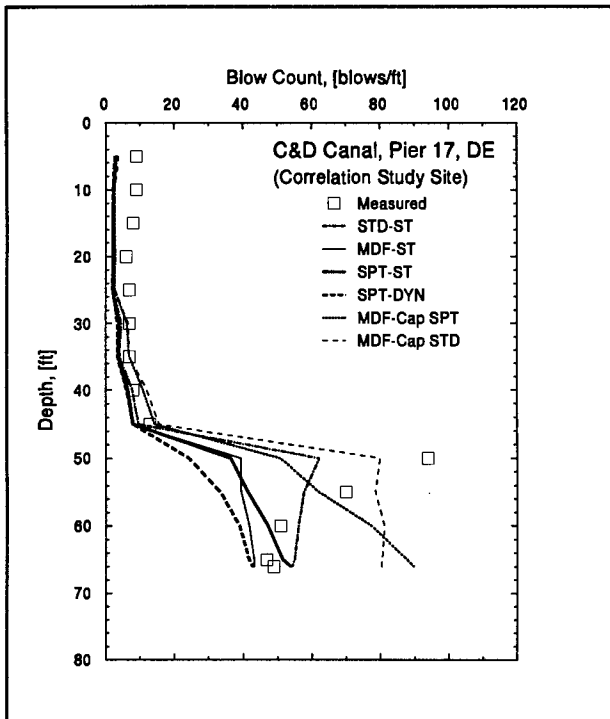


Figure 6.3: Driveability Graphs for C&D Canal, Pier 17, DE

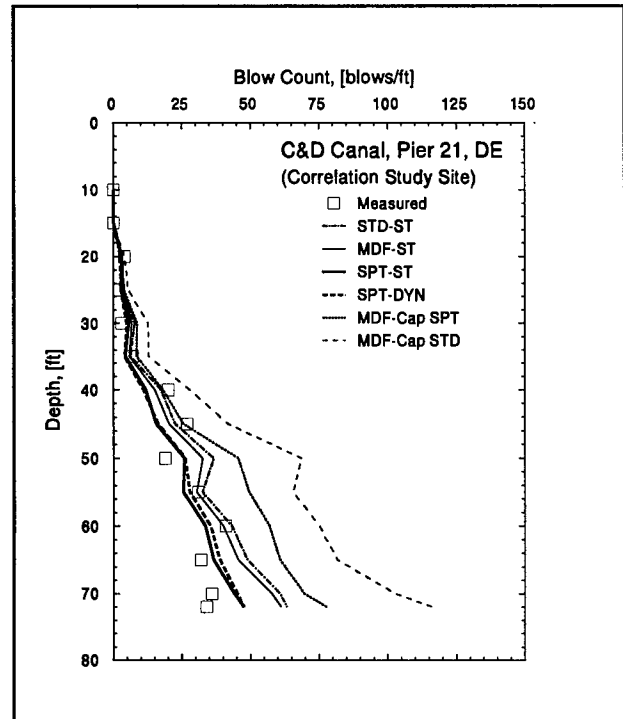


Figure 6.4: Driveability Graphs for C&D Canal, Pier 21, DE

by the last analysis at 105 ft (32 m). This was mainly caused by the relatively high toe resistance, which caused the toe soil constants to have a major effect on the blow count calculation.

Both the STD-ST and SPT-DYN analyses utilized relatively high toe damping values, 0.15 and 0.12 s/ft or 0.49 and 0.39 s/m, respectively, in comparison to the other two methods (0.005 s/ft or 0.02 s/m). This high damping caused a higher calculated blow count. The best blow count match was obtained from SPT-ST. However, even SPT-DYN predicted better than the standard GRLWEAP (STD-ST).

6.4.2 Fore River Bridge, Portland, Maine

The test pile consisted of a closed end steel pipe pile with an outside diameter of 18 in (457 mm), a wall thickness of 0.5 in (12.7 mm) and a total pile length of 59.9 ft (18 m). The pile was driven to a final penetration of 53 ft (16.2 m). The pile driving hammer was a Kobe K-45 with a manufacturer's maximum rated energy of 92.75 kip-ft (125.7 kN-m). The helmet weight was 3.25 kips (14.43 kN), and the hammer cushion consisted of Micarta ($E = 486$ ksi or 162 kPa) which had an area of 576 in² (0.37 m²) and a thickness of 3.5 in (88.9 mm). After installation, the pile was filled with concrete.

Six driveability analyses, listed in table 6.15, were performed. The soil resistance distribution and the Smith soil constants are presented in table 6.9. For the MDF-ST analysis, a toe damping factor of 0.01 s/ft (0.03 s/m) was used. For MDF-Cap STD and MDF-Cap SPT, the toe resistance obtained from SPT-ST was prorated to match the telltale toe resistance obtained from the static load test. A comparison of the blow counts from the six analyses with the measured blow count is presented in figure 6.2 and is also tabulated in table 6.15. The blow count match for the analysis above 42 ft (12.8 m) was poor; from 42 ft to the end of drive SPT-DYN gave the best blow count match. These results suggest that the load test indicated capacity values did not agree with the static resistance encountered during driving.

6.4.3 C&D Canal, Pier 17, Delaware

The test pile driven at this site was a 24-in (610-mm) square prestressed concrete pile with a total length of 75 ft (22.9 m). It was driven to a final penetration of 66 ft (20 m). A Delmag D 46-32 was employed for the pile installation. This hammer has a manufacturer rated energy of 113.16 kip-ft (83.5 kN-m). The helmet weight was 3.57 kips (15.9 kN), and the hammer cushion consisted of 2 in (51 mm) of Conbest. For pile cushioning, 4.5 in (114 mm) oak were used. Six driveability analyses, listed in table 6.16, were performed.

The soil resistance distribution and the Smith soil constants are presented in table 6.10. For the MDF-ST analysis, a toe damping factor of 0.037 s/ft (0.12 s/m) was used. This value was calculated by SPT-ST data at 70 ft or 21.3 m (pile toe depth). The MDF-Cap values were calculated using a correction factor 1.9 on the shaft resistance. The 1.9 factor considered the ratio between pile load test minus SPT-ST, BOR end bearing and SPT-ST indicated BOR shaft resistance. A comparison between the blow counts calculated from the six analyses and the field blow count is presented in figure 6.3 and table 6.16. All six methods gave lower blow counts than the field values at depths above 30 ft (9.1 m), but a reasonable match was achieved between 30 and 45 ft (9.1 and 13.7 m). At 50 and 55 ft (15.2 and 16.8 m), the measured blow counts were much higher than predicted by any method. This high blow count could be due to a high toe resistance at these depths which was missed by the Modified SPT. Indeed, the SPT N-values increased from 12 to 38, from 45 to 50 ft (13.7 to 15.2 m) and 34 at 55 ft (16.8 m). End bearing at these depths were calculated based on 60 ft (18.3 m) Modified SPT compression test, and prorated based on existing SPT N-values. From 60 to 66 ft (18.3 to 20.1 m), all methods gave an acceptable blow count match, except those with the MDF-Cap capacity indicated excessive blow counts. Probably, the best blow count match for the last three analysis depths is the SPT-ST method. However, even SPT-DYN resulted in reasonable final blow count prediction.

6.4.4 C&D Canal, Pier 21, Delaware

The pile size and length, and the driving system at this site were the same as those at Pier 17 except that a 5-in (127-mm) pile cushion was used. The pile was driven to a final penetration of 72 ft (22 m). Again, six driveability analyses were performed and results listed in table 6.17. The soil resistance distribution and the Smith soil constants are presented in table 6.11. For the MDF-ST analysis, a toe damping factor of 0.07 s/ft (0.23 s/m) was used. This value was calculated by SPT-ST at 71 ft or 21.6 m (the depth of pile toe). For MDF-Cap, shaft resistance values were again scaled using a factor 1.9 as determined by and explained for C&D Canal, Pier 17. (For C&D Canal, Pier 21, this factor was actually 1.85, which was considered good agreement between the two piles at the same site.)

A comparison of blow counts from the six analyses and the field blow count is presented in figure 6.4 and tabulated in table 6.17. All except the MDF-Cap methods gave reasonable blow count predictions at depths above 60 ft (18.3 m). From 60 to 72 ft (18.3 to 22.0 m), both STD-ST and MDF-ST overpredicted the blow count compared to measured values. The SPT-ST and SPT-DYN yielded better results though not very accurate. In addition, from 65 to 72 ft (18.3 to 22.0 m), the measured blow count remained constant. However, since the existing SPT N-values did not show a constant behavior calculated blow counts showed a continuously increasing tendency.

Table 6.16: Blow Count Comparison for C&D Canal, Pier 17, Delaware							
Depth [ft]	Blow Count, [BPF]						
	Measured	STD-ST	MDF-ST	SPT-ST	SPT-DYN	MDF-Cap	MDF-Cap
5	9	3	3	3	3	3	4
10	9	2	2	2	2	3	3
15	8	2	2	2	2	3	3
20	6	2	2	2	2	3	3
25	7	2	2	2	2	3	3
30	7	5	4	4	3	6	7
35	7	4	3	4	3	7	7
40	8	8	6	7	6	11	12
45	13	10	8	8	8	14	16
50	94	62	40	37	24	51	80
55	70	58	40	42	33	62	79
60	51	56	42	47	39	77	81
65	47	55	43	52	42	88	80
66	49	54	43	54	43	90	80

Table 6.17: Blow Count Comparison for C&D Canal, Pier 21, Delaware							
Depth [ft]	Blow Count, [BPF]						
	Measured	STD-ST	MDF-ST	SPT-ST	SPT-DYN	MDF-Cap	MDF-Cap
10	0	0	0	0	0	0	0
15	0	0	0	0	0	0	0
20	4	3	3	3	3	3	4
25	2	3	3	3	3	4	5
30	3	8	7	6	5	9	13
35	7	6	6	4	4	8	13
40	20	17	15	12	11	18	28
45	27	23	20	16	16	26	42
50	19	37	33	26	26	46	69
55	31	32	30	26	28	50	66
60	41	43	40	34	35	57	75
65	32	49	46	37	39	61	82
70	36	61	58	44	45	70	103
72	34	63	61	48	47	78	116

Note: 1 ft = 0.305 m; 1 blow per foot [BPF] = 3.3 blows per m [BPM].

6.4.5 White City Bridge, TP3, Florida

The test pile at this site was a 24-in (610-mm) square prestressed concrete pile, with a total length of 50.4 ft (15.4 m). It was driven to a final penetration of 37.2 ft (11.3 m) with a Delmag D 46-02, (rated energy 107.18 kip-ft or 79.1 kN-m). The helmet weight was 6.6 kips (29.3 kN) and the hammer cushion consisted of 3.5 in (89 mm) of Conbest. For pile cushioning, 2.5 in (63.5 mm) of plywood were used. Only three driveability analyses were performed for this site and listed in table 6.18. Because of a good correlation between SPT-ST and load test, no MDF-Cap analyses were performed. Also, for SPT-ST and MDF-ST, the same soil constants resulted and therefore MDF-ST was omitted. The soil resistance distribution and the Smith soil constants are presented in table 6.12.

The blow counts calculated from these three analyses and the measured blow count are presented in figure 6.5 and table 6.18. For depths above 30 ft (9.1 m) penetration, where the toe resistance was relatively small, all methods were in good agreement. From 30 ft (9.1 m) to the end of driving (37.2 ft or 11.3 m), where the toe resistance increased by a factor of about 4, the blow count match deteriorated, probably because of an inaccurate toe quake. It is noteworthy that SPT-DYN performed better than STD-ST (standard GRLWEAP). This site was identified as a large quake site. Further investigation of this site, with the new GRLWEAP soil model, was also performed and discussed in section 6.6.

6.4.6 Apalachicola River Bridge, Florida

The pile at this site was a 24-in (610-mm) square prestressed concrete pile with a 12-in (305-mm) void, and a total length of 93.25 ft (28.4 m). It was driven to a final penetration of 89 ft (27.1 m) with a Vulcan 020 which had a manufacturer's maximum rated energy of 60 kip-ft (44.3 kN-m). The helmet weight was 5.2 kips (23.1 kN), and the hammer cushion consisted of 6 in (152 mm) blue Nylon. For pile cushioning, 6.2 in (157.5 mm) of plywood was used.

Six driveability analyses were performed as per table 6.19 using the soil resistance distribution and the Smith soil constant presented in table 6.13. For the MDF-ST analysis, a toe damping factor of 0.01 s/ft (0.03 s/m) was used. This value was calculated based on dynamic data from 89 ft or 27.1 m (depth of pile toe). The MDF-Cap shaft resistance was calculated by multiplying the SPT-ST shaft resistance with 1.66 which was the ratio of load test (telltale) to SPT-ST shaft resistance. A comparison between the blow counts calculated from the six analyses and the field blow counts is presented in figure 6.6 and in table 6.19.

All except the MDF-Cap methods gave reasonable blow count predictions. Best results were obtained from SPT-ST and SPT-DYN.

Depth [ft]	Blow Count, [BPF]			
	Measured	STD-ST	SPT-ST	SPT-DYN
3	0	7	4	4
6	0	6	3	4
9	4	5	3	3
12	10	7	5	5
15	10	9	5	6
18	8	2	2	2
21	9	2	2	2
24	4	11	7	7
27	8	5	3	3
30	8	6	4	4
33	9	72	36	51
35	30	92	43	55
37.2	112	144	61	82

Depth [ft]	Blow Count, [BPF]						
	Measured	STD-ST	MDF-ST	SPT-ST	SPT-DYN	MDF-Cap	MDF-Cap
10	--	21	14	13	13	14	22
15	--	14	11	10	10	12	17
20	--	7	7	6	7	8	10
25	--	8	7	7	8	10	12
30	9	11	9	9	10	12	15
35	6	6	6	6	7	10	11
40	7	6	6	6	7	10	11
45	10	7	6	7	9	11	12
50	10	13	11	11	12	15	19
55	14	18	14	14	16	19	25
60	35	22	18	18	19	25	32
65	37	29	24	24	25	32	44
70	34	45	36	33	35	44	67
75	39	39	32	31	33	43	60
80	33	40	34	33	34	46	65
85	34	53	44	41	43	63	94
89	48	68	55	51	54	92	150

Note: 1 ft = 0.305 m; 1 blow per foot [BPF] = 3.3 blows per m [BPM].

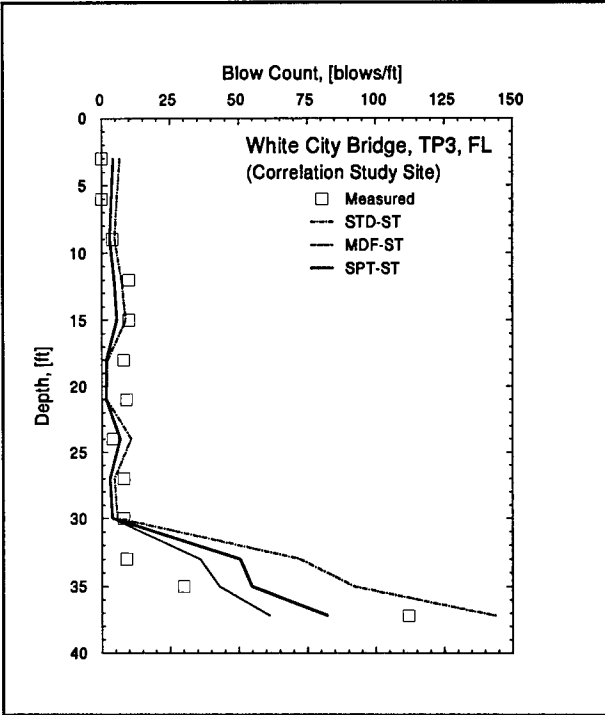


Figure 6.5: Driveability Graphs for White City Bridge, TP3, FL

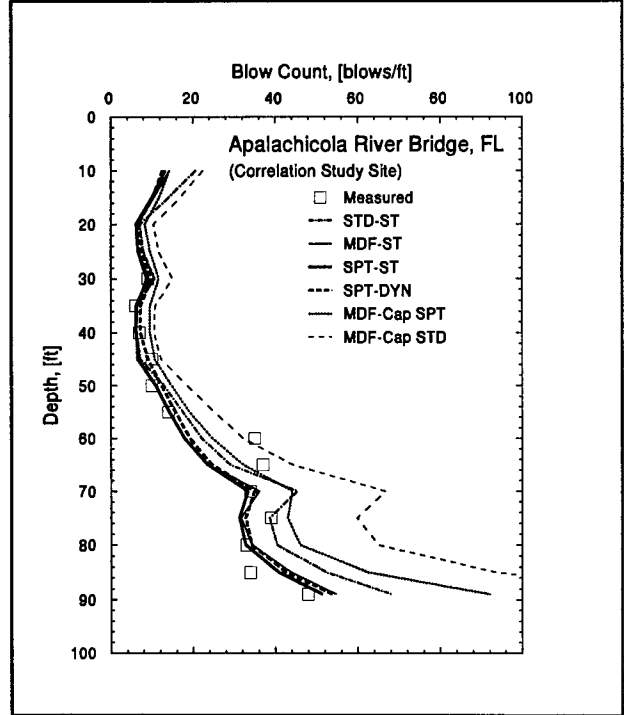


Figure 6.6: Driveability Graphs for Apalachicola River Bridge, FL

6.5 BEARING GRAPH CALCULATIONS

For each of the driveability study presented above, a corresponding bearing graph analysis was also performed for the end of driving pile penetration. The bearing graph analysis requires as an input the shaft resistance as a percentage of total pile capacity. This percentage was calculated based on the results presented in tables 6.1 to 6.6. The Smith soil constants employed for the bearing graph calculations were identical to those used in the driveability study. Dynamic shaft soil resistance parameters were average for the entire length of shaft. Calculated bearing graph analysis results are presented in tables 6.20 through 6.25. The bearing graphs generated by GRLWEAP are presented in appendix A. Bearing graphs were plotted together in figures 6.7 through 6.12. In addition to the static load test capacity, the CAPWAP capacities from EOD and BOR, the standard GRLWEAP at EOD and BOR were also included in these figures. To aid in an understanding of the six methods employed, table 6.26b was added.

Table 6.20: Bearing Graph Comparison for St. Mary, Cleveland, Ohio				
Ultimate Capacity [kips]	Blow Count, [BPF]			
	STD-ST	SPT-ST	SPT-DYN	MDF-ST
50	7	5	7	6
100	13	9	13	11
150	19	13	20	16
200	28	18	31	23
250	46	26	54	36
275	62	31	77	48
300	89	38	124	67
325	147	51	265	106
350	347	74	1289	211
375	6926	113	9999	495
400	--	185	--	--
450	--	433	--	--

Note: 1 kip = 4.45 kN; 1 blow per foot [BPF] = 3.3 blows per m [BPM].

Table 6.21: Bearing Graph Comparison for Fore River Bridge, Portland, Maine						
Ultimate Capacity [kips]	Blow Count, [BPF]					
	STD-ST	SPT-ST	SPT-DYN	MDF-ST	MDF-Cap STD	MDF-Cap SPT
50	0	3	3	0	0	3
100	5	7	7	0	5	7
150	8	11	11	4	8	12
200	11	16	16	6	11	17
250	15	21	21	8	15	22
300	19	27	27	10	19	28
325	21	30	31	12	21	31
350	24	34	34	13	24	35
375	26	38	38	14	26	40
400	29	42	43	16	29	44
450	35	52	54	19	36	55
500	43	67	69	23	43	70
550	52	89	92	28	53	93
600	68	115	121	33	67	120
650	86	156	168	41	85	167
700	117	228	249	49	116	251
750	179	353	389	66	168	376
800	334	537	608	82	280	627
850	707	916	1127	110	633	1357
900	2297	2482	6235	147	1840	9999

Note: 1 kip = 4.45 kN; 1 blow per foot [BPF] = 3.3 blows per m [BPM].

Table 6.22: Bearing Graph Comparison for C&D Canal, Pier 17, Delaware						
Ultimate Capacity [kips]	Blow Count, [BPF]					
	STD-ST	SPT-ST	SPT-DYN	MDF-ST	MDF-Cap STD	MDF-Cap SPT
100	4	5	5	4	4	6
200	10	12	10	8	10	14
300	17	20	17	14	19	24
400	25	28	25	22	27	36
500	36	40	34	30	39	52
600	51	53	44	40	55	64
700	68	60	52	53	70	73
800	78	68	58	65	80	85
900	90	78	65	73	92	100
1000	100	90	74	82	102	119
1100	115	106	82	89	119	148
1200	134	122	91	102	139	178
1300	158	144	104	117	164	220
1400	188	175	121	137	196	286
1500	231	219	143	153	241	388
1600	287	283	170	176	305	591
1700	370	379	204	208	402	1048
1800	457	545	249	252	585	3018
1900	613	842	321	312	970	9999
2000	1037	1487	427	403	2118	9999

Note: 1 kip = 4.45 kN; 1 blow per foot [BPF] = 3.3 blows per m [BPM].

Ultimate Capacity [kips]	Blow Count, [BPF]					
	STD-ST	SPT-ST	SPT-DYN	MDF-ST	MDF-Cap	MDF-Cap
					STD	SPT
100	4	3	3	4	4	3
250	13	10	10	12	13	10
400	25	18	18	24	24	18
550	42	27	26	39	41	26
700	60	36	35	56	57	35
850	69	46	44	67	65	44
1000	83	52	49	77	77	50
1150	100	57	54	92	92	56
1300	125	64	61	112	113	62
1500	164	77	75	151	153	75
1600	192	84	79	176	177	81
1650	207	87	82	186	186	89
1700	225	93	85	200	201	96
1750	248	101	89	216	218	99
1800	276	110	98	239	239	101
1850	311	117	102	266	268	102
1900	354	121	108	297	299	103
2000	482	126	126	389	394	110
2200	--	178	187	928	936	164
2400	--	200	233	--	--	242
2500	--	248	329	--	--	245
2700	--	448	638	--	--	758
2800	--	523	1415	--	--	2250

Note: 1 kip = 4.45 kN; 1 blow per foot [BPF] = 3.3 blows per m [BPM].

Table 6.24: Bearing Graph Comparison for White City Bridge, TP3, Florida			
Ultimate Capacity [kips]	Blow Count, [BPF]		
	STD-ST	SPT-ST	SPT-DYN
50	2	2	2
100	5	3	4
200	14	9	11
300	28	16	23
400	45	26	39
500	77	38	64
550	103	45	86
600	128	57	126
650	157	71	168
700	182	84	223
800	250	97	472
850	316	111	669
900	411	125	--
950	500	130	--
1000	--	141	--
1050	--	154	--
1100	--	171	--
1150	--	190	--
1200	--	217	--
1250	--	236	--
1300	--	295	--
1350	--	320	--
1400	--	367	--
1450	--	425	--

Note: 1 kip = 4.45 kN; 1 blow per foot [BPF] = 3.3 blows per m [BPM].

Table 6.25: Bearing Graph Comparison for Apalachicola River Bridge, Florida						
Ultimate Capacity	Blow Count, [BPF]					
	STD-ST	SPT-ST	SPT-DYN	MDF-ST	MDF-Cap STD	MDF-Cap SPT
100	7	7	7	7	7	7
200	15	14	13	14	16	13
300	24	21	21	21	24	20
400	33	30	29	30	35	29
500	41	37	37	38	44	36
600	52	46	45	47	56	44
700	67	58	58	60	73	56
800	90	78	79	80	103	74
900	124	113	116	112	153	106
1000	179	186	199	161	247	170
1100	298	351	402	262	533	312
1200	720	700	920	573	5534	574

Note: 1 kip = 4.45 kN; 1 blow per foot [BPF] = 3.3 blows per m [BPM]

Table 6.26a: Comparison of Capacity Predictions from Dynamic SPT, GRLWEAP, and Static Load Test								
Pile	Load Test [kips]	Standard GRLWEAP [kips]	SPT-ST [kips]	MDF-ST [kips]	STD-ST [kips]	SPT-DYN [kips]	MDF-Cap SPT [kips]	MDF-Cap STD [kips]
St. Mary	315	370*	410	350	340	320	--	340
Portland, ME	350	470*	160	325	210	160	160	210
C&D 17	1150	1240*	1250	1350	1150	1350	1050	1150
C&D 21	1300	1700*	2000	1350	1300	2000	2020	1350
White City	630	675*	690	690	510	540	--	510
Apalachicola	958	1015*	1110	1120	1115	1060	1115	1030
Ratio to Load Test		1.06-1.34	0.46-1.54	0.93-1.17	0.60-1.16	0.46-1.54	0.43-1.55	0.60-1.08
Average		1.17	1.11	1.08	0.94	1.02	1.01	0.93
Table 6.26b: Method Description								
Source of	SPT-ST	MDF-ST	STD-ST	SPT-DYN	MDF-Cap SPT	MDF-Cap STD		
Static Resistance Values	Modf'd PT Static Tests	Modf'd PT Static Tests	Modf'd PT Static Tests	SPT Dynamic Matching	Pile Load Test	Pile Load Test		
Shaft Damping	SPT Dynamic Matching + Uplift (R_u, q)	GRLWEAP	GRLWEAP	SPT Dynamic Matching	SPT Dynamic Matching + Uplift(R_u, q)	GRLWEAP		
Toe Damping	SPT Dynamic Match w/ SPT Static Values	SPT Dynamic Matching (except Portld)	GRLWEAP	SPT Dynamic Matching	SPT Dynamic Matching w/ Static SPT Values	GRLWEAP		
Quakes	SPT Static Tests	SPT Static Tests	GRLWEAP	SPT Dynamic Matching	SPT Static Tests	GRLWEAP		

*Based on Restrike Test Results; 1 kip = 4.45 kN.

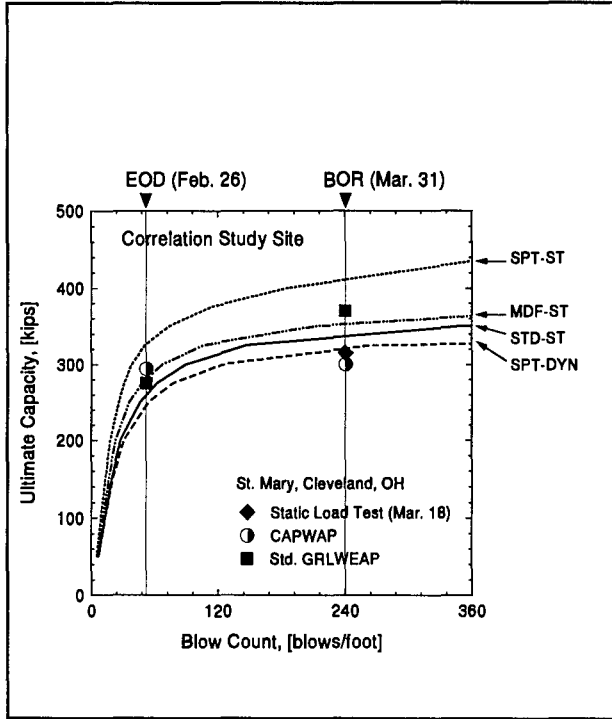


Figure 6.7: Bearing Graphs for St. Mary, Cleveland, OH

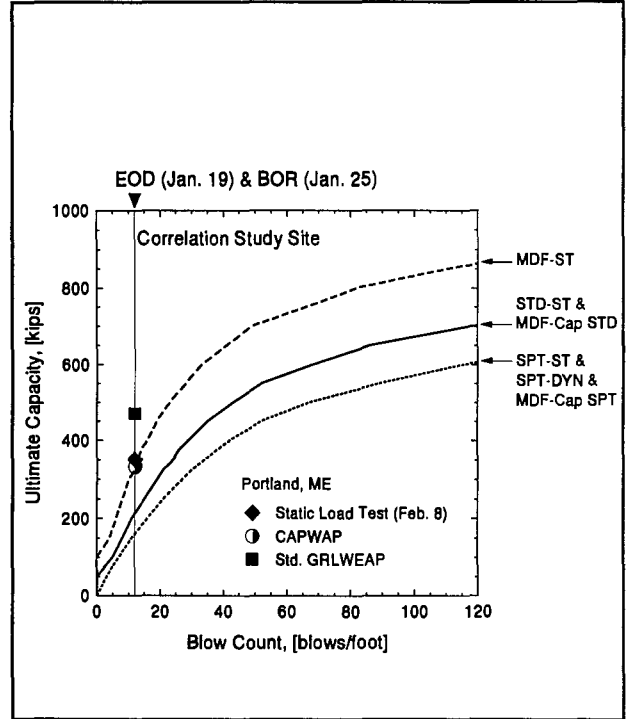


Figure 6.8: Bearing Graphs for Fore River Bridge, Portland, ME

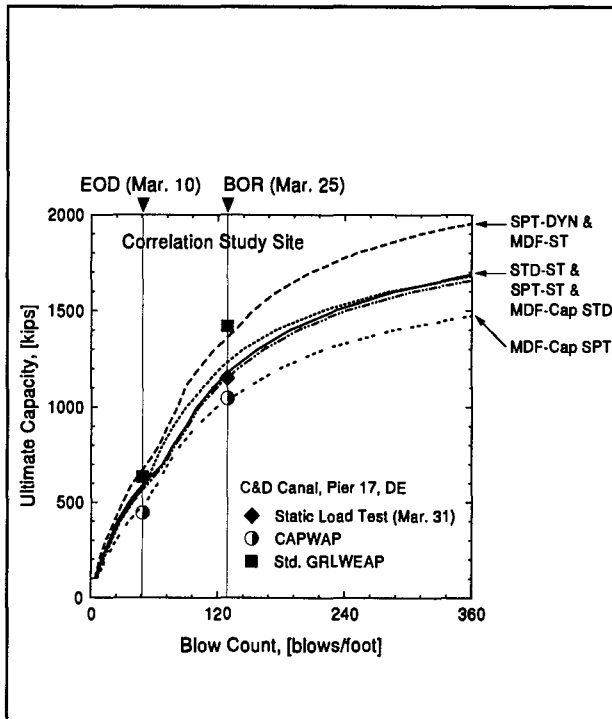


Figure 6.9: Bearing Graphs for C&D Canal, Pier 17, DE

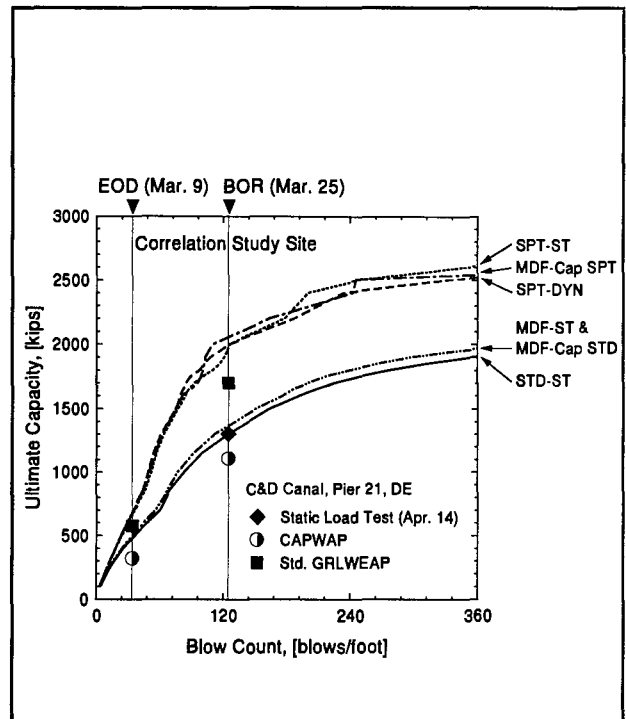


Figure 6.10: Bearing Graphs for C&D Canal, Pier 21, DE

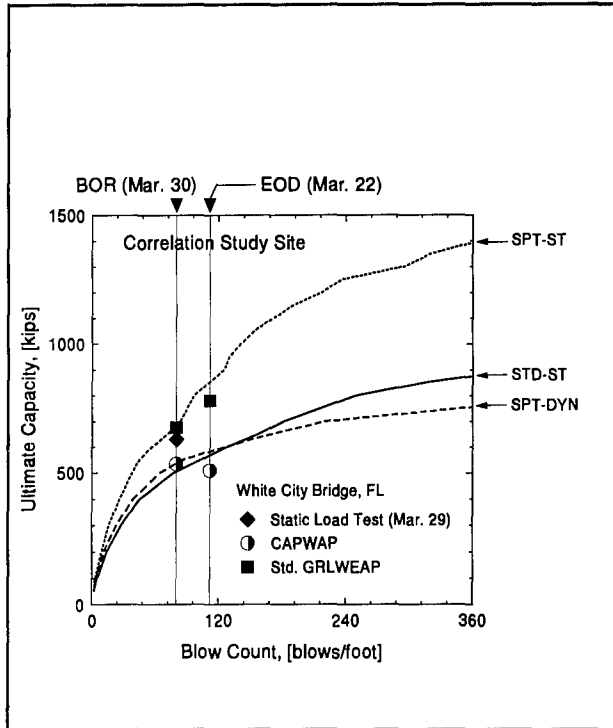


Figure 6.11: Bearing Graphs for White City Bridge, TP3, FL

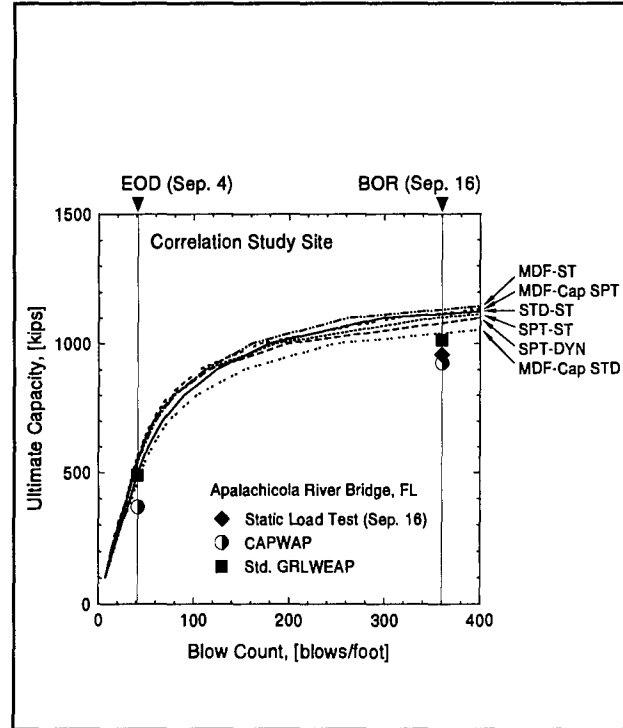


Figure 6.12: Bearing Graphs for Apalachicola Bridge, FL

6.6 TOE PARAMETER STUDY

The effects of a variety of new GRLWEAP toe model parameters on calculated blow count and pile variables at both pile top and toe were investigated in this study. Test Pile Number 3 of the White City Bridge, Florida, was chosen for this study. TP3 was a 24-in (610-mm) square precast, prestressed concrete pile. Dynamic testing was performed on this pile during initial driving and restrike, and therefore pile top force and velocity records were available for both EOD and BOR. The EOD blow count for this pile was 28 blows for 3 in (76 mm) set or 112 BPF (367 BPM) equivalent. A static load test was performed 7 days after the end of driving. The maximum load applied during the static load test was 700 kips with a Davisson's failure load of 630 kips. CAPWAP analysis results performed using the end of driving and beginning of restrike records indicated that the pile experienced mostly end bearing resistance both during EOD and BOR. According to the restrike analysis, soil setup did not cause increase in shaft resistance. For this reason, this pile seemed well suited for the toe parameter study. Since the resistance of the pile is mostly end bearing, the bottom force, velocity and resistance can be calculated very easily using stress wave theory.

As an input to the GRLWEAP analysis, the percentage shaft resistance was assumed to be 3 percent; shaft damping and quake were set to 0.1 s/ft (0.33 s/m) and 0.1 in (2.54 mm), respectively. Because of the low shaft resistance, shaft damping and quake did not have any significant effects on the results. The toe parameters investigated included the toe damping (J_t), toe quake (Q_t), plus three new GRLWEAP parameters gap and hyperbolic factors F1 and F2. This new parameters are defined as follows. The new plug max was not investigated.

Gap is a distance through which the pile toe can move without experiencing soil resistance forces.

Hyperbolic factor F1 is a toe quake multiplier defining the pile toe penetration at which failure is reached as $(F1)(Q_t)$. The shape of the hyperbolic toe load-set curve was described in GRL & Associates, Inc., 1995.

Hyperbolic factor F2 is a toe quake multiplier defining the unloading quake as $(F2)(Q_t)$. Of course, F2 is only reasonable if less than or equal to 1. In other words, the unloading stiffness $R_{ut}/(Q_t F2)$ should be greater than the initial stiffness defined by the nominal quake, Q_t .

Six different cases were studied. For each case, three different values of selected toe parameter(s) were analyzed, and the blow count and computed top and bottom parameters were compared. The computed blow counts calculated for each case are summarized in table 6.27 together with the values of the varied toe parameters. Blank fields indicate a repetition of the same value listed in the row above. Graphs of both the computed top and bottom parameters are presented in figures 6.13 through 6.22 together with measurements for comparison.

Three different blow count computations are presented in table 6.27 and designated as equations (6.1), (6.2), and (6.3). All three blow counts are the inverse of calculated final displacements Δ_i , where i refers to blow count equations (6.1), (6.2) and (6.3). The first equation defines the set as the difference between maximum toe displacement, $\max u_n$, and the average weighted quake which is based on individual segment quakes, q_i , and capacities, R_{ui} . This is the standard GRLWEAP method:

$$\Delta_1 = \max u_n - \sum (R_{ui})(q_i)/R_{ut} \quad (6.1)$$

The second equation simply defines the final set as the toe displacement calculated at the end of the dynamic analysis, *i.e.*, at time t_{end} :

$$\Delta_2 = u_n(t_{end}) \quad (6.2)$$

Table 6.27: Summary of Toe Parameter Study								
Studied Parameter	J _t [s/ft]	Q _t [in]	Gap [in]	F1	F2	Blow count, [BPF]		
						Eq. 6.1	Eq. 6.2	Eq. 6.3
1. Standard	0.15	0.20	0	1.0	1.0	191	9999	2481
2. Quake	0.05	0.15	0	1.0	1.0	96	9999	2317
		0.20				126	9999	2095
		0.40				1606	9999	1444
3. Quake and F1	0.05	0.10	0	4.0	1.0	63	1183	2160
		0.20		2.0		78	9999	1699
		0.3		1.3		140	9999	1537
4. Damping	0.05	0.4	0	1.0	1.0	1606	9999	1444
	0.15					9999	9999	1694
	0.20					9999	9999	1803
5. Gap	0.05	0.1	0	4.0	1.0	63	1183	2160
			0.4			18	29	653
			0.5			15	23	559
6. F2	0.05	0.1	0	4.0	1.0	63	1183	2159
					0.5	59	73	2110
					0.2	51	37	1905
7. Matching Blow Count	0.03	0.2	0	1.0	0.4	118	138	2047

Note: 1 s/ft = 3.28 s/m; 1 in = 25.4 mm; 1 blow per foot [BPF] = 3.28 blows per m [BPM].

The third equation averages the so-called slip values for each segment, *i.e.*, the difference between maximum segment displacement and quake. Thus:

$$\Delta_3 = \sum R_{ui}(\max u_i - q_i)/R_{ut} \quad (6.3)$$

where R_{ui} and R_{ut} are the individual segment capacity and total ultimate capacity, respectively.

Figure 6.13 shows the measured pile top quantities force, velocity and displacement and the associated computed curves for toe quakes of 0.15, 0.20, and 0.40 in (3.8, 5.1, and 10.2 mm). Obviously, since this was a 24-in (610-mm) pile, the 0.2-in (5.1 mm) toe quake would be the standard value. Characteristically, for this White City pile, a second force peak occurred, later than expected from the return of the wave at time $2L/c$. Obviously, none of the three quakes tried, would delay the calculated second force peak enough for a good match. In fact, merely increasing the quake produced a rather large displacement peak.

The toe variables force, velocity and displacement were also calculated from the top measurements using wave propagation theory as for the SPT measurements (assuming no friction effects). These curves, directly calculated from the top measurements were referred to as "measured" bottom curves. For the same three quakes of figure 6.13, bottom variables were calculated and compared in figure 6.14 with these "measured" bottom curves.

The same process was then repeated for other variables and always two figures were plotted as follows:

Figures 6.15 and 6.16 show the effects of varying quake and hyperbolic factor F1 chosen such that the pile displacement at failure, $(F1)(Q_t)$, was equal to 0.4 in (10 mm).

Figures 6.17 and 6.18 are the results for three different toe damping factors.

Figures 6.19 and 6.20 show how the toe gap strongly affects velocities and displacements.

Figure 6.21 and 6.22 summarize results of the variation of unloading factors F2. Effects caused by F2 became apparent only in the late record portion where other parameters had very little effect.

In this study, the toe model components were not used in an attempt to match the measured curves. Instead, an attempt was made to develop trends. For matching, larger quake and damping changes then used in this study would be needed. Also the standard and matching BC (blow count) entries 1 and 7 in table 6.27 did not produce particularly interesting match graphs and were therefore not reproduced as separate figures in this report.

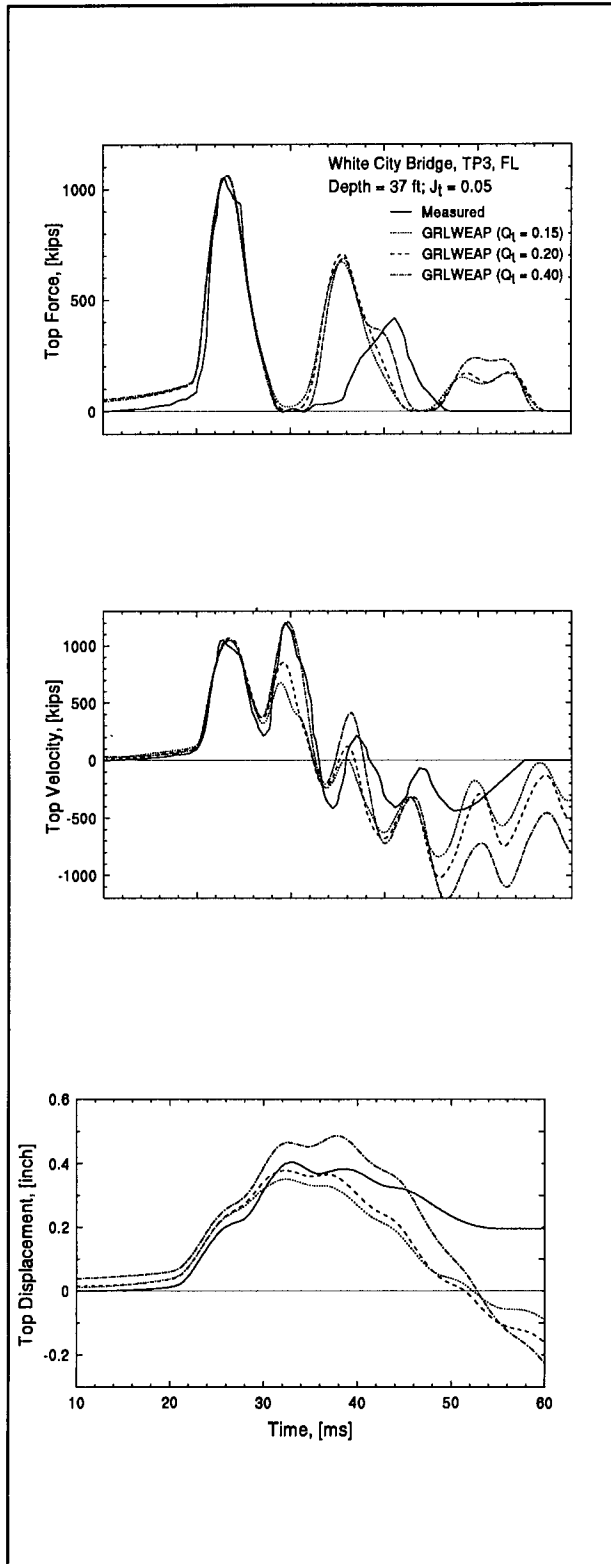


Figure 6.13: Effects of Toe Quake Variations on GRLWEAP Calculated Top Quantities

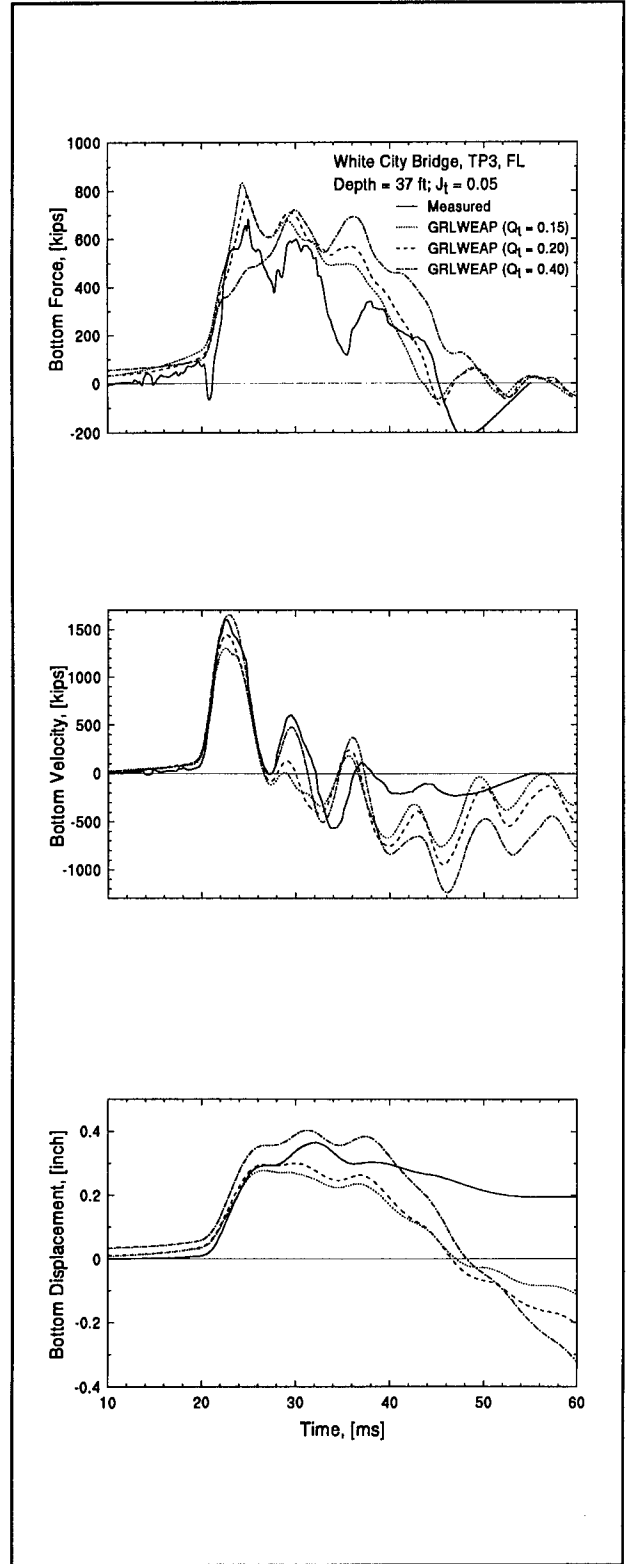


Figure 6.14: Effects of Toe Quake on GRLWEAP Calculated Bottom Quantities

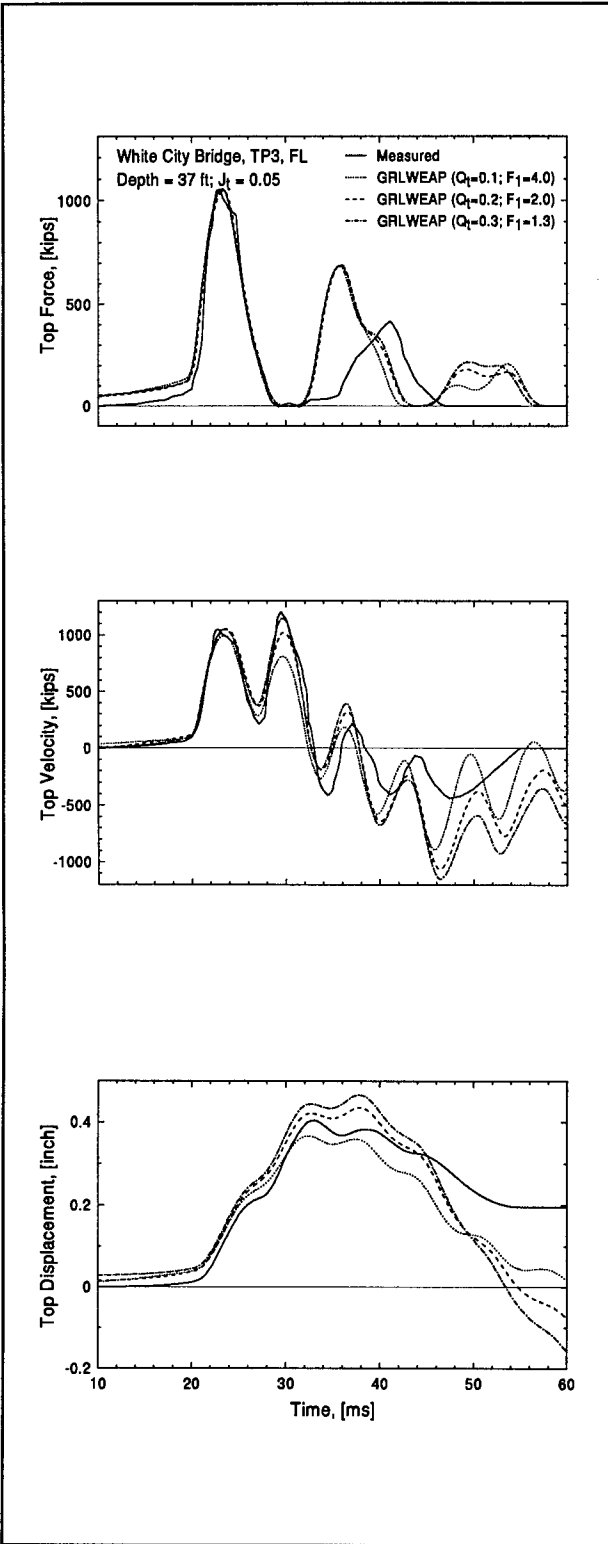


Figure 6.15: Effects of Hyperbolic Factor F_1 on GRLWEAP Calculated Top Quantities

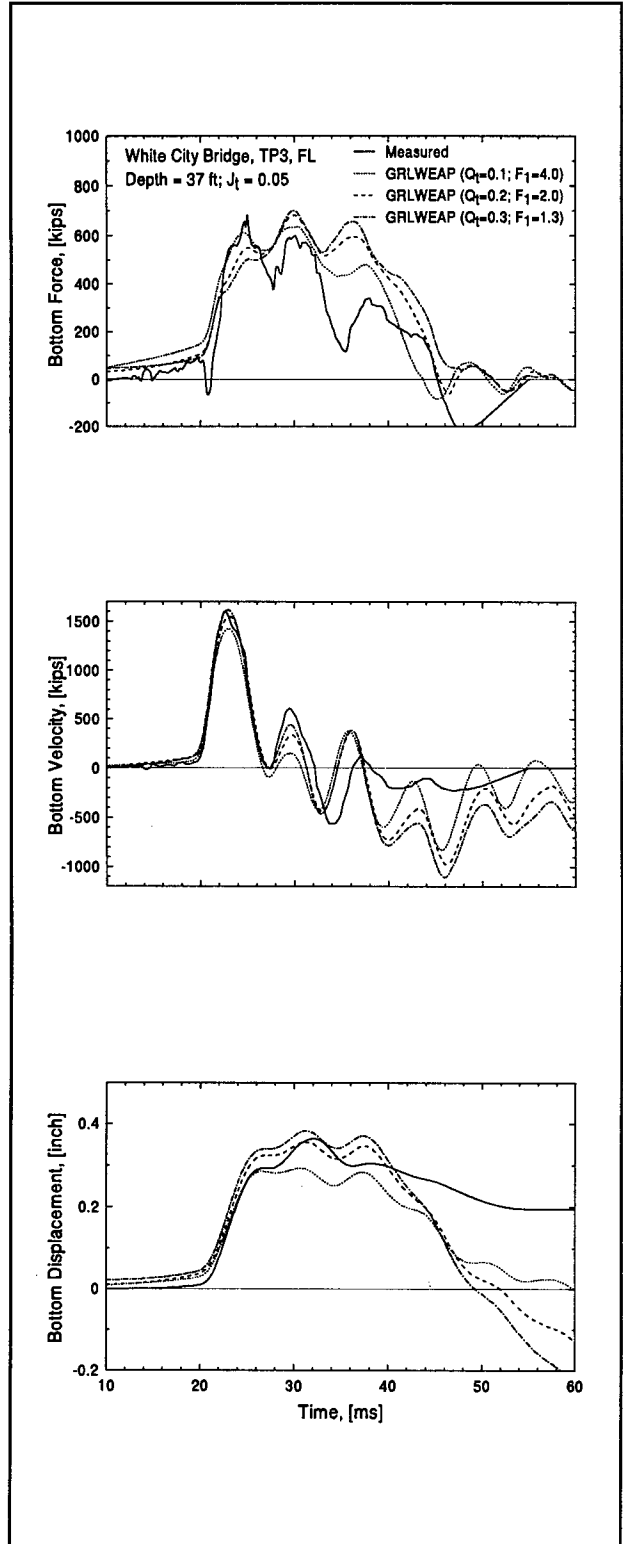


Figure 6.16: Effects of Hyperbolic Factor F_1 on GRLWEAP Calculated Bottom Quantities

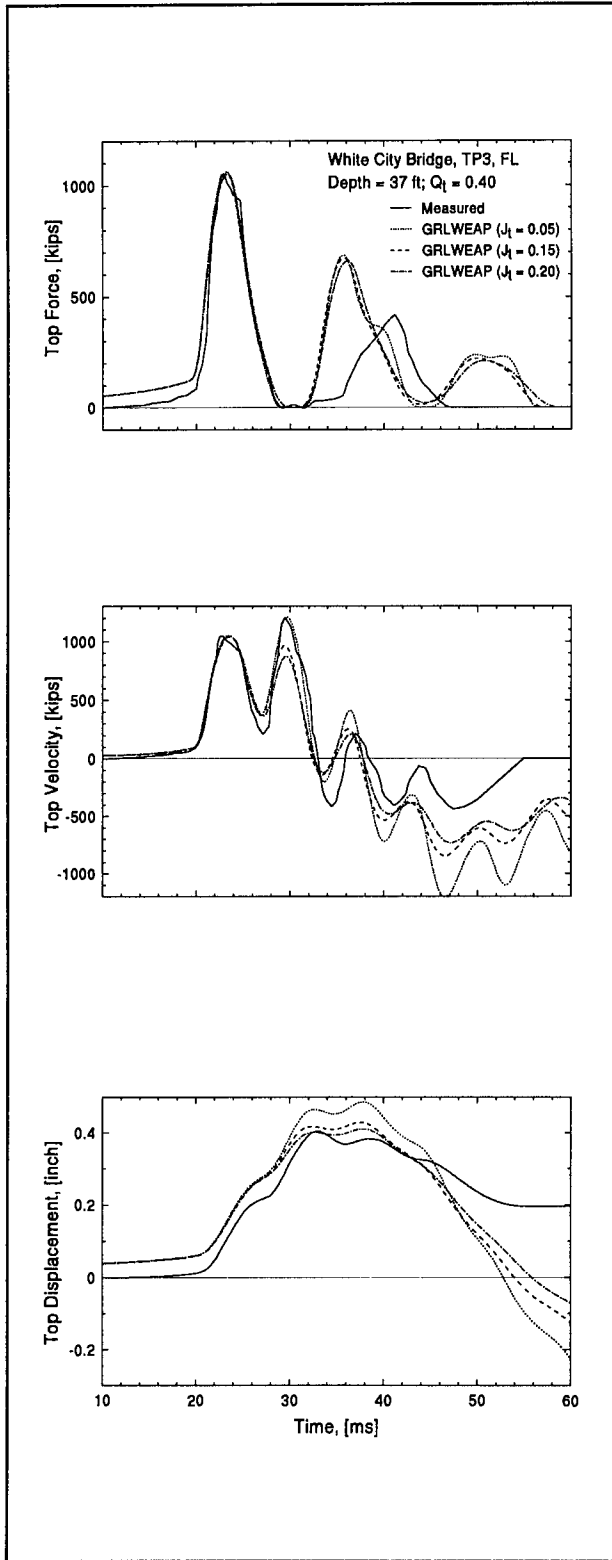


Figure 6.17: Effects of Toe Damping on GRLWEAP Calculated Top Quantities

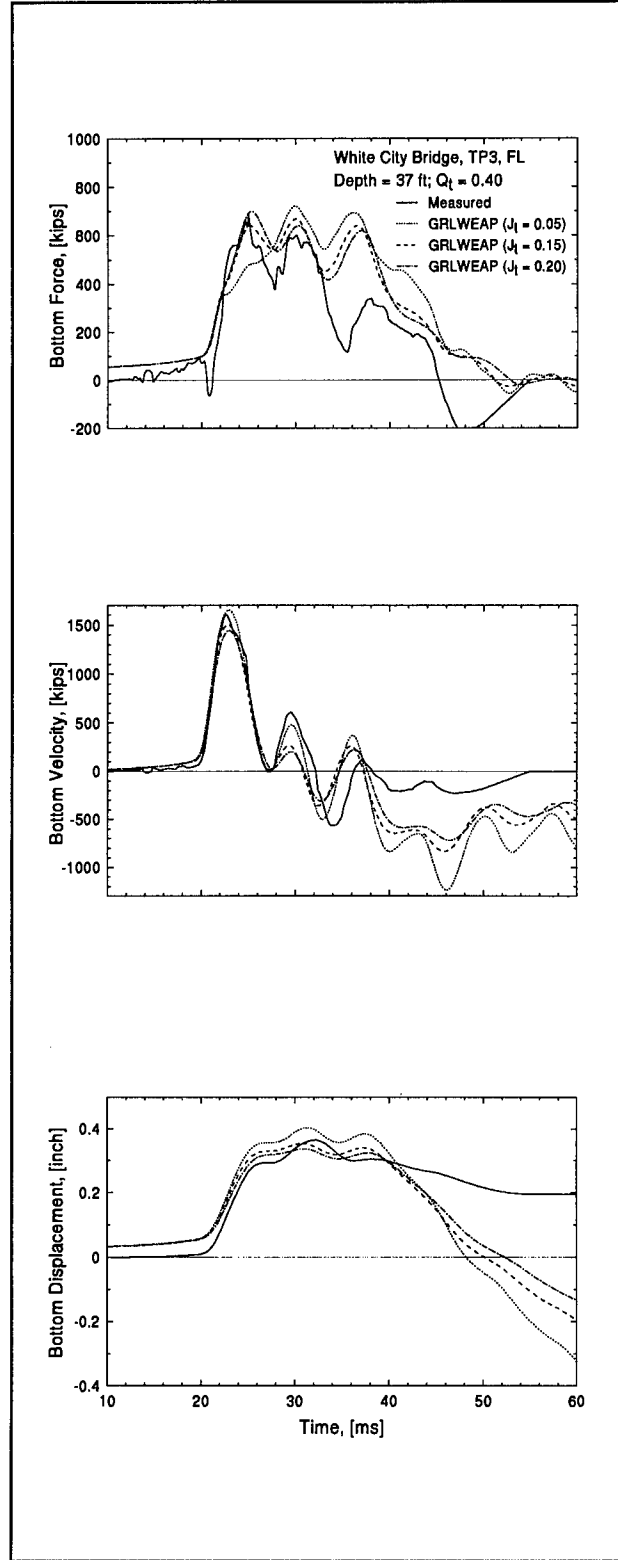


Figure 6.18: Effects of Toe Damping on GRLWEAP Calculated Bottom Quantities

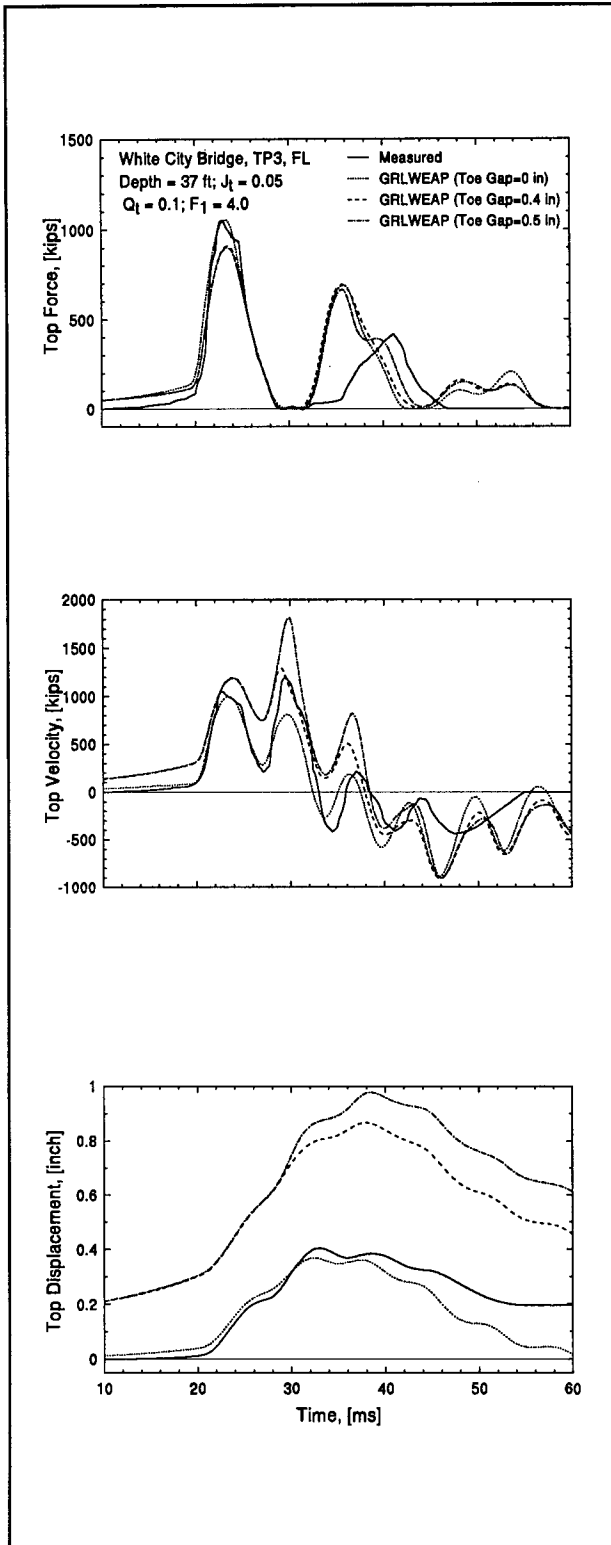


Figure 6.19: Effects of Toe Gap on GRLWEAP Calculated Top Quantities

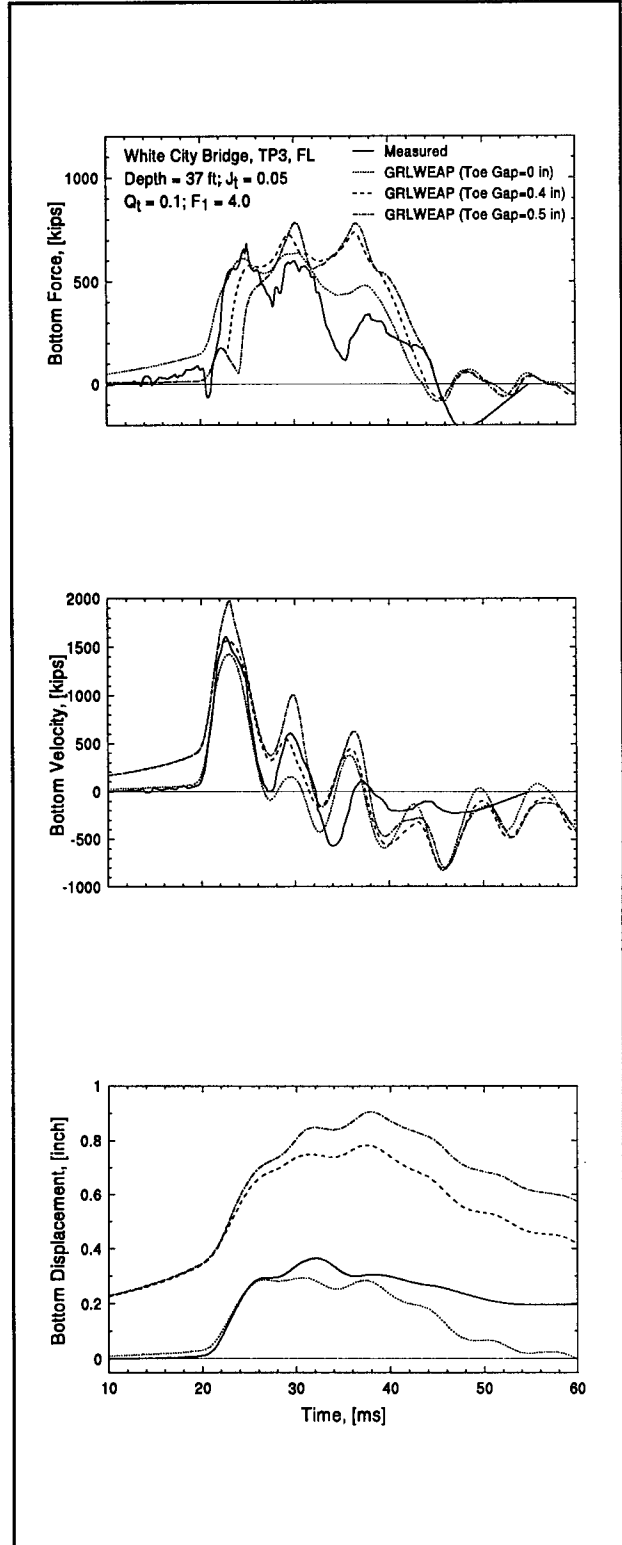


Figure 6.20: Effects of Toe Gap on GRLWEAP Calculated Bottom Quantities

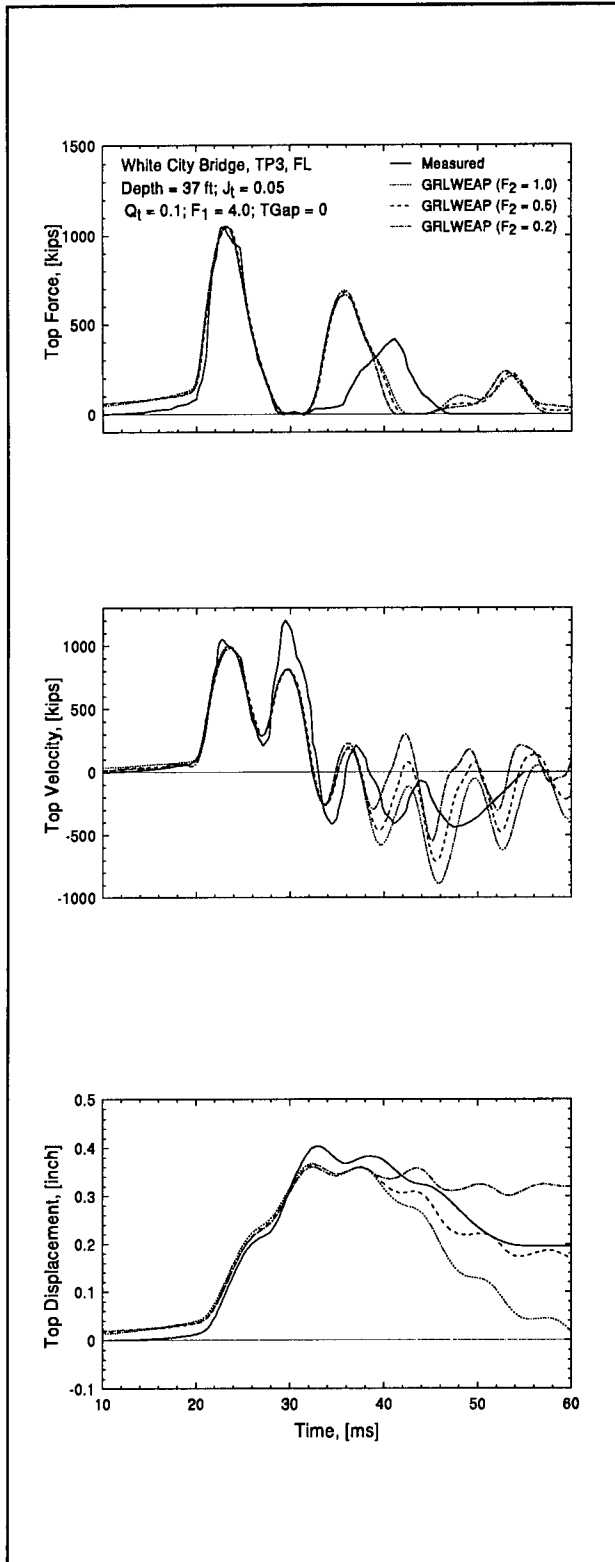


Figure 6.21: Effects of Toe Unloading Quake on GRLWEAP Calculated Top Quantities

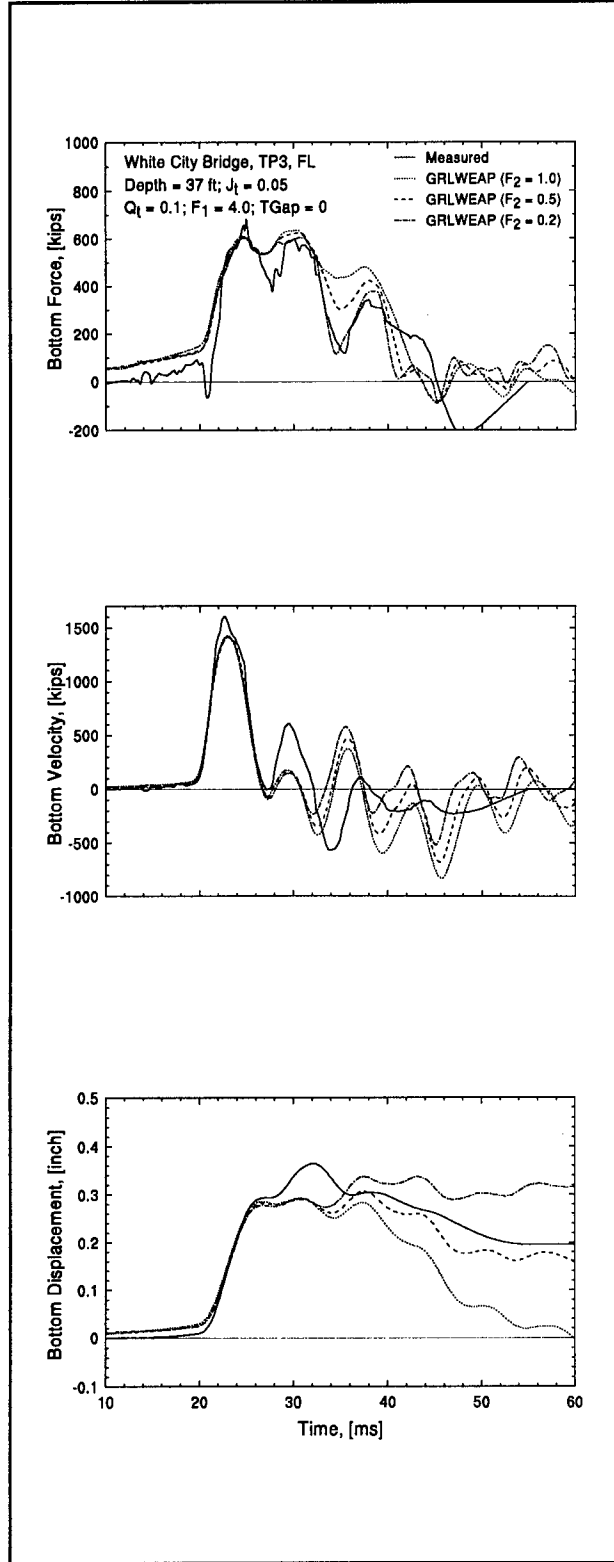


Figure 6.22: Effects of Toe Unloading Quake on GRLWEAP Calculated Bottom Quantities

6.7 DISCUSSION OF RESULTS

6.7.1 Blow Count Predictions

Blow count predictions by the wave equation are in general very sensitive to resistance parameter variations and because of the non-linearity of the blow count resistance relationship, it is difficult to meaningfully assess the quality of blow count predictions. A very simplified attempt at such a comparison will be made here.

The results presented in figures 6.1 through 6.6 generally indicate reasonably good blow count predictions. Considering the EOD blow counts, (for these both uplift and compression test results were available), the SPT-ST and SPT-DYN performed quite well with an average final blow count difference (absolute values) of 14 and 15 blows/ft, respectively, as shown in table 6.28. The average measured final blow count was 52 blows/ft for the six correlation sites. On the average, the predicted blow counts differed from the final ones by 24 and 27 percent (average of absolute values of differences) for the same two methods, respectively. Thus, as far as dynamic wave equation parameters are concerned, the purely dynamic method appears to be as valuable as the much more complicated static method for driveability predictions. Most surprisingly, a mixing of static resistance values from the Modified SPT with standard GRLWEAP dynamic parameters (STD-ST) would yield very poor predictions with 38 blows per ft blow count difference which averages a prediction difference of 69 percent.

6.7.2 Capacity Predictions

Table 6.26a summarizes the capacity predictions from Modified SPT methods together with the load test result itself and ratios of prediction to load test capacity. The standard GRLWEAP capacity predictions, based on the restrrike blow count are also included.

The best capacity predictions were obtained through the MDF-ST method which included standard GRLWEAP shaft parameters, the resistance distribution from Modified SPT static tests and dynamically matched toe parameters (with the exception of Portland whose toe damping factor was arbitrarily set to 0.01 s/ft (0.03 s/m) as determined for White City and Apalachicola.

After investigating these results, the following observations can be made:

Five of the six results were for piles driven into sand

Poor results were only obtained for Portland and C&D 21 using Modified SPT parameters. For Portland, the toe damping was determined too high (0.3 s/ft or 1 s/m) leading to a low capacity prediction; for C&D 21 both low quakes and low damping factors were

Table 6.28: Final Blow Count Comparison Driveability Studies										
	SPT-ST				SPT-DYN			STD-ST		
Site	Measured	Predicted	Pred-Measd		Predicted	Pred-Measd		Predicted	Pred-Measd	
	BPF	BPF	BPF	%	BPF	BPF	%	BPF	BPF	%
St Mary	52	55	3	5.8	84	32	61.5	187	135	245.5
Portland	16	10	6	37.5	14	2	12.5	9	7	12.7
C&D 17	49	54	5	10.2	43	6	12.2	54	5	9.1
C&D 21	34	48	14	41.2	47	13	38.2	63	29	52.7
White City	112	61	51	45.5	82	30	26.8	144	32	58.2
Apalachicola	48	51	3	6.3	54	6	12.5	68	20	36.4
Sum	311	279	82	146.4	324	89	163.8	525	228	414.5
Average	51.8	46.5	13.7	24.4	54.0	14.8	27.3	87.5	38.0	69.1

Note: 1 blow/ft [BPF] = 3.28 blows/m [BPM].

Pred-Measd = the difference between predicted and measured, and percentage over measured.

determined by the Modified SPT. (Quakes were 0.035/0.08 in or 0.9/2 mm on shaft/toe; damping factors were 0.05/0.07 s/ft or 0.16/0.21 s/m on shaft/toe). These low parameters lead to a substantial overprediction of capacity. The Modified SPT toe damping factor, however, appeared to be acceptable.

Relatively low toe damping factors (at most 0.07 s/ft or 0.21 s/m) appeared to yield good capacity results.

Standard GRLWEAP shaft damping parameters appear to yield good results. It is, however, not a simple task to decide which shaft damping factor to use when the shaft soil includes both fine grained and coarse grained materials since the range from 0.05 to 0.20 s/ft (0.16 to 0.65 s/m) can change the capacity appreciably.

Reduced toe damping parameters yielded improved results.

General rules cannot be derived from these observations. However, in these primarily sandy soils, a lower than the usually recommended toe damping factor appears to be reasonable.

6.7.3 Toe Parameter Study

One of the reasons for selecting the White City records for the toe parameter study was the apparent mismatch of forces and velocities at the time of and shortly after the return of the bottom reflected impact wave. The study presented here failed to determine which soil parameter would be responsible for the mismatch. It was therefore concluded that the mismatch was the result of a tension crack in the pile and that only a pile model change (tension slack) could produce a satisfactory force and velocity match.

Even though matching of the recorded signals with GRLWEAP calculated quantities was not successful a few interesting observations were made:

- The analyses presented cannot completely describe the effects of parameter variations on pile forces and motions and on the calculated blow count. Obviously and not unexpectedly, toe quake and hyperbolic factor F_1 have similar effects on forces and motions. Calculated blow counts are primarily affected by the initial quake which is used for the rebound calculation.
- Toe damping has a smoothing effect, however, to achieve a considerable smoothing effect may lead to very high damping factors and excessive blow counts.
- Gaps have to be used with extreme caution and very small values: a gap of 0.2 or

even 0.4 in (5 or 10 mm) leads to very unusual forces and motions and small blow counts (the final set practically increases by the magnitude of the gap in a pure toe resistance case.)

- The only quantities effectively allowing for a match in the later part of the records was the unloading quake included in the hyperbolic model. Reducing the unloading quake (Q_u , F_2) raised the displacement record in the late record portion. Only because of GRLWEAP's blow count calculation based on the maximum toe displacement (eq. 6.1) rather than on the calculated final toe displacement (eq. 6.2), does the GRLWEAP model produce reasonably consistent blow count results in the absence of an unloading quake.

As noted in other studies, a relatively low toe damping factor (0.03 s/ft or 0.1 s/m) did produce a good blow count match.

It is strongly recommended that these new program features be further studied before they are utilized.

CHAPTER 7

PILE CAPACITY AND BLOW COUNT PREDICTION

7.1 INTRODUCTION

In this chapter, the analyses and findings discussed in chapters 5 and 6 were applied to Modified SPT data collected at three verification sites, all located in Florida: Aucilla River Bridge, Vilano Bridge - East Embankment, and Vilano Bridge - West Embankment. The piles at Aucilla and Vilano-East were driven before the Modified SPT was performed. CPT data were also collected at these sites by others and were provided to us prior to the Modified SPT test. All three piles at the verification sites consisted of 18-in (457-mm) square prestressed concrete instrumented with an Osterberg cell at their bottom for static load testing.

To obtain as much information as possible for pile driveability and capacity predictions, the regular SPT procedure was performed at a 5-ft (1.5-m) intervals and the Modified SPT was performed more often than at the correlation sites. At certain depths, all types of tests were performed; regular SPT, uplift test, setup test, redrive test, and compression test. For the driveability prediction, compression tests were performed not only near the final pile toe penetration, but also at several earlier depths.

The pile capacity prediction was based on the results from the Modified SPT uplift and compression tests. The pile toe resistance was based on the compression test results, while the shaft resistance was based on either the uplift test results, or where no uplift test were available, on the results from depths with uplift test, prorated with respect to N-values.

The three methods, discussed in the previous chapter, named the "standard Smith parameters," "SPT parameters," and "Modified parameters" were again used for dynamic soil parameter calculation, each with two capacity values, one from "static" and one from the "dynamic" analysis results.

7.2 MODIFIED SPT DATA ANALYSIS

This analysis type was discussed in section 5.4. Force and velocity records taken near the top of the drill string, calculated force and motion at the sampler toe, and the force matching curves are included in appendix D. The analysis results are presented in tables 7.1 through 7.3 in a form similar to tables 5.7 through 5.12. Exceptions are the lack of a GRLWEAP study of the SPT-system and, since only the flat tip was used in the compression tests, tip type information

was not needed. For more details about the analysis and the information presented in these tables, reference is made to section 5.4.

At the Aucilla River Bridge site, three compression tests were performed, two above and one below the pile tip elevation. At this particular site, the boring hole was lined with a casing whose inside diameter was smaller than the diameter of the specially designed tip, and therefore the special tip could not be used. Instead the drill rod was plugged with a special fitting and used in the compression tests. It was driven 6 in (152 mm) with the standard SPT hammer before performing the compression test. The 6-in (152-mm) penetration might have contributed some shaft resistance; this fact was, however, neglected and all resistance was attributed to the toe. Since the soil type between 10 and 55 ft (3.1 and 16.8 m) depth indicated primarily shaft resistance, more uplift tests were performed than compression tests. Below 55 ft (16.8 m), toe resistance appeared to dominate. A summary of the calculated Smith's soil constants are presented in table 7.1.

At Vilano Bridge - East Embankment, the analysis for soil parameter determination started at the 15 ft (4.6 m) penetration since no static test results were performed above that depth. (At 7-ft or 2.1-m penetration, sand had blown into the casing and the compression test was not successful; at 5- and 10-ft (1.5- and 3.1-m) penetration, only the regular SPT was performed.) The soil type at this site indicated more toe resistance than shaft resistance; therefore, compression tests were performed every 5 ft (1.5 m) prior to the normal SPT. Thus, the compression test was first performed, then the sampler was driven 18 in (457 mm) starting at the depth where the compression test had been done; after that the uplift test was performed. Analysis results are summarized in table 7.2. No setup tests were successfully performed at this site, and therefore, only EOD capacity predictions were available.

At Vilano Bridge - West Embankment, the test pile was designed for a penetration of 62 ft (19 m) with the top 25 ft (7.6 m) predrilled. Therefore, the analysis was performed starting from the 30-ft (9.2-m) penetration. Three compression tests were performed at this site and six uplift tests. A summary results is presented in table 7.3.

7.3 PILE CAPACITY PREDICTION

Pile capacity calculations were based on the ultimate resistance values obtained from the SPT uplift and compression tests. For depths where the toe or shaft resistance were not directly measured, resistance values were calculated by prorating with the SPT N-values. The pile capacity calculations for each verification site are presented in tables 7.4 through 7.6. In these tables, prorated values are listed without brackets and directly measured values are set in parentheses.

Table 7.1: Summary of the Smith Soil Constants for Aucilla River Bridge, Florida

Depth	Soil	Test	Measured	Ultimate	Quake	Damping	Acceleration	Analysis	Figure	Remarks
5	SM	Shaft	18	2.30	0.020	0.100	0.33	Dynamic	D.49	Last Blow, Standard SPT. 30" Drop 1.13 kips on the shaft (Based on the uplift test data at 10 ft)
10	SM	Shaft	4	1.13	0.006	0.250	0.38	Static	D.50	Before Uplift. 20" Drop
			4	1.40	0.006	0.250	0.35	Dynamic		Before Uplift. 20" Drop
				1.13 kips on the shaft (Based on the uplift test data)						
15		Shaft	6	0.75	0.035	0.300	0.32	Dynamic	D.51	Last Blow, Standard SPT. 30" Drop
20	CH	Shaft	4	0.65	0.005	0.300	0.25	Static	D.52	Before Uplift. 30" Drop
			4	0.87	0.030	0.250	0.25	Dynamic		Before Uplift. 30" Drop
				0.92	0.010	0.250	0.50	Static	D.53	After Uplift. 10" Drop.(15 min BOR)
				1.30	0.010	0.150	0.50	Dynamic		After Uplift. 10" Drop.(15 min BOR)
25	CH	Shaft	4	0.78	0.045	0.120	0.30	Dynamic	D.54	Last Blow, Standard SPT. 30" Drop
30	CH	Shaft	4	0.60	0.010	0.150	0.26	Static	D.55	Before Uplift. 30" Drop
			4	1.00	0.030	0.100	0.28	Dynamic		Before Uplift. 30" Drop
				1.04	0.030	0.140	0.52	Static	D.56	After Uplift. 10" Drop.(11 hrs BOR)
				0.70	0.010	0.140	0.52	Dynamic		After Uplift. 10" Drop.(11 hrs BOR)
35	MH	Shaft	5	0.70	0.050	0.130	0.25	Dynamic	D.57	Last Blow, Standard SPT. 30" Drop
40	CL	Shaft	7	1.00	0.013	0.150	0.40	Dynamic	D.58	Last Blow, Standard SPT. 30" Drop
42		Toe	10*	1.90	0.070	0.010	0.20	Static	D.59	Before Compression Test. 20" Drop
			10*	1.10	0.040	0.120	0.20	Dynamic		Before Compression Test. 20" Drop
45	CH	Shaft	4	0.53	0.020	0.190	0.30	Static	D.60	Before Uplift. 30" Drop
			4	0.53	0.060	0.190	0.30	Dynamic		Before Uplift. 30" Drop
50		Shaft	1	0.40	0.025	0.150	0.26	Dynamic	D.61	Standard SPT. 30" Drop
55	Rock	Shaft	57	4.50**	0.047	0.100	0.38	Dynamic	D.62	Last Blow, Standard SPT. 30" Drop No Resistance at the shaft
60		Shaft	45	5.50**	0.100	0.050	0.40	Dynamic	D.63	Last Blow, Standard SPT. 30" Drop No Resistance at the shaft
63		Toe	66*	3.70	0.070	0.120	0.30	Static	D.64	Before Compression Test. 20" Drop
			66*	2.50	0.080	0.300	0.33	Dynamic		Before Compression Test. 20" Drop
65		Shaft	66	3.30**	0.088	0.300	0.33	Dynamic	D.65	Last Blow, Standard SPT. 30" Drop No Resistance at the shaft
67.5		Toe	19*	2.80	0.036	0.050	0.25	Static	D.66	Before Compression Test. 30" Drop
			19*	2.00	0.022	0.100	0.20	Dynamic		Before Compression Test. 30" Drop

Notes: * The drill rod was plugged with a special fitting then driven for 6 in.
 ** This resistance assumed to occur at the sampler tip.
 Rock is Soft Limerock Cemented with Sand.
 1 ft = 0.305 m; 1 kip = 4.45 kN; 1 in = 25.4 mm; 1 s/ft = 0.305 s/m; 1 lb = 4.45 N.

Table 7.2: Summary of the Smith Soil Constants for Vilano Bridge-East, Florida

Depth	Soil	Test	Measured	Ultimate	Quake	Damping	Acceleration	Analysis	Figure	Remarks
15	Toe	4*	0.45	0.040	0.030	0.60	Static	D.68	Before Compression Test. 30" Drop	
		4*	0.33	0.006	0.010	0.60	Dynamic		Before Compression Test. 30" Drop	
15	Shaft	2	0.45	0.100	0.100	0.50	Dynamic	D.69	Last Blow, Standard SPT. 30" Drop	
20	Toe	5*	0.72	0.170	0.010	0.40	Static	D.70	Before Compression Test. 30" Drop	
		5*	0.10	0.100	0.010	0.40	Dynamic		Before Compression Test. 30" Drop	
25	SP Toe	15*	1.60	0.130	0.160	0.45	Static	D.71	Before Compression Test. 30" Drop	
		15*	1.50	0.180	0.150	0.45	Dynamic		Before Compression Test. 30" Drop	
	Shaft	3	0.05	0.010	0.850	0.40	Dynamic	D.72	Before Uplift. 30" Drop	
30	Toe	16*	4.20	0.220	0.120	0.32	Static	D.73	Before Compression Test. 30" Drop	
		16*	3.50	0.300	0.250	0.32	Dynamic		Before Compression Test. 30" Drop	
	Shaft	14	0.45	0.040	2.000	0.40	Static	D.74	Before Uplift. 30" Drop	
		14	3.00	0.050	0.300	0.40	Dynamic		Before Uplift. 30" Drop	
0.76 kips on the shaft										
35	SP Toe	43*	7.30	0.300	0.120	0.62	Static	D.75	Before Compression Test. 30" Drop	
		43*	6.00	0.280	0.120	0.60	Dynamic		Before Compression Test. 30" Drop	
35	Shaft	9	No resistance in the uplift test				Static			
		9	3.5**	0.120	0.050	0.60	Dynamic	D.76	Before Uplift. 30" Drop	
No resistance at the shaft										
40	Toe	19*	8.70	0.300	0.280	0.33	Static	D.77	Before Compression Test. 30" Drop	
		19*	12.00	0.300	0.130	0.30	Dynamic		Before Compression Test. 30" Drop	

Notes: * Using special tip instead of the sampler.

** This resistance is at the sampler tip only.

1 ft = 0.305 m; 1 kip = 4.45 kN; 1 in = 25.4 mm; 1 s/ft = 0.305 s/m; 1 lb = 4.45 N.

Table 7.3: Summary of the Smith Soil Constants for Vilano Bridge-West, Florida

Depth [ft]	Soil Type	Test Type	Measured N-Value	Ultimate	Quake	Damping	Acceleration	Analysis Type	Figure Ref.	Remarks
				Resistance Ru [kips]	Q [in]	Constant J [s/ft]	Constant m [lbs]			
30	OH	Shaft	1	0.45	0.017	0.023	0.65	Static	D.78	Before Uplift. 30" Drop
				0.45	0.027	0.080	0.65	Dynamic		Before Uplift. 30" Drop
35		Shaft	1	0.50	0.012	0.650	0.20	Static	D.79	Before Uplift. 20" Drop
				2.00	0.050	0.100	0.20	Dynamic		Before Uplift. 20" Drop
			1	0.50	0.012	0.200	0.12	Static	D.80	After Uplift. 10" Drop.(1 hr BOR)
				0.50	0.020	0.200	0.12	Dynamic		After Uplift. 10" Drop.(1 hr BOR)
40		Toe	8*	0.15	0.010	0.500	0.70	Static	D.81	Before Compression Test. 10" Drop
				0.15	0.010	0.500	0.70	Dynamic		Before Compression Test. 10" Drop
42	OH	Shaft	1	0.25	0.020	0.700	0.50	Dynamic	D.82	Last Blow. 20" Drop
45	CH	Shaft	1	0.16	0.001	0.700	0.43	Static	D.83	Before Uplift. 20" Drop
				0.16	0.001	0.700	0.43	Dynamic		Before Uplift. 20" Drop
			1	0.31	0.001	0.500	0.50	Static	D.84	After Uplift. 10" Drop.(1 hr BOR)
				0.31	0.020	0.500	0.50	Dynamic		After Uplift. 10" Drop.(1 hr BOR)
50		Shaft	2	0.29	0.001	0.450	0.60	Static	D.85	Before Uplift. 20" Drop
				2	0.16	0.020	0.700	0.58		Dynamic
			2	0.65	0.010	0.800	0.48	Static	D.86	After Uplift. 4" Drop.(14 hrs BOR)
				0.90	0.015	0.500	0.55	Dynamic		After Uplift. 4" Drop.(14 hrs BOR)
52		Toe	2*	0.60	0.020	0.001	0.50	Static	D.88	Before Compression Test. 5" Drop
				0.20	0.001	0.500	0.55	Dynamic		Before Compression Test. 5" Drop
55	OH	Shaft	2	0.26	0.001	0.700	0.48	Static	D.89	Standard SPT. 20" Drop
				2	0.28	0.020	0.600	0.48		Dynamic
			2	0.57	0.010	0.550	0.35	Static	D.90	After Uplift. 4" Drop.(1 hr BOR)
				0.70	0.020	0.500	0.38	Dynamic		After Uplift. 4" Drop.(1 hr BOR)
59	OH	Shaft	1	0.33	0.010	0.250	0.40	Static	D.92	Standard SPT. 30" Drop
				1	0.33	0.010	0.250	0.40		Dynamic
			1	0.49	0.020	1.150	0.30	Static	D.93	After Uplift. 5" Drop.(1 hr BOR)
				0.90	0.023	0.350	0.40	Dynamic		After Uplift. 5" Drop.(1 hr BOR)
62		Toe	10*	1.95	0.080	0.200	0.22	Static	D.96	After Compression Test. 30" Drop
				2.30	0.110	0.150	0.22	Dynamic		After Compression Test. 30" Drop
64	ML	Shaft	8	0.53	0.067	0.300	0.18	Dynamic	D.97	Standard SPT. 30" Drop

Notes: * Using special tip instead of the sampler.
 1 ft = 0.305 m; 1 kip = 4.45 kN; 1 in = 25.4 mm; 1 s/ft = 0.305 s/m; 1 lb = 4.45 N.

Soil Type	Depth [ft]	SPT N-Value		STATIC			DYNAMIC		
		N	N ₆₀	Shaft, [kips/ft]		Toe [kips]	Shaft, [kips/ft]		Toe [kips]
				EOD	BOR		EOD	BOR	
SM	5	18	16	8.64	8.64	229	8.64	8.64	(229)
SM	10	4	4	(8.64)	(8.64)	53	(8.64)	(8.64)	(53)
	15	6	7	6.81	7.84	93	(5.73)	9.29	93
CH	20	4	4	(4.97)*	(7.03)	130	(6.65)	(9.94)	76
CH	25	4	4	4.53	7.50	130	(5.96)	7.64	76
CH	30	4	4	(4.58)*	(7.95)	130	(5.35)	(5.34)	76
MH	35	5	6	6.80	11.25	196	(5.35)	5.35	114
CL	40	7	8	9.06	15.00	261	(7.64)	7.64	151
	42	10**	8	7.06	12.00	(261)	6.21	6.21	(151)
CH	45	4	4	(4.05)*	7.50	130	(4.05)	4.05	(76)
	50	1	1	1.13	1.88	33	(3.06)	3.06	19
Soft	55	57	73	(0.00)	--	426	0.00	--	288
Limerock	60	45	54	0.00	--	315	0.00	--	213
cemented	63	66**	79	0.00	--	(382)	0.00	--	(258)
with sand	65	66	77	0.00	--	372	0.00	--	252
Total: Pile toe at 63 ft				296	416	382	310	348	258

Notes: * The average of these values was used to calculate the shaft resistance distribution.

** The special tip was not used here. Instead the sampler was plugged and driven for 6 in.

1 ft = 0.305 m; 1 kip/ft = 14.6 kN/m; 1 kip = 4.45 kN.

Values in parentheses were calculated from measurement at that depth; other values were calculated by prorating using N values.

Table 7.5: Vilano Bridge - East Embankment, Florida (PSC Pile 18 in Square)									
Soil Type	Depth [ft]	SPT N-Value		STATIC			DYNAMIC		
		N	N ₆₀	Shaft, [kips/ft]		Toe [kips]	Shaft, [kips/ft]		Toe (kips)
				EOD	BOR		EOD	BOR	
SP	5	4	4	0.81	--	60	0.54	--	44
	10	3	3	0.60	--	45	0.40	--	33
	15	2	2	0.40	--	(30)	0.26	--	(22)
	20	5*	4	0.81	--	(47)	0.54	--	(7)
SP	25	3	3	0.60	--	(106)	(0.40)	--	(100)
	30	14	17	(3.44)	--	(278)	(5.78)	--	(231)
SP	35	9	12	(0.00)	--	(482)	(0.00)	--	(396)
Total: Pile toe at 35 ft				34	--	482	40	--	396

Table 7.6: Vilano Bridge - West Embankment, Florida (PSC Pile 18 in Square)									
Soil Type	Depth [ft]	SPT N-Value		STATIC			DYNAMIC		
		N	N ₆₀	Shaft, [kips/ft]		Toe [kips]	Shaft, [kips/ft]		Toe [kips]
				EOD	BOR		EOD	BOR	
OH	30	1	1	(3.44)	3.44	10	(3.44)	3.44	10
	35	1	1	(3.82)	(3.82)	10	(3.82)	(3.82)	10
	40	8*	8	1.96	2.78	(10)	2.45	2.78	(10)
OH	42	1	1	1.22	2.37	10	(1.91)	2.37	10
CH	45	1	1	(1.22)	(2.37)	10	(1.22)	(2.37)	10
	50	2	2	(2.29)	(4.97)	40	2.44	(6.88)	14
	52	2*	2	2.26	4.66	(40)	2.36	6.65	(14)
OH	55	2	2	(1.98)	(4.35)	40	(2.14)	(5.35)	14
OH	59	1	1	(2.52)	(3.75)	40	(2.52)	(6.88)	14
	62	10*	10	7.80	15.29	(129)	3.44	9.28	(152)
ML	64	8	10	11.32	22.16		(4.05)	10.93	
Total: Pile toe at 62 ft.				97	143	129	91	159	152

Notes: (for tables 7.5 and 7.6).

* Using special tip instead of sampler.

1 ft = 0.305 m; 1 kip/ft = 14.6 kN/m; 1 kip = 4.45 kN.

Values in parentheses were calculated from measurement at that depth; other values were calculated by prorating using N values.

Columns 1 and 2 show depth and soil type, respectively. The SPT N-value and the N-value adjusted for 60 percent SPT energy (N_{60}) are presented in columns 3 and 4, respectively (see also chapter 5 and appendix E). The calculated capacity, based on the Modified SPT uplift and compression tests are presented in columns 5 through 7. Using the "Modified SPT DYNAMIC" analyses, capacity results are presented in the last three columns, 8 through 10 (see also chapter 6). These calculated results include the unit shaft resistance at EOD and BOR, and the toe resistance at each depth. The last row in each table indicates the final pile toe depth, the total pile capacity, the total pile shaft resistance and the pile toe resistance at final toe depth. Additional comments on the pile capacity calculations follow.

7.3.1 Aucilla River Bridge, Florida

Reference is made to tables 7.1 and 7.4. The soil was divided into three layers: from the top to 15 ft (4.6 m), from 15 to 50 ft (4.6 to 15.2 m), and from 50 ft (15.2 m) to the final depth of 65 ft (19.8 m). In the third layer, the soil consisted of soft limerock cemented with sand. An uplift test was performed at 55 ft (16.8 m) and showed no resistance; therefore, the shaft resistance within this third layer was assumed to be zero. The toe resistance in the limerock was obtained from the compression test performed at 63 ft (19.2 m).

In the middle layer, three uplift tests were performed at 20, 30 and 45 ft (6.1, 9.1 and 13.7 m). The SPT N-values at these depths were all equal to 4, and similarly the calculated shaft resistance values were close to each other. An average value was, therefore, used to calculate the unit shaft resistance distribution at other depths within this second layer. The toe resistance within the middle layer was calculated based on the value obtained from the Modified SPT compression test at 42 ft (12.8 m).

The unit shaft resistance distribution in the top layer was calculated based on the uplift test results at 10 ft (3.1 m). The relatively high SPT N-value of 18 at 5 ft (1.5 m) and the correspondingly high capacity obtained from dynamic matching were attributed to resistance at the sampler tip. Therefore, the shaft resistance at this depth was assumed to be the same as that obtained from the uplift test at 10 ft (3.1 m), and the difference in total capacity was used to calculate the unit end bearing within this layer.

The "Modified SPT STATIC" analysis at EOD gave a total capacity of 678 kips (3 017 kN) with 382 kips (1 699 kN) toe resistance. Setup tests were performed at 20 and 30 ft (6.1 and 9.1 m), and the results showed a BOR shaft resistance of 416 kips (1 847 kN) for a total capacity of 798 kips (3 543 kN). This yields an overall soil setup factor of 1.18. If the correction factors of 1.66 and 1.90 (see chapter 6) were applied to the shaft resistance from the BOR, the total capacity would range from 1,073 to 1,173 kips (4 764 and 5 208 kN). The "Modified SPT DYNAMIC" analysis yielded somewhat lower toe resistance values. The EOD total capacity of 568 kips

(2 522 kN) was calculated with 258 kips (1 146 kN) toe resistance. At BOR, the shaft resistance increased by 38 kips (170 kN), indicating a setup factor of 1.12.

In addition to the Modified SPT capacity calculations, the pile capacity was also calculated from the CPT results, and from the SPT N-value using the static formula calculations method discussed by Vanikar (1986). The total capacity based on the CPT results was 980 kips (4 359 kN) with 153 kips (679 kN) shaft resistance and 826 kips (3 667 kN) toe resistance. The static formula calculations gave a total capacity of 850 kips (3 774 kN) with 703 kips (3 121 kN) toe resistance. Table 7.7 summarizes all results.

7.3.2 Vilano Bridge - East Embankment, Florida

At this site, two uplift tests were performed at depths of 30 and 35 ft (9.1 and 10.7 m). The Modified SPT test performed at 35 ft (10.7 m) showed no measurable uplift resistance, therefore the uplift results from 30 ft (9.1 m) were used to determine the unit shaft resistance distribution. Setup tests performed at this site did not indicate any gain in shaft resistance. The final pile penetration was 35 ft (10.7 m). The capacity calculations based on table 7.2 are presented in table 7.5.

The "Modified SPT STATIC" analysis produced a total capacity of 516 kips (2 291 kN) with 482 kips (2 140 kN) toe resistance. Factoring the shaft resistance with the correction factor range as for the Aucilla site (1.66 and 1.90) would yield an average total capacity prediction of 540 kips (2 403 kN). The "Modified SPT DYNAMIC" analysis again predicted slightly less: 436 kips (1 936 kN) total capacity with 396 kips (1 758 kN) toe resistance.

As listed in table 7.7, the pile capacity calculation using the CPT results indicated a capacity of 794 kips (3 525 kN) with 126 kips (559 kN) shaft resistance and 668 kips (2 966 kN) toe resistance. The pile capacity based on static formula calculations indicated a total capacity of 221 kips (981 kN) with 113 kips (502 kN) toe resistance.

7.3.3 Vilano Bridge - West Embankment, Florida

The pile at this site had not been driven when the Modified SPT tests were performed. We were advised that the top 25 ft (7.6 m) would be predrilled and that the pile would be driven from 25 ft (7.6 m) to a final pile penetration of 62 ft (18.9 m). Three Modified SPT compression tests and six uplift tests were performed at the future pile driving location. The capacity calculations are presented in table 7.6.

The "Modified SPT STATIC" analysis gave a total pile capacity at EOD of 226 kips (1 003 kN) with 129 kips (573 kN) toe resistance; at BOR the shaft resistance increased from 97 kips (431 kN) to 143 kips (635 kN) for a total capacity of 272 kips (1 208 kN). Thus, the overall predicted setup factor was 1.2. Applying the same correction factors as before (1.66 and 1.90) would yield a capacity range from 366 to 400 kips (1 625 to 1 776 kN). The "Modified SPT DYNAMIC" analysis gave total EOD and BOR capacities of 243 and 311 kips (1 079 and 1 381 kN), and 152 kips (675 kN) toe resistance. In this case, the projected overall setup factor was 1.28. Other capacity predictions (shown in table 7.7) were 283 kips (1 259 kN) for CPT and 136 kips for the static formula calculations.

7.3.4 Discussion of Pile Capacity Prediction

The "Modified SPT STATIC" analysis gave higher capacities at Aucilla and Vilano-East, but lower at Vilano-West when compared to the "Modified SPT DYNAMIC" capacities. While, in general, Modified SPT and CPT yielded similar results, for Vilano-East, the differences were quite significant. At Aucilla and Vilano-West, the total capacities determined from the CPT analysis are comparable to that determined from the Modified SPT. However, shaft resistance and toe resistance component differed by large amounts. The pile capacity based on the static formula calculation (Static Calc.) gave capacities that were quite different from both Modified SPT and CPT.

7.4 DRIVEABILITY ANALYSIS AND BEARING GRAPHS

The soil resistance distribution and the Smith's soil constants calculated earlier were used to perform the driveability and bearing graph analysis. A total of seven driveability and seven bearing graph analyses were performed. The seven analyses consisted of three analyses each using the soil resistance distribution calculated from the "Modified SPT STATIC" and "Modified SPT DYNAMIC" analysis, and one analysis using the soil resistance distribution from static formula calculations which is identified as STD (FHWA). Three analyses using the "Modified SPT STATIC" soil resistance were performed with the following dynamic soil constants: first, standard Smith's soil constants, (STD-ST); second, Smith's soil constants evaluated from the "dynamic" analysis of the Modified SPT data, (SPT-ST); and third, standard Smith's quake and shaft damping and a reduced toe damping factor of 0.01 s/ft (0.03 s/m), (MDF-ST). Three analyses using the "Modified SPT DYNAMIC" soil resistance were also performed with the Smith's soil constants discussed above. The results were identified as STD-DYN, SPT-DYN, and MDF-DYN. Detailed descriptions of these analyses were given in chapter 6. The GRLWEAP soil layer resistance values with Modified SPT dynamic soil parameters are presented in tables 7.8 through 7.10.

Table 7.7: Summary of the Capacity Calculation						
Site & Pile Type	Method	Status	Shaft [kips]	Toe [kips]	Total [kips]	Remarks
Aucilla 18 in Square PSC	Modified SPT	EOD	296	382	678	STATIC
		BOR	416	382	798	STATIC
	Static Calc. CPT	EOD	310	258	568	DYNAMIC
		BOR	348	258	606	DYNAMIC
			147	703	850	
			153	826	980	
Vilano-East 18 in Square PSC	Modified SPT	EOD	34	482	516	STATIC
		BOR	--	--	--	STATIC
	Static Calc. CPT	EOD	40	396	436	DYNAMIC
		BOR	--	--	--	DYNAMIC
			108	113	221	
			126	668	794	
Vilano-West 18 in Square PSC	Modified SPT	EOD	97	129	226	STATIC
		BOR	143	129	272	STATIC
	Static Calc. CPT	EOD	91	152	243	DYNAMIC
		BOR	159	152	311	DYNAMIC
			68	68	136	
			105	178	283	

Note : 1 kip = 4.45 kN.

Table 7.8: Resistance Distribution and Dynamic Parameters for Driveability Analyses of Aucilla River Bridge, Florida

Depth (ft)	Skin Friction (k/ft)	End Bearing (kips)	Skin Quake (in)	Toe Quake (in)	Skin Damping (s/ft)	Toe Damping (s/ft)	Sens.
5.00	8.640	229.000	.006	.070	.230	.010	1.000
10.00	8.640	53.000	.006	.070	.230	.010	1.000
15.00	6.810	93.000	.005	.070	.300	.010	1.000
20.00	4.970	130.000	.005	.070	.300	.010	1.000
25.00	4.530	130.000	.010	.070	.150	.010	1.000
30.00	4.580	130.000	.010	.070	.150	.010	1.000
35.00	6.800	196.000	.010	.070	.150	.010	1.000
40.00	9.060	261.000	.020	.070	.190	.010	1.000
45.00	4.050	130.000	.020	.070	.190	.010	1.000
50.00	1.130	33.000	.020	.070	.190	.010	1.000

a) STATICALLY CALCULATED

Depth (ft)	Skin Friction (k/ft)	End Bearing (kips)	Skin Quake (in)	Toe Quake (in)	Skin Damping (s/ft)	Toe Damping (s/ft)	Sens.
5.00	8.640	229.000	.020	.040	.100	.120	1.000
10.00	8.640	53.000	.056	.040	.250	.120	1.000
15.00	5.730	93.000	.035	.040	.300	.120	1.000
20.00	6.650	76.000	.030	.040	.250	.120	1.000
25.00	5.960	76.000	.045	.040	.120	.120	1.000
30.00	5.350	76.000	.030	.040	.100	.120	1.000
35.00	5.350	114.000	.050	.040	.130	.120	1.000
40.00	7.640	151.000	.013	.040	.150	.120	1.000
45.00	4.050	76.000	.060	.040	.190	.120	1.000
50.00	3.060	19.000	.025	.047	.150	.100	1.000

b) DYNAMICALLY CALCULATED

Notes: 1 ft = 0.305 m; 1 kip/ft = 14.6 kN/m; 1 kip = 4.45 kN; 1 in = 25.4 mm; 1 s/ft = 3.28 s/m.

Table 7.9: Resistance Distribution and Dynamic Parameters for Driveability Analyses of Vilano Bridge - East Embankment, Florida

Depth (ft)	Skin Friction (k/ft)	End Bearing (kips)	Skin Quake (in)	Toe Quake (in)	Skin Damping (s/ft)	Toe Damping (s/ft)	Sens.
5.00	.810	60.000	.100	.040	.100	.030	1.000
10.00	.600	45.000	.100	.040	.100	.030	1.000
15.00	.400	30.000	.100	.040	.100	.030	1.000
20.00	.810	47.000	.100	.170	.100	.010	1.000
25.00	.600	106.000	.100	.130	.100	.160	1.000
30.00	3.440	278.000	.100	.220	.100	.120	1.000

a) STATICALLY CALCULATED

Depth (ft)	Skin Friction (k/ft)	End Bearing (kips)	Skin Quake (in)	Toe Quake (in)	Skin Damping (s/ft)	Toe Damping (s/ft)	Sens.
5.00	.540	44.000	.100	.006	.050	.010	1.000
10.00	.400	33.000	.100	.006	.050	.010	1.000
15.00	.260	22.000	.100	.006	.050	.010	1.000
20.00	.540	7.000	.100	.100	.050	.010	1.000
25.00	.400	100.000	.100	.180	.050	.150	1.000
30.00	5.780	231.000	.100	.300	.050	.250	1.000

b) DYNAMICALLY CALCULATED

Notes: 1 ft = 0.305 m; 1 kip/ft = 14.6 kN/m; 1 kip = 4.45 kN; 1 in = 25.4 mm; 1 s/ft = 3.28 s/m.

Table 7.10: Resistance Distribution and Dynamic Parameters for Driveability Analyses of Vilano Bridge - West Embankment, Florida

Depth (ft)	Skin Friction (k/ft)	End Bearing (kips)	Skin Quake (in)	Toe Quake (in)	Skin Damping (s/ft)	Toe Damping (s/ft)	Sens.
30.00	3.440	10.000	.017	.010	.023	.500	1.000
35.00	3.820	10.000	.012	.010	.200	.500	1.000
42.00	1.220	10.000	.001	.020	.500	.001	1.000
45.00	1.220	10.000	.001	.020	.500	.001	1.000
50.00	2.290	40.000	.010	.020	.800	.001	1.000
55.00	1.980	40.000	.010	.020	.550	.001	1.000
59.00	2.520	40.000	.020	.020	.600	.001	1.000
62.00	7.800	129.000	.020	.080	.600	.200	1.000

a) STATICALLY CALCULATED

Depth (ft)	Skin Friction (k/ft)	End Bearing (kips)	Skin Quake (in)	Toe Quake (in)	Skin Damping (s/ft)	Toe Damping (s/ft)	Sens.
30.00	3.440	10.000	.025	.010	.035	.500	1.000
35.00	3.820	10.000	.020	.010	.200	.500	1.000
42.00	1.910	10.000	.020	.010	.700	.500	1.000
45.00	1.220	10.000	.020	.010	.500	.500	1.000
50.00	2.440	14.000	.015	.010	.500	.500	1.000
55.00	2.140	14.000	.010	.001	.400	.500	1.000
59.00	2.520	14.000	.023	.001	.350	.500	1.000
62.00	3.440	152.000	.023	.110	.350	.150	1.000

b) DYNAMICALLY CALCULATED

Notes: 1 ft = 0.305 m; 1 kip/ft = 14.6 kN/m; 1 kip = 4.45 kN; 1 in = 25.4 mm; 1 s/ft = 3.28 s/m.

The standard Smith model was still used because: first, the exponential damping law was found unnecessary; second, no information for full-scale pile plug masses was available; third, a toe gap was not indicated by the Modified SPT results; and finally, the hyperbolic toe resistance model and radiation damping, both yielded unreliable blow count results.

At Aucilla, the hammer was a Fairchild F-32 with a ram weight of 10.85 kips (48.3 kN), a manufacturer's rated energy of 32.55 kip-ft (44.1 kN-m) and a maximum rated stroke of 3.0 ft (0.91 m). The helmet weight was 1.5 kips (6.7 kN), and the hammer cushion consisted of 5 in (127 mm) of blue polymer with a reported area of 235.6 in² (0.15 m²). The pile cushion consisted of 6 in (152 mm) of plywood. An Osterberg Cell, installed at the pile toe, consisted of two 18-in (457-mm) square steel plates with a total thickness of 1 ft (0.305 m). Because of the Osterberg cell, the pile was modeled nonuniformly with the last foot consisting of steel rather than concrete. The driveability analysis results are presented in appendix A; calculated blow counts are included in table 7.11 and figure 7.4. Since the measured transferred energies are not available to us, no adjustment to the efficiency could be made. In addition to the driveability analyses, bearing graphs were generated for each of the corresponding analysis discussed above (figure 7.1 and table 7.14). These values can be used together with actual blow counts for capacity calculation.

At Vilano - East the hammer was a Delmag D 46-23 with a manufacturer's rated energy of 107.18 kip-ft (145.2 kN-m). The helmet weight was 5.62 kips (25 kN) and the hammer cushion consisted of 2 in (51 mm) of micarta and 1.5 in (38 mm) of aluminum. The hammer cushion area was reported to be 241 in² (0.15 m²). The pile cushion consisted of 9.75 in (248 mm) of plywood. The hammer setting (HS) was reported to be as follows: from zero to 22.7 ft (7 m) penetration HS=2, from 22.7 to 28.2 ft (7 to 8.6 m) HS=3, from 28.2 to 31.6 ft (8.6 to 9.6 m) HS=4, and from 31.6 to 35 ft (9.6 to 10.7 m) HS=3. The driveability analysis results and the bearing graph results are presented in tabular and graphical form in appendix A. Summaries of the driveability analysis and the bearing graphs are presented in figures 7.5 and 7.2, and tables 7.12 and 7.15, respectively.

The driving system at Vilano - West was assumed to be the same as that at Vilano-East with no adjustment to the hammer setting. The results are also presented in appendix A, tables 7.13 and 7.16 and figures 7.3 and 7.6.

Table 7.11: Blow Count Prediction for Aucilla River Bridge, Florida							
Depth [ft]	Blow Count, [BPF]						
	STD-ST	STD-DYN	SPT-ST	SPT-DYN	MDF-ST	MDF-DYN	STD (FHWA)
5	32	32	20	27	21	21	5
10	12	12	11	11	10	10	4
15	23	22	20	21	19	19	5
20	34	25	30	25	28	21	5
25	37	31	34	30	33	27	6
30	41	35	37	33	36	32	8
35	62	46	49	41	51	41	11
40	101	61	73	53	78	53	14
45	64	51	55	46	57	47	16
50	45	43	43	41	44	43	17
55	770	202	434	150	388	144	1193
60	257	123	210	99	172	97	160
63	574	177	369	191	321	130	9999

Table 7.12: Blow Count Prediction for Vilano Bridge - East Embankment, Florida							
Depth [ft]	Blow Count, [BPF]						
	STD-ST	STD-DYN	SPT-ST	SPT-DYN	MDF-ST	MDF-DYN	STD (FHWA)
5	2	0	2	0	0	0	0
10	2	2	2	0	2	0	0
15	2	0	0	0	1	0	2
20	2	0	2	0	2	0	3
25	5	4	5	4	3	2	4
30	18	14	17	19	10	8	7
35	40	31	42	31	25	20	11

Notes: 1 ft = 0.305 m; 1 blow per foot (BPF) = 3.3 blow per m (BPM).

Table 7.13: Blow Count Prediction for Vilano Bridge - West Embankment, Florida							
Depth [ft]	Blow Count, [BPF]						
	STD-ST	STD-DYN	SPT-ST	SPT-DYN	MDF-ST	MDF-DYN	STD (FHWA)
30	2	2	2	2	2	2	2
35	3	3	3	3	3	3	2
40	4	4	3	4	4	4	2
45	4	4	4	5	4	4	3
50	7	5	6	7	5	6	3
55	8	6	7	8	6	7	3
60	11	10	11	14	9	9	5
62	18	20	20	21	15	14	8

Table 7.14: Bearing Graph Prediction for Aucilla River Bridge, Florida							
Ultimate Capacity [kips]	Blow Count, [BPF]						
	STD-ST	STD-DYN	SPT-ST	SPT-DYN	MDF-ST	MDF-DYN	STD (FHWA)
100	13	13	11	12	11	11	13
300	46	46	36	41	39	40	45
400	71	70	51	61	57	60	69
500	124	123	80	102	93	99	114
600	290	286	158	231	194	212	223
700	1215	1183	584	1929	565	636	689
800	9999	9999	9999	9999	9999	9999	9999

Notes: 1 kip = 4.45 kN; 1 blow per foot (BPF) = 3.3 blows per m (BPM).

Ultimate Capacity [kips]	Blow Count, [BPF]						
	STD-ST	STD-DYN	SPT-ST	SPT-DYN	MDF-ST	MDF-DYN	STD (FHWA)
100	5	5	5	5	3	3	5
200	12	12	12	12	7	7	12
300	21	21	22	21	12	13	21
400	29	29	29	29	19	19	29
500	39	39	40	39	24	25	39
550	46	45	46	45	28	28	46
600	54	53	55	53	31	31	54
650	62	61	63	61	35	35	62
700	73	73	75	73	40	40	73
750	87	87	90	87	45	45	87
800	99	98	102	98	49	49	98
900	153	153	160	153	66	69	152
1000	241	238	258	238	87	90	236
1100	497	489	554	489	126	142	481
1200	2159	2084	3118	2084	219	216	1935
1250	9999	9999	9999	9999	276	309	8819
1300					430	617	
1350					770	1255	
1400					9999	3919	

Notes: 1 kip = 4.45 kN; 1 blow per foot (BPF) = 3.3 blows per m (BPM).

Table 7.16: Bearing Graph Prediction for Vilano Bridge - West Embankment, Florida							
Ultimate Capacity [kips]	Blow Count, [BPF]						
	STD-ST	STD-DYN	SPT-ST	SPT-DYN	MDF-ST	MDF-DYN	STD (FHWA)
100	5	5	4	5	4	4	5
200	12	12	9	12	10	10	12
250	18	18	13	18	13	14	18
300	22	22	18	22	19	19	22
350	25	25	21	25	22	22	26
400	30	30	24	29	25	25	30
450	34	34	27	34	28	29	35
500	40	40	30	40	32	33	41
550	46	46	34	46	37	38	47
600	55	55	39	55	43	44	56
700	80	81	51	81	60	63	85
800	132	135	72	135	94	100	146
900	265	280	105	280	167	200	322
950	432	469	130	469	245	295	567
1000	812	923	169	923	406	502	1371
1050	3764	7171	235	7171	774	1086	9999
1100	9999	9999	356	9999	3800	9999	
1150			587		9999		
1200			1235				
1250			9999				

Notes: 1 kip = 4.45 kN; 1 blow per foot (BPF) = 3.3 blows per m (BPM).

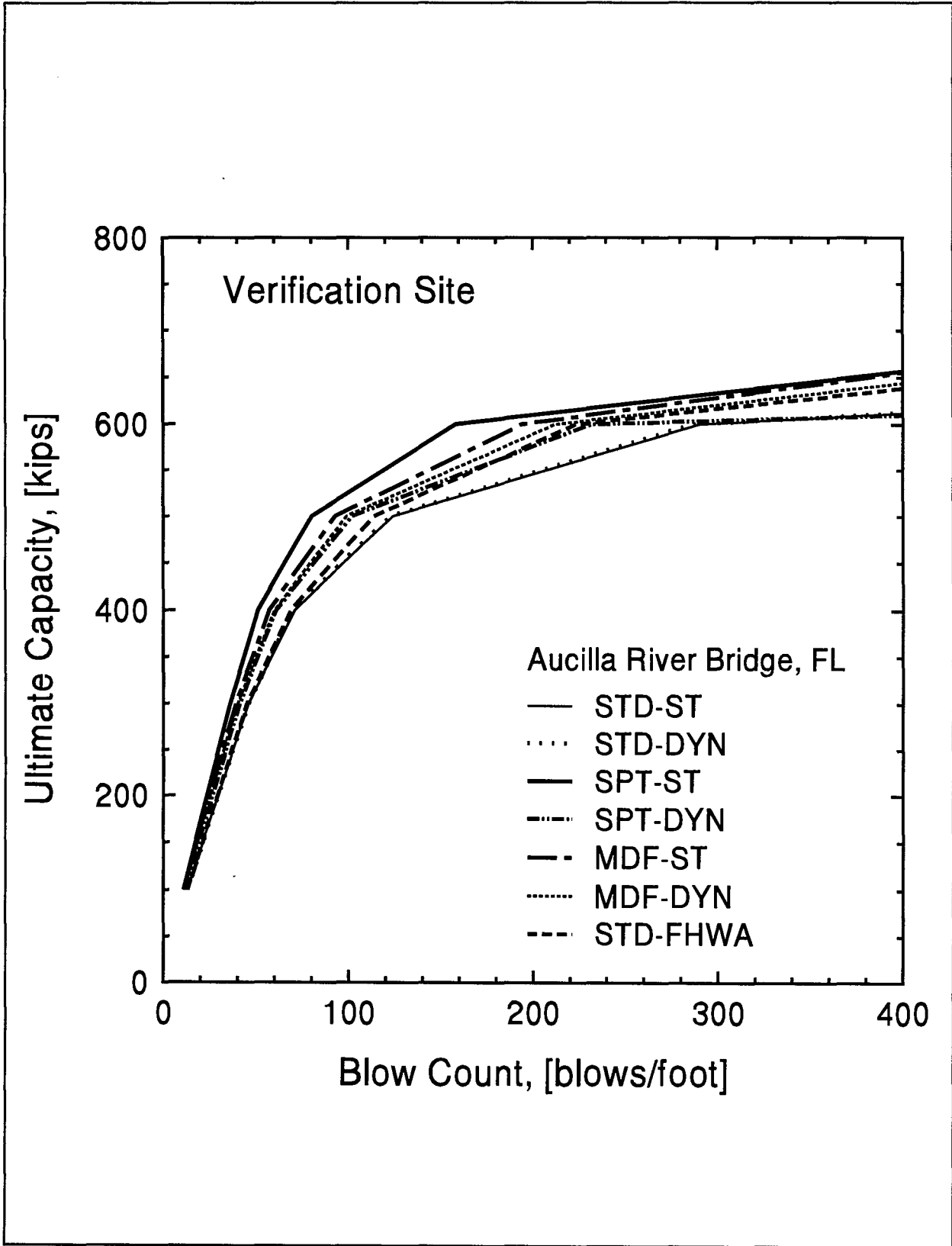


Figure 7.1: Bearing Graph for Aucilla River Bridge, FL from Various Analysis Methods

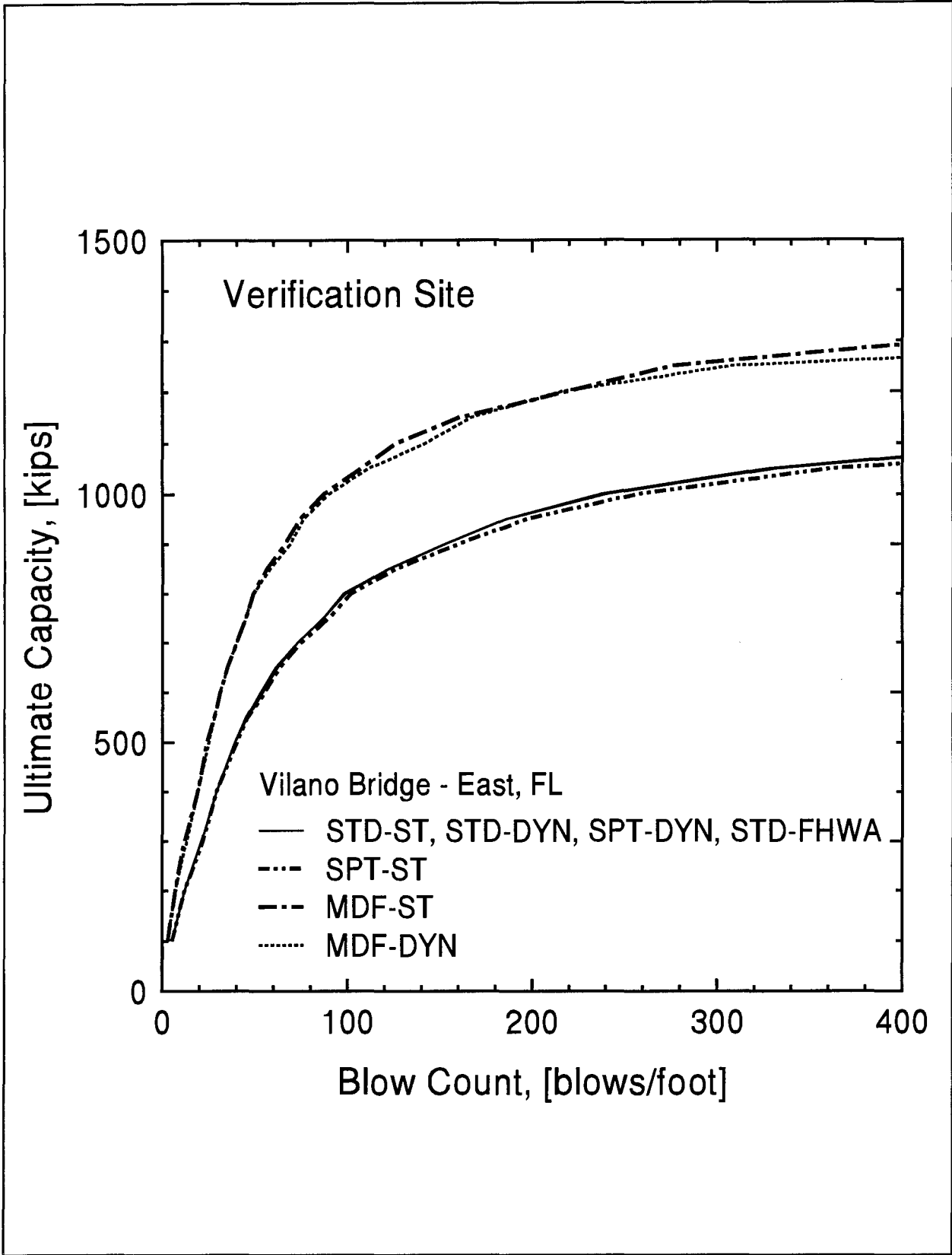


Figure 7.2: Bearing Graph for Vilano Bridge - East, FL from Various Analysis Methods

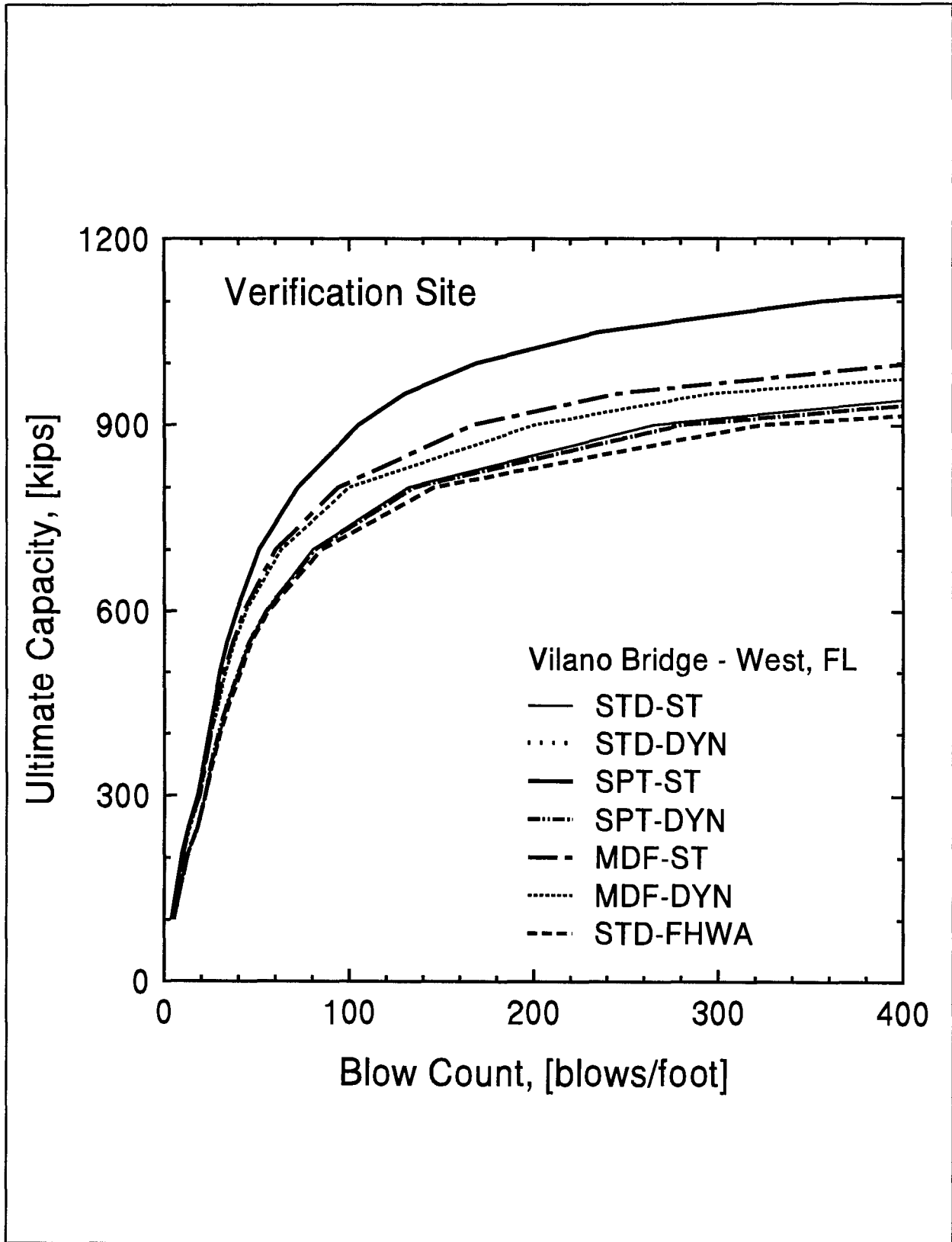


Figure 7.3: Bearing Graph for Vilano Bridge - West, FL from Various Analysis Methods

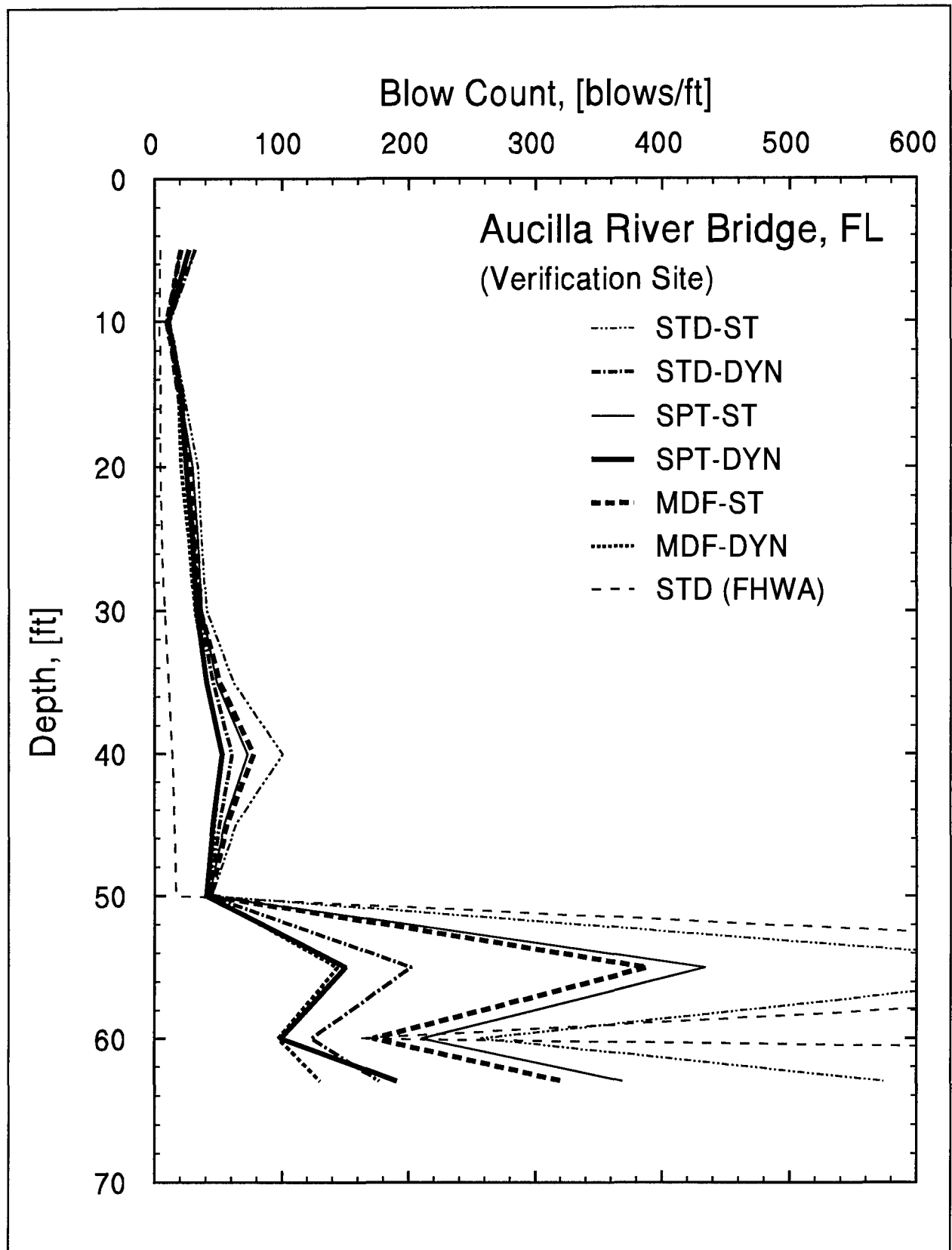


Figure 7.4: Driveability Graph for Aucilla River Bridge, FL from Various Analysis Methods

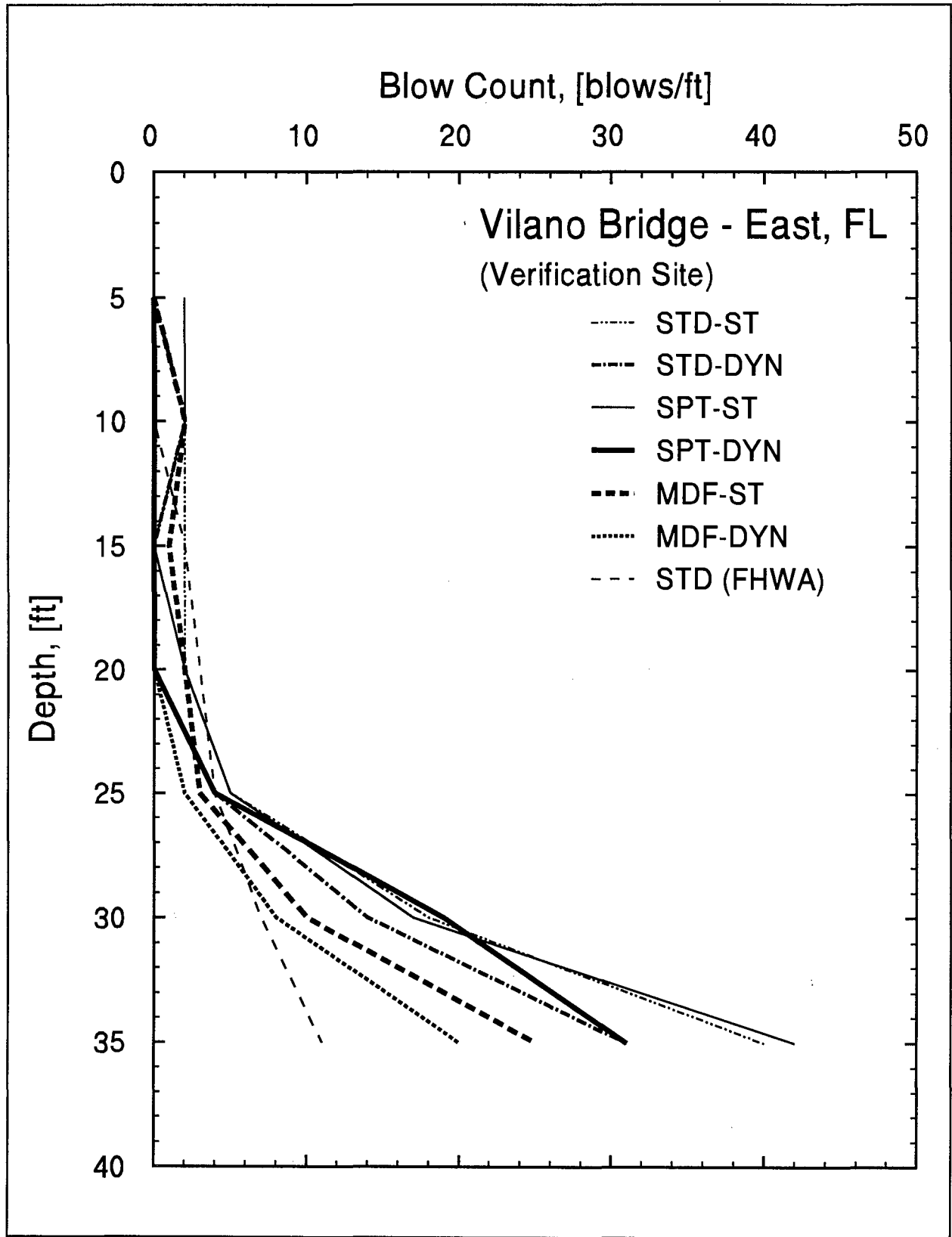


Figure 7.5: Driveability Graph for Vilano Bridge -East, FL from Various Analysis Methods

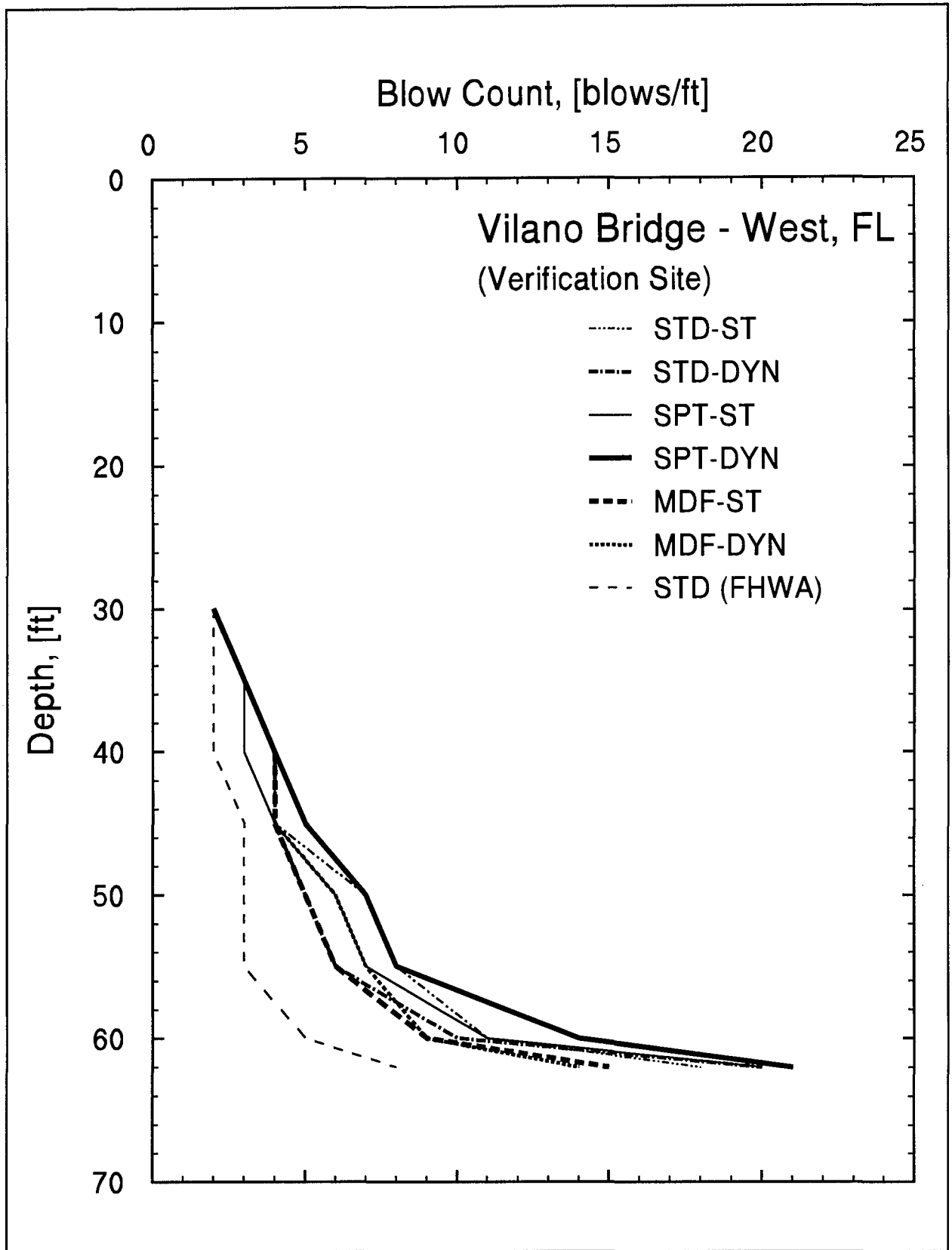


Figure 7.6: Driveability Graph for Vilano Bridge - West, FL from Various Analysis Methods

CHAPTER 8

CONCLUSIONS

The studies described in this report have yielded several important factual results and an improved understanding of the dynamics of the pile-soil interaction. Furthermore, this work has yielded several tangible results, including a literature review, a data base, a set of equipment and a procedure for retrieving static and dynamic soil parameters from standard penetration tests, an enhancement of the GRLWEAP soil model, and other software for data collection and analysis. The following summary presents conclusions on major achievements.

8.1 THE WAVE EQUATION MODEL

The literature does contain several suggestions for a more rational soil model for wave equation analysis. Several recommended model features were incorporated in the wave equation analysis program, GRLWEAP, during the course of this research project; rational, additional soil parameters to be used in the wave equation approach would include the CAPWAP model parameters which are essential for signal matching, among them primarily the toe parameters plug and gap and, in addition, hyperbolic load-set relationship. Making the soil models of the widely used CAPWAP and GRLWEAP programs more similar will hopefully lead to a better agreement between both approaches.

To date new soil model features have not produced any clear improvements over the traditional approach. However, there are clear improvements associated with allowing unit shaft resistance to be an input value, such as reducing data preparation effort and simplifying driveability analyses. This has been added to GRLWEAP, and as a consequence it is, of course, necessary to introduce pile circumference into the wave equation approach for the calculation of ultimate resistance forces. This approach clearly is not only advantageous to the inexperienced user who usually does not understand how the wave equation analysis can function without pile size as an input quantity, but also allows for a more realistic analysis of non-uniform piles. With pile size available, dynamic soil parameters like quakes can be automatically calculated. Further efforts towards simplifying the data input effort would eventually allow for a combined static and dynamic analysis of raw soil data, and yield both static load-set curve and bearing graph, or blow counts and driving stresses versus depth.

8.2 THE DATA BASE

A data base of more than 150 statically and dynamically tested piles was generated of which almost 100 cases met strict requirements of completeness. It was concluded that because of these strict requirements the data base was not necessarily a statistically representative sample of the average foundation pile.

The data base cases used for a variety of correlation studies clearly show that end of driving wave equation analyses typically underpredict. However, restrike based capacity predictions tend to have a greater variance even though their means are closer to the load test capacity.

The data base was also used to correlate CAPWAP results, which clearly demonstrated that a major error source of dynamically calculated results is the time difference between static and dynamic test. This work resulted in a recommendation for radiation damping model parameters.

8.3 DYNAMIC SOIL PARAMETERS

The literature study did contain various recommendations for dynamic soil parameters for the standard Smith soil model. In general, these recommendations did not differ much from those currently used.

Smith type dynamic soil resistance parameters, in particular damping factors, were also back calculated from the data base cases. Of course, since an accurate bearing capacity value was only known for the time when restrike dynamic data was taken after comparable waiting times, these calculated dynamic parameters pertained to restrike situations for which uncertainties about blow count and corresponding hammer energy level made the correlation work somewhat unreliable. There also seemed to be other reasons why the resulting damping factors displayed significant scatter. For example, for the same test piles with several restrikes, earlier restrike tests produced lower damping factors than later restrikes. It is, therefore, safe to assume that grain size distribution is an insufficient soil type identifier for dynamic soil parameter assessment.

The variability of restrike soil damping values obtained from back calculation by wave equation was similar to that determined by CAPWAP best match analyses.

In addition to damping, apparent setup factors were calculated from end of driving wave equation analyses. These factors, applied to end of driving bearing capacity predictions, would yield an estimate of long-term capacity values and therefore eliminated the need for restrike tests. Reverse, for driveability the statically calculated bearing capacity may be divided by the setup factor to yield the static resistance component during driving.

8.4 THE MODIFIED SPT

Clearly the greatest effort in this study was devoted to (a) the development and first application of test equipment for the Modified SPT, (b) to the performance of this test, and (c) to the calculation of static and dynamic resistance parameters for both SPT and full-scale piles based on the Modified SPT results.

On 10 sites, tests were performed with the Modified SPT. On six sites, static load test piles had prior been installed and tested. On three sites, static and dynamic tests were to be performed later. One test site was abandoned.

The Modified SPT included both static and dynamic measurements during and after the standard sampler driving without affecting the N-values measured. The dynamic measurements included hammer impact velocity, drill rod top force and velocity during sampler driving and during driving of the rod with a special tip. The sampler was statically uplift tested at various extraction rates and after a variety of waiting times. Additional shaft unit resistance values were calculated from torque tests. The special tip equipped rod was also statically compression tested yielding load-displacement curves.

It was concluded that a flat end tip would produce results better comparable with full-scale pile toe behavior than cone tips which had a lower end bearing and quake.

It was concluded that the simple torque test gave unit shaft resistance values which agreed well with those from uplift. Thus, the Modified SPT can be simplified if vertical set information is not needed.

It was also concluded that the unit end bearing could be determined from the toe resistance of the sampler; therefore, the special tip test might be replaced with a compression test on the sampler itself. This is especially true in those frequent cases where shaft resistance is negligible compared to the sampler end bearing. It was also found that the dynamic measurements generally yielded reliable toe or shaft resistance values compared to the static shaft or special tip measurements.

Shaft resistance values were usually low and did not allow for rate effect measurements that could be clearly distinguished from setup or other effects. However, where dynamic or static rate effects could be measured, calculation of the apparent exponent approximately yielded unity which suggests that the original Smith damping approach was satisfactory. It is felt that the exponential damping law of the literature has only very limited practical applications.

Static unit toe resistance, both from sampler bottom and a special tip, showed good correlation with full-scale test piles. For the shaft, for which both uplift and torque tests were performed, correction factors up to 1.9 had to be applied to the sampler shaft unit resistance to yield agreement with full-scale pile unit shaft resistance. Reasons for this correction might be a disturbed soil near the upper part of the sampler and a lower densification around the sampler compared to a large displacement pile. Granular soils required larger corrections than fine grained soils.

Static values calculated from "dynamic" analysis on the Modified SPT records showed good agreement with static values obtained from static uplift or compression tests performed with the Modified SPT, and with full-scale test pile results.

The Modified SPT indicated relatively low toe damping factors in clay, e.g., $J_t = 0.03$ s/ft (.1 s/m), for what was considered a driving situation (in contrast to restriking). Such low factors indeed yielded realistic blow counts for the full-scale piles analyzed. Furthermore, low toe damping factors when applied to bearing capacity calculations would yield higher and therefore, on average, better EOD bearing capacity predictions. For granular soils, no clear trends for improved toe damping was observed.

The flat end tip indicated a very realistic post failure strain hardening behavior in granular soils. This information could be used for better load-set predictions and more economical failure criteria definitions.

Large quake sites can be identified from either static or dynamic Modified SPT measurements. For the two sites, White City and Portland, that had indicated large full-scale pile toe quakes, the Modified SPT also indicated relatively high quakes.

The Modified SPT results indicated that GRLWEAP suggested shaft soil parameters are satisfactory for **end of driving** situations. These values are Smith shaft damping factors of 0.2 s/ft (0.66 s/m) for cohesive soils and 0.05 s/ft (0.16 s/m) for non-cohesive soils, and shaft quakes of 0.1 in (2.5 mm). Admittedly, however, since sampler friction was always relatively low, the data had insufficient resolution and therefore not accurately assessed.

For restrike situations, a much greater variation in both shaft and toe damping must be expected. For example, tests in soft clays indicated very high restrike damping factors.

As for the Modified SPT procedure itself, it was, of course, more time consuming than normal SPT operations. However, since torque measurements can replace the uplift test and since dynamic measurements can replace the special tip static compression test, a significant improvement in the economy of the Modified SPT is possible without loss of major test benefits.

CHAPTER 9

RECOMMENDATIONS

The methods employed and/or developed during this project are promising and should be further developed and refined for improved prediction methods on pile behavior. In particular, the following additional work is recommended for the data base:

1. Further expand the data base including also cases which are not perfect but provide important information about pile behavior (e.g., cases with refusal blow counts may be of interest if the load test capacity is relatively low; driving records are of interest even if the static load test did not fail, etc.)

For improved dynamic soil parameters, particularly for improved long-term capacities based on EOD readings:

2. Perform additional correlation studies; in particular, pursue the question whether or not lower end of driving damping factors in clays, and larger quakes for large piles should be recommended. Check end of driving results with recommended setup factors for the end of driving analyses.
3. Investigate a better system than soil grain size distribution for shaft dynamic soil damping and make recommendations for increased damping factors for restrike analyses.
4. Develop a better understanding of whether and how dynamic soil parameters change after driving and during setup periods.

For an improved wave equation software:

5. For both improved stress and capacity/driveability predictions, utilize the hyperbolic toe resistance for large quake cases; include the plug feature automatically for open end piles and the toe gap for low friction piles. Improve calculation of blow count for hyperbolic analyses.
6. Develop the wave equation approach for automatic setup loss/gain based on waiting times and energy dissipated in the soil utilizing the recommended and rechecked setup factors.

7. For restrike evaluation by wave equation, damping or setup factors must be developed using instrumented dynamic tests and CAPWAP, ideally with static load test confirmation.

For dynamic testing and CAPWAP:

8. The automatic CAPWAP procedure should be expanded to allow for realistic radiation damping. Automatic CAPWAP is generally the more acceptable solution as it avoids, in the minds of critics, the uniqueness question.

For the Modified SPT the following work is proposed:

9. Devising the necessary hardware to improve the torque measurement and to allow for torque measurements without top transducer exchange.
10. Develop a quicker means for static and dynamic end bearing tests. It is proposed that this test only be performed in addition to the usual sampler test driving where high end bearing values would make both bearing capacity calculation and driveability very important and difficult.
11. Prepare software allowing for automated evaluation of static and dynamic resistance parameters, in particular for cohesionless soils toe quake, toe damping and toe static resistance, during driving. For the shaft, these values could be similarly determined in cohesive soils.
12. Prepare specifications for Modified SPT data collection and evaluation.

NTIS does not permit return of items for credit or refund. A replacement will be provided if an error is made in filling your order, if the item was received in damaged condition, or if the item is defective.

Reproduced by NTIS

National Technical Information Service
Springfield, VA 22161

*This report was printed specifically for your order
from nearly 3 million titles available in our collection.*

For economy and efficiency, NTIS does not maintain stock of its vast collection of technical reports. Rather, most documents are printed for each order. Documents that are not in electronic format are reproduced from master archival copies and are the best possible reproductions available. If you have any questions concerning this document or any order you have placed with NTIS, please call our Customer Service Department at (703) 487-4660.

About NTIS

NTIS collects scientific, technical, engineering, and business related information — then organizes, maintains, and disseminates that information in a variety of formats — from microfiche to online services. The NTIS collection of nearly 3 million titles includes reports describing research conducted or sponsored by federal agencies and their contractors; statistical and business information; U.S. military publications; audiovisual products; computer software and electronic databases developed by federal agencies; training tools; and technical reports prepared by research organizations worldwide. Approximately 100,000 *new* titles are added and indexed into the NTIS collection annually.

For more information about NTIS products and services, call NTIS at (703) 487-4650 and request the free *NTIS Catalog of Products and Services*, PR-827LPG, or visit the NTIS Web site <http://www.ntis.gov>.

NTIS

***Your indispensable resource for government-sponsored
information—U.S. and worldwide***







U.S. DEPARTMENT OF COMMERCE
Technology Administration
National Technical Information Service
Springfield, VA 22161 (703) 487-4650
